

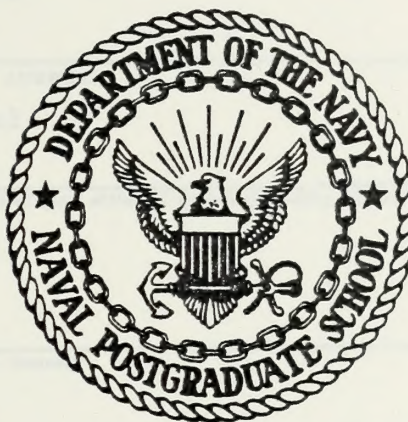
COMPUTER SIMULATION OF THE ANGULAR
DISPERSION OF SPUTTERED COPPER ISOTOPES
AND A POSSIBLE "LIQUID SPLASH" EFFECT

Patrick Wayne Kelly

DUDLEY KNOX LIBRARY
NAVAL POSTGRADUATE SCHOOL

NAVAL POSTGRADUATE SCHOOL

Monterey, California



THESIS

COMPUTER SIMULATION OF THE ANGULAR
DISPERSION OF SPUTTERED COPPER ISOTOPES
AND A POSSIBLE "LIQUID SPLASH" EFFECT

by

Patrick Wayne Kelly, Sr.

June 1977

Thesis Advisor:

Don E. Harrison, Jr.

Approved for public release; distribution unlimited.

T178652

REPORT DOCUMENTATION PAGE		READ INSTRUCTIONS BEFORE COMPLETING FORM
1. REPORT NUMBER	2. GOVT ACCESSION NO.	3. RECIPIENT'S CATALOG NUMBER
4. TITLE (and Subtitle) Computer Simulation of the Angular Dispersion of Sputtered Copper Isotopes and a Possible "Liquid Splash" Effect		5. TYPE OF REPORT & PERIOD COVERED Masters Thesis June 1977
7. AUTHOR(s) Patrick Wayne Kelly, Sr.		6. PERFORMING ORG. REPORT NUMBER
9. PERFORMING ORGANIZATION NAME AND ADDRESS Naval Postgraduate School Monterey, CA 93940		8. CONTRACT OR GRANT NUMBER(s)
11. CONTROLLING OFFICE NAME AND ADDRESS Naval Postgraduate School Monterey, CA 93940		10. PROGRAM ELEMENT, PROJECT, TASK AREA & WORK UNIT NUMBERS
14. MONITORING AGENCY NAME & ADDRESS (if different from Controlling Office)		12. REPORT DATE June 1977
		13. NUMBER OF PAGES 259
		15. SECURITY CLASS. (of this report) UNCLASSIFIED
		15a. DECLASSIFICATION/DOWNGRADING SCHEDULE
16. DISTRIBUTION STATEMENT (of this Report) Approved for public release; distribution unlimited		
17. DISTRIBUTION STATEMENT (of the abstract entered in Block 20, if different from Report)		
18. SUPPLEMENTARY NOTES		
19. KEY WORDS (Continue on reverse side if necessary and identify by block number) Sputtering Computer Simulation Sputtered Isotopes		
20. ABSTRACT (Continue on reverse side if necessary and identify by block number) The NPS computer simulation model was modified to study the angular dispersion and ring of sputtering sites formation of sputtered copper isotopes. The sputtering ratio as a function of the ion mass and the microcrystallite size needed to contain low-energy events were also investigated. A shift in the ejection angles of sputtered Cu (63) isotopes toward the surface normal is observed. When the "primary knock-on atom" was a light		

isotope, all of the sputtered atoms were ejected more nearly normal to the surface. The predominance of sputtered atoms in the $\langle 100 \rangle$ and $\langle 101 \rangle$ directions from the impact atom indicated an ease of momentum transfer in these directions. Results obtained from studies based upon a grid of impact points compares very favorably with the results obtained when randomly selected impact points were used. The rings of sputtered atoms present a "Liquid Splash" effect.

Approved for public release; distribution unlimited.

Computer Simulation of the Angular
Dispersion of Sputtered Copper Isotopes
and a Possible "Liquid Splash" Effect

by

Patrick Wayne Kelly, Sr.
Lieutenant, United States Navy
B.S.E.E., University of Colorado, 1971

Submitted in partial fulfillment of the
requirements for the degree of

MASTER OF SCIENCE IN PHYSICS

from the

NAVAL POSTGRADUATE SCHOOL

June 1977

ABSTRACT

The NPS computer simulation model was modified to study the angular dispersion and ring of sputtering sites formation of sputtered copper isotopes. The sputtering ratio as a function of the ion mass and the microcrystallite size needed to contain low-energy events were also investigated.

A shift in the ejection angles of sputtered Cu (63) isotopes toward the surface normal is observed. When the "primary knock-on atom" was a light isotope, all of the sputtered atoms were ejected more nearly normal to the surface. The predominance of sputtered atoms in the $\langle 100 \rangle$ and $\langle 101 \rangle$ directions from the impact atom indicated an ease of momentum transfer in these directions. Results obtained from studies based upon a grid of impact points compares very favorably with the results obtained when randomly selected impact points were used. The rings of sputtered atoms present a "liquid splash" effect.

TABLE OF CONTENTS

LIST OF FIGURES.....	8
ACKNOWLEDGEMENTS.....	15
I. INTRODUCTION.....	16
II. RESEARCH OBJECTIVES.....	21
A. ANGULAR DISPERSION OF ISOTOPES.....	21
B. LIQUID SPLASH EFFECT.....	21
C. ENERGY CONTAINMENT.....	22
D. ION/ATOM MASS RATIO.....	22
III. SIMULATION MODEL MODIFICATIONS.....	24
A. MICROCRYSTALLITE SIZE.....	25
B. CRYSTAL BOUNDARIES.....	26
C. ISOTOPE GENERATION.....	27
D. TARGET IMPACT AREAS.....	27
E. LATTICE FOLDING.....	28
F. ATOM SPUTTERING PROBABILITY.....	28
G. EJECTION ANGLES.....	29
H. VARIABLE-SHOT SELECTION.....	29
I. RANDOMLY SELECTED IMPACT POINTS.....	30
IV. RESULTS.....	32
A. 9X9 MICROCRYSTALLITE.....	33
1. (100) Orientation.....	33
a. 100-eV Ions.....	34
(1) Helium Ions.....	34
(2) Neon Ions.....	35
(3) Argon Ions.....	35
(4) Copper Ions.....	38
(5) Krypton Ions.....	38
(6) Xenon Ions.....	39
(7) Gold Ions.....	39
(8) Mercury Ions.....	39

b.	1-keV Results.....	40
(1)	Helium Ions.....	41
(2)	Neon Ions.....	41
(3)	Argon Ions.....	42
(4)	Copper Ions.....	42
(5)	Krypton Ions.....	43
(6)	Xenon Ions.....	43
(7)	Gold Ions.....	43
(8)	Mercury Ions.....	44
c.	2-keV Results.....	44
2.	(110) Orientation - 100 eV.....	45
a.	Argon Ions.....	46
b.	Mercury Ions.....	47
3.	(111) Orientation - 100eV.....	47
a.	Argon Ions.....	48
b.	Mercury Ions.....	49
B.	LARGER LATTICES.....	49
1.	100-eV Containment.....	50
2.	17x4x17 Microcrystallite.....	51
a.	Copper Ions.....	51
b.	Mercury Ions.....	53
c.	Sputtering Mechanism Traces.....	54
3.	Ion/Atom Mass Ratio.....	55
C.	RANDOM IMPACT POINTS.....	56
V.	CONCLUSIONS AND RECOMMENDATIONS.....	58
A.	SIMULATION MODEL.....	58
B.	CONTAINMENT.....	59
C.	ANGULAR DISPERSION.....	60
D.	RING FORMATION.....	60
E.	ION/ATOM MASS RATIO.....	61
F.	RANDOMLY SELECTED IMPACT POINTS.....	62
G.	FUTURE RESEARCH.....	62
Appendix A:	ISOTOPE GENERATION.....	64
Appendix B:	LATTICE FOLDING.....	66

A.	(100) ORIENTATION FOLDING.....	67
B.	(110) ORIENTATION FOLDING.....	67
C.	(111) ORIENTATION FOLDING.....	68
Appendix C:	GLOSSARY.....	70
Appendix D:	COMPUTER PROGRAM.....	95
FIGURES.....		129
LIST OF REFERENCES.....		256
INITIAL DISTRIBUTION LIST.....		259

LIST OF FIGURES

1. Sputtering Summary - (100) 2keV Cu/Ne ⁺ KSE-B.....	129
2. Sputtering Summary - (100) 2keV Cu/Au ⁺ KSE-B.....	129
3. 9x4x9, (100) Orientation Microcrystallite.....	130
4. 9x4x9, (110) Orientation Microcrystallite.....	131
5. 9x4x9, (111) Orientation Microcrystallite.....	132
6. Microcrystallite Boundaries.....	133
7. Intrinsic Geometry of Target Impact Areas.....	134
8. Reduced Representative Impact Areas.....	135
9. Expanded Impact Area - (100) Orientation.....	136
10. Expanded Impact Area - (110) Orientation.....	137
11. Expanded Impact Area - (111) Orientation.....	138
12. (100) and (110) Orientation Folding Geometry.....	139
13. (111) Orientation Folding Geometry.....	140
14. Sputtering Ratio vs. Ion Atomic Number - (100), 100-eV, 9x4x9.....	141
15. Sputtering Summary - (100), 100-eV, Cu/He ⁺	142
16. Ring Probability - (100), 100-eV, Cu/He ⁺	143
17. Angular Dispersion - (100), 100-eV, Cu/He ⁺	144
18. Sputtering Summary - (100), 100-eV, Cu/Ne ⁺	145
19. Ring Probability - (100), 100-eV, Cu/Ne ⁺	146

20.	Angular Dispersion - (100), 100-eV, Cu/Ne+.....	147
21.	Sputtering Summary - (100), 100-eV, Cu/Ar+.....	148
22.	Ring Probability - (100), 100-eV, Cu/Ar+.....	149
23.	Angular Dispersion - (100), 100-eV, Cu/Ar+ Gibson-II.....	150
24.	Angular Dispersion - (100), 100-eV, Cu/Ar+ KSE-B.....	151
25.	Sputtering Mechanism Trace - (100), 100-eV, Cu/Ar+, Gibson-II.....	152
26.	Sputtering Summary - (100), 100-eV, Cu/Cu+.....	153
27.	Ring Probability - (100), 100-eV, Cu/Cu+.....	154
28.	Angular Dispersion - (100), 100-eV, Cu/Cu+.....	155
29.	Sputtering Summary - (100), 100-eV, Cu/Kr+.....	156
30.	Ring Probability - (100), 100-eV, Cu/Kr+.....	157
31.	Angular Dispersion - (100), 100-eV, Cu/Kr+.....	158
32.	Sputtering Summary - (100), 100-eV, Cu/Xe+.....	159
33.	Ring Probability - (100), 100-eV, Cu/Xe+.....	160
34.	Angular Dispersion - (100), 100-eV, Cu/Xe+.....	161
35.	Sputtering Summary - (100), 100-eV, Cu/Au+.....	162
36.	Ring Probability - (100), 100-eV, Cu/Au+.....	163
37.	Angular Dispersion - (100), 100-eV, Cu/Au+.....	164
38.	Sputtering Summary - (100), 100-eV, Cu/Hg+.....	165
39.	Ring Probability - (100), 100-eV, Cu/Hg+.....	166
40.	Angular Dispersion - (100), 100-eV, Cu/Hg+ Gibson-II.....	167

41.	Angular Dispersion - (100), 100-eV, Cu/Hg ⁺ KSE-B.....	168
42.	Sputtering Ratio vs. Ion Atomic Number - (100), 1-keV, 9x4x9.....	169
43.	Sputtering Summary - (100), 1-keV, Cu/He ⁺	170
44.	Ring Probability - (100), 1-keV, Cu/He ⁺	171
45.	Angular Dispersion - (100), 1-keV, Cu/He ⁺	172
46.	Sputtering Summary - (100), 1-keV, Cu/Ne ⁺	173
47.	Ring Probability - (100), 1-keV, Cu/Ne ⁺	174
48.	Angular Dispersion - (100), 1-keV, Cu/Ne ⁺	175
49.	Sputtering Summary - (100), 1-keV, Cu/Ar ⁺	176
50.	Ring Probability - (100), 1-keV, Cu/Ar ⁺	177
51.	Angular Dispersion - (100), 1-keV, Cu/Ar ⁺	178
52.	Sputtering Summary - (100), 1-keV, Cu/Cu ⁺	179
53.	Ring Probability - (100), 1-keV, Cu/Cu ⁺	180
54.	Angular Dispersion - (100), 1-keV, Cu/Cu ⁺	181
55.	Sputtering Summary - (100), 1-keV, Cu/Kr ⁺	182
56.	Ring Probability - (100), 1-keV, Cu/Kr ⁺	183
57.	Angular Dispersion - (100), 1-keV, Cu/Kr ⁺	184
58.	Sputtering Summary - (100), 1-keV, Cu/Xe ⁺	185
59.	Ring Probability - (100), 1-keV, Cu/Xe ⁺	186
60.	Angular Dispersion - (100), 1-keV, Cu/Xe ⁺	187
61.	Sputtering Summary - (100), 1-keV, Cu/Au ⁺	188
62.	Ring Probability - (100), 1-keV, Cu/Au ⁺	189
63.	Angular Dispersion - (100), 1-keV, Cu/Au ⁺	190

64.	Sputtering Summary - (100), 1-keV, Cu/Hg+	191
65.	Ring Probability - (100), 1-keV, Cu/Hg+	192
66.	Angular Dispersion - (100), 1-keV, Cu/Hg+	193
67.	Sputtering Ratio vs. Ion Atomic Number - (100), 2-keV, 9x4x9	194
68.	Sputtering Summary - (110), 100-eV, Cu/Ar+ Gibson-II	195
69.	Ring Probability - (110), 100-eV, Cu/Ar+ Gibson-II	196
70.	Angular Dispersion - (110), 100-eV, Cu/Ar+ Gibson-II	197
71.	Angular Dispersion - (110), 100-eV, Cu/Ar+ Gibson-II	198
72.	Sputtering Summary - (110), 100-eV, Cu/Ar+ KSE-B	199
73.	Ring Probability - (110), 100-eV, Cu/Ar+ KSE-B	200
74.	Angular Dispersion - (110), 100-eV, Cu/Ar+ KSE-B	201
75.	Angular Dispersion - (110), 100-eV, Cu/Ar+ KSE-B	202
76.	Sputtering Summary - (110), 100-eV, Cu/Hg+ KSE-B	203
77.	Ring Probability - (110), 100-eV, Cu/Hg+ KSE-B	204
78.	Angular Dispersion - (110), 100-eV, Cu/Hg+	205
79.	Sputtering Summary - (111), 100-eV, Cu/Ar+	206
80.	Atom Probability - (111), 100-eV, Cu/Ar+	207

81.	Angular Dispersion - (111), 100-eV, Cu/Ar ⁺ Gibson-II.....	208
82.	Angular Dispersion - (111), 100-eV, Cu/Ar ⁺ KSE-B.....	209
83.	Angular Dispersion - (111), 100-eV, Cu/Ar ⁺ KSE-B.....	210
84.	Sputtering Summary - (111), 100-eV, Cu/Hg ⁺ Gibson-II.....	211
85.	Sputtering Summary - (111), 100-eV, Cu/Hg ⁺ KSE-B.....	212
86.	Atom Probability - (111), 100-eV, Cu/Hg ⁺	213
87.	Angular Dispersion - (111), 100-eV, Cu/Hg ⁺ Gibson-II.....	214
88.	Angular Dispersion - (111), 100-eV, Cu/Hg ⁺ KSE-B.....	215
89.	Angular Dispersion - (111), 100-eV, Cu/Hg ⁺ KSE-B.....	216
90.	Sputtering Summary - (110), 100-eV, Cu/Hg ⁺ 13x6x13.....	217
91.	Sputtering Summary - (111), 100-eV, Cu/Hg ⁺ 13x4x13.....	218
92.	Sputtering Ratio vs. Ion Atomic Number.....	219
93.	Sputtering Ratio vs. Lattice Size.....	220
94.	Sputtering Summary - (100), 100-eV, Cu/Cu ⁺	221
95.	Atom Probability - (100), 100-eV, Cu/Cu ⁺	222
96.	Angular Dispersion - (100), 100-eV, Cu/Cu ⁺	223
97.	Sputtering Summary - (100), 200-eV, Cu/Cu ⁺	224

98.	Atom Probability - (100), 200-eV, Cu/Cu+.....	225
99.	Angular Dispersion - (100), 200-eV, Cu/Cu+.....	226
100.	Sputtering Summary - (100), 500-eV, Cu/Cu+.....	227
101.	Atom Probability - (100), 500-eV, Cu/Cu+.....	228
102.	Angular Dispersion - (100), 500-eV, Cu/Cu+.....	229
103.	Sputtering Summary - (100), 1-keV, Cu/Cu+.....	230
104.	Atom Probability - (100), 1-keV, Cu/Cu+.....	231
105.	Angular Dispersion - (100), 1-keV, Cu/Cu+.....	232
106.	Sputtering Summary - (100), 100-eV, Cu/Hg+.....	233
107.	Atom Probability - (100), 100-eV, Cu/Hg+.....	234
108.	Angular Dispersion - (100), 100-eV, Cu/Hg+.....	235
109.	Sputtering Summary - (100), 200-eV, Cu/Hg+.....	236
110.	Atom Probability - (100), 200-eV, Cu/Hg+.....	237
111.	Angular Dispersion - (100), 200-eV, Cu/Hg+.....	238
112.	Sputtering Summary - (100), 500-eV, Cu/Hg+.....	239
113.	Atom Probability - (100), 500-eV, Cu/Hg+.....	240
114.	Angular Dispersion - (100), 500-eV, Cu/Hg+.....	241
115.	Sputtering Summary - (100), 1-keV, Cu/Hg+.....	242
116.	Atom Probability - (100), 1-keV, Cu/Hg+.....	243
117.	Angular Dispersion - (100), 1-keV, Cu/Hg+.....	244
118.	Sputtering Mechanism Trace - (100), 100-eV, Cu/Uc+, KSE-B, 17x4x17.....	245
119.	Sputtering Mechanism Trace - (100), 100-eV, Cu/Uc+, KSE-B, 9x4x9.....	246

120.	Sputtering Ratio vs. Ion/Target Atom	
	Atomic Mass Ratio.....	247
121.	Sputtering Ratio vs. Ion/Target Atom	
	Atomic Mass Ratio.....	248
122.	Placement of 144 Random Shots.....	249
123.	Sputtering Summary - Random Points	
	(100), 100-eV, Cu/Hg ⁺ , KSE-B, 11x4x11.....	250
124.	Sputtering Summary - Grid Points	
	(100), 100-eV, Cu/Hg ⁺ , KSE-B, 11x4x11.....	251
125.	Atom Sputtering Probability - Random Points	252
126.	Atom Sputtering Probability - Grid Points	253
127.	Angular Dispersion - Random Points	254
128.	Angular Dispersion - Grid Points	255

ACKNOWLEDGEMENTS

A digital computer simulation requires the assistance and cooperation of many personnel not directly concerned with the research. I am indebted to the staff of the Computer Center Naval Postgraduate School (NPS) for their help in processing rapidly the large number of runs required to gather and analyze the data.

I am especially grateful to Dr. Don E. Harrison, Jr. at NPS for his encouragement and supervision in this research effort. Also invaluable were the many hours of stimulating discussion with Professor Harrison and Gary L. Smith, a friend and fellow student, concerning sputtering and modeling along with the endless exchange of ideas, techniques, and solutions.

To my wife, Jan, and our three sons, I express my sincere appreciation for their devotion, patience, and understanding throughout this research.

I. INTRODUCTION

The phenomena of physical sputtering have been extensively studied since it was first mentioned in Philosophical Transactions by Grove in 1852. Sputtering is the ejection of atomic material from a target resulting from bombardment by an energetic particle. Most scientific investigation has been restricted to ionic bombardment because the ion can easily be accelerated to any desired velocity. Sputtering has defied complete physical description because of complicated mechanisms, difficulty in treating the behavior of a many-body system, and an incomplete understanding of the interacting forces and potentials in crystal structures.

Early experiments typically determined the "sputtering ratio" of single and polycrystalline materials. The "sputtering ratio" (interchangeable with sputtering yield - Y) is defined as the number of target atoms ejected from the surface per incident ion.

In 1923, Kingdon and Langmuir [1] bombarded thoriated tungsten with various ions in a glow discharge tube. This was a special case of sputtering since the thin surface film of thorium on a tungsten substrate was sputtered rather than the tungsten itself. The results of this experiment qualitatively suggested an ejection mechanism.

A few years later, Blechschmidt and von Hippel [2,3] proposed a theory which described sputtering as an evaporation of surface atoms (an emission mechanism). Earlier, von Hippel [4] had found by spectroscopic analysis

that at least some sputtered atoms were in an excited state. The sputtering theory showed that atoms in the region of impact could rapidly acquire thermal energy if the kinetic energy of the incident ion was converted to thermal energy at the target surface. If an atom acquired a sufficient amount of thermal energy, it would then evaporate from the surface, some atoms evaporating while in an excited state.

Direct application of statistical methods to sputtering was made by Harrison [5] who envisioned the interaction of two distribution functions (the crystal lattice and the ion beam). These models, based on statistical methods, implicitly accept ejection-type mechanisms.

One of the most important contributions to the study of sputtering was made by Wehner [6] in 1953. He discounted the evaporation theory and presented strong evidence for a momentum transfer process. Shortly after Wehner's findings were reported, Henschke [7] proposed a theory of sputtering based solely on classical theory, treating normal and oblique incidence sputtering separately. His concept of normal incidence sputtering required many-body collisions in which the ion was eventually reflected outward to sputter surface atoms. This theory was plausible for oblique incidence sputtering; however, the case for normal incidence sputtering required that the ion be reflected inside the crystal.

Wehner and Rosenberg [8] reported that in the sputtering of polycrystalline metals at low ion energy (normal incidence) more material is ejected obliquely than in a direction normal to the target surface. This is due to the fact that less than a full (180°) overall direction change of momentum is more favorable for sputtering because this requires fewer number of successive collisions for atom ejection. In 1960, Wehner and Anderson [9] reported

sputtering patterns from single crystal targets which showed an anisotropic spread of energy from a collision center and atoms which are preferentially ejected in close-packed directions.

When an atom collides with another which has a higher mass, the scattering angle can vary between 0° and 180° . In a collision with a lower mass atom the scattering is confined to between 0° and 90° (thus backward reflection cannot occur). In low-energy sputtering of multi-element targets, Winters and Sigmund [10] showed theoretically that a significant contribution to sputtering, called "single reflective collisions", arises from the reflection of lower mass atoms from underlying heavier atoms. For a detailed discussion of momentum reversal, see Harrison and Magnuson [11].

In 1962, Wehner et al [12] published a compilation of sputtering yields for metals and semiconductors in the 100-600 eV range. In 1966, Wehner, Anderson, and KenKnight [13] published the results of a study that covered almost a decade of research in low-energy sputtering. A few of the numerous topics discussed included more accurate and improved techniques for analyzing the sputtered mass, the temperature dependence of sputtering yields of various metals bombarded by atomic and polyatomic ions in the 2.8 to 10 keV range, the effect of oxygen on ion ejection patterns, and the spatial distribution of ejected atoms in metals and semiconductors.

A few low-energy sputtering experiments [14, 15, 16, 17, 18], which lend themselves to direct comparison with these simulations, investigate the behavior of the sputtering ratio as a function of ion energy, lattice orientation, target material, and ion angle of incidence.

Paralleling the experimental investigation of the sputtering yield and the development of mass spectrographic analysis was the attempt to model the sputtering mechanism through the use of computer simulation. In 1960, Gibson, Goland, Milgram, and Vineyard [19], the first investigators to use computer simulation as a means of studying radiation damage, set forth the criteria that must be satisfied before the simulation method could be applied to crystals. Reference [19] gives a very detailed description of the simulation method. Basically, they built a computer model to represent metallic copper and studied radiation damage events at low and moderate ranges of energy up to 400 eV. In their model, one atom in the stationary lattice was given an arbitrary kinetic energy and direction of motion, as though it had been struck by a bombarding particle, and was allowed to interact with the remaining atoms in the lattice. This resulted in cascades of independent binary collisions. It is well established that sputtering of solids by ion bombardment is the result of successive independent approximately binary collisions somewhat as if these collisions take place with or between separate gas atoms. Low-energy ion scattering studies [20] have shown that the approximately binary scattering behavior still holds at bombarding energies as low as those approaching the sputtering thresholds.

In 1967, Harrison, Levy, Johnson, and Effron [21] used a computer to simulate the bombardment of face-centered-cubic (fcc) copper single crystals by an argon ion. From their studies, the sputtering mechanisms in the fcc crystal were isolated and identified. They reported, for ion energies less than 10 keV, the sputtering process occurred predominately within three atomic layers of the surface. The computer simulation included only a repulsive force between the atoms. The equations of motion for the

many-body system were computed using an "average-force" algorithm rather than a "central-difference" algorithm, see Harrison, Gay, and Effron [22]. In 1972, Harrison, Moore, and Holcombe [23] in continuing efforts to develop a more realistic computer model incorporated a Cu-Cu potential function which included an attractive potential, surface layer relaxation, and surface binding energy for the (100), (110), and (111) copper planes. They reported improved agreement between experimental and simulation results, but the original interpretation of the low-energy sputtering mechanisms in fcc copper crystals remained unchanged.

Computer simulation of physical processes is still in a very infant state because the available processing speed of existing computers severely limits the sophistication of the models. However, past investigations were quite successful in identifying the mechanisms which occur when energetic particles interact with crystal atoms. The ability to observe these mechanisms is an advantage peculiar to the computer simulation because each crystal atom is identified by a number for the mathematical calculation, and its complete track can be labeled and recorded. The tracks of selected atoms can be examined to determine the dynamics of the atoms which exit the front surface.

II. RESEARCH OBJECTIVES

A. ANGULAR DISPERSION OF ISOTOPES

Recently, Wehner [24] reported that the isotope ratio in metal deposits obtained by sputtering a flat target at low ion energy (100eV) under normal incidence is a function of the ejection angle. He investigated the bombardment of a Cu(63-65) target with 100 eV Hg ions. He reported that the lighter isotopes are enriched in a direction normal to the target surface. This research was a computer simulation investigation of Wehner's studies of angular dispersion of isotopes in a monocrystalline copper lattice.

B. LIQUID SPLASH EFFECT

In preliminary NPS simulation studies, after analysis of data, a predominance of sputtered atoms occurred at certain distances from the center of the lattice representative area in which the ion impacts occur. Figures 1 and 2 [25] depict the top layer of a copper fcc crystal respectively bombarded by neon and gold ions at 2 keV. The numbers represent the number of times that the atom was sputtered in 36 events (shots). The dark triangle in the center represents the target impact area. All 36 events are directed into this representative area. The darkened ellipses highlight the atoms most often sputtered and suggest a ring outward from the center (especially for the Cu-Au interaction).

Macklin and Metaxas [26] experimentally investigated the splashing of liquid drops on deep and shallow liquid layers. They published high speed photographs which showed liquid splashes that might be analogous to surface atoms being ejected from the surface and a few eventually sputtering.

This research was an investigation of "ring formation" or "liquid splash" effect of sputtered atoms. Determination was made of the probability that a congregate of atoms at a given distance from the impact area reference will sputter.

C. ENERGY CONTAINMENT

As with any computer simulation, a trade-off must be made between the accuracy and detail desired and the size and time requirements imposed by computer availability. Because of this constraint a limit exists on the size of the monocrystalline lattice used in the simulation. This research was an investigation to determine the size lattice required to contain a low energy event.

D. ION/ATOM MASS RATIO

In July of 1976, Eer Nisse [27], reported experimental confirmation of a monotonic dependence of Y with the atomic number. He investigated the yield of a gold target impacted by 40 keV ions up to the atomic number of gold. This monotonic dependence is predicted by a sputtering theory of Sigmund [28]. However, computer simulation data of previous NPS studies [29] indicate that the monotonic dependence of

the sputtering ratio on the ion mass ceases to be valid for ion/atom mass ratios greater than one. This research was an investigation of the sputtering ratio versus ion atomic number for a wide range of ion/atom ratios.

III. SIMULATION MODEL MODIFICATIONS

The basic simulation model used in this research has been developed by the NPS group over the last decade [21, 23, 31, 32]. A brief description of this model and the alterations made to it for this research follow. For detailed discussions of the simulation method, the reader is directed to references 19, 20, 21, and 23. A detailed description of the mathematical model has been published [22].

In the development of the computer model, the lattice unit (LU) proves to be a convenient unit of length, and is used extensively. One $LU = a_0/2$, where a_0 is the cubic lattice constant, the atomic spacing as determined by x-ray crystallographic studies. For copper, $a_0 = 3.615$ angstroms.

Certain properties of the program and results are best considered in the framework of a specific run. Each run is begun by constructing a target microcrystallite whose sites represent the equilibrium positions of copper atoms near the surface of a fcc crystal. The target atom - target atom interaction is represented by the Born-Mayer Gibson type II (Gibson-II) repulsive potential function.

Each ion of the beam is represented by a single neutral atom of the desired element [30]. The ion is placed at the point on its trajectory such that its velocity vector determines the point of impact. The term bullet and ion are used interchangeably throughout this report for the incident particle to avoid confusing it with target atoms.

The bullet-target potential function was always either the Gibson-II or that determined by the Kinetic Secondary Electron (KSE-B) Potential [30]. These two potential functions seem to represent a reasonable range of "hard" and "soft" potential functions.

As reported by Harrison, Moore, and Holcombe [23], the attractive forces between the atoms in the crystal are so small, when compared to the forces which occur in even moderately energetic collisions, that they may be safely neglected in sputtering simulations. Also, in order to use the smaller reduced target areas, the ions must be normally incident. Even though the computer program still retained the capability to utilize attractive potentials and obliquely incident ions, they were not used in this investigation.

A. MICROCRYSTALLITE SIZE

Initial discussion to establish research objectives revealed the advantages gained from using a symmetrical lattice that could be folded and rotated so that atoms sputtered by ions incident at all possible impact points would become available for analysis. A lattice with each layer a square and having an odd number of atoms along each boundary was needed. The lattice generation program as previously used could handle this change with no alterations.

Figures 3, 4, and 5 show a roughly isometric projection of the labeled atoms in a 9x4x9 (100) orientation, a 9x6x9 (110) orientation, and a 9x4x9 (111) orientation of a fcc microcrystallite respectively. This type of projection, first used by Harrison and Delaplain [31], with the distance

between layers in the Y direction exaggerated, and the atoms represented by 20° ellipses has proved to be a valuable tool for analyzing the computer programs and for displaying data. The first number in each lattice is atom number two, with atom number one being the bullet.

From previous studies, it was clear that at the low energy levels considered the sputtering mechanisms were confined to the surface layers [21]. For this reason, the (100) and (111) orientation microcrystallites were only four layers deep. The (110) orientation lattice generation program constructs a lattice which has significantly fewer atoms and its layers are closer together. In an attempt to increase the number of atoms in the lattice while keeping the required computer time below that of the (100) and (111) orientation programs, the (110) orientation microcrystallite was set at six layers deep.

B. CRYSTAL BOUNDARIES

The previous simulation program contained a microcrystallite with established boundaries that were not consistent with the development of the potential functions. Since the potential function is truncated at the nearest-neighbor separation (ROE), all boundaries (except the top surface) were set at ROE. This is justified by the fact that an atom outside these boundaries is farther from the crystal than the potential truncation radius. The upper surface boundary was set by starting a small distance from the lattice surface, and increasing the distance in succeeding runs until the total yield was independent of the distance. For computational efficiency this distance should be set as small as possible.

Figure 6 shows a drawing of the microcrystallite in solid lines and the plane boundaries in dashed lines. The boundaries which are defined in the Glossary (Appendix C) are shown as planes at the distance from the microcrystallite surface cited above.

C. ISOTOPE GENERATION

In order to study the angular dispersion of sputtered isotopes, a method for generating a microcrystallite with the correct isotope ratio and masses was needed. The method used assigned an additional variable to each atom that identified the atom "type". The atoms were classified according to two types; type 1 - least abundant, heavier isotope and type 2 - most abundant, lighter isotope. Appendix A is a detailed discussion of how the correct isotope ratio was obtained and each atom properly identified with the correct mass.

D. TARGET IMPACT AREAS

A representative area must contain all possible impact points upon a particular surface, that is any point in the surface must be projectable into a point of the representative area. Figure 7 shows the intrinsic geometry of the three fcc orientations and the complete sets of impact points for each representative area. Figure 8 shows the reduced sets of impact points from which the complete sets are generated by reflection and rotation. Figures 9, 10, and 11 show an expanded view of the target impact areas and the actual impact points used. The individual impact points are those used in previous simulations for normal

incidence. This simplification, which greatly reduces the computer running time, is only possible when the ion is normally incident.

E. LATTICE FOLDING

In order to investigate the ring formation or "liquid splash" effect, it was necessary to develop a means of folding the results obtained from the reduced target area. This requirement was satisfied by writing three subroutines; KFOLDA, KFOLDB, and KFOLDC. Appendix B gives a detailed description of the "folding" logic and the geometry of each orientation. Figure 12 shows how the (100) and (110) orientation reduced representative areas were folded to obtain the complete representative areas. Figure 13 shows how the (111) orientation reduced representative area was folded and summed to obtain the complete representative area.

F. ATOM SPUTTERING PROBABILITY

A means of taking the folded data and calculating a conditional probability that an atom would sputter from a particular ring was needed. This was accomplished by writing the subroutine KPROB. In this subroutine, the distance from each atom to the reference (0,0) point in the reduced representative impact area was calculated. then all atoms at each distance were checked and the atom sputtering count was summed. This sum was divided by the total number of sputs from all the shots. This quotient was the

conditional probability that a given ring at a known distance would sputter an atom given the atoms that had already sputtered.

KPROB performs the above calculations. However, a very interesting result is obtained by dividing the conditional probability obtained above by the number of atoms in a particular ring. This result was a conditional probability that an atom at a given distance from the impact point would sputter.

G. EJECTION ANGLES

The ejection angle is defined as the angle between the atom's velocity vector and the surface normal. A tally was kept of each atom's ejection angle, grouped in five degree intervals. This tally was recorded separately for each isotope. To provide a quick analysis of the data, a program (HISTO) was written to print out a histogram of the number of sputtered atoms ejected in each interval for each isotope.

H. VARIABLE-SHOT SELECTION

The previous program was only flexible enough to allow either a single-shot run or all 36 shots. As the size of the lattice and the ion's energy were increased, the computer run time for a set of 36 shots became unmanageable (12 - 18 hours). At this point, a variable size shot "package" was developed. The features included the ability to specify the number of shots desired and the starting impact point of the "package". The final summary for the

particular package run was printed out. The packages had to be combined by hand calculations in order to get the total information for a particular run. Even so, this procedure allowed runs to be made with larger lattices and higher energies (i.e. the containment studies) that previously would have been prohibitively long.

I. RANDOMLY SELECTED IMPACT POINTS

To obtain more angular dispersion data for the low-energy, (100) orientation events, a modification was made to the simulation model. This modification replaced the systematic method of incrementing the impact point over a grid of points in the representative target area with a random-shot capability. Again, the IMSL GGUB routine was used to generate uniformly distributed, psuedo-random numbers. The first random number was labeled the x coordinate in the impact area. The second random number was labeled the z coordinate and tested to determine if it was inside the impact area z boundaries determined by the value of the x coordinate. If this test was passed sucessfully, these values for the x and z coordinates were used. However, if the test did not pass (the x and z coordinates were outside the impact area), the two original numbers were discarded, two more were selected, and the process was repeated again.

This random impact point did not effect the variable - shot selection feature. But, enough random numbers had to be generated to allow for those points that did not fall into the impact area.

The results of randomly bombarding the impact area will be discussed later. This feature was incorporated in response to other investigators suggestion that the grid of impact points be compared with a randomly bombarded impact area.

IV. RESULTS

The three lattice orientation models for the copper target were utilized in computer simulation runs in which 100-eV, 200-eV, 500-eV, and 1-keV normally incident ions bombarded the target. The ion masses varied from 4 amu (He^+) to over 200 amu (Hg^+). The lattice was constructed with copper atoms of either the natural mass (63.54 amu) or the proper ratio of isotopes (63.93 amu and 64.93 amu). The lattice size varied from a $9 \times 4 \times 9$, (100) orientation of 162 atoms to a $17 \times 4 \times 17$, (100) orientation of 578 atoms.

Computer runs were made for various permutations of ion energy, ion mass, lattice orientation, lattice size, and potential function. The summary of each run contained the number of atoms sputtered from each impact point, the number of times each atom sputtered, a histogram showing the angular dispersion of the sputtered atoms for each isotope, the number of sputs for each atom after the folding process, the distance from each ring to the impact area reference point, the number of atoms and the sum of their sputs in each ring, and the probability that each ring contained a sputtered atom.

In the sputtering summaries the numbers in the ellipses indicate the number of times that particular atom sputtered in the simulation. The dark areas, a triangle for the (100) and (111) orientations and a rectangle for the (110) orientation, indicate the location of the target impact area. The atom that is struck by the ion is called the "primary knock-on atom" (hereafter PKA). Since different seeds were used to generate the random isotope sites, a

letter L or H denotes whether the sputtered atom was a light or heavy isotope. Wherever possible, the results for the Gibson-II and KSE-B potential functions were combined. In the figures displaying the sputtering summary and the mechanism tracing, some of the lower layers were omitted. However, all atoms were included in all calculations. In the 100-eV results all the sputtered atoms are shown. Wherever a direction in the lattice is specified, it is always with respect to that particular lattice axes. The top surface is always an XZ plane.

A. 9X9 MICROCRYSTALLITE

Initially, all simulations used a 9x9 lattice to determine the sputtering ratio as a function of the ion mass at 100 eV and 1 keV. The model was modified to include the isotope generator, the symmetrical folding of the summary, the angular dispersion of sputtered isotopes, and the "ring sputtering" probabilities.

1. (100) Orientation

The (100) orientation microcrystallite was constructed in a lattice consisting of 162 atoms. The lattice was 9 atoms in the X and Z directions and 4 atoms deep in the Y direction, hence 9x4x9. Figure 3 shows an isometric projection of the lattice and its atom numbering scheme. Figure 9 shows an expanded view of the grid of 36 impact points used.

a. 100-eV Ions

Of primary importance was the investigation of the angular dispersion of isotopes reported by Wehner [24]. His experiments were conducted with 100-eV mercury ions bombarding a copper target. These conditions were ideal to simulate with modifications to the existing model.

The sputtering simulations for a normally incident, 100-eV ion were run using He^+ , Ne^+ , Ar^+ , Cu^+ , Kr^+ , Xe^+ , Au^+ , and Hg^+ ions. Figure 14 shows the sputtering ratio as a function of the ion mass for both potential functions. As mentioned in the objectives, a decrease in the yield was evident for the heavier ions. The KSE-B curve shows a more natural, smooth behavior than that of Gibson-II.

(1) Helium Ions. The results when 100-eV helium ions impact the target area are shown in figures 15, 16, and 17. Figure 15 shows the sputtering summaries using (a) Gibson-II, resulting in a sputtering ratio of 0.444, and (b) KSE-B, resulting in a sputtering ratio of 0.111. The predominance of the sputtered atoms in the $\langle 100 \rangle$ and $\langle 101 \rangle$ directions is quite evident. Figure 16 shows the conditional probability that a ring of atoms, as a function of the ring distance from the impact area reference point, will contain an atom that sputtered for (a) Gibson-II and (b) KSE-B. The term "ring sputtering" probability, henceforth ring probability, was used as a label to mean the above conditional probability. The relative amplitudes of the ring probabilities could be misleading because the calculation does not take into effect the number of atoms in each ring. Again, the predominance of rings that contain atoms in the $\langle 100 \rangle$ and $\langle 101 \rangle$ directions is evident. The

peak of the KSE-B curve was closer to the center than the Gibson-II peaks, which were spread out all the way to the lattice edges. Figure 17 shows the angular dispersion results for (a) Gibson-II and (b) KSE-B. The particular seed used in the psuedo-random number generator to locate the isotope random sites was such that only light isotopes sputtered in this case.

(2) Neon Ions. The results when 100-eV neon ions impact the target area are shown in figures 18, 19, and 20. Figure 19 shows that for the light mass of the neon ion, atoms on the lattice boundary are sputtered using (a) Gibson-II and (b) KSE-B. Gibson-II resulted in a sputtering ratio of 0.889, while the sputtering ratio for KSE-B was 0.806. Figure 19 shows that the Ne^+ sputtered atoms were further away from the lattice center than the He^+ , for both (a) Gibson-II and (b) KSE-B. This was confirmed by the increased number of next-nearest neighbor atoms (in the $\langle 101 \rangle$ direction) sputtering. Figure 20 indicates that some of the heavier isotopes sputtered for (a) Gibson-II and (b) KSE-B. There were not enough sputtered atoms to notice any trend in the isotope angular dispersion.

(3) Argon Ions. The argon simulations were used to investigate the "reflective collision" theory. Argon ions of 100-eV energy bombarded the target area using both of the potential functions. In the random isotope site locations, the PKA (atom 22) was a heavy isotope, while three (52, 58, and 67) of the four atoms directly underneath were light isotopes. Four simulations were run using each of the potential functions; (1) the random isotope sites, (2) forcing the PKA to a light isotope, (3) forcing the PKA to a heavy isotope and all four atoms underneath to a light isotope, and (4) forcing the PKA to a light isotope and all four atoms underneath to a heavy isotope. The remainder of the lattice isotopes were unchanged.

Figure 21 shows the sputtering summaries for all four combinations using (a) Gibson-II and (b) KSE-B. In all four cases, identical atoms sputtered independent of isotope locations. Gibson-II resulted in sputtering ratios of 1.056, while KSE-B resulted in sputtering ratios of 0.944. Figure 22 illustrates the ring probability in all four cases for (a) Gibson-II and (b) KSE-B. Figure 23 illustrates the angular dispersion of ejected atoms, using Gibson-II, for (a) case (1), (b) case (2), (c) case (3), and (d) case (4). No light isotopes were sputtered. Figure 24 illustrates the same results for KSE-B.

Since at least four atoms were ejected into a different five degree window for Gibson-II, the sputtering mechanisms were checked. The most active event occurred when the impact area was struck by the ion at impact point 4060 (impact displaced 0.40 LU in the X direction and 0.60 LU in the Z direction from the center of the PKA, hence 4060). Four atoms were sputtered at this point. A single-impact program was run at this point with the output listing the positions, velocities, kinetic energy, and potential energy of each atom with a total energy greater than 0.1 eV. The listing was printed once every five timesteps. A timestep is the time interval between dynamic calculations. It is variable and determined as the time required for the fastest moving atom to move 0.1 LU from its previous position. In real time the timestep is on the order of 10^{-15} seconds. Figure 25 illustrates atom trajectories in the sputtering of atoms 17, 32, 57, and 77. In cases (3) and (4), the sputtering mechanisms were the same displaying only a slight difference in the ejection angles and the velocities of the sputtered atoms.

The argon ion collides with atom 22 (PKA) and atom 27 by timestep 5, pushing them down and under atoms 17 and 32 respectively. The ion continued downward and collided with atom 67 by timestep 15. The ion reflected back up through the hole vacated by atoms 22 and 27. By timestep 15, atoms 17 and 32 were moving upward. Atom 67 moved down colliding with atoms 107 and 112 by timestep 20. Atoms 107 and 112 squeezed [21] under atoms 102 and 117 respectively. Atoms 102 and 117 were moving up by timestep 30, and struck atoms 57 and 77 from below by timestep 40. By this time, atoms 17 and 32 had moved far enough above the lattice with sufficient upward velocity to be classified as "sputs". Atom 17 was ejected at an angle of 33.56° to the surface normal with an upward velocity of 2924 m/sec for case (3), and at an angle of 33.36° with a velocity of 2974 m/sec for case (4). Atom 32 was ejected at an angle of 33.65° with an upward velocity of 2926 m/sec for case (3), and at an angle of 33.56° with a velocity of 2918 m/sec for case (4). Atoms 57 and 77 continued upward through the holes left by the sputtered atoms 17 and 32. As atom 57 passed through this hole its trajectory was bent closer to the surface normal by atoms 12, 16, and 21. Likewise, atom 77 was reflected upward by atoms 28, 33, and 37. By timestep 75, atoms 57 and 77 were far enough above the lattice surface with sufficient upward velocity to be classified as "sputs". Atom 57 was ejected at an angle of 18.12° with an upward velocity of 2967 m/sec for case (3), and at an angle of 17.75° with a velocity of 2882 m/sec for case (4). Atom 77 sputtered at an angle of 25.04° with an upward velocity of 2799 m/sec for case (3), and at an angle of 24.75° with a velocity of 2859 m/sec for case (4).

It is noted that when the PKA was a light isotope, all of the sputtered atoms were ejected closer to the surface normal. Also noted is the remarkable symmetry of ejection angles and velocities of the sputtered atoms.

(4) Copper Ions. The results when 100-eV copper ions impact the target area are shown in figures 26, 27, and 28. Figure 26 shows the sputtering summaries for (a) Gibson-II, resulting in a sputtering ratio 0.944, and (b) KSE-B, resulting in a sputtering ratio of 1.111. Gibson-II simulations with Ar^+ and Cu^+ were the only runs that had atoms sputter from the second layer. Also, these two ions resulted in the highest sputtering ratios for both potential functions. These results further indicate a maximum sputtering ratio occurs near an ion/atom mass ratio of unity. Figure 27 illustrates a continued spread outward of the ring probability for (a) Gibson-II and (b) KSE-B. Figure 28 illustrates the angular dispersion results for (a) Gibson-II and (b) KSE-B.

(5) Krypton Ions. The results when 100-eV krypton ions impact the target area are shown in figures 29, 30, and 31. Figure 29 shows the sputtering summaries for (a) Gibson-II, resulting in a sputtering ratio of 0.694, and (b) KSE-B, resulting in a sputtering ratio of 1.139. Here, a maximum in the sputtering ratio was reached for KSE-B, while the sputtering ratio for Gibson-II dropped drastically. Figure 30 illustrates a continued outward spread of the ring probabilities for (a) Gibson-II and (b) KSE-B. It is noticed that the outward spread still occurred, even though the Gibson-II yield decreased. Figure 31 illustrates the angular dispersion results for (a) Gibson-II and (b) KSE-B.

(6) Xenon Ions. The results when 100-eV xenon ions impact the target area are shown in figures 32, 33, and 34. Figure 32 shows the sputtering summaries for (a) Gibson-II, resulting in a sputtering ratio of 0.556, and (b) KSE-B, resulting in a sputtering ratio of 1.028. Figure 33 illustrates the ring probabilities for (a) Gibson-II and (b) KSE-B. The outward spread of the ring probability peaks is still seen for KSE-B, while Gibson-II remained constant. Figure 34 illustrates the angular dispersion results for (a) Gibson-II and (b) KSE-B.

(7) Gold Ions. The results when 100-eV gold ions impact the target area are shown in figures 35, 36, and 37. Figure 35 shows the sputtering summaries for (a) Gibson-II, resulting in a sputtering ratio of 0.528, and (b) KSE-B, resulting in a sputtering ratio of 0.778. Figure 36 illustrates the ring probabilities for (a) Gibson-II and (b) KSE-B. Gibson-II has settled out with approximately equal probability of sputtering from atoms in the first two rings in the $\langle 101 \rangle$ direction. In the case of KSE-B, a shift from the first and second rings in the $\langle 100 \rangle$ direction toward the second ring in the $\langle 101 \rangle$ direction is noticed. Figure 37 illustrates the angular dispersion results for (a) Gibson-II and (b) KSE-B.

(8) Mercury Ions. These Hg^+ bombardment results are compiled from the sets of simulation runs used to investigate the "reflective collision" theory. Figure 38 shows the sputtering summaries for all four cases, in which the masses of the PKA and the four atoms underneath are varied. The results for (a) Gibson-II were identical in all four cases, resulting in a sputtering ratio of 0.528. The sputtering ratio was 0.743 using KSE-B in a lattice consisting of atoms with only the natural mass. The results for (b) KSE-B depended on the order of the heavy over light

interaction. When the PKA was a heavy isotope, shown in figure 38(b), the sputtering ratio was 0.7229. However, when the PKA was a light isotope, atom 30 sputtered an additional time (denoted by ▲) and the sputtering ratio became 0.750. Figure 39 illustrates the ring probabilities for (a) Gibson-II, which remained relatively unchanged, and (b) KSE-B, which still displayed a shift to the second ring in the 101 direction. Figure 40 illustrates the angular dispersion results for Gibson-II. Figure 41 shows the angular dispersion results for KSE-B. Again, atom 30 sputtered an additional time. The additional ejection angle is denoted by ▲.

b. 1-keV Results

The 1-keV events were obviously not contained in the 9x4x9 microcrystallite. However, the simulations were run to compare the sputtering ratios with experimental results. Also, the dependence of the sputtering on ion mass was investigated. Useful information can be obtained about the ring probabilities and isotope angular dispersion at this higher energy. The 162 atom, 9x4x9 microcrystallite, with the correct ratio of copper isotopes at random sites, was used. Even though all atoms were used in the calculations and the printout provided information on all atoms, only the top layer results are shown in the figures. Even in the worse case (Cu/Ar⁺, Gibson-II), more than 86 per cent of the sputtered atoms were from the top layer.

The sputtering simulations for normally incident, 1-keV ions were run using He⁺, Ne⁺, Ar⁺, Cu⁺, Kr⁺, Xe⁺, Au⁺, and Hg⁺ ions. Figure 42 shows the sputtering ratio as a function of the ion mass for both potential functions. As expected, the sputtering ratios have

increased. However, they are no longer smooth and continuous, but exhibit a randomness, as if each was independent of the others.

All the 1-keV simulations used the same random isotope sites. The letters L and H, denoting light or heavy isotopes, appear only in the Cu/Ne⁺, KSE-B summary (more different atoms sputtered - but not the highest sputtering ratio).

(1) Helium Ions. The results when 1-keV helium ions impact the target area are shown in figures 43, 44, and 45. Figure 43 shows the sputtering summaries for (a) Gibson-II, resulting in a sputtering ratio of 1.914, and (b) KSE-B, resulting in a sputtering ratio of 2.833. In both cases, boundary atoms sputtered. Figure 44 illustrates the ring probabilities for (a) Gibson-II and (b) KSE-B. Both display a large action-reaction effect, as if a bomb were dropped at the center and everything out from the center was blasted upward. Figure 45 illustrates the angular dispersion results for (a) Gibson-II and (b) KSE-B.

(2) Neon Ions. The results when 1-keV neon ions impact the target area are shown in figures 46, 47, and 48. Figure 46 shows the sputtering summaries for (a) Gibson-II, resulting in a sputtering ratio of 3.686, and (b) KSE-B, resulting in a sputtering ratio of 4.500. Most of the surface atoms were sputtered, indicating that the energy (or momentum) spread out over the entire lattice surface. Figure 47 illustrates the ring probabilities for (a) Gibson-II and (b) KSE-B. The KSE-B simulation indicates a spreading outward of the sputtered atoms. The Gibson-II simulation not only exhibits increased sputtering of atoms further from the center, but it also clearly shows a shift in the number of sputtered atoms from those at 2.83 LU in the <101> direction to those at 3.16 LU in the <103>

direction. As mentioned earlier, this could be artificial because the ring at 3.16 LU is the first ring to contain eight atoms. Figure 48 illustrates the angular dispersion results for (a) Gibson-II and (b) KSE-B.

(3) Argon Ions. The results when 1-keV argon ions impact the target area are shown in figures 49, 50, and 51. Figure 49 shows the sputtering summaries for (a) Gibson-II, resulting in a sputtering ratio of 3.806, and (b) KSE-B, resulting in a sputtering ratio of 4.611. Figure 50 illustrates the ring probabilities for (a) Gibson-II and (b) KSE-B. The Gibson-II simulation continued to increase in the outward direction at the expense of the atoms at 3.16 LU in the $\langle 103 \rangle$ direction. However, the KSE-B simulation reversed its trend and the ring probability for the close-in rings (1.41 LU and 2.00 LU) increased at the expense of the ring at 2.83 LU and the rings further out from the center. Figure 51 illustrates the angular dispersion results for (a) Gibson-II and KSE-B.

(4) Copper Ions. The results when 1-keV copper ions impact the target area are shown in figures 52, 53, and 54. Figure 52 shows the sputtering summaries for (a) Gibson-II, resulting in a sputtering ratio of 3.028, and (b) KSE-B, resulting in a sputtering ratio of 3.972. These low sputtering ratios not only disagree with a monotonic increase in the yield with mass, but are drastically low for the maximum to occur at a ion/atom mass ratio of unity. Figure 53 illustrates the ring probabilities for (a) Gibson-II and (b) KSE-B. The Gibson-II simulation showed an unexpected change. The ring probability increased for the rings at 2.00 LU ($\langle 100 \rangle$ direction) and 3.16 LU ($\langle 103 \rangle$ direction). This trend was also displayed in the KSE-B simulation, where it starts to occur in the Cu/Ar⁺ simulation. Figure 54 illustrates the angular dispersion results for (a) Gibson-II and (b) KSE-B.

(5) Krypton Ions. The results when 1-keV krypton ions impact the target area are shown in figures 55, 56, and 57. Figure 55 shows the sputtering summaries for (a) Gibson-II, resulting in a sputtering ratio of 2.833, and (b) KSE-B, resulting in a sputtering ratio of 3.917. Note that the sputtering ratio, for both potential functions, continues to decrease with increased ion mass. Figure 56 illustrates the ring probabilities for (a) Gibson-II and (b) KSE-B. Both potential function simulations continue to exhibit the trend to establish a peak at 2.00 LU in the $\langle 100 \rangle$ direction and at 3.16 LU in the $\langle 103 \rangle$ direction. However, the KSE-B simulation shows significantly larger ring probability at 3.16 LU. Figure 57 illustrates the angular dispersion results for (a) Gibson-II and (b) KSE-B.

(6) Xenon Ions. The results when 1-keV xenon ions impact the target area are shown in figures 58, 59, and 60. Figure 58 shows the sputtering summaries for (a) Gibson-II, resulting in a sputtering ratio of 2.333, and (b) KSE-B, resulting in a sputtering ratio of 3.472. Both potential functions continued to show a decrease in the sputtering ratio with an increase in the mass of the ion. Figure 59 illustrates the ring probabilities for (a) Gibson-II and (b) KSE-B. All the previous trends, except an increased ring probability at 3.16 LU were shattered. Figure 60 illustrates the angular dispersion results for (a) Gibson-II and (b) KSE-B.

(7) Gold Ions. The results when 1-keV gold ions impact the target area are shown in figures 61, 62, and 63. Figure 61 shows the sputtering summaries for (a) Gibson-II, resulting in a sputtering ratio of 2.778, and (b) KSE-B, resulting in a sputtering ratio of 4.167. A definite increase in the sputtering ratio occurred. Figure 62 illustrates the ring probabilities for (a) Gibson-II and (b)

KSE-B. No new trends were noted, except that the ring at 3.16 LU continues to dominate and the other ring probabilities fluctuate. Figure 63 illustrates the angular dispersion results for (a) Gibson-II and (b) KSE-B.

(8) Mercury Ions. The results when 1-keV mercury ions impact the target area are shown in figures 64, 65, and 66. Figure 64 shows the sputtering summaries for (a) Gibson-II, resulting in a sputtering ratio of 2.778, and (b) KSE-B, resulting in a sputtering ratio of 4.278. These simulations resulted in no change in the sputtering ratio for Gibson-II, and only a slight increase for KSE-B. Figure 65 illustrates the ring probabilities for (a) Gibson-II and (b) KSE-B. Only insignificant changes occurred compared to the gold ion results. Figure 66 illustrates the angular dispersion results for (a) Gibson-II and (b) KSE-B.

c. 2-keV Results

The 2-keV ion simulations were the earliest runs made. No isotope information was obtained. As a consequence, the only results are the sputtering ratio versus ion mass curve, figure 67, for both potential functions. They exhibit an even more erratic behavior than did the 1-keV simulations. The sputtering summaries frequently show atoms sputtered from the third layer, and rarely an atom sputtered from the fourth layer. At certain impact points as many as 25 atoms sputtered. The small, 9x4x9 microcrystallite was effectively blasted apart by the 2-keV ions.

2. (110) Orientation 100 eV

The effort devoted to (110) orientation simulation runs was very limited due to the higher priority assigned to the (100) orientation runs. As a result, only the argon and mercury ion simulations at 100 eV were run. Still needing investigation are the sputtering ratio as a function of ion mass and sputtering mechanism traces.

The (110) orientation microcrystallite was constructed in a lattice consisting of 123 copper isotopes. In the random isotope site locations, the PKA (14) was a light isotope, as were three (33, 36, and 37) of the four atoms underneath the PKA. Figure 4 shows an isometric projection of the lattice and its numbering scheme. Figure 10 shows an expanded view of the grid of 36 impact points used. A 9x6x9 lattice was used with no increase in computer time required to complete a run.

Two sets of simulations were run to investigate the "reflective collision" theory. Four runs were made in each set of simulations for each potential function. The impact area was bombarded by 100-eV, argon and mercury ions. The four runs consisted of; (1) the random isotope sites (PKA was a light isotope), (2) forcing the PKA to a heavy isotope, (3) forcing the PKA to a light isotope and all four atoms underneath to a heavy isotope, and (4) forcing the PKA to a heavy isotope and all four atoms underneath to a light isotope. The remainder of the lattice isotopes were unchanged.

a. Argon Ions

The results when 100-eV argon ions impact the target area are shown in figures 68-75. Figure 68 shows the sputtering summaries using Gibson-II for all four cases. Case (1) and case (3), shown in figure 68(a), resulted in a sputtering ratio of 0.839. Case (2) and case (4), shown in figure 68(b), resulted in a sputtering ratio of 0.861. A predominance of sputtered atoms in the $\langle 100 \rangle$ and $\langle 101 \rangle$ directions is evident. Figure 69 illustrates the ring probabilities for (a) case (1) and case (3), and (b) case (2) and case (4) using Gibson-II. Notice that an atom at the boundary (in the $\langle 101 \rangle$ direction) sputtered. Figure 70 illustrates the angular dispersion results for (a) case (1), and (b) case (3) using Gibson-II. Figure 71 shows the same information for (a) case (2), and (b) case (4).

Figure 72 shows the sputtering summaries using KSE-B for all four cases. Case (3) resulted in a sputtering ratio of 0.750, while case (1) sputtered atom 26 one additional time (denoted by \blacktriangle) and had a sputtering ratio of 0.778. Case (1) and case (3) are shown in figure 72(a). Case (2) resulted in a sputtering ratio of 0.778, while case (4) sputtered atom 8 one additional time and had a sputtering ratio of 0.805. Case (2) and case (4) are shown in figure 72(b). Again, it is evident that only atoms in the $\langle 100 \rangle$ and $\langle 110 \rangle$ directions sputtered. Figure 73 illustrates the ring probabilities, using KSE-B, for (a) case (1) and case (3), and (b) case (2) and case (4). The close-in trend, similar to that of Gibson-II, is evident, as are the sputtered atoms at the boundary in the $\langle 101 \rangle$ direction. Figure 74 illustrates the angular dispersion

results, using KSE-B, for (a) case (1) , and (b) case (3) . Figure 75 shows the same information for (a) case (2), and (b) case (4) .

b. Mercury Ions

The results when 100-eV mercury ions impact the target area are shown in figure 76, 77, and 78. Figure 76(a) shows the sputtering summaries for all four cases, using Gibson-II. Case (1), case (2), and case (4) resulted in a sputtering ratio of 0.278. Case (3) sputtered atom 13 one additional time (denoted by \blacktriangle) and had a sputtering ratio of 3.05. Figure 76(b) shows the sputtering summaries for all four cases, using KSE-B, which resulted in sputtering ratios of 0.222. Figure 77 illustrates the ring probabilities for (a) Gibson-II and (b) KSE-B. Figure 78 illustrates the angular dispersion results for (a) Gibson-II and (b) KSE-B.

No significant trends were noted in the (110) orientation. However, the ease with which atoms sputtered in the $\langle 101 \rangle$ direction is evident.

3. (111) Orientation 100eV

Like the (110) orientation, the (111) orientation did not receive extensive attention. Both the sputtering ratio as a function of the ion mass, and sputtering mechanism traces need further investigation.

The (111) orientation microcrystallite is constructed in a $9 \times 4 \times 9$ lattice consisting of 163 atoms. In the random isotope site locations, the PKA (22) was a light isotope, as were three (58, 63, and 67) of the four atoms

underneath the PKA. Figure 5 shows an isometric projection of the lattice and its numbering scheme. Figure 11 shows an expanded view of the grid of 21 impact points used.

Two sets of simulations were run to investigate the "reflective collision" theory. Four runs were made in each set of simulations for each potential function. The target was bombarded by 100-eV argon and mercury ions. The four runs consisted of; (1) the random isotope sites (PKA was a light isotope), (2) forcing the PKA to a heavy isotope, (3) forcing the PKA to a light isotope and all four atoms underneath to a heavy isotope, and (4) forcing the PKA to a heavy isotope and all four atoms underneath to a light isotope. The remainder of the lattice isotopes were unchanged.

a. Argon Ions

The results when 100-eV argon ions impact the target area are shown in figures 79-83. Figure 79 shows the sputtering summaries for (a) Gibson-II, resulting in sputtering ratios of 0.857, and (b) KSE-B, resulting in sputtering ratios of 0.762. For KSE-B, case (2), atom 16 sputtered one additional time (denoted by ▲), resulting in a sputtering ratio of 0.810. Figure 80 illustrates the ring probabilities for (a) Gibson-II and (b) KSE-B. It was unexpected that, for KSE-B, all of the sputtered atoms are in the $\langle 101 \rangle$ direction in the ring at 2.83 LU. Figure 81 illustrates the Gibson-II angular dispersion results for (a) case (1) and case (3), and (b) case (2) and case (4). Figure 82 illustrates the KSE-B angular dispersion results for (a) case (1) and (b) case (3). Figure 83 shows the same results for (a) case (2), and (b) case (4).

b. Mercury Ions

The results when 100-eV mercury ions impact the target area are shown in figures 84-89. Figure 84(a) shows the sputtering summaries, using Gibson-II, for case (1), case (2), and case (4), which resulted in sputtering ratios of 0.476. Case (3) had a sputtering ratio of 0.381 and is shown in figure 84(b). Figure 85 shows the sputtering summaries using the KSE-B. Case (3) resulted in a sputtering ratio of 0.762, while case (1) sputtered two additional atoms (12 and 14 - denoted by \blacktriangle) and has a sputtering ratio of 0.857. Case (1) and case (3) are shown in figure 85(a). Case (2) and case (4), shown in figure 85(b), have sputtering ratios of 0.952. Figure 86 illustrates the ring probabilities for (a) Gibson-II and (b) KSE-B. Again, it is evident that the only sputtered atoms are in the ring at 2.83 LU, in the $\langle 101 \rangle$ direction. Figure 87 illustrates the Gibson-II angular dispersion results for (a) case (1), case (2), and case (4), and (b) case (3). Figure 88 illustrates the KSE-B angular dispersion results for (a) case (1) and (b) case (3). Figure 89 shows the same information for (a) case (2), and (b) case (4).

B. LARGER LATTICES

The erratic behavior of the sputtering ratio as a function of the ion mass, indicates that the microcrystallite is not containing the event. Originally, "containment" was defined as "no boundary atoms sputtering." Based on this definition, none of the 100-eV events were contained in the (100) orientation or (110) orientation 9x9 microcrystallites. However, in the (111) orientation, 100-eV events were contained. The sputtering summaries for

mercury ions bombarding a 13x6x13, (110) orientation microcrystallite containing 255 atoms are shown in figure 90. Figure 90(a) is for Gibson-II, while figure 90(b) is for KSE-B. Comparison of figure 90 with figure 76, confirmed that the 9x6x9 microcrystallite did not contain the 100-eV, mercury event. Based on the original definition of containment, the 13x6x13 microcrystallite did not contain the Gibson-II simulation run.

In the (111) orientation, the sputtering summaries for mercury ions bombarding a 13x4x13 microcrystallite containing 339 atoms are shown in figure 91. Figure 91(a) is for Gibson-II, while figure 91(b) is for KSE-B. Comparison of figure 91 with figures 84 and 85, indicate that even though the 9x4x9 lattice had no boundary atoms sputtered, the sputtering ratio increases when a 13x4x13 lattice is used.

1. 100-eV Containment

Based on the above information, the definition for "containment" was changed to: "an event is contained when an increase in the microcrystallite size does not result in any further increase in the yield." Earlier simulations resulted in larger yields for KSE-B. For this reason, KSE-B was used to investigate the size microcrystallite needed to contain a 100-eV event.

The sputtering ratio as a function of the ion mass was examined for the (100) orientation. Figure 92 shows the results for 9x4x9, 11x4x11, and 11x6x11 microcrystallites. Additionally, simulations were run for copper (largest sputtering ratio) and mercury ions for 13x4x13, 13x6x13, and 17x4x17 microcrystallites. Based on the new definition of containment, 100-eV helium and xenon events are contained in

a 9x4x9 microcrystallite because an 11x4x11 microcrystallite produces the same yield. However, the argon, copper, and krypton events were not contained. Further increase of the microcrystallite size demonstrated that the 100-eV, copper event is contained by a 13x4x13 microcrystallite. Figure 92 also illustrates that the maximum sputtering ratio occurs when the ion/atom mass ratio is approximately unity. Figure 93 shows the same information in a plot of sputtering ratio versus lattice size for all eight ions.

2. 17x4x17 Microcrystallite

Asuming that all 100-eV events are contained by a 17x4x17 microcrystallite, the effect of increasing the ion energy was investigated. The reason for this investigation was to determine how energetic an event could be contained by a 17x4x17 microcrystallite. And to compare higher energy events with experimental results. The reason for not increasing the lattice size without limit was obviously to keep the computer run time within reason. Again, only KSE-B with mercury and copper ions were investigated.

a. Copper Ions

The results when 100-eV copper ions impact the target area are shown in figures 94, 95, and 96. Figure 94 shows the sputtering summary with a sputtering ratio of 1.389. Containment for the 100-eV copper event had already been established. Figure 95 illustrates the "atom sputtering probability", henceforth called the "probability". The "probability" is the "ring sputtering probability" divided by the number of atoms in each ring. The dimensions for "probability" is sputs per atom divided by the total sputs at a fixed distance from the impact area

reference point. Figure 95 indicates an enhancement of sputtered atoms in the $\langle 100 \rangle$ and $\langle 101 \rangle$ directions. Figure 96 illustrates the angular dispersion results.

Results for the 200-eV copper ion simulations are shown in figures 97, 98, and 99. Figure 97, the sputtering summary with a sputtering ratio of 2.889, shows that boundary atoms are sputtered, and that the event definitely is not contained. Figure 98 illustrates the "probability" results and indicates that an atom farther out had increased chances of sputtering. Figure 99 illustrates the angular dispersion results. A bias toward light isotopes closer to the normal is evident.

The results for the 500-eV copper ion simulations, with a sputtering ratio of 4.028, are shown in figures 100, 101, and 102. Again, boundary atoms are sputtered and a slight shift outward of the "probability" is noticed. Figure 102 illustrates the angular dispersion results which showed that more light isotopes are ejected more nearly normal to the lattice surface.

the 1-keV, copper ion results with a sputtering ratio of 7.083, are shown in figures 103, 104, and 105. Figure 103, the sputtering summary, shows a very large number of the surface atoms sputtered. Boundary atoms in every direction are sputtered. This increased spreading outward was confirmed in figure 104, which shows the "probabilities" relatively level. Figure 105 illustrates the angular dispersion results.

Obviously, the 200-eV, 500-eV, and 1-keV copper events are not contained, even in a $17 \times 4 \times 17$ microcrystallite.

b. Mercury Ions

The results for the 100-eV mercury ion simulations are shown in figures 106, 107, and 108. Again, the 11x4x11 lattice has already been determined to contain the 100-eV, mercury event. Figure 106 shows the sputtering summary with a sputtering ratio of 0.833. Figure 107 illustrates the "probability", and like the copper simulation, was predominant in the $\langle 101 \rangle$ direction. Figure 108 illustrates the angular dispersion results.

The 200-eV mercury ion results, with a sputtering ratio of 1.722, are shown in figures 109, 110, and 111. Figure 109, the sputtering summary, shows an outward spreading of the sputtered atoms. However, no boundary atoms were sputtered and the 200-eV, mercury event is tentatively classified as "contained". Figure 110 confirms the outward shift in "probability". Figure 111 illustrates the angular dispersion results, which indicate a greater number of heavy isotopes sputtering than the isotope ratio would justify.

The 500-eV mercury ion results, with a sputtering ratio of 3.667, are shown in figures 112, 113, and 114. Figure 112, the sputtering summary, indicates that boundary atoms are sputtered. Figure 113 illustrates the continued outward spreading of sputtered atoms. Figure 114 illustrates the angular dispersion results, and the number of heavy to light isotopes closer to the correct ratio.

The 1-keV mercury ion results, with a sputtering ratio of 6.139, are shown in figures 115, 116, and 117. Figure 115 shows that boundary atoms are sputtered. Figure 116 shows the "probability" still spreading outward. Figure 117 illustrates the angular dispersion results.

The "probability" figures for both the copper and mercury ions are remarkably similar and display the same trends.

c. Sputtering Mechanism Traces

The containment studies indicated that, as the lattice size was increased, the sputtering ratio increased. Investigation into the similarities of the 17x4x17 and 9x4x9 microcrystallites, indicated that atom 108 (17x4x17) sputtered twice in 36 events. This corresponds to atom 40 in the 9x4x9 microcrystallite, which did not sputter in 36 events. Sputtering mechanism trace runs were performed to determine the sputtering mechanism involved in the sputtering of atom 108. Atom 108 sputtered when ions impacted at points 50 (impact point displaced 0.50 LU in the Z direction only) and 60 (impact point displaced 0.6 LU in the Z direction only).

Figure 118 illustrates the atom trajectories in the sputtering of atom 108 from impact point 50 (the mechanism is the same for impact point 60). The copper ion struck atoms 74 (PKA) and 91 forcing them down by timestep 15. As atom 91 was moving downward, atoms 99, 100, and 108 prevented atom 91 flying off in the positive Z direction, and channeled it downward. By timestep 25, atom 91 had collided with atom 224, reversing its direction. At timestep 30, atom 91 was forcing atom 108 upward from underneath. Atom 91 transferred almost all of its energy (momentum) to atom 108 and had less than 0.1 eV by timestep 45. As atom 108 was going upward, it also had a velocity in the positive Z direction of greater than 6000 m/sec. Atoms 116, 117, and 125 bent atom 108 upward quite radically. The velocity in the Z direction had been reduced to less than 700 m/sec by timestep 50. By timestep 60, atom 108 was far

enough above the lattice surface, with sufficient velocity to be classified as a sput. Atom 108 was ejected at an angle of 19.23° to the surface normal with an upward velocity of 3206 m/sec.

Quite evident is the role atoms 116, 117, and 125 have in channeling atom 108 upward. In the $9 \times 4 \times 9$ lattice, atom 40 (a boundary atom) corresponds to atom 108. And nothing equivalent exists for atoms 116, 117, and 125. Investigation was then made to determine whether an atom corresponding to atom 108 could be sputtered in the $9 \times 4 \times 9$ lattice by using the same impact point on a different PKA. In this simulation, atom 31, corresponding to atom 108 in the larger lattice, was expected to sputter. Figure 119 illustrates the atom trajectories when the copper ion struck the new PKA (atom 13) at impact point 50. Atom 31 was ejected at an angle of 20.17° with an upward velocity of 3127 m/sec. The mechanism is the same, and the importance of boundary atoms is very evident.

Additional runs were made on the $9 \times 4 \times 9$ lattice bombarding atom 13 at impact points 50 and 60. At both points, comparison is made between runs with (1) only atoms of the natural mass, , and natural mass, and (2) forcing atom 22 (91) to a heavy isotope and atom 67 (224) to a light isotope. In all four cases, the sputtering mechanism is the same. The differences in the ejection angles and upward velocities, for each impact point, are less than 0.4° and 75 m/sec respectively.

3. Ion/Atom Mass Ratio

Sigmund [28] proposed a theory that the maximum sputtering yield increases as a function of energy. However, results of this investigation strongly indicate a

dependence on the ratio of the ion mass to the target atom mass. A rearrangement of Sigmund's theoretical curves (figure 16b, ref. 28) to show the sputtering ratio as a function of the ion/atom mass ratio results in figure 120. The curves shown by Sigmund are predicted for 200-eV, 600-eV, 1-keV, and 5-keV ions bombarding an aluminum target. Figure 120 illustrates that Sigmund's theory would predict the sputtering ratio to increase as a function of the ion/atom mass ratio. Figure 121 shows experimental results obtained by Wehner and is presented by Sigmund (figure 12, ref. 28) to support his theory. This figure has been replotted to show the sputtering ratio as a function of the ion/atom mass ratio. The results were obtained by bombarding a copper target with 100-eV, 200-eV, and 600-eV ions. Experimental results plotted in this manner show a decrease in the sputtering ratio with an ion/atom mass ratio greater than unity, in disagreement with the theory proposed by Sigmund. Results obtained in the present investigation completely agree with the shape of experimental data shown in figure 121.

C. RANDOM IMPACT POINTS

In response to other investigators' suggestion that the target impact area be bombarded randomly rather than the systematic grid of impact points, the computer program was slightly modified. Since additional data were desired for mercury events, Hg^+ was used as the incident ion. The KSE-B potential function was used. Earlier results revealed that the 100-eV, mercury ion event was contained in an $11 \times 4 \times 11$ microcrystallite.

Figure 122 illustrates the (100) orientation impact area that was struck at the 144 randomly selected impact points. A few gaps are evident, but the randomness is very apparent. Figures 123-128 show a comparison of the results from a randomly bombarded impact area and the results from the grid of impact points. Since the number of events were not the same, the sputtering summaries indicate a sputtering ratio for each atom. Figure 123 shows the normalized sputtering summary for the randomly selected impact points. Figure 124 shows the same information using the grid of impact points. The four groups of 36 randomly selected impact points had a mean sputtering ratio of 0.812 with a variance of 0.0048. Additional runs (not shown), combined with the four previous groups to give a total of 21 groups of 36 randomly selected impact points (756 shots), resulted in a mean sputtering ratio of 0.782 with a variance of 0.016. This compares very favorably with a sputtering ratio of 0.778 using the grid of impact points. Figures 125 and 126 show the "probability" results for the randomly selected impact points and the grid of impact points respectively. It is quite evident that they are almost identical. Figure 127 illustrates the angular dispersion results for randomly selected impact points. A definite shift of the lighter isotopes toward the surface normal is observed. Figure 128 illustrates the same information for the grid of impact points. The absence of the shift of the light isotopes toward the normal is noted.

V. CONCLUSIONS AND RECOMMENDATIONS

A. SIMULATION MODEL

The more sophisticated a simulation model becomes, the more uncertain are its results. Some of these uncertainties are now beginning to appear in this model.

The lattice generators can now construct randomly positioned isotopes. Symmetrical unfolding of the event results is the reverse of the folding required to reduce the representative impact area. The model can now display the ejection angle of the sputtered isotopes in a histogram for visual comparison. It now determines the distance from the surface layer center to each ring of sputtered atoms, the number of atoms and the number of times each atom sputters in each ring, and the probability that that each ring contained an atom that was sputtered. Other modifications were made in the model to approximate more nearly a meaningful physical description. These include changes in the distances from the lattice surface at which calculations are truncated, the depth of lattice needed to prevent any change in the yield, and a systematic determination of the distance above the surface at which an atom is declared to have sputtered.

B. CONTAINMENT

The containment of an event is paramount in a complete description of the sputtering process. However, it is less significant when studying mechanisms and trends.

Based on the definition of containment (no increase in yield with an increase in the microcrystallite size), the 100-eV results showed that a 9x4x9, (100) orientation microcrystallite contained only the helium and xenon events. The 100-eV, mercury event is contained in an 11x4x11 lattice. To contain a 100-eV copper event, which had the largest yield, a 13x4x13 lattice was needed. Sputtering mechanism traces revealed the importance of boundary atoms in deflecting and channeling atoms in the sputtering process. By choosing the PKA to be an atom other than the one at the surface layer center, the effect of an increased lattice size could be duplicated.

Investigation with a 17x4x17 microcrystallite revealed that Gibson-II potential function simulations are more difficult to contain than when using the KSE-B potential function. Only the 100-eV, copper event was contained using Gibson-II, while using KSE-B the 100-eV and 200-eV, copper events were contained. It is quite obvious that to contain any higher-energy events would require a microcrystallite so large that the computer run time would be prohibitive.

C. ANGULAR DISPERSION

Because the low-energy events resulted in so few sputtered atoms, the angular dispersion results for any particular ion are inconclusive. A trend of light isotope enrichment is observed when the results from numerous runs are combined. For example, the histograms of the four sets of 36 randomly selected impact points show a definite shift of the lighter isotopes to smaller ejection angles. In his report on the enrichment of lighter isotopes in the normal direction, Wehner [24] noted only a 0.6% enrichment in Cu (63). The number of sputtered isotopes was not sufficient to detect this small difference.

The "reflective collision" theory, which Wehner suggests to be the cause, was observed to have very little effect on the sputtered atoms. Investigation revealed that in most of the simulation runs, the same atoms sputtered independent of its isotope type or the various positions of the lattice isotopes. When the PKA was a light isotope, the atoms that did sputter were ejected more nearly normal to the surface. Varying the isotope type of the PKA, atoms that were known to sputter, and some of the target atoms that they collided with resulted in differences in the ejection angle normal of less than 0.4° .

D. RING FORMATION

Results definitely show that the sputtering mechanisms do produce a formation of rings of sputtered atoms around the impact area. The results indicate that the transfer of

momentum along the $\langle 100 \rangle$ and $\langle 101 \rangle$ directions in the surface layer is relatively easy. The predominance of sputtering of next-nearest neighbors, in the $\langle 101 \rangle$ direction is evident. For example, at 100-eV, all simulations using an ion of the mass of argon or greater sputtered the same atoms, but with different frequencies. The particular atoms that sputter do not appear to be dependent on the mass of the incident ion. However, the number of times the atom sputters does appear to be dependent on the ion mass. Ring and atom sputtering probabilities clearly show the sputtered atoms from certain site directions and the distances of the sites from the center of the PKA.

A trend was noted: as the energy and mass of the ion is increased, the sputtered atoms come from sites which appear to spread outward from the impact area. These higher-energy events give the appearance of a "liquid splash", with the size of the crater dependent on the ion energy and mass.

E. ION/ATOM MASS RATIO

The results of this investigation do not support a monotonic increase in the sputtering ratio with increased ion mass as implied in figures of Sigmund[28] and Eer Nisse [27]. All the plots showing the sputtering ratio as a function of the ion mass, clearly indicate a maximum near an ion/atom mass ratio of one. At ion/atom mass ratios greater than one, the sputtering ratio appears to become asymptotic to a lower value. This may be an artifact of the computer model. These plots also highlight the containment problem. The behavior of the sputtering ratio, for larger ion/atom mass ratios, is erratic because the microcrystallite does not contain the event.

The general shape of the sputtering ratio curve, when plotted as a function of the ion/atom mass ratio, is in agreement with the experimental data of Wehner and his co-workers. Results conclusively show that the ion/atom mass ratio is an important factor in the determination of the sputtering ratio.

F. RANDOMLY SELECTED IMPACT POINTS

The sputtering ratio obtained using the grid of impact points is extremely close to that obtained when randomly selected impact points were used. The similarity between the sputtering summaries and the atom sputtering probabilities are quite evident. The quantity of data obtained with the randomly selected impact points was required to confirm that light isotope enrichment was present.

Based on the comparison of results obtained from the randomly selected impact points and from the grid of impact points, the systematic method of "walking" through the grid seems completely justified.

G. FUTURE RESEARCH

Even the more than 1000 hours of computer time used in running these simulations did not begin to encompass the permutations and combinations of parameters that need to be investigated.

The (110) and (111) orientations need to be studied in depth. The few sputtering mechanisms observed were the same as those for the (100) orientation. However, the sputtering ratio as a function of the ion mass, containment requirements, ring formation, and angular dispersion of isotopes need further investigation. It is highly recommended that the effect of momentum transfer along certain directions be investigated.

APPENDIX A

ISOTOPE GENERATION

All atoms in the lattice were one of two types; type 1 - the heavier, least abundant isotope, or type 2 - the lighter, most abundant isotope. The average atomic weight of copper is 63.54 amu. The isotope weights are 62.93 amu and 64.93 amu with natural abundances of 69.1% and 30.9% respectively.

The lattice was generated with either the isotope masses and their corresponding abundance or the weighted average of the isotope masses with an abundance of 100%. Initially, all atoms were forced to the type 2 atom in the lattice generator. If the isotope lattice was desired, the International Mathematical and Statistical Library (ISML) routine GGUB was called. This routine generates a uniformly distributed set of psuedo - random numbers between zero and one. Each of these random numbers was assigned to a particular atom and was tested to see if it was less than or equal to 0.309. If the number was less than this test value (the abundance of the least abundant isotope), the atom was changed to a type 1 atom. A seed for the random number generator, for the particular size lattice to be generated, was chosen by trial and error which would produce the correct number of atoms above and below the test value to assure the correct isotope ratio.

A feature was designed to allow any number of the atom masses (types) to be selectively changed after the lattice had been generated. This feature was incorporated to investigate the changes and effects of picking heavy/light, heavy/heavy, or light/light collision atoms. This would facilitate the dynamic investigation of the "reflective collision" theory proposed by Winters and Sigmund [10].

The dynamics of the simulation remained unchanged except that all calculations that were dependent on target atom mass were modified to use the correct mass.

The simulation was now capable of generating a lattice with the correct isotope ratio and masses with randomly selected sites.

APPENDIX B

LATTICE FOLDING

As mentioned in the simulation model development, a lattice that was symmetrical about the folding axes was required. Once this was achieved by the lattice generators, it was necessary to fold the lattice in a manner such that, after the folds, the reduced representative impact area was identical to the complete representative impact area. After these folds were performed correctly and in the right sequence, the results were identical to that obtained if the complete representative impact area had been bombarded systematically.

After each fold, the sputtering count for all atoms that were symmetric about the folding axis were summed. The summing process started with the first atom in a layer to the highest numbered atom in that layer. After this process, the sputtering count for each atom was twice what the sum was since the sputs were summed each time a symmetric atom was encountered. This doubling effect of each fold was corrected by scaling the sputtering count of each atom after all the folds in a layer were completed. All necessary folds were then performed on each successive layer.

A. (100) ORIENTATION FOLDING

Figure 12 shows the (100) orientation reduced representative impact area folding geometry. The reduced 36 impact point area, when folded, represents the complete 288 impact point area.

Since the (100) orientation impact area is a 45° - 45° triangle, three folds were required to complete the folding process. The first fold was along the diagonal. The first fold was along the diagonal axis, the second along the horizontal axis, and the third along the vertical axis. The diagonal fold process for all layers was the same. However, the horizontal and vertical folds were modified depending on which layer was being folded.

After all the folds in a layer for the (100) orientation were complete, the sputtering count for each atom was divided by eight to correctly scale the results.

B. (110) ORIENTATION FOLDING

Figure 12 also shows the (110) orientation reduced representative impact area folding geometry. The reduced 36 impact point area, when folded, represents the complete 144 impact point area.

Since the (110) orientation reduced impact area is a rectangle, two folds were required to complete the folding process. The first fold was along the horizontal axis and the second fold was along the vertical axis. The diagonal

fold was not necessary. The horizontal and vertical folds (exactly the same as for the (100) orientation) were modified depending on which layer was being folded.

After all the folds in a layer for the (110) orientation were complete, the sputtering count for each atom was divided by four to correctly scale the results.

C. (111) ORIENTATION FOLDING

The (111) orientation was by far the most difficult to determine. Figure 13 shows the (111) orientation reduced representative impact area folding geometry. The reduced 21 impact point area, when folded, represents the complete 126 impact point area.

Since the (111) orientation impact area is a 30° - 60° triangle three folds along the diagonals resulted in the overlap shown in Figure 13. However, if the set of three folding sequences were summed the results could be scaled to represent the complete impact area. The number one fold was along the positive slope diagonal axis, the number two fold was along the negative slope diagonal axis, and the number three fold was along the vertical axis.

Before each sequence of folds, the sputtering count for each atom was reinitialized to the original value. The first sequence (1,2,3) was performed and upon completion the sputtering count for each atom was divided by eight to correctly scale the results. The second sequence (1,2,1) was performed and again the sputtering count for each atom was divided by eight for scaling. The third sequence (1,3,2) was performed and again the sputtering count for each atom was divided by eight for scaling.

Finally, the results obtained from each sequence was summed and the final sputtering count for each atom was divided by four to correctly scale the results due to the summing process.

Since the geometry of the (111) orientation was complicated and not fully developed, the folding process was performed only for the first layer.

APPENDIX C

GLOSSARY

ABUN1, ABUN2

The abundance of the target's isotopes.

AC

A distance measurement used in impact point generation.

ALFA, ALFA2

The cosine of the angle between vectors R_1, R_2 , - squared.

ALPHA

Input Morse potential parameter.

ANGLE

The angle between the direction of motion of an ejected atom and the surface normal in degrees.

AVE

The sputtering ratio.

AXT, AYT, AZT

Components of the random thermal displacement.

BENRGY

The lattice binding energy in ev.

BIND

Negative of the total potential energy (TPOT) at time zero. Retained for energy conservation checks.

BMAS

The mass of the bullet in amu.

BQZ

A fcc crystal constant $-(1/\text{ROOT}(3))$.

BUL

The bullet heading Hollarith.

BX, BZ

Unscaled x,z coordinates of the impact point.

BXMAX, BXMIN

X direction boundaries of the target impact area.

BZMAX, BZMIN

Z direction boundaries of the target impact area.

CELS

A frictional force multiplier when frictional forces are included in the program.

CGB1, CGB2

Morse potential parameters.

CGD1, CGD2

Morse potential parameters.

CGF1, CGF2

Morse force function parameters.

CF0, CF1, CF2

Force parameters of the cubic fit between Morse and Born-Mayer functions.

CO, CORF

"Phonon" displacement correlation parameter used as an option in WARM.

CORN

$1 - \text{CORF}$.

COX, COY, COZ

Directional cosines of the incoming ion's velocity vector, relative to the surface normal.

COXI, COYI, COZI

Negative values of COX, COY, COZ.

CP0, CP1, CP2, CP3

Potential parameters of cubic fit between Morse and Born-Mayer functions.

CVBD

A ratio used to avoid repeated division.

CVD

Distance conversion factor - angstroms to meters.

CVE

Energy conversion factor - ev to joules.

CVED

A ratio used to avoid repeated division, CVE/CVD , used to convert exponential potential functions to forces.

CVM

Mass conversion factor - amu to kg.

CVR

Conversion factor - lattice units to angstroms.

DBXMAX, DBZMAX

Upper boundary limits for the target impact area.

DCON

Input Morse potential parameter.

DFF

The distance closer than ROE that an atom is to the bullet. Used when forces are turned on or off.

DIST

The distance between any two atoms.

DNN(I)

Distance to the Ith ring in lattice units.

DRX, DRY, DRZ

Components of DIST.

DT

Length of each timestep in seconds.

DTI

Number of lattice units the most energetic atom can move in one timestep.

DTOD

DT over distance - a ratio used to avoid repeated division.

DTOM1, DTOM2

DT over target isotope mass - a ratio used to avoid repeated division.

DTOMB

DT over bullet mass - a ratio used to avoid repeated division.

DX(I), DY(I), DZ(I)

Change in the position of the Ith atom.

EMAX

The velocity squared of the fastest atom. Used to make ETEST.

ETEST

The kinetic energy of the most energetic atom.

ETHR

Energy threshold to escape the surface.

EV

Primary energy of the bullet in ev.

EVR

Primary energy of the bullet in kev. R indicates a read-in and saved value.

EXA, EXB

Input Born-Mayer potential function for the target atom - target atom interaction.

FA

The temporary component force increment on an atom.

FAC

The decrement size used in SETUP in locating the ion impact point.

FINISH

The elapsed program running time in seconds.

FLAT

A lattice unit in angstroms.

FM

A small number used in checking potential energy zero point.

FMAX

The maximum frequency of occurrence in the histogram intervals.

FORCE

A numerical value of the force function for a specific pair of atoms.

FPTC

The corrective force at ROE.

FRC

Numerical value of the target force function at ROE.

FRAN

A real variable for number of passes completed at termination.

FRANR

The reciprocal of FRAN.

FREQ1, FREQ2

Number of events in each interval of the histogram.

FSCAL

A histogram scale factor.

FTDI

A parameter used to determine DT by maximum energy method.

FXA

A Born-Mayer force function parameter.

FX(I), FY(I), FZ(I)

Components of the total force on the Ith atom.

HBMAS

Half Bullet Mass - a ratio used to avoid repeated division.

HDTOD

Half DT over distance - a ratio used to avoid repeated division.

HDTOM

Half DT over most abundant isotope mass - a ratio used to avoid repeated division.

HDTOMB

Half DT over bullet mass - a ratio used to avoid repeated division.

HTMAS1, HTMAS2

Half target isotope mass - a ratio used to avoid repeated division.

IBOX1, IBOX2

Ejected atom angle tally keeper.

ICOUNT

Flag used in sequencing.

IDEEP

The first frozen layer. in the target microcrystal.

IET

Elapsed time in 2.6 microsecond blocks. Used to determine actual elapsed time.

IFPM

The atom number of any target atom that has its mass constrained due its isotope ratio.

IFLAG

Flag used in sequencing.

IFM

The isotope type (heavy or light) of any target atom that has its mass constrained due to its isotope ratio.

IFT

A number used as a constant when generating pseudo-random numbers.

IH1

Alphanumeric array of the program heading.

IH2

Alphanumeric array of the Morse parameters.

IHB(1), IHB(2), IHB(3), IHB(4), IHB(5), IHB(6)
Alphanumeric array describing the bullet.

IHBPOT
The type of ion-atom potential.

IHBULL
The bullet elemental symbol or name.

IHS
Alphanumeric array for the type and orientation of the crystal.

IHT
Alphanumeric array describing the target.

IHT(1), IHT(2), IHT(3), IHT(4), IHT(5), IHT(6)
Alpha numeric array describing the target.

IHTARG
The target elemental symbol or name.

IHTPOT
The type of target atom - target atom potential.

ILATT
A flag used in the lattice generators.

ILAYER
A variable used to identify which layer is being folded.

ILL
The number of the last atom in the first layer.

IMF

The mass of each target atom with the correct isotope ratio.

IN

The number of intervals in the histograms.

INDEX

A variable used in determining phase in a dynamics cycle step.

INT

The width of the intervals in the histograms.

IOR

The target plane of incidence.

IOUT

Flag used in sequencing.

IPASS

The number of passes (shots) completed.

IPNUM

The impact point number.

IPNUMS

Scaled impact point number.

I PROG

Input variable used to skip attractive potential.

IRAN

Random number seed used in NORMAL subroutine which generates pseudo-random numbers.

IRANGE

The upper limit in the histograms.

IREAD

The number of atoms which have the isotope type constrained externally.

ISEEDA, ISEEDB, ISEEDC

Seeds used in the uniform random number generator which determines the isotope ratio and distribution.

ISSET

Flag used in sequencing.

ISHUT

A parameter used to shut down the program.

ISNUM

The atom number of a sputtered atom.

ISOGEN

A flag used as an option to generate the target atom masses with isotope or single element values.

ISPX, ISPZ

Initial start point x,z coordinates.

IT

Unscaled x coordinate used in lattice generation.

ITEMP

The lattice temperature in degrees Kelvin.

ITIME

Flag used in sequencing.

ITT

An odd-even integer used to determine atom site location.

IX, IY, IZ

The number of x,y,z, planes in the crystal.

IXP, IYP, IZP

Crystal dimensions in x,y,z.

JN

The numerical value of the histogram intervals.

JOUT

A histogram sequencing variable.

JSCAL

A histogram scale factor.

JT

Unscaled y coordinate used in lattice generation.

JTS

Variable used to establish atom site.

JTT

Variable used to establish atom site.

K2SUM

The square of the sputtering count which is used in calculating the variance.

KATOM

The number of atoms in a ring.

KFIRST

A sequencing variable.

KRING

The highest numbered ring in a layer.

KSPUT

The number of sputs from all atoms in a ring.

KSUM

The total sputtering count before folding.

KT

Unscaled z coordinate used in lattice generation.

LCUT(I)

Used to identify an Ith atom which can be omitted from the force and potential calculations by changing LCUT(I) from zero to one.

LD

The highest numbered atom in a mobile layer.

LL

The highest numbered atom in the entire crystal.

LL2, LL3

Twice and triple the value of LL.

LNUM(I)

The number of times the Ith atom sputters after all shots in the target impact area.

LNUMF(I)

The number of times the Ith atom sputters after all shots and the summary is complete and folded.

LNUMI(I)

The number of times the Ith atom sputters after all shots but before folding the summary.

LS

Sum of the Miller index integers.

LSS

Variable used to identify the type of surface.

LSUR

The lattice surface type.

LTYPE

The type of lattice (i.e. fcc).

MAX

A height scale factor used in the histograms.

MCRO

The number of simultaneous equations solved by CROSYM.

N1

NLAY - 1, a sorting variable.

NCT

Increments the timestep interval.

NCTT, ND

Data output interval in number of timesteps. Also the timestep interval between potential energy calculations.

NF1

A sequencing variable.

NFIRST

The number of the first atom in a given layer.

NLAY

The highest numbered atom in a given layer.

NLAY1

The highest numbered atom in the first layer.

NLINE

The line number in the output block.

NOTH

A Hollarith consisting of blanks.

NPAGE

A page numbering variable.

NRAN

Variable for number of passes (shots) completed at termination.

NRS

A restart flag.

NS

The next timestep number at which output will be printed.

NSHOTS

The number of passes (shots) to be completed in a program. Used to break up an extremely large, many-shot program into a few small programs with manageable computer run time.

NSPUT(I)

The number of atoms that sputter for the Ith impact point.

NSR

The first timestep where output is printed.

NSS

Flag to print final output status of current shot.

NT

The timestep number.

NTT

Timestep number limit before shut down.

PAC

Parameter for bullet force function correction.

PBMAS

Bullet mass in kg.

PEXA, PEXB

Input Born-Mayer potential function parameters for the bullet-target interaction.

PFIV

Point five (0.5).

PFPTC

Bullet force function evaluated at ROE.

PFRC

Bullet-atom repulsive force interaction evaluated at ROE.

PFXA

Bullet force function parameter.

PKE(I)

The kinetic energy of the Ith atom.

PNEG

Total negative potential energy in the lattice.

PNUM

Alphanumeric variable for the impact point number.

POT

The potential energy between two atoms.

PPE(I)

The potential energy of the Ith atom.

PPOS

Total positive potential energy in the lattice.

PPTC

Bullet potential function evaluated at ROE.

PROB

The probability that an atom will sputter from a given ring.

PTC

Target atom potential function evaluated at ROE.

PTE(I)

The total energy of the Ith atom.

QM

A small number used in checking the kinetic energy zero point.

QUIT

Coutoff variable checked against the total potential energy which can be used as a shut down criterion.

R1, R1S

Distance from (0,0) impact point to the initial bullet position.

R1, R1Y, R1Z

The x,y,z components of R1S.

R2

Magnitude of vector from impact point to the first atom hit by the bullet.

R3

Magnitude of vector from impact point to bullet start position.

R1, R2

Scalar product of vectors R1, R2.

R2SQ

R2 squared.

RAD

The angle between the direction of an ejected atom and the surface normal in radians.

RADDEG

Conversion factor - radians to degrees.

RAN(I)

A list of normally distributed random numbers.

RANGE

A scaling variable used in the histogram.

RBX, RBZ

Unscaled x,z coordinates of the impact area reference point.

RDIST

The distance between an atom and the center point of its layer.

RE

Input Morse potential parameter.

RINCR

The RANGE increments.

RMIDPT

The midpoint of each interval in the histogram.

ROE, ROE2

Nearest neighbor distance - squared.

ROEA

The maximum cutoff for the Born-Mayer potential.

ROEB

The minimum cutoff for the Morse potential.

ROEC, ROEC2

The maximum cutoff for the Morse potential - squared.

ROEM

Defines the region where the repulsive force function must be modified.

RX(I), RY(I), RZ(I)

X,y,z coordinates of the Ith atom at any time.

RXBL, RYBL, RZBL

Maximum negative x,y,z coordinates an atom may move before it is LCUT.

RXBM, RYBM, RZBM

Maximum positive x,y,z coordinates an atom may move before it is LCUT.

RXF, RYF, RZF

Final x,y,z coordinates of the Ith atom when it is LCUT.

RXI(I), RYI(I), RZI(I)

The Ith atom's initial x,y,z coordinates.

RXK(I), RYK(I), RZK(I)

Temporary x,y,z coordinates of the Ith atom during the force cycle.

RXS, RYS, RZS

Scaled x,y,z coordinates of the impact point.

SAVE

One-half POT.

SBX, SBZ

Scaled x,z coordinates of the impact point.

SCALE

A scaling variable for the frequency of events in the histogram.

SCX, SCY, SCZ

The x,y,z lattice scale factors used to convert the generated lattice to match a real crystal.

SCXR, SCZR

The inverse of SCX and SCZ - a ratio used to avoid repeated division.

SDIST

The square of the distance from the center of a layer to an atom.

SETIME

A library subroutine used to keep track of run time .

SLOW

A cutoff velocity variable checked against a long DT.

SPDX, SPDZ

The fraction of the target impact area that the impact points are incremented.

SPX, SPZ

The x,z components of the distance from the impact area reference point to the impact point.

SSCZ

A z scale factor used in the (111) orientation lattice generation.

STD

The standard deviation of the sputtering ratio.

STOPER

This variable stops calculating and saves 60 seconds for compilation and output.

SUR

Alphanumeric variable describing the surface.

TA, TAMP

The thermal amplitude of the lattice.

TAR

Alphanumeric variable describing the target element.

TARGET

Alphanumeric variable describing the target element.

TAS

A scale factor - $TAMP/ROOT(3.0)$.

TASF, TASN

Random thermal amplitude scale constants.

TE
The total kinetic and potential energy of all the atoms.

TEMP
The temperature of the lattice in degrees Kelvin.

TESTE
A termination test of energy.

TFAC
A time factor ratio used to determine DT by maximum force methods.

THERM
Mean thermal energy of a lattice atom. Used in shut-down tests.

TIME
The elapsed calculating time in seconds.

TITLE1, TITLE2
The titles for the histogram outputs.

TMAS1, TMAS2
The target isotope masses in amu.

TPKE
The total kinetic energy of all the atoms.

TPOT
The total potential energy of all the atoms.

TRUN
The time the program is to run in minutes.

VEL

The velocity calculation - $\text{SQRT}(\text{ev}/\text{HBMAS})$.

VSS

A temporary storage variable for the velocity components.

VTEST

A test velocity used to determine if the atom has sufficient velocity (energy) to escape the surface.

VTs

A scale factor - $0.8 * \text{VTEST}$.

VX(I), VY(I), VZ(I)

The x,y,z components of the Ith atom's velocity.

VXS, VYS, VZS

The x,y,z components of the bullet's initial velocity.

XDIST

The x component of the distance from the center of a layer to the atom.

XMAX, XMIN

The x planes to determine whether two atoms are close enough to interact.

YLAX(I)

The crystal relaxation of the Ith layer in the -y direction.

YMAX, YMIN

The y planes to determine whether two atoms are close enough to interact.

ZDIST

The z component of the distance from the center of a layer to the atom.

ZE

Absolute zero (0.0).

ZMAX, ZMIN

The z planes to determine whether two atoms are close enough to interact.

ZSTOP

Used to print out a warning header that a pass was terminated before completion.

APPENDIX D

COMPUTER PROGRAM

OLD3 IS OLD1 MODIFIED TO INCREASE SPEED
 ROLD IS OLD3 WITH 'WARMED' LATTICE
 RING IS RPF MODIFIED TO FOLD LATTICE AND
 STUDY RING FORMATION/SPUTTERING
 RMAS IS RING MODIFIED TO STUDY TARGET ISOTOPES
 RANG IS RMAS MOD. TO STUDY ANGULAR DISPERSION

DIMENSION DX(600),DY(600),DZ(600)
 DIMENSION RXK(600),RYK(600),RZK(600)
 DIMENSION PKE(600),PTE(600)
 DIMENSION NSPUT(50),IPNUMS(50)
 DIMENSION ISNUM(20),ISEQ(600)
 DIMENSION RXF(600),RYF(600),RZF(600)
 DIMENSION IBOX1(20),IBOX2(20),RANNUM(250)
 DIMENSION FREQ1(80),FREQ2(80),RANGE(20),TITLE1(24),
 X TITLE2(24)
 DIMENSION HCTOM(2)
 DIMENSION IFFM(600),IFM(600)
 COMMON/COM1/RX(600),RY(600),RZ(600),LCUT(600),LL,LD
 COMMON/COM2/RCE,RCE2,ROEM,AC,PAC,PPTC,PTC,PFPTC,FPTC,
 X FM,PFIV,TPCT
 COMMON/COM3/EXA,EXB,FXA,PEXA,PEXB,PFXA,THERM
 COMMON/COM4/IX,IY,IZ,IXP,IYP,SCX,SCY,SCZ,IDEEP,
 X RBX,RBZ
 COMMON/COM4A/LNUM(600),LNUMI(600),LNUMF(600)
 COMMON/COM5/FX(600),FY(600),FZ(600),PPE(600)
 COMMON/COM6/COXI,COYI,CCZI,RXS,RYS,RZS,FAC
 COMMON/COM7/R1,LSS,SPX,SPZ,COX,CCY,COZ,YLAX(20),ILL
 COMMON/COM8/VX(600),VY(600),VZ(600)
 COMMON/COM8A/VXS(600),VYS(600),VZS(600)
 COMMON/COM11/RXI(600),RYI(600),RZI(600)
 COMMON/COM13/RAN(1800),IRAN,TASN,TASF,LL2,LL3
 COMMON/COM14/AXT(600),AYT(600),AZT(600)
 COMMON/COM16/BMAS,TMAS1,TMAS2,ABUN1,ABUN2,IFNUM
 COMMON/COM16A/BX,BY,BZ,EDISP,CVR
 COMMON/COM17/TIME,NT,DT,DTI,TEMP,CELS,EV,NPAGE,NLINE
 COMMON/COM18/ITEMP,TAMP,CORF
 COMMON/COM20/IH1(20),IHS(10),IHT(6),IHB(6),IHTARG(2),
 X IHBULL(2)
 COMMON/COM21/IHBPCT(2),IHTPCT(2),SUR(2),IH2(10),ICR,
 X LSR
 COMMON/COM22/ROEA,RCEB,RCEC,ROEC2,CPO,CP1,CF2,CP3,CFO,
 X CF1,CF2,CGC1,CGD2,CGB1,CGB2,CGF1,CGF2,IPRCG
 COMMON/COM23/SPDX,SPDZ,DBXMAX,DBZMAX,SSCZ
 COMMON/COM24/DNN(100),KATOM(100),KSPUT(100),PROB(100)
 COMMON/COM24A/KSUM,KRING,RDIST(600)
 COMMON/COM25/IMF(600),ISOGEN
 COMMON/COM30/ISEEDA,ISEEDB,ISEEDC
 COMMON/COMA/A(4,5),MCRO
 9005 FCRMAT (20A4)
 9010 FCRMAT (20A4)
 9020 FCRMAT (10A4,I3,2A4,I2,3I3,2F3.0,2F5.2,I2)
 9030 FCRMAT (2A4,A4,F8.3,2A4,2F10.5,F8.5,3F7.4,I3)
 9035 FCRMAT (F5.2,I5)


```

904C FCRMAT(10A4,3F5.2,3F8.5,I1)
9050 FCRMAT(2X,I3,15(I3,1X,I1,2X))
9080 FCRMAT(5X,3F5.3,4I5,2F8.6,2X,A4,3F6.4)
9105 FCRMAT(11X,F5.0)
9600 FCRMAT(//)
9601 FCRMAT(1H1)
9620 FCRMAT(1X,3(I5,4X,I1,4X,3F6.2,8X))
9630 FCRMAT(105X,4HPAGE,I3,/,1H1)
964C FCRMAT(' BINDING ENERGY =',F6.2,', TEST SPEED =',
X F10.2,', M/SEC',', SAFETY FACTOR SPEED =',F10.2,
X ' M/SEC',/,1H1)
9680 FCRMAT(2X,'ATCM',2X,'LCUT',9X,'VX',9X,'VY',9X,'VZ',
X 8X,'RXF',8X,'RYF',8X,'RZF',8X,'PPE',8X,'PKE',8X,
X 'PTE'//)
9681 FCRMAT(1X,'ATOM DX',6X,'DY',6X,'DZ',7X,'VX',7X,'VY',
X 7X,'VZ',7X,'KE',8X,'PE',8X,'TE',7X,'RX',6X,'RY',6X,
X 'RZ',4X,'LCUT ISEQ',/)
9682 FCRMAT(15,3F8.3,3F9.1,3F10.4,3F8.3,I4,3X,I4)
9685 FCRMAT(2X,I3,3X,I3,5X,3(F8.1,3X),6(F8.3,3X))
969C FCRMAT(74X,F10.3,'EV, TOTAL KINETIC ENERGY',F10.3,
X 'EV, TOTAL POTENTIAL ENERGY',F10.3,'EV, TOTAL',
X ' ENERGY',/,9X,'TOTAL POSITIVE POTENTIAL ENERGY IS',
X F10.3,'TOTAL NEGATIVE POTENTIAL ENERGY IS',F10.3)
9695 FCRMAT(3X,'ATOM & POTENTIAL SURF',5X,'VX',7X,'VY',7X,
X 'VZ',10X,'PKE',6X,'PPE',6X,'PTE KEV CCX COY',/)
9701 FCRMAT(' IFT =',I10,', IRAN =',I10,', LL =',I5,/)
9800 FCRMAT(1X,2I5,2A4,I4,A4,1X,3F9.1,2F9.4,F5.1,1X,2F6.3)
9805 FCRMAT(5X,'SPUTTERED ATCM / ANGLE WITH NCRML'//)
9810 FCRMAT(//,' AT',F7.1,' EV, THE FOLLOWING ATCMS WERE',
X ' SPUTTERED: ',20I4,/)
9815 FCRMAT(1X,5(5X,I3,3X,F7.4))
982C FCRMAT(' THERE ARE NO SPOTS AT ',F8.1,'EV')
984C FCRMAT(25X,'SUMMARY OF TARGET IMPACT AREA',/,25X,
X 'FOLDED TO REPRESENT TOTAL COVERAGE'//)
9845 FCRMAT(1X,'ATOM NUMBER / TIMES SPUTTERED ')
985C FCRMAT(//,' SPUTTERING RATIO WAS',F6.3,
X ' THE VARIANCE WAS',F8.3,', FCR',I4,
X ' IMPACT POINTS, THE STD DEV OF THE MEAN WAS',
X F6.3,/)
986C FCRMAT(2X,'STATISTICAL SUMMARY FOR',I4,'IMPACT POINTS'
X ' AT ',F5.1,'KEV',/)
9865 FCRMAT(' NUMBER OF TIMES EACH ATCM SPUTTERED'//)
9870 FCRMAT(10(I6,I4))
9875 FCRMAT(//,' BINDING ENERGY WAS',F6.2,' EV, TEST SPEED'
X ' WAS',F10.2,' M/SEC, SPUTTERED ATOM COUNT IS',I5)
9880 FCRMAT(1X,3(' RING DISTANCE ATCMS SPOTS PROB '))
9885 FCRMAT(1X,3(' NN(',I2,')',2X,F6.3,3X,I2,5X,I3,3X,
X F6.3,1X))
989C FCRMAT(25X,'PROBABILITY THAT A RING OF ATCMS SPUTTERS'
X //)
9895 FCRMAT(25X,'SPUTTERED ATOMS ANGULAR DENSITY'//)
990C FCRMAT(2X,'INCREMENTS ARE IN',F4.2,' DEGREE INTERVALS'
X /)
9905 FCRMAT(2X,'ANGLE (DEGREES) / NUMBER OF ATCMS'//)
9910 FCRMAT(2X,19(I3,3X),I3)
9915 FCRMAT(3X,I2,2(1X,F4.2))
9920 FCRMAT(' 00-05 05-10 10-15 15-20 20-25 25-30 30-35',
X ' 35-40 40-45 45-50 50-55 55-60 60-65 65-70 70-75',
X ' 75-80 80-85 85-90'//)
9925 FCRMAT(' 00-10 10-20 20-30 30-40 40-50 50-60 60-70',
X ' 70-80 80-90'//)
993C FCRMAT(' NUMBER OF ATOMS CHANGED WAS',I4/, ' ATOMS',
X ' CHANGED AND ISOTOPE TYPE ARE')
9935 FCRMAT(1X,13(I3,2X,I1,3X))
9940 FCRMAT(1X,'SCX=',F7.4,' SCY=',F7.4,' SCZ=',F7.4)
9945 FCRMAT(3(I10,10X),I5)
995C FCRMAT(' ISEED =',I10)
9955 FCRMAT(1X,'*** THIS SHOT WAS TERMINATED BEFORE IT',
X ' WAS COMPLETED',/,4X,' ZSTOP=1 THE CURRENT',
X ' TIMESTEP EXCEEDED THE LIMIT',/,14X,'ANY SPOTS',
X ' ARE REMOVED FROM THE SUMMARY')
9960 FCRMAT(1X,'*** THIS SHOT WAS TERMINATED BEFORE IT',

```



```

X      ' WAS COMPLETED'//,14X,' ISHUT=1  TIME RAN OUT'//,
X      14X,' ANY SPUTS ARE REMOVED FRM THE SUMMARY')
9965  FCRMAT(4X,' IMPACT PCINT ',I5)
9970  FCRMAT(4X,'BX=',F6.4,'BZ=',F6.4)
9975  FCRMAT(8X,'NOT IN TARGET AREA',/)
      CALL CVFLOW
      CALL SETIME
      READ (5,9005) TITLE1
      READ (5,9005) TITLE2
      READ(5,9105) TRUN
      STOPER=TRUN*60.0-60.0
      FINISH=0.0
      ILATT=0
      MCRC=4
      NCTT=10
      TESTE=2.0
          BIND=0.0
          CVB=0.774E-9
      BENRGY=2.0
      ISHUT=0
      LC=0
      FM=1.0E-10
      PFIV=0.5
      CM=0.01
      SLCW=1.0E-14
      WRITE(6,9601)
      DO 1 I=1,20
      IECX1(I)=0
      IECX2(I)=0
1  CCNTINUE
      DO 2 I=1,600
      LNUM(I)=0
      LCCT(I)=0
      RXK(I)=0.0
      RYK(I)=0.0
      RZK(I)=0.0
      VX(I)=0.0
      VY(I)=0.0
      VZ(I)=0.0
      RX(I)=0.0
      RY(I)=0.0
      RZ(I)=0.0
      FX(I)=0.0
      FY(I)=0.0
      FZ(I)=0.0
      PTE(I)=0.0
      PKE(I)=0.0
      PPE(I)=0.0
      RXI(I)=0.0
      RYI(I)=0.0
2  RZI(I)=0.0
      READ ( 5,9010) IH1
      READ(5,9020)IHS,IOR,SUR,LSS,IX,IY,IZ,RBX,RBZ,CTI,RCE2,
X  LTYPE
      READ (5,9030) IHBULL,BUL,BMAS,IHBPOT,PEXA,PEXB,XXXX
      READ(5,9030)IHTARG,TAR,TMAS1,IHTPOT,EXA,EXB,FLAT,TMAS2
X  ,ABUN1,ABUN2,ISOGEN
      READ (5,9040) IH2,ROEA,ROEB,ROEC,DCCN,ALPHA,RE,IAPCG
5  READ(5,9080)EVR,SPX,SPZ,NTT,NSR,NC,IDEEP,COX,COY,ITEMP
X  ,TA,CO,ETHR
      READ(5,9945) ISEEDA,ISEEDB,ISEEDC,NSHOTS
      READ (5,9915) IRANGE,RMIDPT,RINCR
      READ (5,9050) IREAD,(IFFM(J),IFM(J),J=1,IREAD)
      IF(EVR.LE.0.0) GO TO 9999
      IF(ISOGEN.NE.0) GC TO 33
      TMAS2=63.54
      ABUN1=C.000
      ABUN2=1.000
33  CCNTINUE
      TAMP=TA
      CCRF=CC
      IPASS=1

```



```

NCTT=ND
IF(ILATT.NE.0) GO TO 10
      MAKE HEADING HOLLARITH

```

```

IFE(1)=IHBULL(1)
IFB(2)=IHBULL(2)
IFE(3)=IHTARG(1)
IFB(4)=IHTARG(2)
IFB(5)=IHBPCT(1)
IFB(6)=IHBPCT(2)
IFT(1)=IHB(3)
IFT(2)=IHB(4)
IFT(3)=IHB(3)
IFT(4)=IHB(4)
IFT(5)=IHTPCT(1)
IFT(6)=IHTPCT(2)

```

MAKE CONSTANTS

```

RACDEG=57.2957795
RCE=SQRT(RCE2)
EV=EVR*1000.0
NS=NSR
      FAC=0.1
RCM=RCE-CTI
CVR=0.5*FLAT
CVE=1.6021E-19
CVM=1.6604E-27
CVC=CVR*1.0E-10
CVED=CVE/CVD
RXBL=-RCE
RYBL=-0.8
RZBL=-RCE
IXP=(IX+1)/2
IYP=(IY+1)/2
IZP=(IZ+1)/2
PEMAS=BMAS*CVM
HEMAS=0.5*PBMAS/CVE
PTMAS1=TMAS1*CVM
PTMAS2=TMAS2*CVM
HTMAS1=0.5*PTMAS1/CVE
HTMAS2=0.5*PTMAS2/CVE
VTEST=-SQRT(2.0*ETHR*CVE/PTMAS2)
VTS=0.8*VTEST

```

MAKE REPULSIVE POTENTIALS

```

FXA=ALOG(-EXB*CVED)+EXA
PFXA=ALOG(-PEXB*CVED)+PEXA
AC=ALOG(CVED)+EXA
PAC=AC-EXA+PEXA
PTC=EXP(EXA+EXB*ROE)
FRC=EXP(FXA+EXB*RCE)
FPTC=EXP(AC+EXB*RCE)
PFPTC=EXP(PAC+PEXB*ROE)
PFRC=EXP(PFXA+PEXB*RCE)
PPTC=EXP(PEXA+PEXB*ROE)

```

GENERATE THE LATTICE

```

      IF (IOR.EQ.100) GO TO 6
      IF (IOR.EQ.110) GO TO 7
      IF (IOR.EQ.111) GO TO 8
6 CALL KF100
  GC TO 9
7 CALL KF110
  GC TO 9
8 CALL KF111
  GC TO 9
9 CCNTINUE
  IF (IOR.EQ.100) THETA=1.0000

```



```

IF (IOR.EQ.110) THETA=C.0000
IF (IOR.EQ.111) THETA=(SQRT(1.5)/3.0)/(SQRT(2.0)/2.0)
IF (ISOGEN.EQ.0) GC TO 12
DC 12 I=1,IREAD
J=IFFM(I)
IMF(J)=IFM(I)
12 CCNTINUE
DC 65 I=2,LL,3
K=I+1
J=I+2
65 WRITE(6,9620) I, IMF(I), RXI(I), RYI(I), RZI(I), K, IMF(K),
X RXI(K), RYI(K), RZI(K), J, IMF(J), RXI(J), RYI(J), RZI(J)
WRITE(6,9600)
WRITE(6,9930) IREAD
WRITE(6,9935) (IFFM(J), IFM(J), J=1, IREAD)
WRITE(6,9600)
WRITE(6,9940) SCX, SCY, SCZ
LL2=2*LL
LL3=3*LL
R1S=R1
ILATT=1
NFACE=1
BX=RBX*SCX
EZ=RBZ*SCZ
SBX=BX
SEZ=BZ
RXBM=(IX-1)*SCX+RCE
RYBM=(IY-1)*SCY+RCE
RZBM=(IZ-1)*SCZ+RCE
10 CCNTINUE
CCZ=1.0-CCX*COX-CCY*COY
COZ=ABS(COZ)
CCZ=SQRT(COZ)
CCXI=-CCX
CCYI=-CCY
CCZI=-CCZ
IFT=ITIME(II)
IRAN=2*IFT+1
IF (IRAN.LT.0) IRAN=-IRAN
BXMIN=BX
BXMAX=BX+DBXMAX
BZMIN=BZ
EZMAX=EZ+DBZMAX
IF (IOR.NE.100) GO TO 25
IF (SPX.EQ.0.0) GO TO 25
BZMAX=BZMAX-10.0*SPX*SPDZ
BZMIN=BZMIN+10.0*SPX*SPDZ
25 IF (IOR.NE.111) GO TO 30
IF (SPX.EQ.0.0) GO TO 30
BZMAX=BZMAX-5.0*SFX*SPDZ
BZMIN=BZMIN+5.0*SFX*SPDZ
30 CCNTINUE
BX=(RBX+SPX)*SCX
BY=(RYI(4)+C.001)*SCY
EZ=(RBZ+SPZ)*SCZ
SCXR=1.0/SCX
SCZR=1.0/SCZ
IF (IOR.EQ.111) SCZR=1.0/SSCZ

```

PREPARE TO WARM LATTICE

```

IFT=ITIME(II)
IRAN=2*IFT+1
IF (IRAN.LT.0) IRAN=-IRAN
WRITE(6,9600)
WRITE(6,9701) IFT, IRAN, LL
WRITE(6,9640) ETHR, VTEST, VTS
IF (TAMP.EQ.C.0) GC TO 40
TAS=TAMP/SQRT(3.0)
CCRN=1.0-CCRF
TASN=TAS*CCRN
TASF=TAS*CCRF

```

C
C
C

C
C
C

EACH REPLICA STARTS HERE

```
40 CCNTINUE
   IF(IPASS.GT.NSHOTS) GO TO 1000
   IF(TAMP.GT.C.O) CALL WARM
50 CCNTINUE
   TIME=0.0
   NS=NSR
   NT=0
   NSS=0
   NCT=0
   INDEX=J
   ZSTCP=0.0
   SPX=(BX-SBX)*SCXR
   SPZ=(BZ-SBZ)*SCZR
   ISPX=(SPX+0.001)*100.0
   ISPZ=(SPZ+0.001)*100.0
   IPNUM=100*ISPX+ISPZ
   IPNUMS(IPASS)=IPNUM
   R1=R1S
```

C
C
C

RECONSTRUCT LATTICE

```
   ISEQ(1)=0
   CC 60 I=2,LL
   LCLT(I)=0
   ISEQ(I)=0
   RX(I)=RXI(I)
   RY(I)=RYI(I)
   RZ(I)=RZI(I)
   PTE(I)=0.0
   PPE(I)=0.0
   VX(I)=0.0
   VY(I)=0.0
   VZ(I)=0.0
60 CCNTINUE
   IF(TAMP.NE.C.O) CALL WARM
   RXS=BX
   RYS=BY
   RZS=BZ
   R1=R1+FAC
   CALL SETUP
   LCLT(1)=0
   RXI(1)=RX(1)
   RYI(1)=RY(1)
   RZI(1)=RZ(1)
   PPE(1)=0.0
   VEL=SQRT(EV/HBMAS)
   VX(1)=VEL*CCX
   VY(1)=VEL*CCY
   VZ(1)=VEL*CCZ
   FCTI=DTI*CVC
   CT=FDTI/VEL
```

C
C
C

BEGIN TIMESTEP CYCLE

```
100 DTCD=DT/CVD
   FCTCD=0.5*DTCD
   DTCM1=DT/PTMAS1
   DTCM2=DT/PTMAS2
   HCTCM(1)=0.5*DTOM1
   FCTCM(2)=0.5*DTOM2
   DTCMB=DT/PBMAS
   FCTOMB=C.5*DTOMB
200 CALL STEP
   IF(INDEX.GT.J) GO TO 250
```

C
C
C

FIRST HALF OF TIMESTEP

```
210 INDEX=1
   I=1
```



```

      IF(LCUT(I).EQ.2) GO TO 215
      IF(LCUT(I).NE.3) GO TO 220
      RXK(I)=RX(I)
      RYK(I)=RY(I)
      RZK(I)=RZ(I)
      RX(I)=RX(I)+DTOD*(HDTOMB*FX(I)+VX(I))
      RY(I)=RY(I)+DTOD*(HDTOMB*FY(I)+VY(I))
      RZ(I)=RZ(I)+DTOD*(HDTOMB*FZ(I)+VZ(I))
      GC TO 220
215  RX(I)=RX(I)+DTOD*VX(I)
      RY(I)=RY(I)+DTOD*VY(I)
      RZ(I)=RZ(I)+DTOD*VZ(I)
220  CC 240 I=2,LL
      IF(LCUT(I).EQ.2) GO TO 235
      IF(LCUT(I).GT.0) GO TO 240
      J=IMF(I)
      RXK(I)=RX(I)
      RYK(I)=RY(I)
      RZK(I)=RZ(I)
      RX(I)=RX(I)+DTOD*(HDTOM(J)*FX(I)+VX(I))
      RY(I)=RY(I)+DTOD*(HDTOM(J)*FY(I)+VY(I))
      RZ(I)=RZ(I)+DTOD*(HDTOM(J)*FZ(I)+VZ(I))
      GC TO 240
235  RX(I)=RX(I)+DTOD*VX(I)
      RY(I)=RY(I)+DTOD*VY(I)
      RZ(I)=RZ(I)+DTOD*VZ(I)
240  CCNTINUE
      GC TO 200

```

SECOND HALF OF TIMESTEP

```

250  CCNTINUE
      INDEX=0
      EMAX=0.0
      TIME=TIME+DT
      NT=NT+1
      I=1
      IF(LCUT(I).NE.0) GO TO 260
      VSS=VX(I)
      VX(I)=VSS+HDTOMB*FX(I)
      RX(I)=RXK(I)+(VX(I)+VSS)*HDTOD
      VSS=VY(I)
      VY(I)=VSS+HDTOMB*FY(I)
      RY(I)=RYK(I)+(VY(I)+VSS)*HDTOD
      VSS=VZ(I)
      VZ(I)=VSS+HDTOMB*FZ(I)
      RZ(I)=RZK(I)+(VZ(I)+VSS)*HDTOD
      FX(1)=0.0
      FY(1)=0.0
      FZ(1)=0.0
      PKE(I)=VX(I)*VX(I)+VY(I)*VY(I)+VZ(I)*VZ(I)
      EMAX=PKE(I)
      K=I
      PKE(I)=PKE(I)*HBMAS
260  CC 290 I=2,LL
      IF(LCUT(I).NE.0) GO TO 290
      J=IMF(I)
      VSS=VX(I)
      VX(I)=VSS+HDTOM(J)*FX(I)
      RX(I)=RXK(I)+(VX(I)+VSS)*HDTOD
      VSS=VY(I)
      VY(I)=VSS+HDTOM(J)*FY(I)
      RY(I)=RYK(I)+(VY(I)+VSS)*HDTOD
      VSS=VZ(I)
      VZ(I)=VSS+HDTOM(J)*FZ(I)
      RZ(I)=RZK(I)+(VZ(I)+VSS)*HDTOD
      FX(I)=0.0
      FY(I)=0.0
      FZ(I)=0.0
      PKE(I)=VX(I)*VX(I)+VY(I)*VY(I)+VZ(I)*VZ(I)
      IF(PKE(I).LT.EMAX) GO TO 280
      EMAX=PKE(I)

```



```

      K=I
280  IF(IMF(I).EQ.1) GO TO 282
      PKE(I)=HTMAS2*PKE(I)
      GC TO 290
282  PKE(I)=HTMAS1*PKE(I)
290  CCNTINUE

```

TEST FOR PRINT OR TERMINATION

```

      CALL GETIME(IET)
      CALL SETIME
      FINISH= IET *2.6E-05 +FINISH
      IF(FINISH.GT.STOPER) GO TO 370
      IF(IMF(K).EQ.1) GO TO 293
      ETEST=HTMAS2*EMAX
      GC TO 294
293  ETEST=HTMAS1*EMAX
294  CCNTINUE
      IF(ETEST.LE.TESTE) GO TO 380
      NCT=NCT+1
      IF(NCT.NE.NCTT) GO TO 360
      NCT=0
      DC 305 I=1,LL
      IF(LCUT(I).GT.0) GO TO 305
      PPE(I)=C.0
305  CCNTINUE
      CALL ENERGY
307  DC 350 I=1,LL
      IF(LCUT(I).GT.0) GO TO 350
      IF(RY(I).LT.RYBL.AND.VY(I).LT.0.0) GO TO 320
      IF(RX(I).LT.RXBL.OR.RX(I).GT.RXBM) GO TO 310
      IF(RZ(I).LT.RZBL.OR.RZ(I).GT.RZEM) GO TO 310
      IF(RY(I).LT.RYBM) GO TO 350
310  LCUT(I)=1
      RXF(I)=RX(I)
      RYF(I)=RY(I)
      RZF(I)=RZ(I)
      PTE(I)=PKE(I)+PPE(I)
      GC TO 350
320  IF(I.EQ.1) GO TO 310
      IF(PPE(I).GT.0.0001) GO TO 350
      PTE(I)=PKE(I)+PPE(I)
      IF(PTE(I).LT.0.0) GO TO 350
      LCUT(I)=2
      RXF(I)=RX(I)
      RYF(I)=RY(I)
      RZF(I)=RZ(I)
350  CCNTINUE

```

TEST FOR OUTPUT OF CURRENT STATUS

```

360  DT=FDTI/SQRT(EMAX)
      IF(NT.GE.NTT) GO TO 380
      GO TO NEXT TIMESTEP
      IF(NS.NE.NT) GO TO 100
      GC TO 400
370  ISFUT=1
      GC TO 400
380  NSS=1
      IF(NT.GE.NTT) ZSTCP=1.0

```

CALCULATE POTENTIAL ENERGY AND PRINT STATUS OF THE CURRENT TIMESTEP

```

400  CCNTINUE
      TFCT=0.0
      PFCS=0.0
      FNEG=0.0
      DC 450 I=1,LL
      IF(ISEQ(I).EQ.1) ISEQ(I)=2

```



```

        IF(LCUT(I).NE.0) GC TO 450
        PPE(I)=0.0
        PTE(I)=0.0
450  CCNTINUE
        CALL ENERGY
595  PTE(1)=PKE(1)+PPE(1)
        TFKE=PKE(1)
600  CC 625 I=2,LL
        TFKE=TFKE+PKE(I)
        IF(PPE(I).GT.0.0) GO TO 615
        FNEG=FNEG+PPE(I)
        GC TC 620
615  PPCS=PPCS+PPE(I)
620  PTE(I)=PKE(I)+PPE(I)
625  CCNTINUE
        TE=TPKE+TPOT+BIND
        IF((NSS.NE.0) .AND. (ZSTOP.EQ.0.0)) GO TO 950
        CALL KPRINT
        WRITE(6,9681)
730  CC 750 I=1,LL
        IF(PTE(I).LT.0.1) GO TC 750
        IF(ISEQ(I).EQ.0) ISEQ(I)=1
        DX(I)=RX(I)-RXI(I)
        DY(I)=RY(I)-RYI(I)
        DZ(I)=RZ(I)-RZI(I)
        WRITE(6,9682) I,DX(I),DY(I),DZ(I),VX(I),VY(I),VZ(I),
X PKE(I),PPE(I),PTE(I),RX(I),RY(I),RZ(I),LCUT(I),ISEQ(I)
750  CCNTINUE
        WRITE(6,9690) TPKE,TPCT,TE,PPOS,PNEG
        IF(ISHUT.NE.0) GO TO 972
        IF(ZSTOP.NE.0.0) GO TO 973
        WRITE(6,9630) NPAGE
        NPAGE=NPAGE+1
        NS=NS+NC

```

```

C
C
C      GO TO NEXT TIMESTEP

```

```

        GC TO 100
950  CCNTINUE

```

```

C
C
C      TERMINATE REPLICA AND THEN
      PRINT FINAL STATUS OF CURRENT PASS

```

```

        J=1
        K=C
        IK=0
        CC 960 I=1,LL
        IF(LCUT(I).LT.2) GO TO 960
        IF(VY(I).GT.VTEST) GO TO 960
        K=K+1
        ISNUM(J)=I
        LNUM(I)=LNUM(I)+1
        J=J+1
960  CCNTINUE
        KK=K
        NSPUT(IPASS)=KK
        CALL KPRINT
        IF(KK.EQ.0) GO TO 972
        WRITE(6,9810) EV,(ISNUM(I),I=1,KK)
        WRITE(6,9600)
        WRITE(6,9695)
        DO 968 II=1,KK
        I=ISNUM(II)
        WRITE(6,9800) IPNUM,I,BUL,TAR,IOR,SUR(1),VX(I),VY(I),VZ
X(I),PKE(I),PPE(I),PTE(I),EVR,COX,CCZ
968  CCNTINUE
        CC 969 I=2,LL
        IF(LCUT(I).EQ.2 .AND. VY(I).LT.VTS) WRITE(6,9800)
X IPNUM,I,BUL,TAR,IOR,SUR(1),VX(I),VY(I),VZ(I),PKE(I),
X PPE(I),PTE(I),EVR
969  CCNTINUE

```

C

C DETERMINE SPUTTERED ATOM ANGLE

```

C
  IF(KK.EQ.0) GO TO 972
  WRITE (6,9600)
  WRITE(6,9805)
  DO 970 I=1, KK
  L=ISNUM(I)
  RAC=ATAN(SQRT(VX(L)**2+VZ(L)**2)/(-VY(L)))
  ANGLE=RAC*RADDEG
  J=IFIX((ANGLE/RINCR)+1.0)
  IF(IMF(L).EQ.1) IBOX1(J)=IBOX1(J) +1
  IF(IMF(L).EQ.2) IBOX2(J)=IBOX2(J) +1
  WRITE (6,9815) L, ANGLE
970 CCNTINUE
  IF((ISHUT.EQ.1) .CR. (ZSTOP.EQ.1.0)) GO TO 972
  WRITE(6,9630) NPAGE
  NPAGE=NPAGE+1
  GO TO 990
972 IF(ISHUT.EQ.0) GO TO 973
  WRITE(6,9965) IPNUM
  WRITE(6,9600)
  WRITE(6,9960)
  NSPLT(IPASS)=0
  IPASS=IPASS-1
  NSHOTS=NSHOTS-1
  GO TO 975
973 IF(ZSTCF.EQ.0) GO TO 974
  WRITE(6,9965) IPNUM
  WRITE(6,9600)
  WRITE(6,9955)
  NSPLT(IPASS)=0
  IPASS=IPASS-1
  NSHOTS=NSHOTS-1
  GO TO 975
974 WRITE(6,9820) EV
975 WRITE(6,9630) NPAGE
  NPAGE=NPAGE+1

```

C C C DEFINE NEW REPLICA OR TERMINATE

```

990 IPASS=IPASS+1
  IF(ISHUT.NE.0) GO TO 1000
  BZ=BZ+SPDZ
  IF(BZ.LE.BZMAX) GO TO 40
  BX=BX+SPDX
  IF(BX.GT.BXMAX) GO TO 1000
  IF(IGR.EQ.100) BZMIN=BZMIN+SPDZ
  IF(IGR.EQ.111) BZMIN=BZMIN+SPDZ/2.0
  BZ=BZMIN
  IF(IGR.EQ.100) BZMAX=BZMAX-SPDZ
  IF(IGR.EQ.111) BZMAX=BZMAX-SPDZ/2.0
  GO TO 40

```

C C C PRINT SUMMARY OF ALL SHOTS

```

1000 CCNTINUE
  CALL KPRINT
  WRITE (6,9600)
  NRAM=IPASS-1
  WRITE(6,9860) NRAM, EVR
  WRITE(6,9870) ((IPNUMS(I), NSPUT(I)), I=1, NRAM)
  KSUM=0
  K2SUM=0
  DO 1005 I=1, NRAM
  KSUM=KSUM+NSPUT(I)
  K2SUM=K2SUM+NSPUT(I)**2
1005 CCNTINUE
  FRAN=NRAM
  FRANR=1.0/FRAN
  AVE=FLOAT(KSUM)*FRANR
  VAR=FLOAT(K2SUM)*FRANR-AVE**2
  STD=VAR*FRANR

```



```

      STD=SQRT(STD)
      WRITE (6,9600)
      WRITE (6,9875) ETHR,VTEST,KSUM
      WRITE (6,9850) AVE,VAR,NRAN,STD
      WRITE (6,9600)
      WRITE (6,9865)
      WRITE (6,9870) (I,LNUM(I),I=1,LL)
      WRITE (6,9600)
      WRITE (6,9930) IREAD
      WRITE (6,9935) (IFFM(J),IFM(J),J=1,IREAD)
      IF(IOR.NE.100) GO TO 1007
      WRITE (6,9950) ISEEDA
1007  IF(IOR.NE.110) GO TO 1008
      WRITE (6,9950) ISEECB
1008  IF(IOR.NE.111) GO TO 1009
      WRITE (6,9950) ISEEC
1009  CCNTINUE
      WRITE (6,9630) NPAGE
      NPAGE=NPAGE+1
      CALL KPNT

```

```

C
C      FOLD FINAL SUMMARY

```

```

      IF (IOR.EQ.100) GC TO 1011
      IF (IOR.EQ.110) GC TO 1012
      IF (IOR.EQ.111) GC TO 1013
1011  CALL KFCLDA
      GC TO 1014
1012  CALL KFCLDB
      GC TO 1014
1013  CALL KFCLDC
1014  WRITE (6,9600)
      WRITE (6,9840)
      WRITE (6,9845)
      WRITE (6,9870) (I,LNUM(I),I=1,LL)
      WRITE (6,9600)

```

```

C
C      DETERMINE RING SPUTTERING PROBABILITY

```

```

1015  CALL KPROB
      WRITE (6,9890)
      WRITE (6,9880)
      CC 1020 I=1,KRING,3
      J=I+1
      K=I+2
      WRITE (6,9885) I,DNN(I),KATOM(I),KSPUT(I),PROB(I),J,
X      DNN(J),KATOM(J),KSPUT(J),PROB(J),K,DNN(K),KATOM(K),
X      KSPUT(K),PROB(K)
1020  CCNTINUE
      WRITE (6,9600)
      WRITE (6,9630) NPAGE
      NPAGE=NPAGE+1
      CALL KPNT
      WRITE (6,9600)

```

```

C
C      DRAW ISOTOPE HISTOGRAMS

```

```

1025  CC 1030 I=1,IRANGE
      FREQ1(I)=IBCX1(I)
      FREQ2(I)=IBCX2(I)
1030  CCNTINUE
      RANGE(1)=RMIDPT
      CC 1040 I=2,IRANGE
      J=I-1
      RANGE(I)= RANGE(J)+RINCR
1040  CCNTINUE
      IN=-IRANGE
      CALL HISTO(IN,FREQ1,RANGE,TITLE1)
      WRITE (6,9600)
      WRITE (6,9895)
      WRITE (6,9900) RINCR
      IF (IRANGE.EQ.9) WRITE (6,9925)

```



```

IF (IRANGE.EQ.18) WRITE(6,9920)
WRITE (6,9910) (IBOX1(J),J=1,IRANGE)
WRITE (6,9600)
WRITE (6,9600)
CALL HISTO(IN,FREQ2,RANGE,TITLE2)
WRITE (6,9600)
WRITE (6,9855)
WRITE (6,9900) RINCR
IF (IRANGE.EQ.9) WRITE (6,9925)
IF (IRANGE.EQ.18) WRITE(6,9920)
WRITE (6,9910) (IBOX2(J),J=1,IRANGE)
WRITE (6,9600)
WRITE (6,9630) NPAGE
NPAGE=NPAGE+1
IF(ISHUT.EQ.0) GO TO 5
9999 STCP
END

```


SLEROUTINE SETUP

THIS S/R FINDS THE STARTING POINT FOR EACH
IMPACT POINT IN THE TARGET AREA

```

CCMMCN/COM1/RX(600),RY(600),RZ(600),LCUT(600),LL,LD
CCMMCN/CCM2/RCE,RCE2,ROEM,AC,PAC,PPTC,PTC,PFPTC,FPTC,
X FM,PFIV,TPCT
CCMMCN/COM6/COXI,COYI,CCZI,RXS,RYS,RZS,FAC
CCMMCN/CCM7/R1,LSS,SPX,SPZ,COX,CCY,COZ,YLAX(20),ILL
CCMMCN/COM11/RXI(600),RYI(600),RZI(600)
I=1
100 R1=R1-FAC
IF(R1.LT.0.0) GO TO 300
R1X=R1*COXI+RXS
R1Y=R1*COYI+RYS
R1Z=R1*CCZI+RZS
XMIN = R1X-ROE
YMIN = R1Y-ROE
ZMIN = R1Z-ROE
XMAX = R1X+ROE
YMAX = R1Y+ROE
ZMAX = R1Z+ROE
CC 195 J=2,LL
IF(LCUT(J).GT.0) GO TO 195
IF(RY(J).GE.YMAX) GO TO 195
IF(RY(J).LE.YMIN) GO TO 195
IF(RX(J).GT.XMAX) GO TO 195
IF(RX(J).LE.XMIN) GO TO 195
IF(RZ(J).GE.ZMAX) GO TO 195
IF(RZ(J).LE.ZMIN) GO TO 195
CRX=RX(J)-R1X
DRY=RY(J)-R1Y
CRZ=RZ(J)-R1Z
DIST=DRX**2+DRY**2+DRZ**2
IF(DIST.GE.ROE2) GO TO 195
CC TO 200
195 CCNTINUE
CC TO 100
200 CCNTINUE
R2SQ=(RXI(J)-RXS)**2+(RYI(J)-RYS)**2+(RZI(J)-RZS)**2
R2=SQRT(R2SQ)
R1R2=(R1X-RXS)*(RXI(J)-RXS)+(R1Y-RYS)*(RYI(J)-RYS)+
X (R1Z-RZS)*(RZI(J)-RZS)
ALFA=R1R2/(R1*R2)
ALFA2=ALFA*ALFA
R3=R2*ALFA+SQRT(R2SQ*ALFA2-R2SQ+RCE2)
RX(1)=R3*COXI+RXS
RY(1)=R3*COYI+RYS
RZ(1)=R3*CCZI+RZS
RETURN
300 RX(1)=RXS
RY(1)=RYS
RZ(1)=RZS
9700 FCRMAT(41) THIS DID NOT LOCATE A PROPER START POINT)
WRITE ( 6,9700)
RETURN
END

```

SLEROUTINE WARM

THIS IS A MODEL 3 WARMER
EACH ATOM IS DISPLACED AN AMOUNT DETERMINED

BY ITS THERMAL AMPLITUDE

```

COMMON/COM1/RX(600),RY(600),RZ(600),LCUT(600),LL,LD
COMMON/COM13/ RAN(1800),IRAN,TASN,TASF,LL2,LL3
COMMON/COM14/ AXT(600),AYT(600),AZT(600)
AXT(1)=0
AYT(1)=0
AZT(1)=0
CALL NCFMAL(IRAN,RAN,LL3)
DO 1100 I=2,LL
  AXT(I)=RAN(I)
  AYT(I)=RAN(I+LL)
  AZT(I)=RAN(I+LL2)
  RX(I)=RX(I)+TASN*AXT(I)+TASF*AXT(I-1)
  RY(I)=RY(I)+TASN*AYT(I)+TASF*AYT(I-1)
  RZ(I)=RZ(I)+TASN*AZT(I)+TASF*AZT(I-1)
1100 CONTINUE
RETURN
END

```

SLERCUTINE KF100

LATTICE GENERATOR FOR A FCC (100) ORIENTATION
 LATTICE IS DEVELOPED IN THE X DIRECTION, THEN
 THE Z DIRECTION, THEN FINALLY THE Y DIRECTION

```

COMMON/COM1/RX(600),RY(600),RZ(600),LCUT(600),LL,LD
COMMON/COM2/RCE,RCE2,ROEM,AC,PAC,PPTC,PTC,PFPTC,FPTC,
X FM,PFIV,TPCT
COMMON/COM4/IX,IY,IZ,IXP,IYP,SCX,SCY,SCZ,IDEEP,
X FBX,RBZ
COMMON/COM7/R1,LSS,SPX,SPZ,COX,CCY,COZ,YLAX(20),ILL
COMMON/COM11/RXI(600),RYI(600),RZI(600)
COMMON/COM23/ SPDZ,DBXMAX,DBZMAX,SSCZ
COMMON/COM25/IMF(600),ISOGEN
COMMON/COM30/ ISEEDA, ISEEDB, ISEEDC
DIMENSION R(600)
9001 FCRMAT(' ISEED=',I10//)
9690 FCRMAT(35X,'SUMMARY OF ATOMS   FCC (100) CRIENTATION'
X  /,35X,'MASS 1 IS THE HEAVIER/LEAST ABUNDANT ISOTCPE',
X  //,3('  ATOM  MASS              POSITION              '),/)
LC=0
N=600
DO 3 I=2,N
  IMF(I)=2
3 CONTINUE
ISEED=ISEEDA
WRITE (6,9001) ISEED
WRITE (6,9690)
IF (ISOGEN.EQ.0) GO TO 4

      GENERATE RANDOM MASSES

CALL GSUB(ISEED,N,R)
DO 4 I=2,N
  IF(R(I).LE.C.309) IMF(I)=1
4 CONTINUE
DO 5 I=3,IY
5 YLAX(I)=0.0

      DETERMINE ORIENTATION PARAMETERS

SCX=1.0
SCY=1.0
SCZ=1.0
SFCX=0.1

```



```

SFCZ=0.1
LEXMAX=0.501
LEZMAX=1.001
YLAX(1)=-0.12
YLAX(2)=-0.03

```

GENERATE THE LATTICE

```

M=2
JT=0
Y=-SCY
CC 60 J=1,IY
Y=Y+SCY
KT=0
Z=-SCZ
CC 59 K=1,IZ
Z=Z+SCZ
IT=0
X=-SCX
CC 58 I=1,IX
X=X+SCX
ITT=IT+JT+KT
IF (ITT-(ITT/2)*2) 57,30,57
30 RXI(M)=X
RYI(M)=Y+YLAX(J)
RZI(M)=Z
M=M+1
57 CCNTINUE
IT =IT+1
58 CCNTINUE
KT=KT+1
59 CCNTINUE
IF (JT.EQ.0) ILL=M-1
JT = JT + 1
IF (JT.EQ.IDEEP) LD=M-1
60 CCNTINUE
LL=M-1
IF (LD.EQ.0) LD=LL-1
IF (COY.EQ.0) GO TO 120
GC TO ( 70,80,90),LSS
70 R1=RCE/ABS(COY)
GC TO 100
80 ISPX=RBX
ISPZ=RBZ
N=(IX/2)*ISPZ+ISPX/2+3
IF (IX-(IX/2)*2) 83,85,83
83 N=N+ISPX/2
85 LCLT(N)=1
R1=2.0
LCLT(2)=-1
GC TO 100
90 M=2
RXI(M)=RBX*SCX
RYI(M)=-SCY+YLAX(1)
RZI(M)=(RBZ+1.0)*SCZ
R1=(ROE+SCY)/ABS(COY)
100 CCNTINUE
110 RETURN
120 R1=1.5
RETURN
END

```

SLROUTINE KF110

LATTICE GENERATOR FOR A FCC (110) ORIENTATION
 LATTICE IS DEVELOPED IN THE X DIRECTION, THEN
 THE Z DIRECTION, THEN FINALLY THE Y DIRECTION


```

C      CCMCN/COM1/RX(600),RY(600),RZ(600),LCUT(600),LL,LD
      CCMCN/COM2/RCE,RCE2,ROEM,AC,PAC,PPTC,PTC,PFPTC,FPTC,
X      FM,PFIV,TPCT
      CCMCN/COM4/IX,IY,IZ,IXP,IYP,SCX,SCY,SCZ,IDEEP,
X      RBX,RBZ
      CCMCN/COM7/R1,LSS,SPX,SPZ,COX,CCY,COZ,YLAX(20),ILL
      CCMCN/COM11/RXI(600),RYI(600),RZI(600)
      CCMCN/COM23/SPDX,SPDZ,DBXMAX,DBZMAX,SSCZ
      CCMCN/COM25/IMF(600),ISOGEN
      CCMCN/COM30/ISEEDA,ISEEDB,ISEEDC
      DIMENSION R(600)
9001  FORMAT(' ISEED=',I10//)
9690  FORMAT(35X,'SUMMARY OF ATOMS   FCC (110) ORIENTATION'
X      /,35X,'MASS 1 IS THE HEAVIER/LEAST ABUNDANT ISOTCPE'
X      /,3('  ATOM  MASS              POSITION              '),/)
      LC=C
      N=600
      DO 3 I=2,N
      IMF(I)=2
3  CCNTINUE
      ISEED=ISEEDB
      WRITE (6,9001) ISEED
      WRITE (6,9690)
      IF (ISOGEN.EQ.0) GC TO 4

C      C      GENERATE RANDOM MASSES

      CALL GSUB(ISEED,N,R)
      DO 4 I=2,N
      IF(R(I).LE.C.309) IMF(I)=1
4  CCNTINUE
      DO 5 I=3,IY
5  YLAX(I)=0.0

C      C      DETERMINE ORIENTATION PARAMETERS

      RC=1.0/SQRT(2.0)
      SCX=RC
      SCY=RC
      SCZ=1.0
      SPDX=0.2*SCX
      SPDZ=0.2*SCZ
      DBXMAX=SCX+C.01
      DBZMAX=SCZ+C.01
      YLAX(1)=-0.15
      YLAX(2)=-0.03

C      C      GENERATE THE LATTICE

      M=2
      JT=0
      Y=-SCY
      DO 60 J=1,IY
      Y=Y+SCY
      KT=0
      Z=-SCZ
      DO 59 K=1,IZ
      Z=Z+SCZ
      IT=0
      X=-SCX
      DO 58 I=1,IX
      X=X+SCX
      IF(IT-(IT/2)*2) 21,11,21
11  IF(JT-(JT/2)*2) 57,12,57
12  IF(KT-(KT/2)*2) 57,30,57
21  IF(JT-(JT/2)*2) 22,57,22
22  IF(KT-(KT/2)*2) 30,57,30
30  RXI(M)=X
      RYI(M)=Y+YLAX(J)
      RZI(M)=Z
      M=M+1

```



```

57 CCNTINUE
   IT = IT + 1
58 CCNTINUE
   KT = KT + 1
59 CCNTINUE
   JT = JT + 1
   IF (JT.EQ.IDEEP) LD=M-1
60 CCNTINUE
   LL=M-1
   IF (LD.EQ.0) LD=LL-1
   IF (COY.EQ.0) GO TO 120
   GC TO ( 70,80,90),LSS
70 R1=RCE/ABS(COY)
   GC TO 100
80 ISPX=SPX
   ISPZ=SPZ
   N=(IX+1)/2*ISPZ/2+ISPX+2
   LCUT(N)=1
   R1=RCE/ABS(COY)
   LCUT(2)=-1
   GC TO 100
90 N=2
   RXI(M)=(SPX+1.0)*SCX
   RYI(M)=-SCY+YLAX(1)
   RZI(M)=(SPZ+1.0)*SCZ
   R1=(RCE+SCY)/ABS(COY)
100 CCNTINUE
110 RETURN
120 R1=1.5
   RETURN
END

```

SLERCUTINE KF111

LATTICE GENERATOR FOR A FCC (111) ORIENTATION
 LATTICE IS DEVELOPED IN THE X DIRECTION, THEN
 THE Z DIRECTION, THEN FINALLY THE Y DIRECTION

```

COMMON/COM1/RX(600),RY(600),RZ(600),LCUT(600),LL,LD
COMMON/COM2/RCE,RCE2,ROEM,AC,PAC,PPTC,PTC,PFPTC,FPTC,
X FM,PFIV,TPCT
COMMON/COM4/IX,IY,IZ,IXP,IYP,SCX,SCY,SCZ,IDEEP,
X REX,RBZ
COMMON/COM7/R1,LSS,SPX,SPZ,COX,CCY,COZ,YLAX(20),ILL
COMMON/COM11/RXI(600),RYI(600),RZI(600)
COMMON/COM23/SPDX,SPDZ,DBXMAX,DBZMAX,SSCZ
COMMON/COM25/IMF(600),ISOGEN
COMMON/COM30/ISEEDA,ISEEDB,ISEEDC
DIMENSION R(600)
9001 FORMAT(' ISEED=',I10//)
9690 FORMAT(35X,'SUMMARY OF ATOMS   FCC (111) ORIENTATION'
X //,35X,'MASS 1 IS THE HEAVIER/LEAST ABUNDANT ISOTCPE'
X //,3('  ATOM  MASS              POSITION              '),/)
   LC=C
   N=600
   DC 3 I=2,N
   IMF(I)=2
3 CCNTINUE
   ISEED=ISEEDC
   WRITE (6,9001) ISEED
   WRITE (6,9690)
   IF (ISOGEN.EQ.0) GO TO 4

      GENERATE RANDOM MASSES

CALL GGLB(ISEED,N,R)
DC 4 I=2,N

```



```

      IF(R(I).LE.0.309) IMF(I)=1
4  CCNTINUE
      DC 5 I=3,IY
5  YLAX(I)=0.0

```

DETERMINE ORIENTATION PARAMETERS

```

      SCX=1.0/SQRT(2.0)
      SCY=2.0/SQRT(3.0)
      SCZ=SQRT(1.5)
      SSCZ=2.0*SCZ/3.0
      SPCX=0.2*SCX
      SPCZ=0.2*SSCZ
      CBXMAX=SCX+0.01
      CEZMAX=SSCZ+0.01
      YLAX(1)=-0.05
      YLAX(2)=-0.01

```

GENERATE THE LATTICE

```

      M=2
      JT=C
      Y=-SCY
      CC 60 J=1,IY
      Y=Y+SCY
      JTS=JT+JT/3
      Z=-SCZ
      KT=C
      CC 59 K=1,IZ
      Z=Z+SCZ
      IT=C
      X=-SCX
      DC 58 I=1,IX
      X=X+SCX
      IN=IT+JTS+KT
      IF(IN-(IN/2)*2) 57,30,57
30  RXI(M)=X
      RYI(M)=Y+YLAX(J)
      IF(JT-3*(JT/3)) 41,45,41
41  JTT=JT
42  JTT=JTT-3
      IF(JTT) 43,45,42
43  JTT=JTT+3
      ZP=JTT
      RZI(M)=Z+ZP*SSCZ
      GC TO 50
45  RZI(M)=Z
50  M=M+1
57  CCNTINUE
      IT=IT+1
58  CCNTINUE
      KT=KT+1
59  CCNTINUE
      JT=JT+1
      IF(JT.EQ.IDEEP) LC=M-1
60  CCNTINUE
      LL=M-1
      IF(LD.EQ.0) LD=LL-1
      IF(COY.EQ.0) GO TO 120
      GC TC ( 70,80,90),LSS
70  R1=RCE/ABS(COY)
      LCLT(2)=-1
      GC TO 100
80  ISPX=SPX
      ISPZ=SPZ
      N=IX*(ISPZ/2)+ISPX+2
      LCLT(N)=1
      R1=RCE/ABS(COY)
      GC TC 100
90  M=2
      RXI(M)=SPX*SCX
      RYI(M)=-SCY+YLAX(1)

```



```

RZI(M)=(SPZ+1.0)*SCZ
R1=(ROE+SCY)/ABS(COY)
100 CCNTINUE
110 RETURN
120 R1=1.5
RETURN
END

```

SUBROUTINE ENERGY

THIS S/R CALCULATES THE MUTUAL POTENTIAL ENERGIES
THIS S/R ALLOWS ATTRACTIVE POTENTIALS
THIS IS THE MUNDKUR HIGH SPEED VERSION

```

CCMMCN/COM1/RX(600),RY(600),RZ(600),LCUT(600),LL,LD
CCMMCN/COM2/RCE,RCE2,ROEM,AC,PAC,PPTC,PTC,PFPTC,FPTC,
X FM,PFIV,TFCT
CCMMCN/COM3/EXA,EXB,FXA,PEXA,PEXB,PFXA,THERM
CCMMCN/COM5/FX(600),FY(600),FZ(600),PPE(600)
CCMMCN/COM22/ROEA,RCEB,ROEC,ROEC2,CPO,CPI,CF2,CP3,CF0,
X CF1,CF2,CGD1,CGD2,CGB1,CGB2,CGF,IPOG
I=1
IF(LCUT(I).NE.0) GO TO 200
IF=I+1

```

INITIAL POTENTIAL ENERGY INTERACTION
MAXIMUM DISTANCE BOUNDARIES

```

XMAX = RX(I)+ROE
YMAX = RY(I)+ROE
ZMAX = RZ(I)+ROE
XMIN = RX(I)-ROE
YMIN = RY(I)-ROE
ZMIN = RZ(I)-ROE

```

TEST TO DETERMINE IF BULLET AND ATOMS
ARE CLOSE ENOUGH TO INTERACT

```

CC 195 J=IP,LL
IF(LCUT(J).GT.0) GO TO 195
IF(RY(J).GE.YMAX) GO TO 195
IF(RY(J).LE.YMIN) GO TO 195
IF(RX(J).GT.XMAX) GO TO 195
IF(RX(J).LE.XMIN) GO TO 195
IF(RZ(J).GE.ZMAX) GO TO 195
IF(RZ(J).LE.ZMIN) GO TO 195

```

TEST TO DETERMINE IF THE ATOMS ARE INSIDE A
CIRCLE OF RADIUS ROE FROM THE BULLET

```

DRX=RX(J)-RX(I)
DRY=RY(J)-RY(I)
DRZ=RZ(J)-RZ(I)
DIST=DRX**2+DRY**2+DRZ**2
IF(DIST.GE.ROE2) GO TO 195
DIST=SQRT(DIST)

```

CALCULATION OF THE POTENTIAL ENERGY

```

PCT=EXP(PEXA+PEXB*DIST)-PPTC
IF(POT.LE.0.00001) POT=0.0
TFCT=TPCT+PCT
SAVE=PFIV*PCT
PPE(I)=PPE(I)+SAVE
PPE(J)=PPE(J)+SAVE

```

```

195 CCNTINUE
200 CCNTINUE

```



```

CC 300 I=2,LD
IF(LCUT(I).GT.0) GC TO 300
IF=I+1
XMAX = RX(I)+ROE
XMIN = RX(I)-ROE
YMAX = RY(I)+ROE
YMIN = RY(I)-ROE
ZMAX = RZ(I)+ROE
ZMIN = RZ(I)-ROE

```

TEST TO DETERMINE IF THE ATOMS
ARE CLOSE ENOUGH TO INTERACT

```

CC 295 J=IP,LL
IF(LCUT(J).GT.0) GC TO 295
IF(RY(J).GE.YMAX) GO TO 295
IF(RY(J).LE.YMIN) GO TO 295
IF(RX(J).GE.XMAX) GO TO 295
IF(RX(J).LE.XMIN) GO TO 295
IF(RZ(J).GE.ZMAX) GO TO 295
IF(RZ(J).LE.ZMIN) GO TO 295
DRX=RX(J)-RX(I)
DRY=RY(J)-RY(I)
DRZ=RZ(J)-RZ(I)
DIST=DRX**2+DRY**2+DRZ**2
IF(DIST.GE.ROE2) GC TO 295
DIST=SQRT(DIST)

```

CALCULATION OF THE POTENTIAL ENERGY

```

PCT=EXP(EXA+EXB*DIST)-PTC
IF(POT.LE.0.00001) POT=0.0
280 TPCT=TPCT+PCT
SAVE=PFIV*PCT
PPE(I)=PPE(I)+SAVE
PPE(J)=PPE(J)+SAVE
295 CCNTINUE
300 CCNTINUE
DC 310 I=1,LL
IF(LCUT(I).EQ.0) GC TO 310
TPCT=TPCT+PPE(I)
310 CCNTINUE
RETURN
END

```

SLBRROUTINE STEP

THIS S/R CALCULATES THE FORCES BETWEEN ATOMS
ATTRACTIVE FORCES ARE ALLOWED BETWEEN ATOMS
THIS IS THE MUNDKUR HIGH SPEED VERSION

```

CCMMCN/COM1/RX(600),RY(600),RZ(600),LCUT(600),LL,LD
CCMMCN/CCM2/RCE,RCE2,ROEM,AC,PAC,FPPTC,PTC,PFPTC,FPTC,
X FM,PFIV,TPOT
CCMMCN/COM3/EXA,EXB,FXA,PEXA,PEXB,PFXA,THERM
CCMMCN/COM5/FX(600),FY(600),FZ(600),PPE(600)
CCMMCN/COM22/ROEA,ROEB,ROEC,ROEC2,CPO,CPI,CP2,CP3,CFO,
X CF1,CF2,CGD1,CGD2,CGB1,CGB2,CGF,IPROG
I=1
IF(LCUT(I).NE.0) GO TO 200
IF=I+1

```

INITIAL FORCE DISTANCE BOUNDARIES

```

XMAX = RX(I)+ROE
YMAX = RY(I)+ROE

```



```

ZMAX = RZ(I)+ROE
XMIN = RX(I)-ROE
YMIN = RY(I)-ROE
ZMIN = RZ(I)-ROE

```

```

TEST TO DETERMINE IF BULLET AND ATOMS ARE
CLOSE ENOUGH TO INTERACT AND WHICH FORCE
FUNCTION TO USE

```

```

CC 195 J=IP,LL
IF(LCUT(J).GT.0) GO TO 195
IF(RY(J).GE.YMAX) GO TO 195
IF(RY(J).LE.YMIN) GO TO 195
IF(RX(J).GT.XMAX) GO TO 195
IF(RX(J).LE.XMIN) GO TO 195
IF(RZ(J).GE.ZMAX) GO TO 195
IF(RZ(J).LE.ZMIN) GO TO 195

```

```

TEST TO DETERMINE IF ATCM IS INSIDE A CIRCLE
OF RADIUS ROE FROM THE BULLET

```

```

DRX=RX(J)-RX(I)
DRY=RY(J)-RY(I)
DRZ=RZ(J)-RZ(I)
DIST=DRX**2+DRY**2+DRZ**2
IF(DIST.GE.ROE2) GO TO 195
DIST=SQRT(DIST)
IF(DIST.GT.RCEM) GO TO 165

```

```

ACTUAL FORCE FUNCTION DETERMINED FROM THE
BCRM-MEYER BULLET-ATCM PCTENTIAL

```

```

FCRCE=EXP(PFXA+PEXB*DIST)
GO TO 180

```

```

165 CFF=ROE-DIST
IF(DFF.LT.1.0E-10) GO TO 195

```

```

AN AVERAGE FORCE FUNCTION FOR THE BULLET-ATCM
INTERACTION AT TURNON

```

```

FCRCE=(EXP(PAC+PEXB*DIST)-PFPTC)/CFF
IF(FM.GT.FCRCE) GO TO 195

```

```

180 FCD =FORCE/DIST
FA = FCD*DRX
FX(J) = FX(J)+FA
FX(I) = FX(I)-FA
FA = FCD*DRY
FY(J) = FY(J)+FA
FY(I) = FY(I)-FA
FA = FCD*DRZ
FZ(J) = FZ(J)+FA
FZ(I) = FZ(I)-FA

```

```

195 CCNTINUE
200 CCNTINUE

```

```

CC 300 I=2,LD
IF(LCUT(I).GT.0) GO TO 300
IF=I+1
XMIN = RX(I)-ROE
XMAX = RX(I)+ROE
YMIN = RY(I)-ROE
YMAX = RY(I)+ROE
ZMIN = RZ(I)-ROE
ZMAX = RZ(I)+ROE

```

```

TEST TO DETERMINE WHETHER ATOMS ARE CLOSE
ENOUGH TO INTERACT AND WHICH FORCE FUNCTION
TO USE.

```

```

DC 295 J=IP,LL
IF(LCUT(J).GT.0) GO TO 295
IF(RY(J).GE.YMAX) GO TO 295
IF(RY(J).LE.YMIN) GO TO 295

```



```

IF(RX(J).GE.XMAX) GC TO 295
IF(RX(J).LE.XMIN) GO TO 295
IF(RZ(J).GE.ZMAX) GO TO 295
IF(RZ(J).LE.ZMIN) GO TO 295
CRX=RX(J)-RX(I)
DRY=RY(J)-RY(I)
CRZ=RZ(J)-RZ(I)
DIST=DRX**2+DRY**2+DRZ**2
IF(DIST.GE.ROE2) GO TO 295
DIST=SQRT(DIST)
IF(DIST.GT.ROEM) GC TO 265

```

ACTUAL FORCE FUNCTION DETERMINED FROM THE
CU-CU (GIB-II) POTENTIAL FUNCTION

```

FCRCE=EXP(FXA+EXB*DIST)

```

```

GC TO 280

```

```

265 DFF=ROE-DIST

```

```

IF(DFF.LT.1.0 E-10) GO TO 295

```

AN AVERAGE FORCE FUNCTION FOR THE ATCM-ATCM
INTERACTION AT TURN ON

```

FCRCE=(EXP(AC+EXB*DIST)-FPTC)/DFF

```

```

IF(FM.GT.FORCE) GC TO 295

```

```

280 FCC=FORCE/DIST

```

```

FA=FOD*CRX

```

```

FX(J)=FX(J)+FA

```

```

FX(I)=FX(I)-FA

```

```

FA=FOD*DRY

```

```

FY(J)=FY(J)+FA

```

```

FY(I)=FY(I)-FA

```

```

FA=FOD*DRZ

```

```

FZ(J)=FZ(J)+FA

```

```

FZ(I)=FZ(I)-FA

```

```

295 CCNTINUE

```

```

300 CCNTINUE

```

```

RETURN

```

```

END

```

SUBROUTINE KPRINT

THIS SUBROUTINE PRINTS THE PAGE HEADING

```

CCMMCN/COM1/RX(600),RY(600),RZ(600),LCUT(600),LL,LD

```

```

CCMMCN/COM3/EXA,EXB,FXA,PEXA,PEXB,PFXA,THERM

```

```

CCMMCN/COM4/IX,IY,IZ,IXP,IYP,SCX,SCY,SCZ,IDEEP,

```

```

X RBX,RBZ

```

```

CCMMCN/COM7/R1,LSS,SPX,SPZ,CCX,CCY,COZ,YLAX(20),ILL

```

```

CCMMCN/COM11/RXI(600),RYI(600),RZI(600)

```

```

CCMMCN/COM16/BMAS,TMAS1,TMAS2,ABUN1,ABUN2,IPNUM

```

```

CCMMCN/COM16A/BX,BY,BZ,EDISP,CVR

```

```

CCMMCN/COM17/TIME,NT,DT,DTI,TEMP,CELS,EV,NPAGE,NLINE

```

```

CCMMCN/COM18/ ITEMP,TAMP,CORF

```

```

CCMMCN/COM20/IH1(20),IHS(10),IHT(6),IHB(6),IHTARG(2),

```

```

X IHBULL(2)

```

```

CCMMCN/COM21/IHBPCT(2),IHTPOT(2),SUR(2),IH2(10),IOR,

```

```

X LSLR

```

```

CCMMCN/COM22/ROEA,ROEB,ROEC,ROEC2,CPO,CP1,CP2,CP3,CFO,

```

```

X CF1,CF2,CGC1,CGD2,CGB1,CGB2,CGF1,CGF2,IPRCG

```

```

9610 FORMAT(2CX,20A4,/,4CX,10A4,///)

```

```

9640 FCRMAT(' ',I3,' ) PLANE ',2A4,' SURFACE, PRIMARY',

```

```

X ' ENERGY =',F7.1,' EV, CRYSTAL SIZE (' ,I2,' X ' ,I2,

```

```

X ' X ' ,I2,' ), IMPACT PCINT ' ,I9/)

```

```

9645 FCRMAT(' TARGET -',2A4,20X,' BULLET -',2A4,7X,

```

```

X ' LATTICE UNIT =',F7.4,' ANG')

```

```

9650 FCRMAT(' MASS1 =',F7.2,2X,' ABUNDANCE =',F5.3,6X,

```



```

X 'MASS =' ,F7.2,9X,'LATTICE TEMPERATURE =' ,A4,
X 'THERMAL AMPLITUDE =' ,F7.4)
9652 FCRMAT(' MASS2 =' ,F7.2,2X,'ABUNDANCE =' ,F5.3,
X 29X,'CORRELATION =' ,F5.3,/)
9655 FCRMAT(12X,2(2A4,1X),2A4,3X,5HPEXA=,F9.5,2X,5HPEXB=,
X F9.5,2X,5HPEXA=,F9.5/)
9660 FCRMAT(12H POTENTIAL ,2(2A4,1X),2A4,3X,5HPEXA =,F9.5,
X 2X,5HPEXB =,F9.5,2X,5HPEXA =,F9.5)
9665 FCRMAT(30H TARGET POINT ON CRYSTAL X =,F7.3,', Y =',
X F7.3,', Z =',F7.3,13H, COS TO X =,F8.5,
X 12H, CCS TO Z =,F8.5)
9670 FCRMAT(30H PRIMARY START POINT (LU) X =,F7.3,5H, Y =,
X F7.3,5H, Z =,F7.3/)
9675 FCRMAT(/,TIMESTEP ,I4,40X,' ELAPSED TIME (SEC) =' ,
X E10.4,', LAST TIMESTEP WAS =' ,E10.4/)
9725 FCRMAT(' CUT-OFF AT',F5.2,', WHEN R =' ,F6.3,' LU,MORSE
X POTENTIAL PARAMETERS ARE',10A4,/,10X,' CGD1 =' ,
X F8.4,', CGD2 =' ,F8.4,', CGB1 =' ,F8.4,', CGB2 =' ,
X F8.4,', CGF1 =' ,F8.4,', CGF2 =' ,F8.4,/)
9730 FCRMAT(' WHEN',F8.4,' <R<',F8.4,' THE MATCHING POTENTI
X AL PARAMETER ARE',/,3X,' CPC =' ,E12.4,', CP1 =' ,
X E12.4,', CP2 =' ,E12.4,', CP3 =' ,E12.4,/,7X,' CFO =' ,
X E12.4,', CF1 =' ,E12.4,', CF2 =' ,E12.4,/)
9740 FCRMAT(11H THE FIRST ,I3,22H ATOMS ARE BLOCKED, ,I3,
X 24H LAYERS ARE FREE TO MOVE,/)
WRITE ( 6,9610) I-1,IHS
WRITE ( 6,9640) ICR,SUR,EV,IX,IY,IZ,IPNUM
WRITE ( 6,9645) IHTARG,IHBULL,CVR
WRITE (6,9650) TMA51,ABUN1,BMAS,ITEMP,TAMP
WRITE (6,9652) TMA52,ABUN2,CORF
WRITE ( 6,9660) IHT,EXA,EXB,FXA
WRITE ( 6,9655) IHB,PEXA,PEXB,PEXA
WRITE ( 6,9665) BX,BY,BZ,COX,CCY,CCZ
WRITE ( 6,9670) RXI(1),RYI(1),RZI(1)
IF(IPROG.NE.4) GO TO 100
WRITE ( 6,9730) RCEA,ROEB,CPO,CP1,CP2,CP3,CFO,CF1,CF2
WRITE(6,9725)ROEC,ROEB,IH2,CGD1,CGD2,CGB1,CGB2,CGF1,
X CGF2
100 WRITE ( 6,9675) NT,TIME,DT
NLINE=1
RETURN
END

```

SLBROUTINE KPNT

THIS SUBROUTINE PRINTS THE HEADING
FOR OUTPUT THAT IS FILED

```

CCCMCN/COM4/IX,IY,IZ,IXP,IYP,SCX,SCY,SCZ,IDEEP,
X RBX,RBZ
CCCMCN/COM16/BMAS,TMA51,TMA52,ABUN1,ABUN2,IPNUM
CCCMCN/COM16A/BX,BY,BZ,EDISP,CVR
CCCMCN/COM17/TIME,NT,DT,DTI,TEMP,CELS,EV,NPAGE,NLINE
CCCMCN/COM20/IH1(20),IHS(10),IHT(6),IHB(6),IHTARG(2),
X IHBULL(2)
CCCMCN/COM21/IHBPCT(2),IHTPOT(2),SUR(2),I-2(10),IOR,
X LSUR
9640 FCRMAT(' (' ,I3,' ) PLANE',10X,' ION ENERGY =' ,F7.1,10X,
X 'CRYSTAL SIZE (' ,I2,' X',I2,' X',I2,' )',/)
9645 FCRMAT(' TARGET -',2A4,20X,' BULLET -',2A4,6X,
X 'PCTENTIAL ',2(2A4,1X),2A4)
9650 FCRMAT(' MASS 1 =' ,F7.2,2X,'ABUNDANCE =' ,F5.3,4X,
X 'MASS =' ,F7.2,16X,2(2A4,1X),2A4)
9652 FCRMAT(' MASS 2 =' ,F7.2,2X,'ABUNDANCE =' ,F5.3,/)
WRITE (6,9640) IOR,EV,IX,IY,IZ
WRITE (6,9645) IHTARG,IHBULL,IHT
WRITE (6,9650) TMA51,ABUN1,BMAS,IHB

```



```

WRITE (6,9652) TMS2,ABUN2
RETURN
END

```

```

SUBROUTINE HISTO(IN,FREQ1,RANGE,TITLE1)

```

```

      THIS SUBROUTINE DRAWS THE HISTORAM (FREQUENCY
      VS. EJECTED ANGLE) FOR THE TYPE 1 HEAVY ATOMS

```

```

      DIMENSION FREQ1(20),RANGE(20),JOUT(20),TITLE1(24)
      DIMENSION PCUT(20)
      DATA NOTH/' ','/','K','*','*','*','/'
3  FCFMAT('OINTERVAL',2X,19(F5.1,1X),F5.1)
4  FCFMAT('/',8X,24A4/)
5  FCFMAT('OFREQUENCY',20I6)
6  FCFMAT('OINTERVAL',2X,19(F5.1,1X),F5.1)
7  FCFMAT(' ','-',128(' ','-'))
      WRITE (6,4) TITLE1
      JN=IN
      INT=0
      IF(JN.GT.0) GO TO 10
      INT=1
      JN=-JN
10  DO 12 I=1,JN
12  JCLT(I)=FREQ1(I)
      WRITE (6,5) (JOUT(I),I=1,JN)
      WRITE (6,7)

      FIND LARGEST FREQUENCY

      FMAX=0.
      DO 20 I=1,JN
      IF(FREQ1(I).GT.FMAX) FMAX=FREQ1(I)
20  CCNTINUE

      SCALE

      JSCAL=1
      IF(FMAX.GT.60.) JSCAL=(FMAX+59.)/60.
      FSCAL=JSCAL
      DO 50 I=1,JN
50  JCLT(I)=NOTH
      MAX=FMAX/FSCAL
      DO 80 I=1,MAX
      X=MAX-(I-1)
      DO 70 J=1,JN
      IF(FREQ1(J)/FSCAL.GE.X) JOUT(J)=K
70  CCNTINUE
      IX=X*FSCAL
80  WRITE (6,2) IX,(JOUT(J),J=1,JN)
      2 FCFMAT(I6,4X,20(2X,A4))
      WRITE (6,7)
      IF(INT.EQ.1) GO TO 16
      WRITE (6,3) (RANGE(J),J=1,JN)
      GO TO 15
16  DO 51 I=1,JN
51  PCUT(I)=RANGE(I)
      WRITE (6,6) (PCUT(I),I=1,JN)
15  CCNTINUE
      WRITE (6,100)
100 FCFMAT(1X,'MIDPOINT'/)
      RETURN
      END

```


SLROUTINE HISTO(IN,FREQ2,RANGE,TITLE2)

THIS SUBROUTINE DRAWS THE HISTORAM (FREQUENCY
VS. EJECTED ANGLE) FOR THE TYPE2 LIGHT ATOMS

```

DIMENSION FREQ2(20),RANGE(20),JOUT(20),TITLE2(24)
DIMENSION PCUT(20)
DATA NOTH/' ',K/'****'/
2  FCFMAT(I6,4X,2J(2X,A4))
3  FCFMAT('0INTERVAL',2X,19(F5.1,1X),F5.1)
4  FCFMAT('/',8X,24A4/)
5  FCFMAT('0FREQUENCY',20I6)
6  FCFMAT('0INTERVAL',2X,19(F5.1,1X),F5.1)
7  FCFMAT('-',128('-',))
WRITE (6,4) TITLE2
JN=IN
INT=0
IF(JN.GT.0) GO TO 10
INT=1
JN=-JN
10 DC 12 I=1,JN
12 JCLT(I)=FREQ2(I)
WRITE (6,5) (JOUT(I),I=1,JN)
WRITE (6,7)

FIND LARGEST FREQUENCY

FMAX=0.
CC 20 I=1,JN
IF(FREQ2(I).GT.FMAX) FMAX=FREQ2(I)
20 CCNTINUE

SCALE

JSCAL=1
IF(FMAX.GT.60.) JSCAL=(FMAX+59.)/60.
FSCAL=JSCAL
DC 50 I=1,JN
50 JCLT(I)=NOTH
MAX=FMAX/FSCAL
CC 80 I=1,MAX
X=MAX-(I-1)
CC 70 J=1,JN
IF(FREQ2(J)/FSCAL.GE.X) JOUT(J)=K
70 CCNTINUE
IX=X*FSCAL
80 WRITE (6,2) IX,(JOUT(J),J=1,JN)
WRITE (6,7)
IF(INT.EQ.1) GO TO 16
WRITE (6,3) (RANGE(J),J=1,JN)
GO TO 15
16 CC 51 I=1,JN
51 PCUT(I)=RANGE(I)
WRITE (6,6) (POUT(I),I=1,JN)
15 CCNTINUE
WRITE (6,100)
100 FCFMAT(1X,'MIDPOINT'/)
RETURN
END

```

SLROUTINE KFOLDA

THIS SUBROUTINE STATISTICALLY FOLDS THE
TARGET IMPACT AREA FOR THE FCC (100) CRYSTAL
LATTICE TO REPRESENT FULL COVERAGE

15C CCNTINUE
GC TO 210

CC
C SECOND (HORIZONTAL) FOLD - EVEN LAYERS

16C K=NLAY-IX/2+1
DO 200 J=NFIRST,NLAY
LNUM(J)=LNUM(J)+LNUM(K)
IF(J.EQ.K) LNUM(J)=2*LNUM(J)
LNUM(K)=LNUM(J)
ICCOUNT=ICCOUNT+1
IF(ISET.EQ.1) GO TO 180
IF(ICCOUNT.GT.IX/2) GO TO 170
K=K+1
GC TO 200
170 ISET=1
K=K-IX+1
ICCOUNT=1
GC TO 200
180 IF (ICCOUNT.GT.IX/2+1) GO TO 190
K=K+1
GC TO 200
190 ISET=0
K=K-IX+1
ICCOUNT=1
200 CCNTINUE
210 DO 220 J=NFIRST,NLAY
LNUM(J)=LNUM(J)/2
220 CCNTINUE

C
C THIRD (VERTICAL) FOLD - ODD LAYERS

ICCOUNT=1
ISET=0
GC TO (230,280,230,280,230,280), ILAYER
23C K=NFIRST+IX/2
DO 270 J=NFIRST,NLAY
LNUM(J)=LNUM(J)+LNUM(K)
IF(J.EQ.K) LNUM(J)=2*LNUM(J)
LNUM(K)=LNUM(J)
ICCOUNT=ICCOUNT+1
IF(ISET.EQ.1) GO TO 250
IF(ICCOUNT.GT.IX/2 +1) GO TO 240
K=K-1
GC TO 270
240 ISET=1
K=K+IX-1
ICCOUNT=1
GC TO 270
250 IF (ICCOUNT.GT.IX/2) GO TO 260
K=K-1
GC TO 270
260 ISET=0
K=K+IX-1
ICCOUNT=1
270 CCNTINUE
GC TO 330

C
C THIRD (VERTICAL) FOLD - EVEN LAYERS

280 K=NFIRST+IX/2-1
DO 320 J=NFIRST,NLAY
LNUM(J)=LNUM(J)+LNUM(K)
IF(J.EQ.K) LNUM(J)=2*LNUM(J)
LNUM(K)=LNUM(J)
ICCOUNT=ICCOUNT+1
IF(ISET.EQ.1) GO TO 300
IF(ICCOUNT.GT.IX/2) GO TO 290
K=K-1
GC TO 320
290 ISET=1
K=K+IX-1


```

      ICCUNT=1
      GC TO 320
300  IF(ICOUNT.GT.IX/2+1) GO TO 310
      K=K-1
      GC TO 320
310  ISET=0
      K=K+IX-1
      ICCUNT=1
320  CCNTINUE
330  CC 340 J=NFIRST,NLAY
      LNUM(J)=LNUM(J)/2
340  CCNTINUE
      ILAYER=ILAYER+1
      NFIRST=NLAY+1
      IF(ILAYER.GT.IY) GO TO 350
      GC TO 10
350  RETURN
      ENC

```

SLEROUTINE KFOLDB

THIS SUBROUTINE STATISTICALLY FOLDS THE
TARGET IMPACT AREA FOR THE FCC (110) CRYSTAL
LATTICE TO REPRESENT FULL COVERAGE

```

      CCMCN/COM1/RX(600),RY(600),RZ(600),LCUT(600),LL,LD
      CCMCN/COM4/IX,IY,IZ,IXP,IYP,SCX,SCY,SCZ,IDEEP,
X   REX,RBZ
      CCMCN/COM4A/ LNUM(600),LNUMI(600),LNUMF(600)
      CCMCN/COM21/IHBPOT(2),IHTPOT(2),SUR(2),IF2(10),IOR,
X   LSLR
      ILAYER=1
      NFIRST=2

```

DETERMINE THE FIRST ATOM AND THE LARGEST
NUMBERED ATOM IN EACH LAYER

```

10  GC TO (20,30,40,30,40,30),ILAYER
20  NLAY=((IX+1)/2)*((IZ+1)/2)+1
      NLAY1=NLAY
      GC TO 50
30  NLAY=NLAY + (IX/2)*(IZ/2)
      GC TO 50
40  NLAY=NLAY+NLAY1-1
50  ICCUNT=1
      GC TO (60,90,60,90,60,90),ILAYER

```

SECCND (HCRIZONTAL) FOLD - ODD LAYERS

```

60  K=NLAY-IX/2
      CC 80 J=NFIRST,NLAY
      LNUM(J)=LNUM(J)+LNUM(K)
      IF(J.EQ.K) LNUM(J)= 2*LNUM(J)
      LNUM(K)=LNUM(J)
      ICCUNT=ICCUNT+1
      IF (ICCUNT.GT. IX/2 +1) GO TO 70
      K=K+1
      GC TO 80
70  K=K-IX
      ICCUNT=1
80  CCNTINUE
      GC TO 120

```

SECCND (HCRIZONTAL) FOLD - EVEN LAYERS

```

90  K=NLAY-IX/2 +1
      CC 110 J=NFIRST,NLAY

```



```

      CCMCN/COM21/IHBPCT(2),IHTPCT(2),SUR(2),IH2(10),ICR,
X  LSLR
      CC 1 J=2,LL
        LNUMF(J)=0
        LNUMI(J)=LNUM(J)
1  CCNTINUE
      ICCT=0
      ITIME=1
      NLAY=((LL-2)/(IY/2))/2+2
2  NFIRST=2+ IX/2
      ICCUNT=0
      ISET=0
      K=NLAY-IX/2
      J=NFIRST
5  CCNTINUE

```

FIRST (+ SLOPE DIAGONAL) FOLD - FIRST LAYER

```

      LNUM(J)=LNUM(J)+LNUM(K)
      IF (J.EQ.K) LNUM(J)=2*LNUM(J)
      LNUM(K)=LNUM(J)
      ICCUNT=ICCUNT+1
      IF (ISET.EQ.0 .AND. ICOUNT.EQ.1) GO TO 10
      IF (ISET.EQ.0 .AND. ICOUNT.EQ.2) GO TO 15
      IF (ISET.EQ.0 .AND. ICOUNT.EQ.3) GO TO 20
      IF (ISET.EQ.2 .AND. ICOUNT.EQ.1) GO TO 22
      IF (ISET.EQ.2 .AND. ICOUNT.EQ.2) GO TO 15
      IF (ISET.EQ.2 .AND. ICOUNT.EQ.3) GO TO 10
      IF (ISET.EQ.2 .AND. ICOUNT.EQ.4) GO TO 35
      IF (ICOUNT.EQ.4 .OR. ICOUNT.EQ.8 .OR. ICCUNT.EQ.13
X  .CR. ICOUNT.EQ.17) GO TO 25
      IF (ICCUNT.EQ.20) GO TC 30
      J=J+1
      K=K+5
      GC TO 5
10  J=J+(IX-3)/2
      K=K-IX
      GC TO 5
15  J=J+1
      K=K+(IX+1)/2
      GC TO 5
20  ISET=ISET+1
      ICCUNT=0
22  J=J+2
      K=K-14
      GC TO 5
25  K=K-19
      J=J+1
      GC TO 5
30  ISET=ISET+1
      ICCUNT=0
      J=J+1
      K=K+5
      GC TO 5
35  IF (ICOUNT.EQ.1) GO TO 150
      GC TO (50,50,100),ITIME

```

SECCND (- SLOPE DIAGONAL) - FIRST LAYER

```

50  CCNTINUE
      NFIRST=2
      IFLAG=0
      ICCUNT=0
      ISET=0
      ICCT=0
      K=NLAY
      J=NFIRST
55  CCNTINUE
      LNUM(J)=LNUM(J)+LNUM(K)
      IF (J.EQ.K) LNUM(J)=2*LNUM(J)
      LNUM(K)=LNUM(J)
      ICCUNT=ICCUNT+1

```



```

IF (ISET.EQ.0 .AND. ICOUNT.EQ.1) GO TO 60
IF (ISET.EQ.0 .AND. ICOUNT.EQ.2) GO TO 65
IF (ISET.EQ.0 .AND. ICOUNT.EQ.3) GO TO 70
IF (ISET.EQ.2 .AND. ICOUNT.EQ.1) GO TO 72
IF (ISET.EQ.2 .AND. ICOUNT.EQ.2) GO TO 65
IF (ISET.EQ.2 .AND. ICOUNT.EQ.3) GO TO 60
IF (ISET.EQ.2 .AND. ICOUNT.EQ.4) GO TO 85
IF (ICOUNT.EQ.4 .OR. ICOUNT.EQ.17) GO TO 75
IF (ICOUNT.EQ.8 .OR. ICOUNT.EQ.13) GO TO 77
IF (ICOUNT.EQ.20) GO TO 80
J=J+1
K=K-4
GC TO 55
60 J=J+5
K=K-5
GC TO 55
65 J=J+1
K=K-4
GC TO 55
70 ISET=ISET+1
ICOUNT=0
72 J=J+3
K=K+3
GC TO 55
75 J=J+2
K=K+7
GC TO 55
77 J=J+1
K=K+11
GC TO 55
80 ISET=ISET+1
ICOUNT=0
J=J+1
K=K-4
GC TO 55
85 GC TO (100,95,150),ITIME
95 ICLT=1
GC TO 2

```

CC C C THIRD (VERTICAL) FOLD - FIRST LAYER

```

100 CCNTINUE
ICOUNT=1
ISET=0
NFIRST=2
K=NFIRST+IX/2
DC 140 J=NFIRST,NLAY
LNLM(J)=LNLM(J)+LNLM(K)
IF (J.EQ.K) LNLM(J)=2*LNLM(J)
LNLM(K)=LNLM(J)
ICOUNT=ICOUNT+1
IF (ISET.EQ.1) GO TO 120
IF (ICOUNT.GT. IX/2 +1) GO TO 110
K=K-1
GC TO 140
110 ISET=1
K=K+IX-1
ICOUNT=1
GC TO 140
120 IF (ICOUNT.GT. IX/2) GO TO 130
K=K-1
GC TO 140
130 ISET=0
K=K+IX-1
ICOUNT=1
140 CCNTINUE
GC TO (150,150,50),ITIME
150 ITIME=ITIME+1
ICLT=0
ICOUNT=0
DC 152 J=2,NLAY
LNLM(J)=LNLM(J)/8

```



```

      LNUMF(J)=LNUMF(J)+LNUM(J)
152  CCNTINUE
      IF (ITIME.GT.3) GC TO 160
      CC 155 J=2,NLAY
      LNUM(J)=LNUMI(J)
155  CCNTINUE
      GC TO 2
160  CC 170 J=2,NLAY
      LNUM(J)=LNUMF(J)/4
170  CCNTINUE
      K=NLAY+1
      CC 180 J=K,LL
      LNUM(J)=6*LNUM(J)
180  CCNTINUE
      RETURN
      END

```

SUBROUTINE KPROB

KPROB IS DESIGNED TO STUDY THE PROBABILITY
THAT A RING OF ATOMS (AT A GIVEN DISTANCE FROM
THE LAYER CENTER) WILL SPLITTER

```

      CCMCN/COM1/RX(600),RY(600),RZ(600),LCUT(600),LL,LD
      CCMCN/COM4/IX,IY,IZ,IXF,IYP,SCX,SCY,SCZ,IDEEP,
X    FEX,RBZ
      CCMCN/COM4A/ LNUM(600),LNUMI(600),LNUMF(600)
      CCMCN/COM11/RXI(600),RYI(600),RZI(600)
      CCMCN/COM21/IHBPCT(2),IHPCT(2),SUR(2),IH2(10),ICR,
X    LSLR
      CCMCN/COM24/ DNN(100),KATOM(100),KSPUT(100),PROB(100)
      CCMCN/COM24A/ KSLM,KRING,RDIST(600)
      CC 2 I=1,100
      KATCM(I)=0
      KSPLT(I)=0
      FRCB(I)=0.0
2    CCNTINUE

```

DETERMINE THE DISTANCE FROM EACH ATOM TO THE
INITIAL (0,0) POINT OF TARGET IMPACT AREA

```

      CC 5 I=2,LL
      XDIST=RXI(I)-RBX*SCX
      ZDIST=RZI(I)-RBZ*SCZ
      SDIST=XDIST**2 +ZDIST**2
      RCIST(I)=SDIST**.5
5    CCNTINUE
      KFIRST=1
      ILAYER=1
      NFIRST=2
      IF (IOR.EQ.110) GC TO 170
      IF (IOR.EQ.111) GC TO 200

```

DETERMINE THE FIRST ATOM AND THE LARGEST
NUMBERED ATOM IN EACH LAYER FOR 100 LATTICE

```

10  GC TO (20,30,40,50,60,70), ILAYER
20  NLAY=((LL-1)/(IY/2))/2+2
      NLAY1=NLAY
      GC TO 80
30  NLAY=((LL-1)/(IY/2))+1
      GC TO 80
40  NLAY=NLAY1 + NLAY -1
      GC TO 80
50  NLAY = NLAY1 + NLAY -2
      GC TO 80
60  NLAY = NLAY1 + NLAY -3

```



```

GC TO 80
70 NLAY = NLAY1 + NLAY -4
GC TO 80

```

```

C
C      SORT DISTANCES IN A LAYER INTO ASCENDING ORDER
C

```

```

80 N1=NLAY-1
DC 100 I=NFIRST,N1
NF1=I+1
CC 90 J=NF1,NLAY
IF (RDIST(J).GE.RDIST(I)) GO TO 90
SAVE=RDIST(I)
RDIST(I)=RDIST(J)
RDIST(J)=SAVE
90 CCNTINUE
100 CCNTINUE

```

```

C
C      ESTABLISH A RING AT EACH DISTANCE (+ OR - DR)
C

```

```

K=KFIRST
DC 120 I=NFIRST,NLAY
J=I+1
IF (J.GT.NLAY) GO TO 110
IF (RDIST(J)-RDIST(I).GT.0.001) GC TO 110
GC TO 120
110 DNN(K)=RDIST(I)
K=K+1
120 CCNTINUE

```

```

C
C      REINITIALIZE THE DISTANCE FROM EACH ATOM
C      TO THE REFERENCE (0,0) POINT OF IMPACT AREA
C

```

```

CC 145 I=2,LL
XCIST=RXI(I)-RBX*SCX
ZCIST=RZI(I)-RBZ*SCZ
SCIST=XCIST**2 + ZCIST**2
RDIST(I)=SCIST**.5
145 CCNTINUE

```

```

C
C      DETERMINE THE NUMBER OF ATOMS AND SPOTS FROM
C      ATOMS IN EACH RING
C

```

```

KRING=K-1
DC 150 J=KFIRST,KRING
CC 140 I=NFIRST,NLAY
IF (ABS(RDIST(I)-DNN(J)).LT.0.001) GO TO 130
GC TO 140
130 KATOM(J)=KATOM(J)+1
KSPUT(J)=KSPUT(J)+LNUM(I)
140 CCNTINUE

```

```

C
C      DETERMINE THE PROBABILITY OF AN ATOM IN EACH
C      RING SPUTTERING
C

```

```

IF (KSUM.EQ.0) KSUM=1
IF (IOR.EQ.100) PROB(J)=FLOAT(KSPUT(J))/(FLCAT(KSUM)*
X 8.0)
IF (IOR.EQ.110) PROB(J)=FLOAT(KSPUT(J))/(FLCAT(KSUM)*
X 4.0)
IF (IOR.EQ.111) PROB(J)=FLOAT(KSPUT(J))/(FLCAT(KSUM)*
X 6.0)
150 CCNTINUE
ILAYER=ILAYER+1
NFIRST=NLAY+1
KFIRST=K
155 IF (ILAYER.GT.IY) GO TO 160
IF (IOR.EQ.100) GC TO 10
IF (IOR.EQ.110) GC TO 170
IF (IOR.EQ.111) GC TO 200
160 RETURN

```

```

C
C      DETERMINE THE FIRST ATOM AND THE LARGEST

```



```

C          NUMBERED ATOM IN EACH LAYER FOR 110 LATTICE
C
17C GC TO (180,190,195,190,195,190),ILAYER
18C NLAY=((IX+1)/2)*((IZ+1)/2)+1
    NLAY1=NLAY
    GC TO 8C
19C NLAY=NLAY + (IX/2)*(IZ/2)
    GC TO 8C
195 NLAY=NLAY+((IX+1)/2)*((IZ+1)/2)
    GC TO 8C

```

```

C          DETERMINE THE FIRST ATOM AND THE LARGEST
C          NUMBERED ATOM IN EACH LAYER FOR 111 LATTICE
C
20C GC TO (210,220,230,240),ILAYER
21C NLAY=((LL-2)/(IY/2))/2+2
    NLAY1=NLAY
    GC TO 8C
22C NLAY=((LL-2)/(IY/2))+1
    GC TO 8C
23C NLAY=NLAY1+NLAY-1
    GC TO 8C
24C NLAY=NLAY1+NLAY-1
    GC TO 8C
    END

```

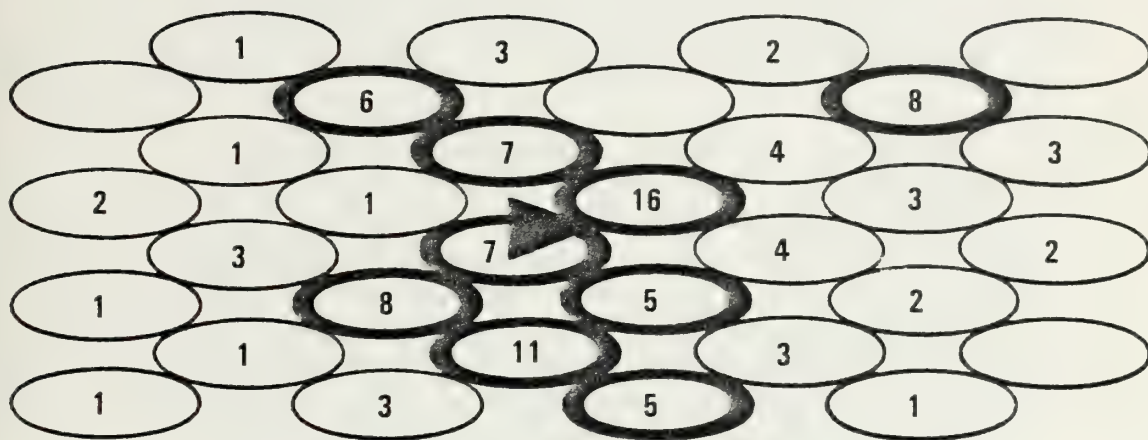



Figure 1 - Sputtering Summary - (100) 2keV Cu/Ne+ KSE-B

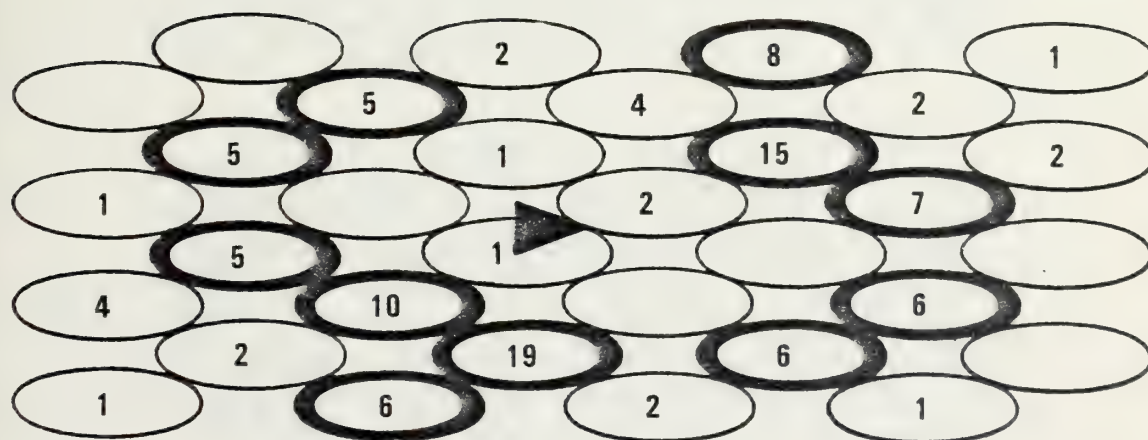


Figure 2 - Sputtering Summary - (100) 2keV Cu/Au+ KSE-B

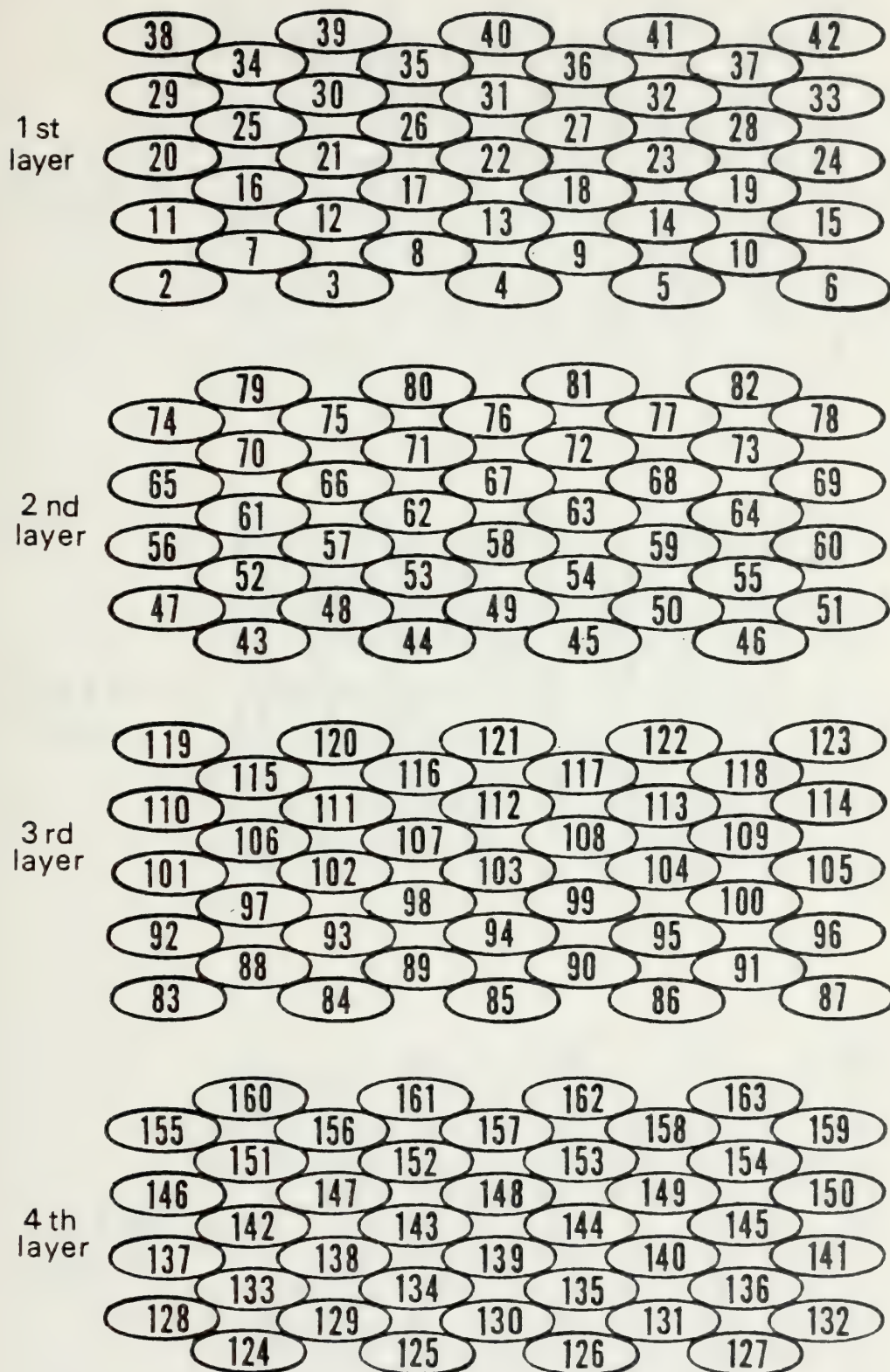
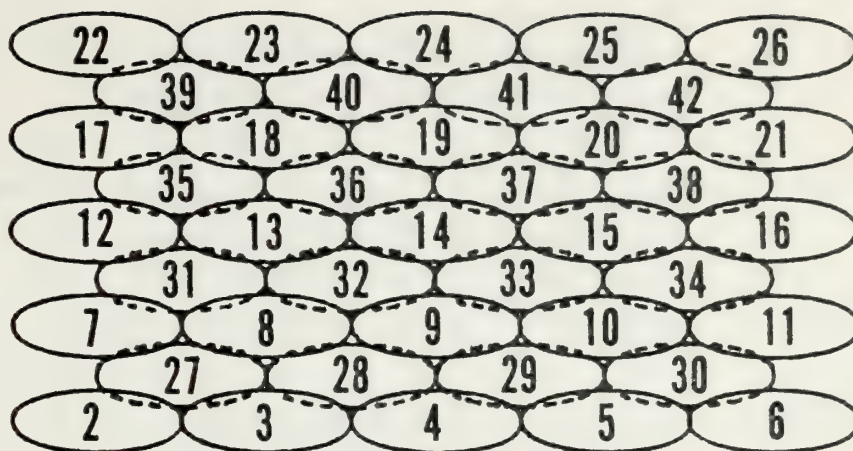
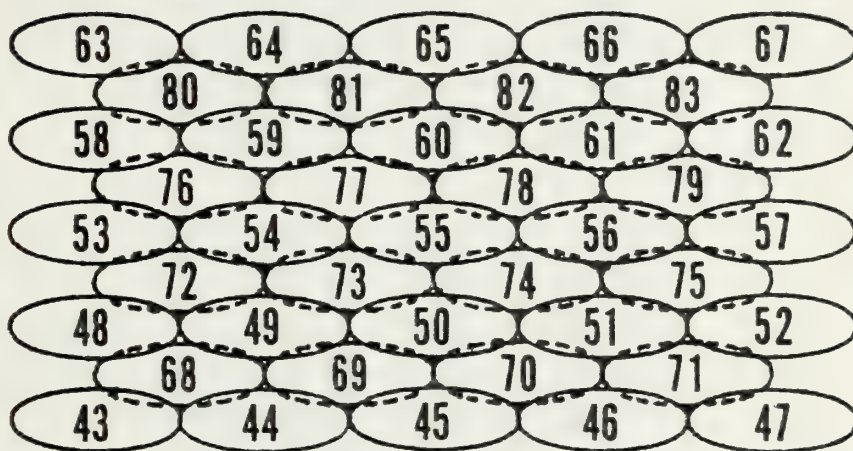


Figure 3 - 9x4x9, (100) Orientation Microcrystallite

1st & 2nd
layers



3rd & 4th
layers



5th & 6th
layers

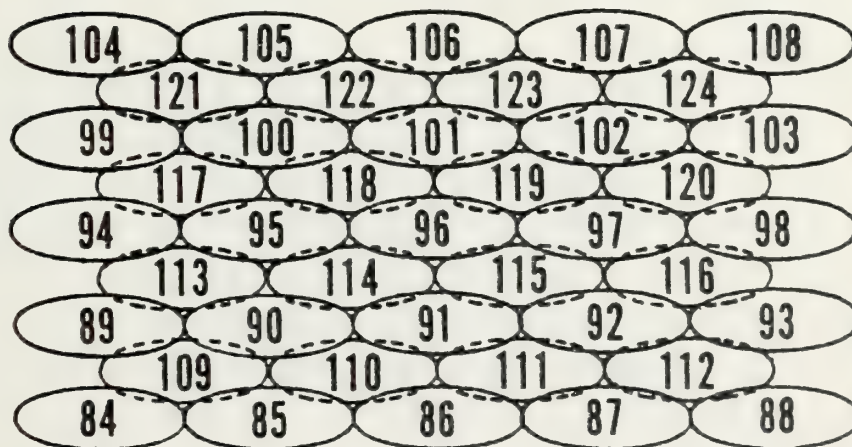


Figure 4 - 9x4x9, (110) Orientation Microcrystallite

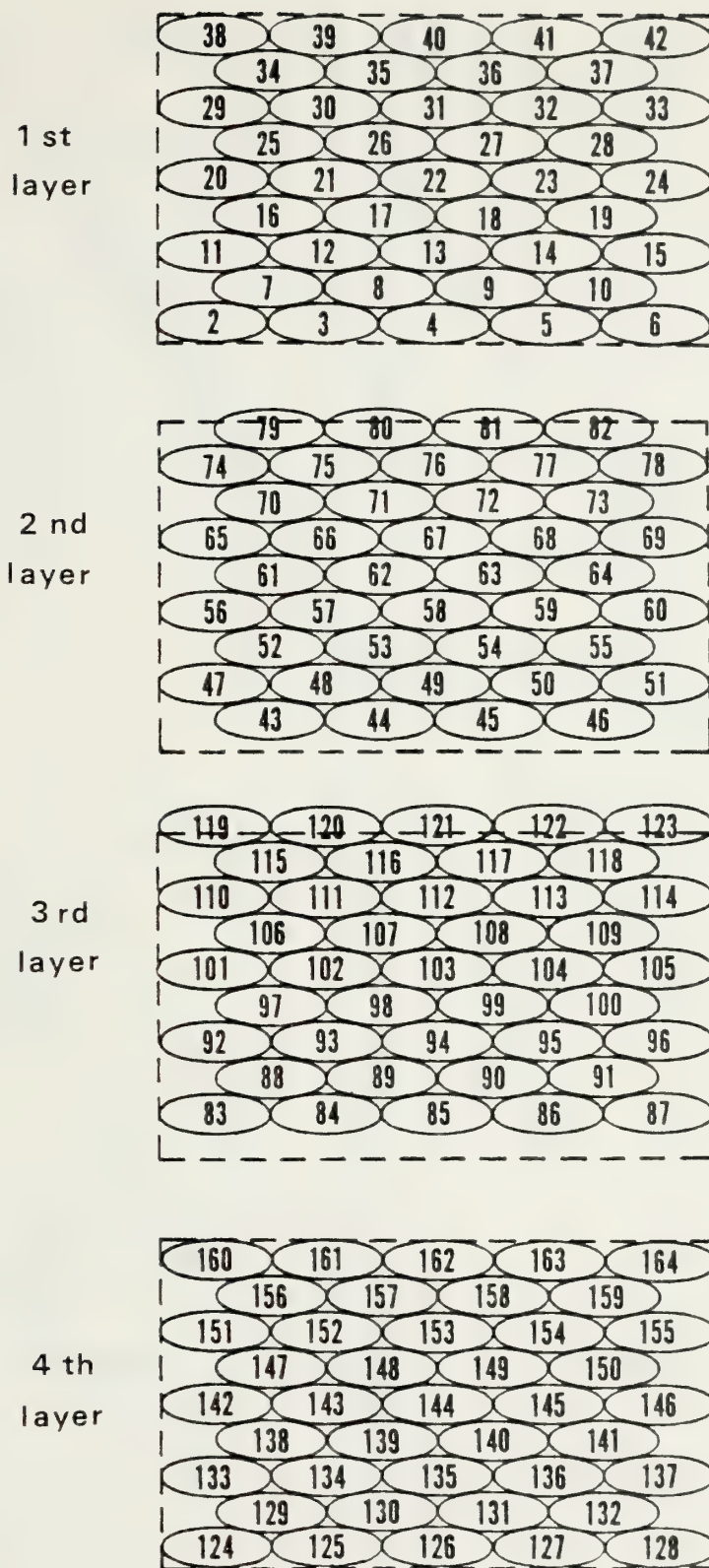


Figure 5 - 9x4x9, (111) Orientation Microcrystallite

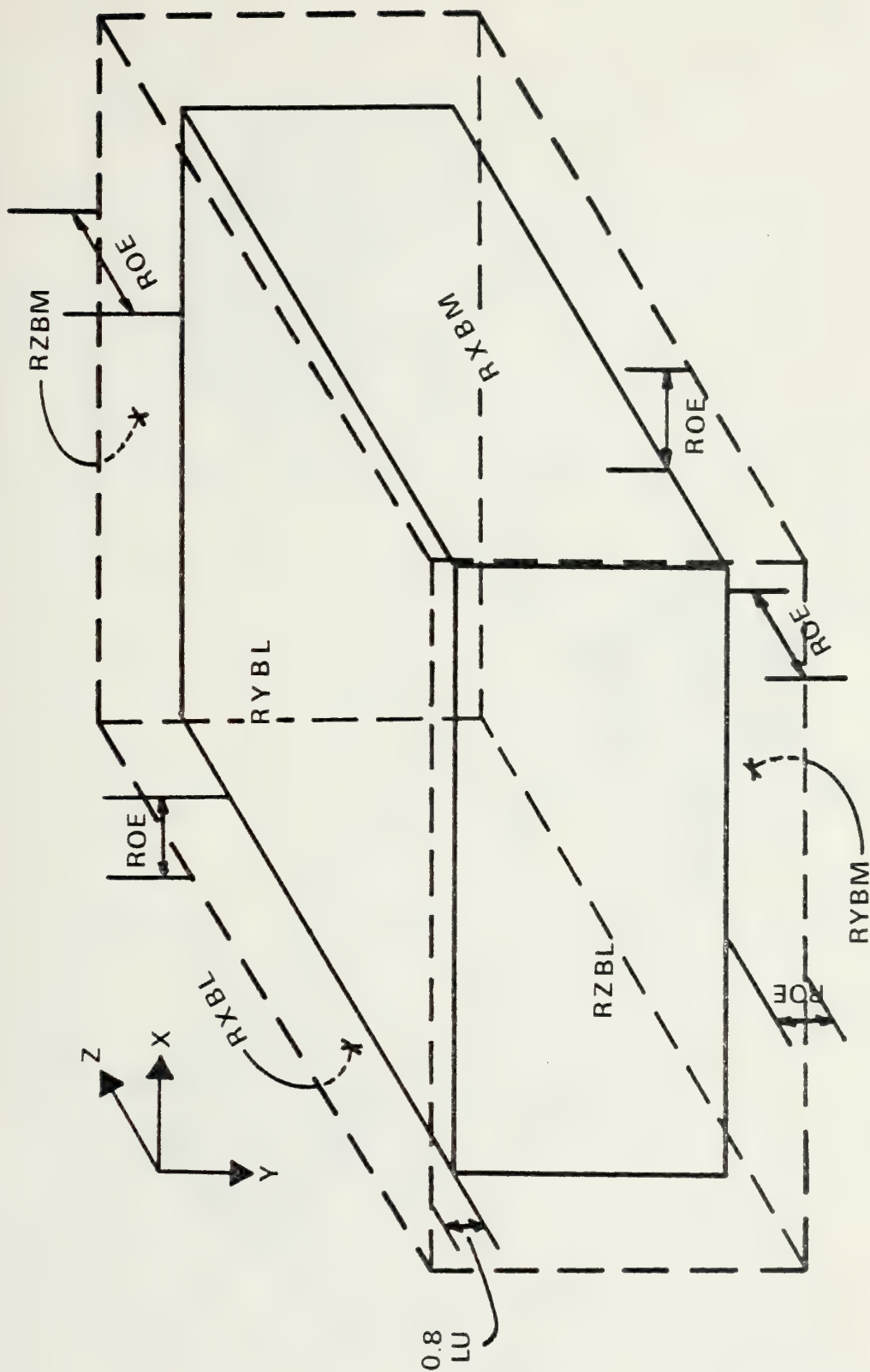


Figure 6 - Microcrystallite Boundaries

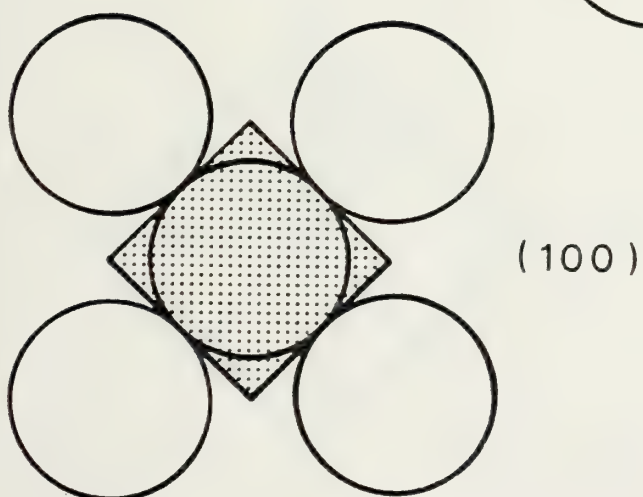
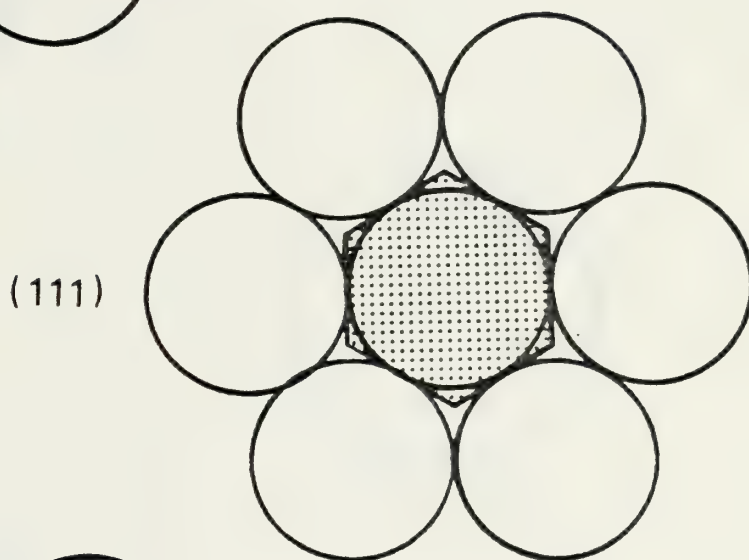
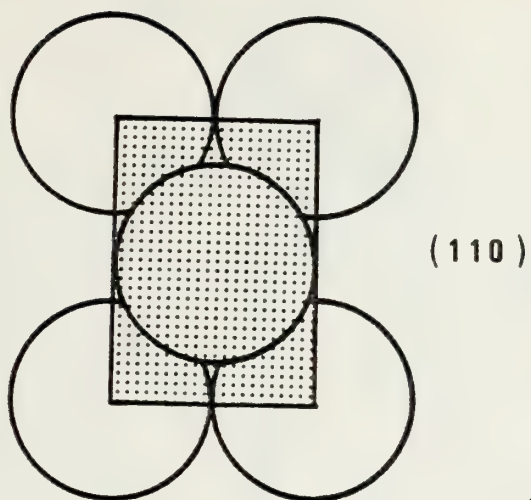
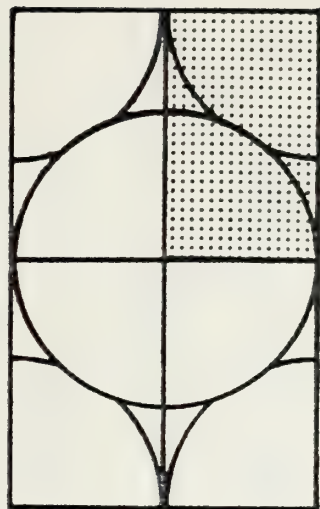
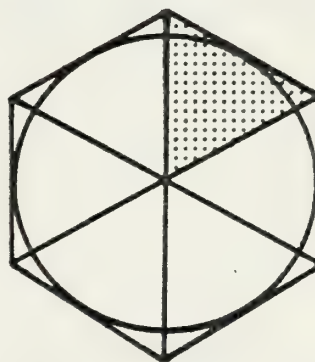


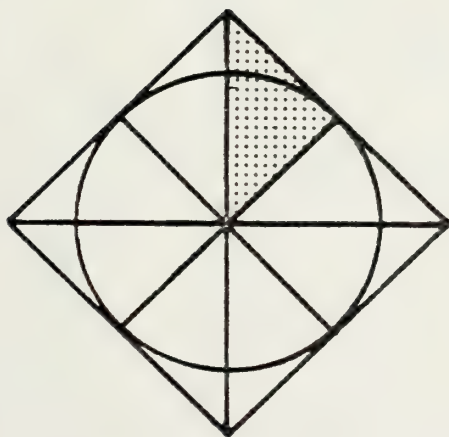
Figure 7 - Intrinsic Geometry of Target Impact Areas



(110)



(111)



(100)

Figure 8 - Reduced Representative Impact Areas

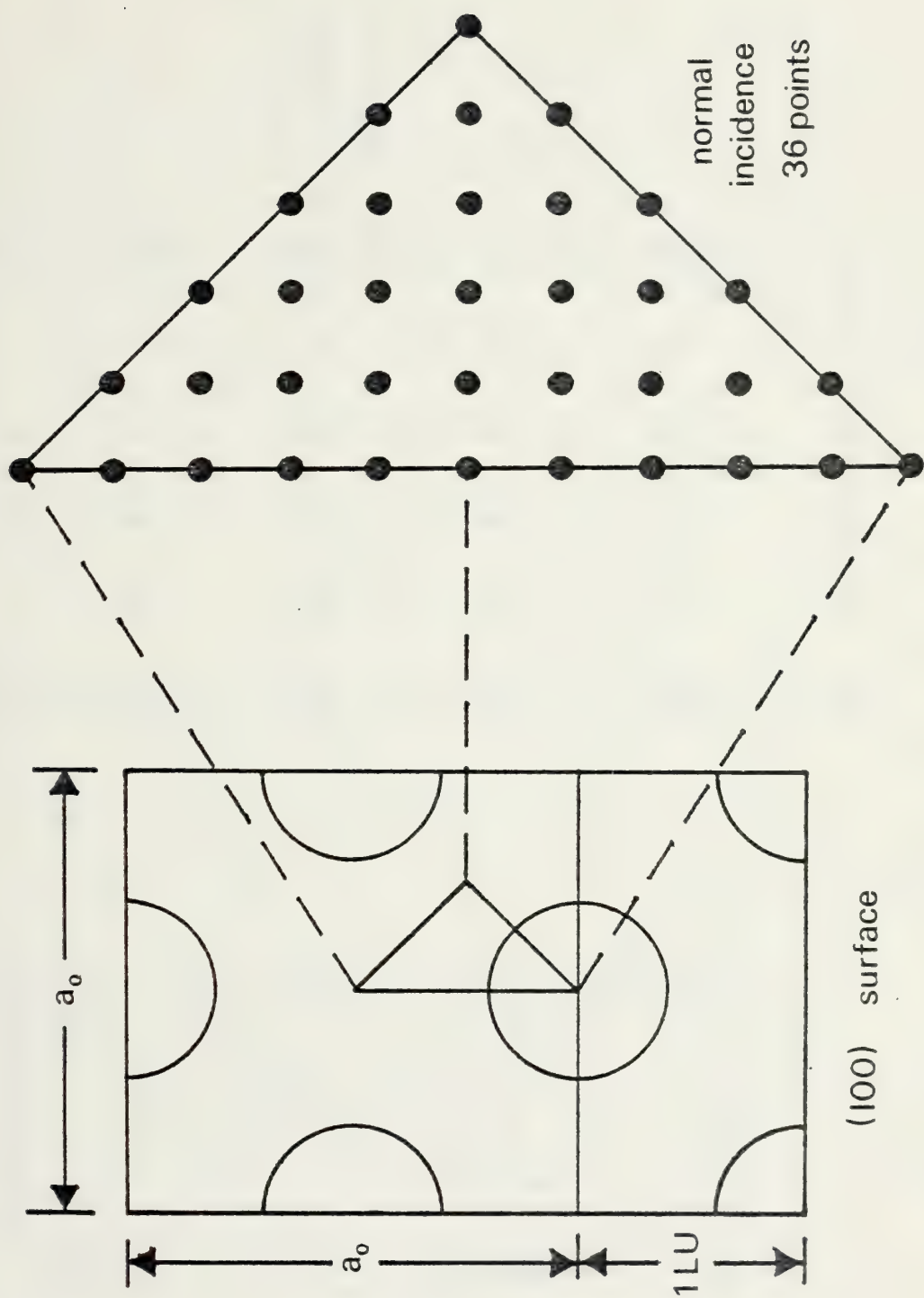


Figure 9 - Expanded Impact Area - (100) Orientation

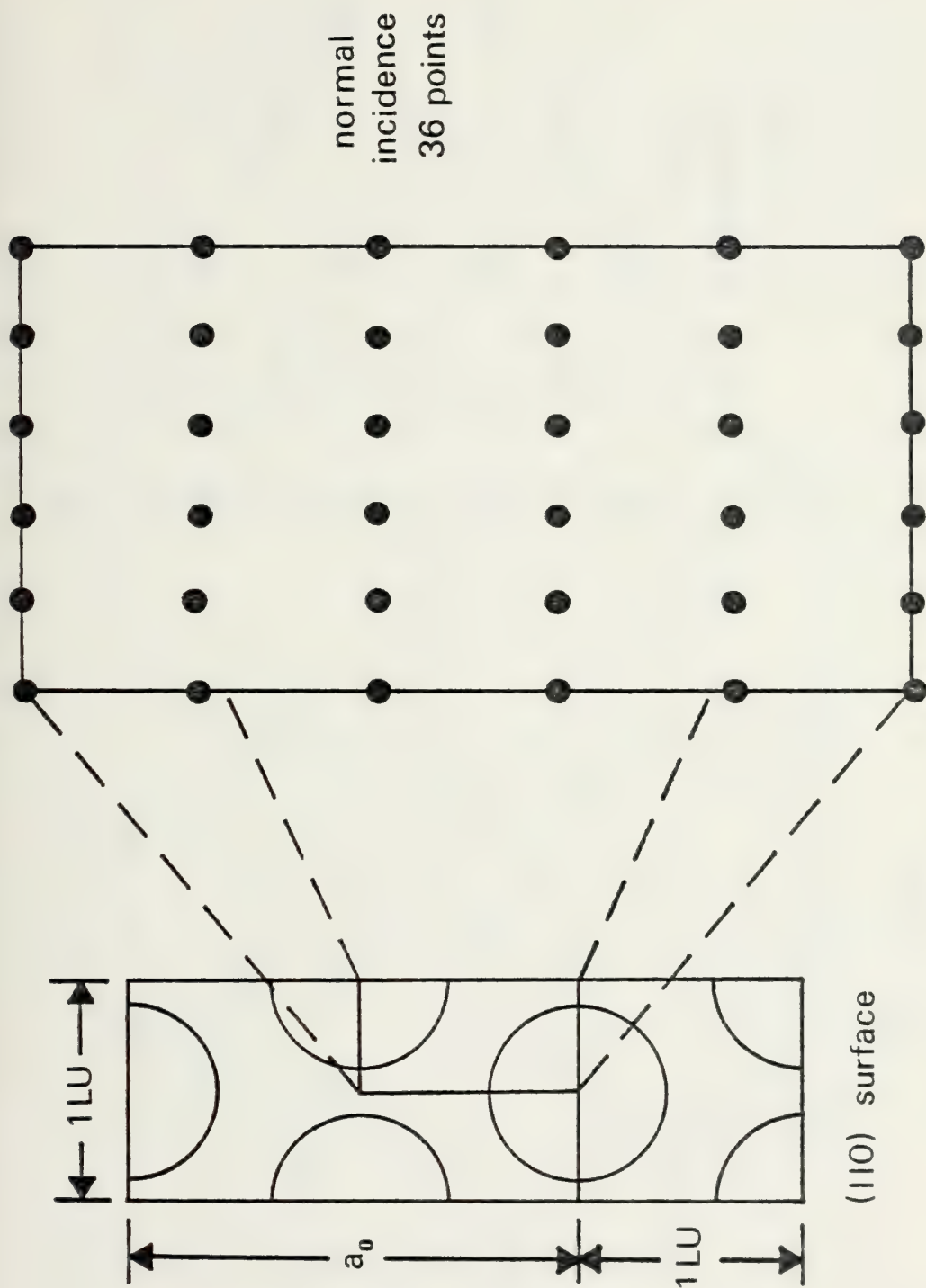


Figure 10 - Expanded Impact Area - (110) Orientation

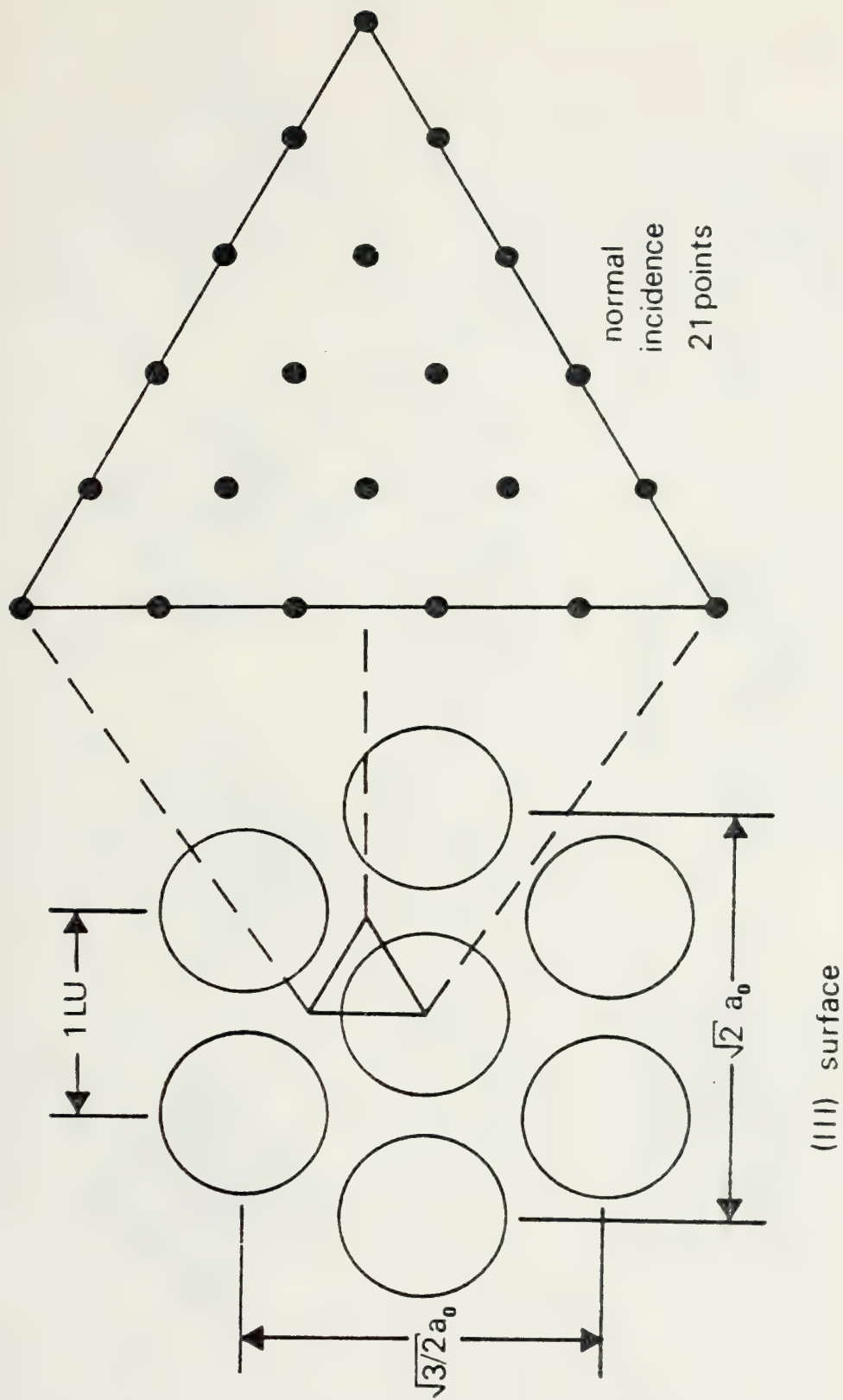
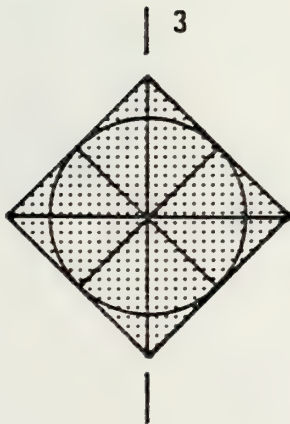
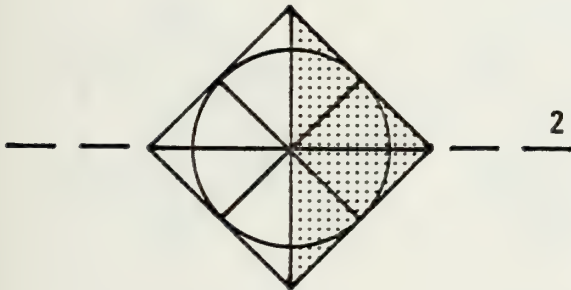
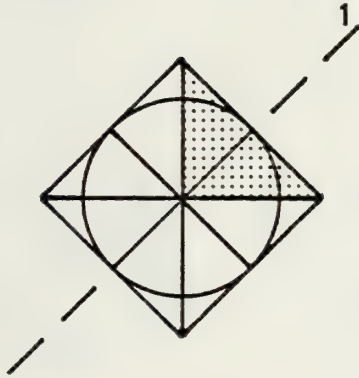
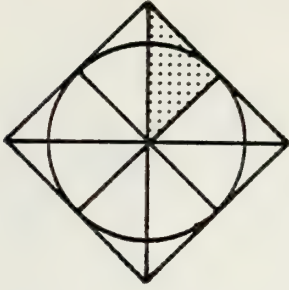


Figure 11 - Expanded Impact Area - (111) Orientation

(100)



(110)

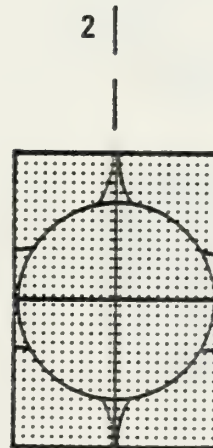
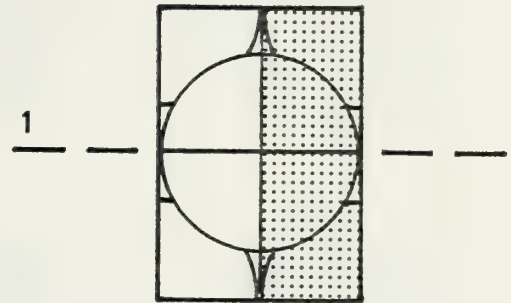
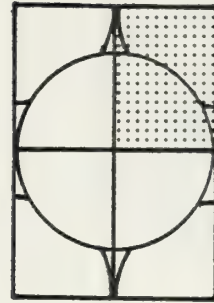


Figure 12 - (100) and (110) Orientation Folding Geometry

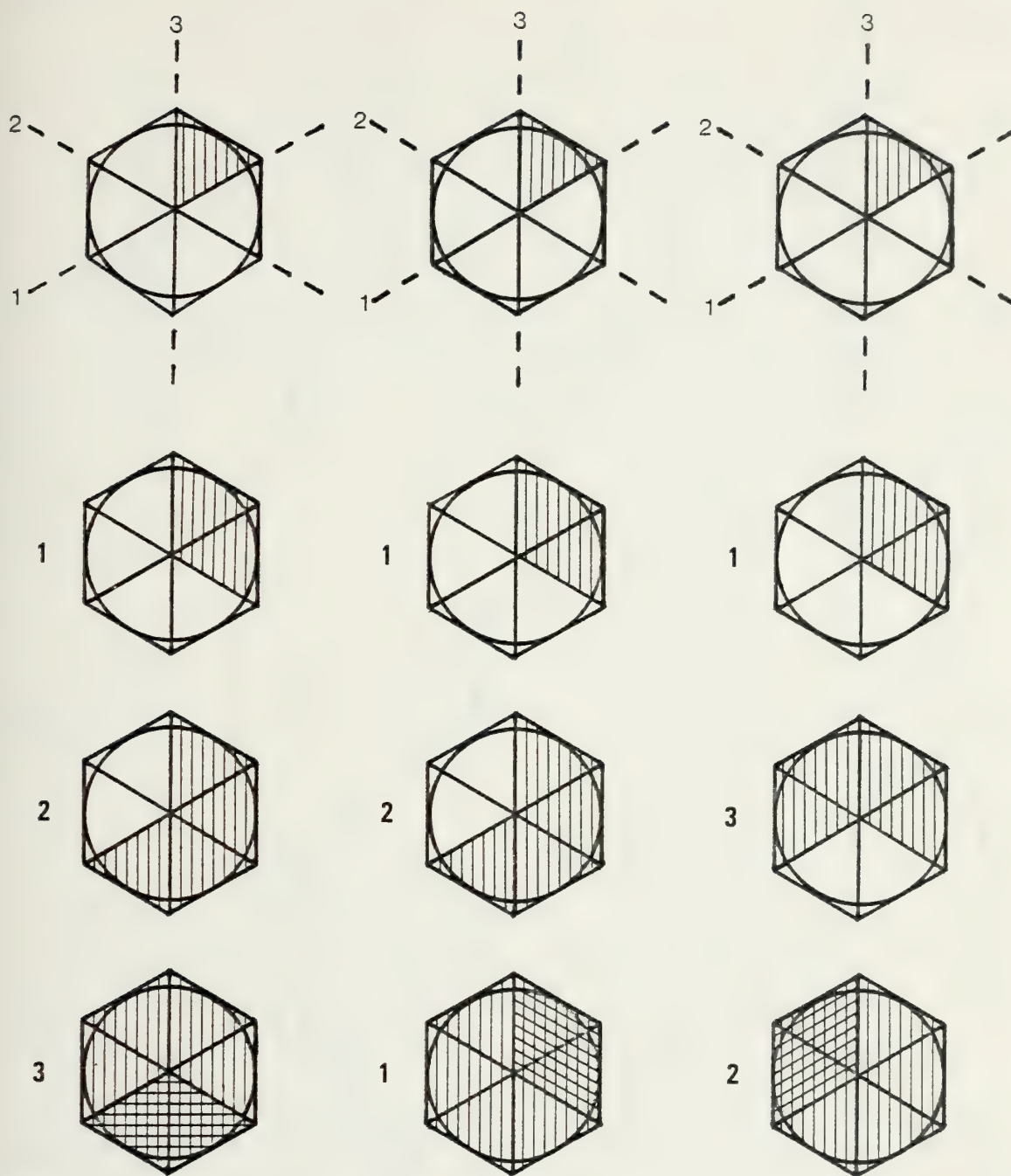


Figure 13 - (111) Orientation Folding Geometry

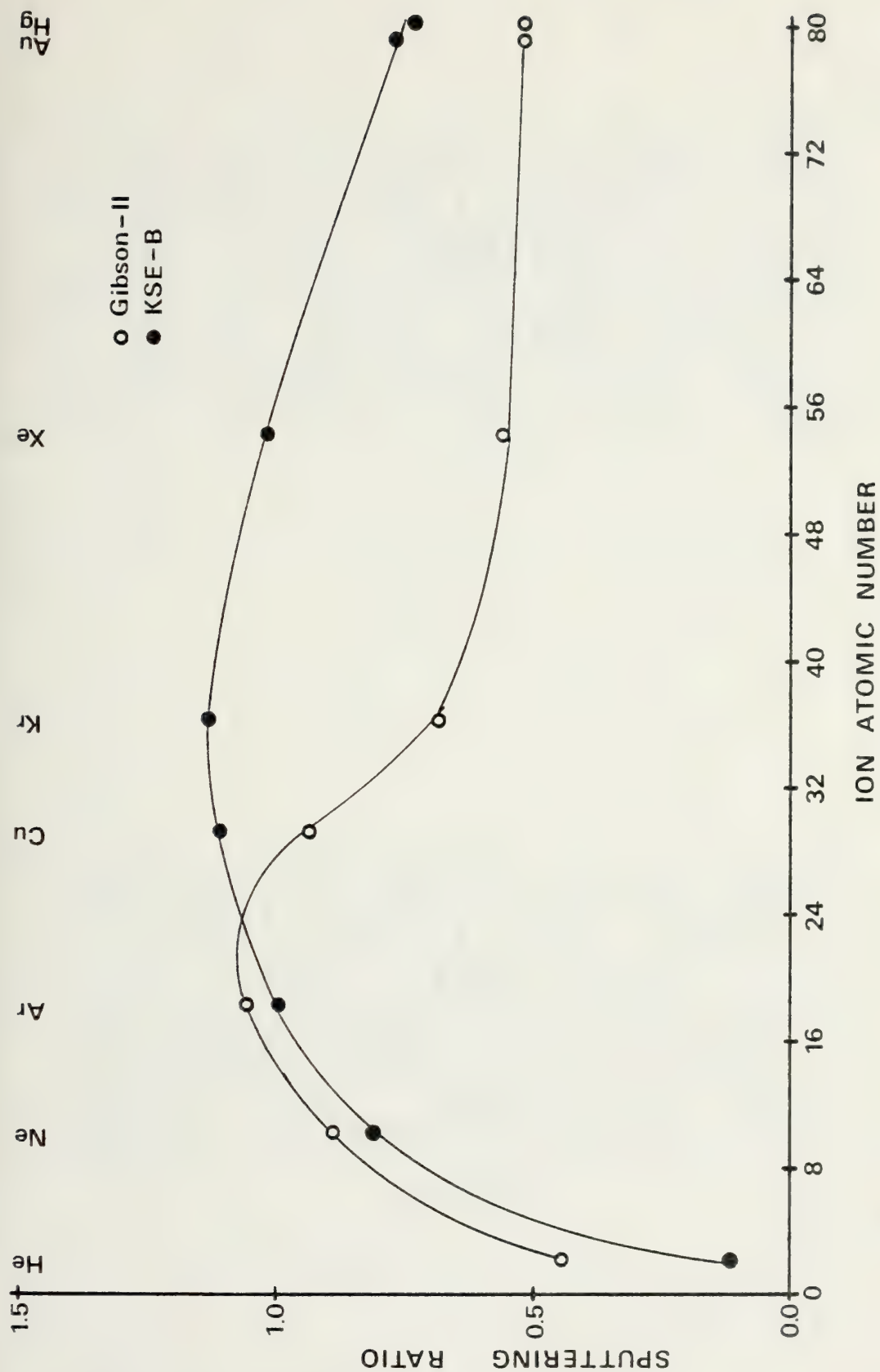
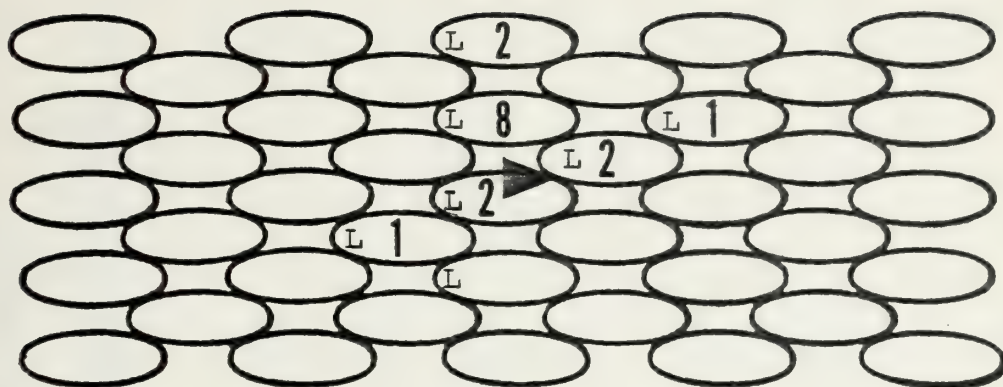
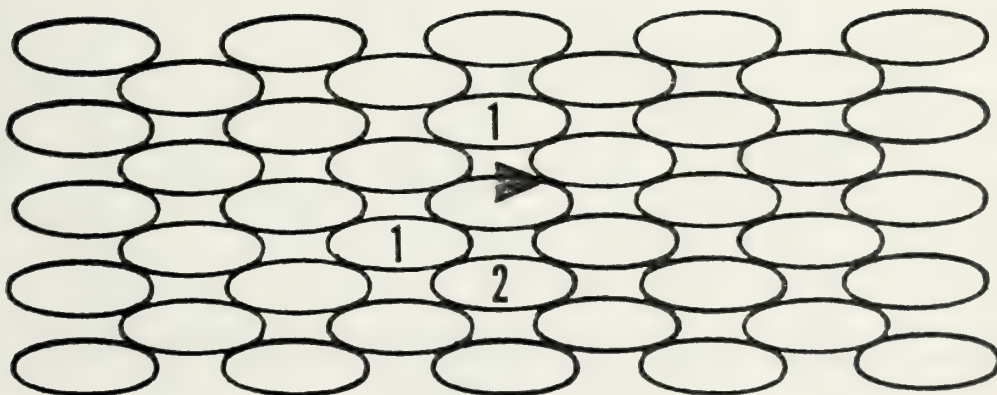


Figure 14 - Sputtering Ratio vs. Ion Atomic Number - (100), 100-eV, 9x4x9



(a) Gibson-II



(b) KSE-B

Figure 15 - Sputtering Summary - (100), 100-eV, Cu/H⁺

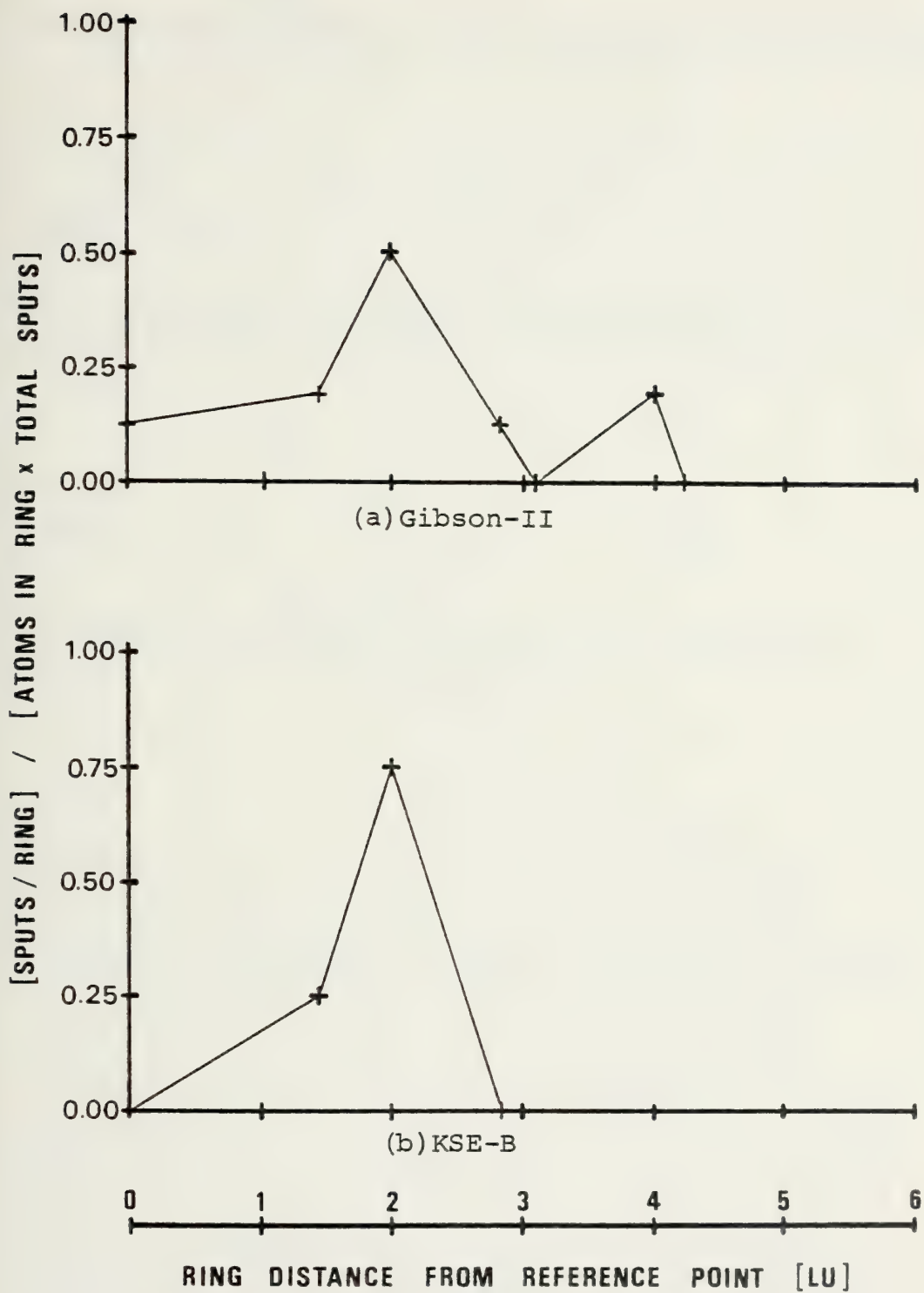
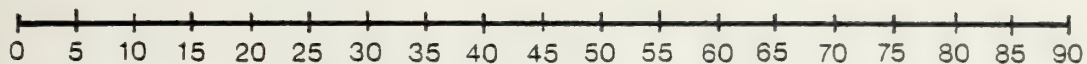


Figure 16 - Ring Probability - (100), 100-eV, Cu/ i^{+}

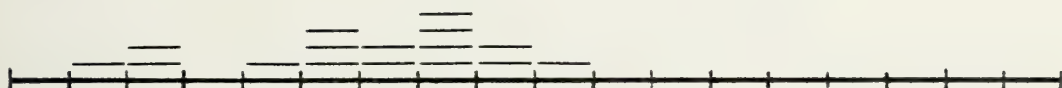
Ejection Angle (Degrees)



Heavy



Light

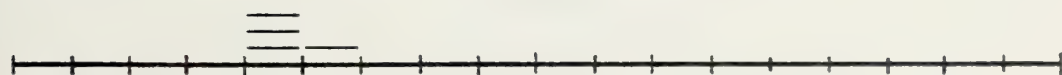


(a) Gibson-II

Heavy

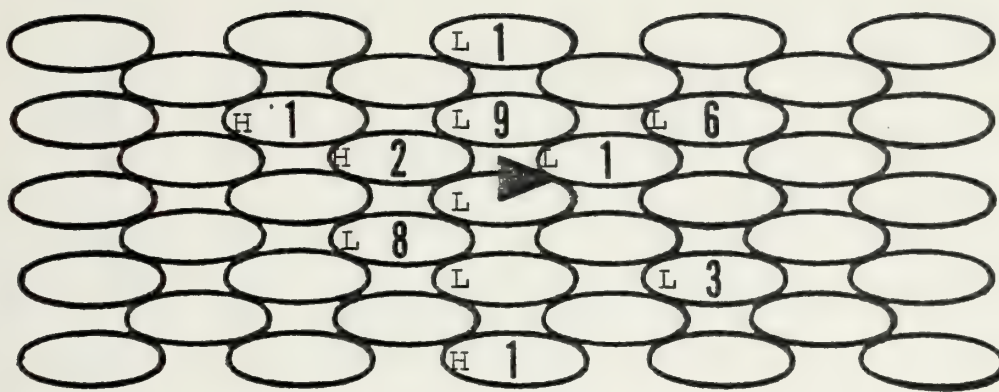


Light

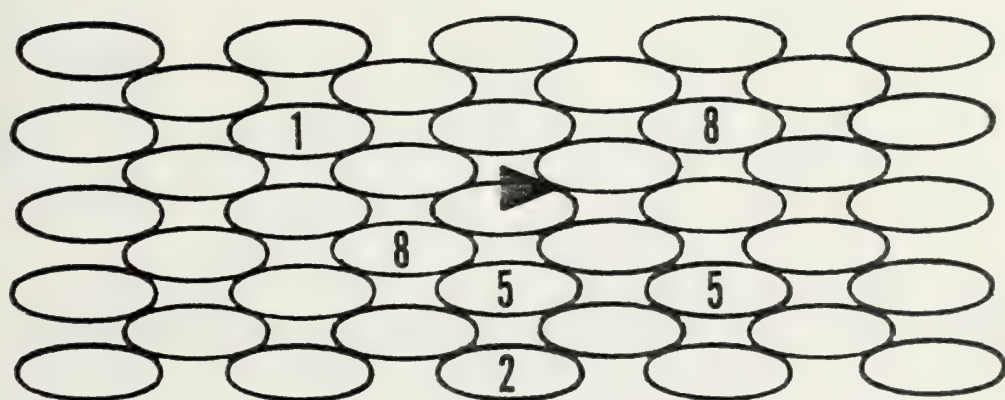


(b) KSE-B

Figure 17 - Angular Dispersion - (100), 100-eV, Cu/He⁺



(a) Gibson-II



(b) KSE-B

Figure 18 - Sputtering Summary - (100), 100-eV, Cu/Ne⁺

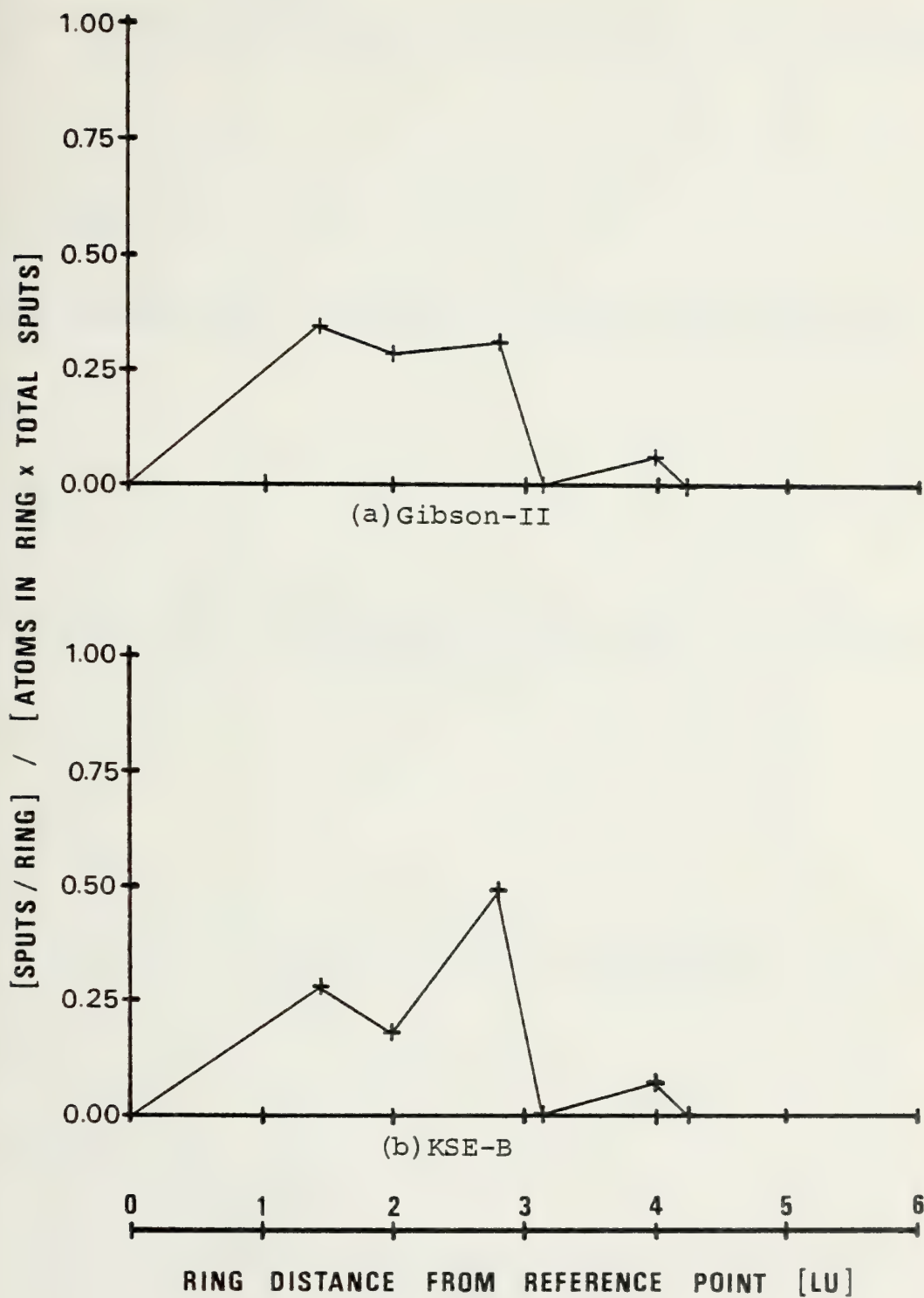
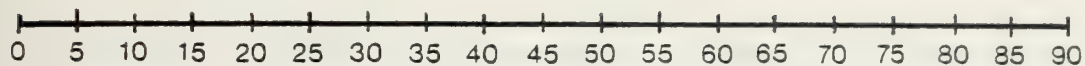


Figure 19 - Ring Probability - (100), 100-eV, Cu/Ne+

Ejection Angle (Degrees)



Heavy



Light

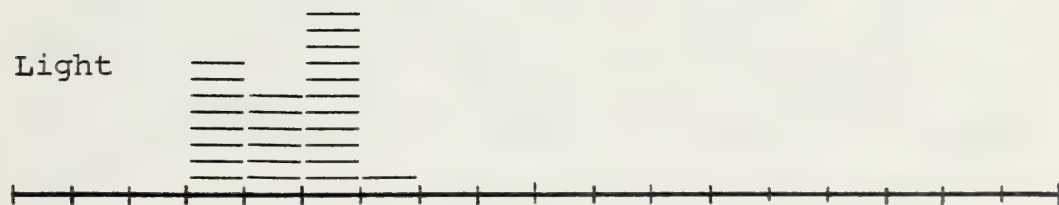


(a) Gibson-II

Heavy

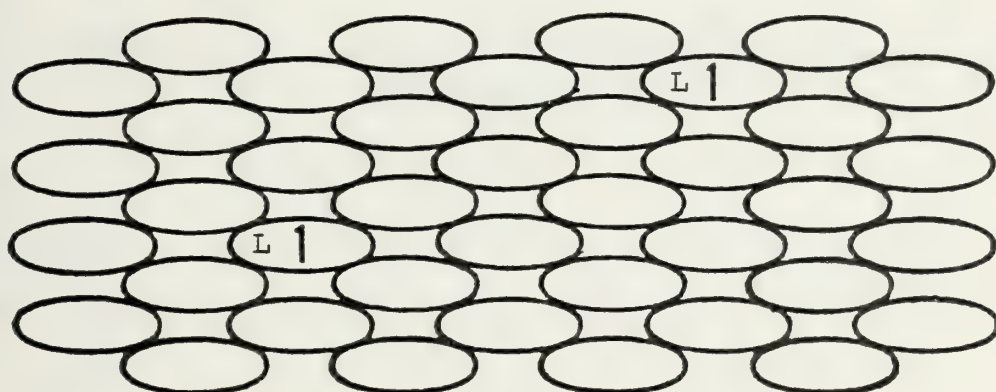
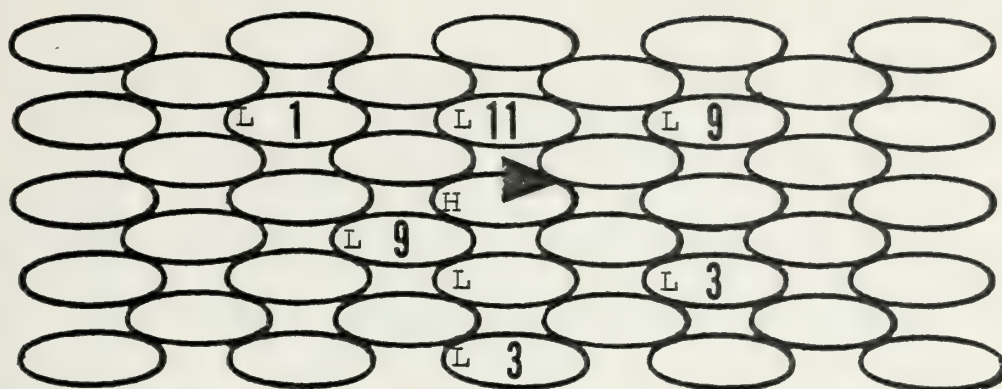


Light

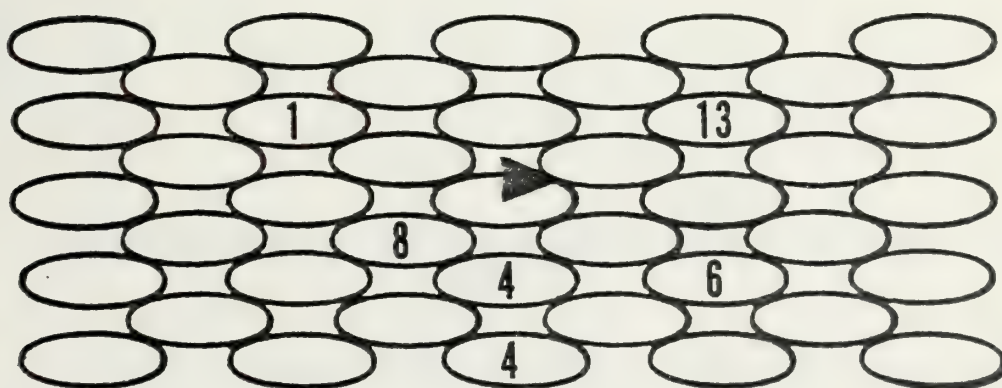


(b) KSE-B

Figure 20 - Angular Dispersion - (100), 100-eV, Cu/Ne⁺



(a) Gibson-II



(b) KSE-B

Figure 21 - Sputtering Summary - (100), 100-eV, Cu/Ar⁺

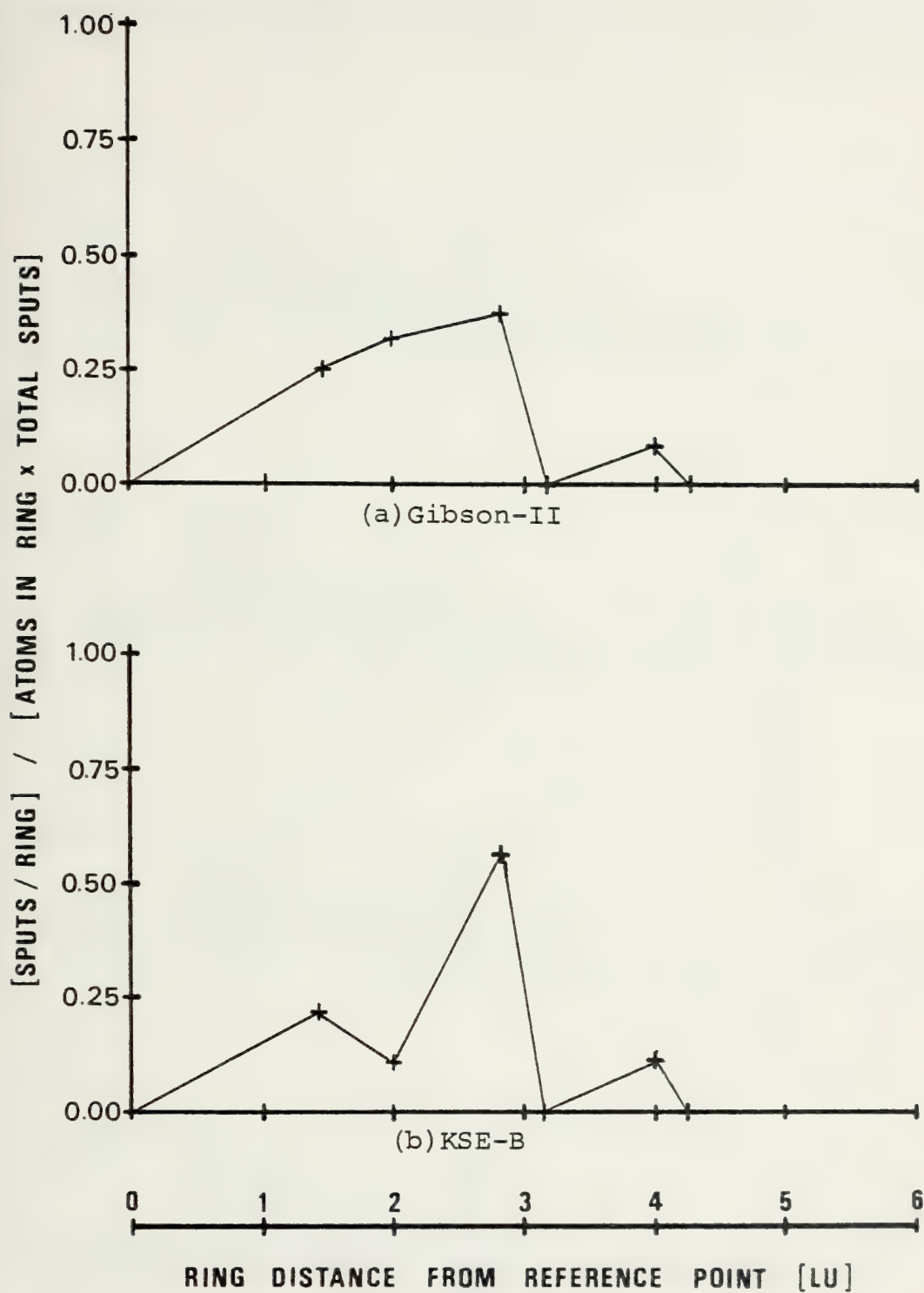
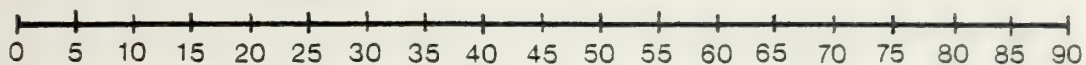
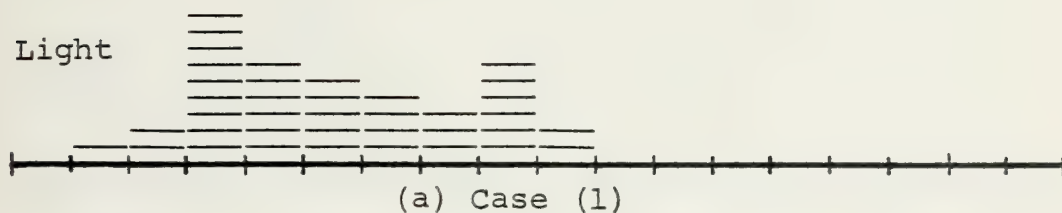


Figure 22 - Ring Probability - (100), 100-eV, Cu/Ar⁺

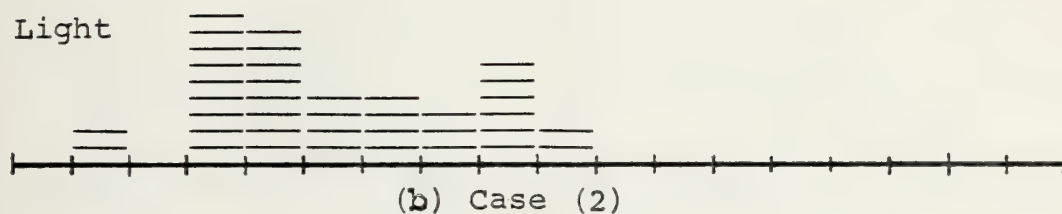
Ejection Angle (Degrees)



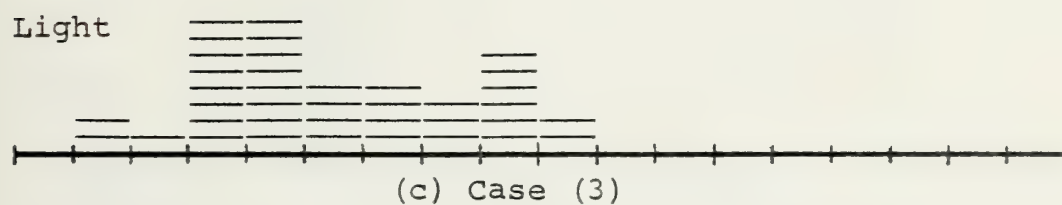
Light



Light



Light



Light

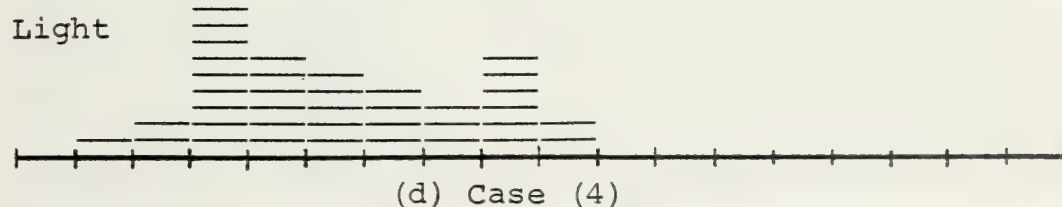


Figure 23 - Angular Dispersion - (100), 100-eV, Cu/Ar⁺
Gibson-II

Ejection Angle (Degrees)

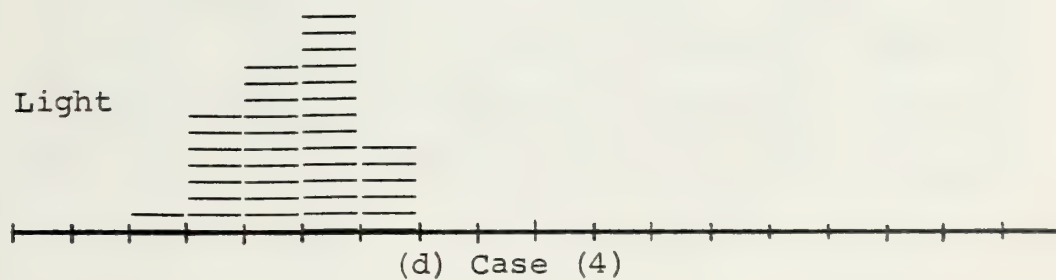
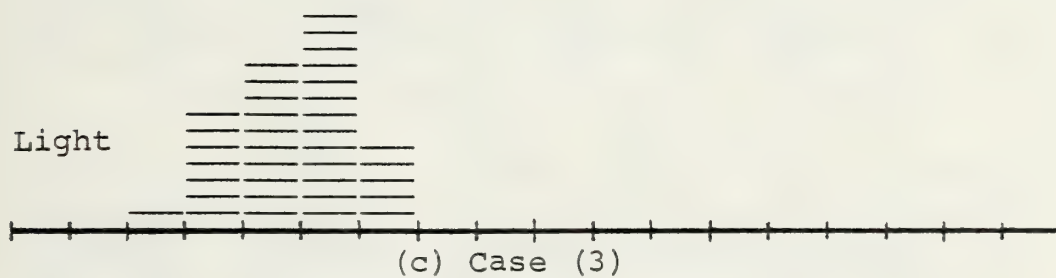
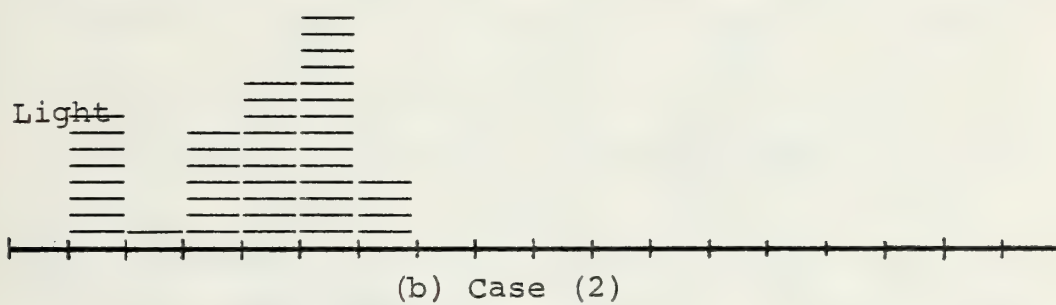
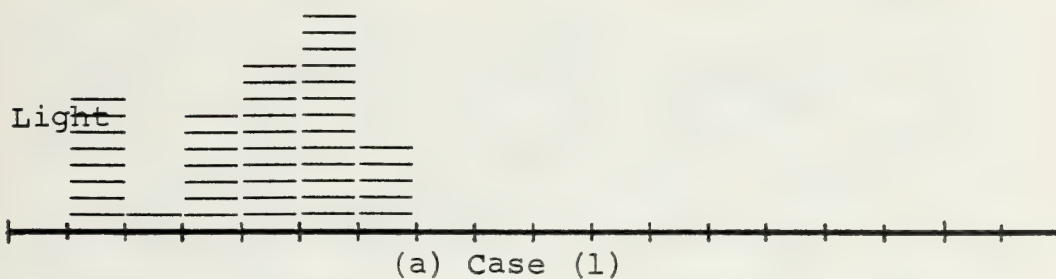
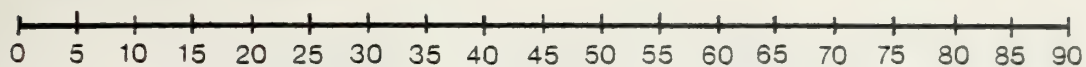
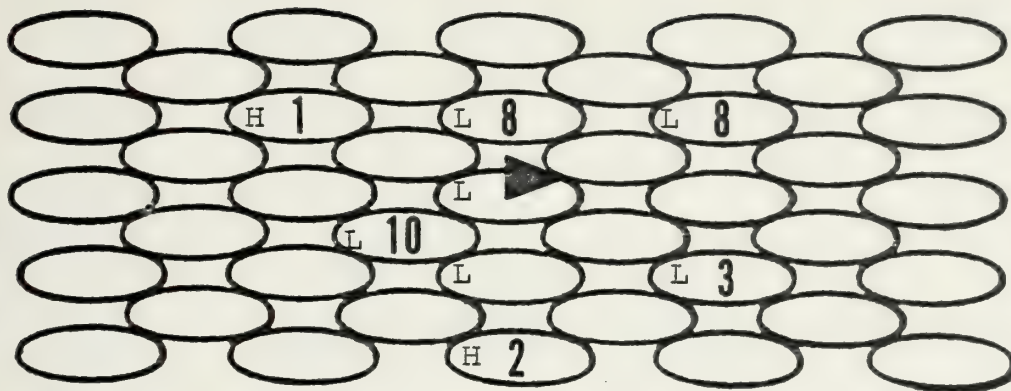
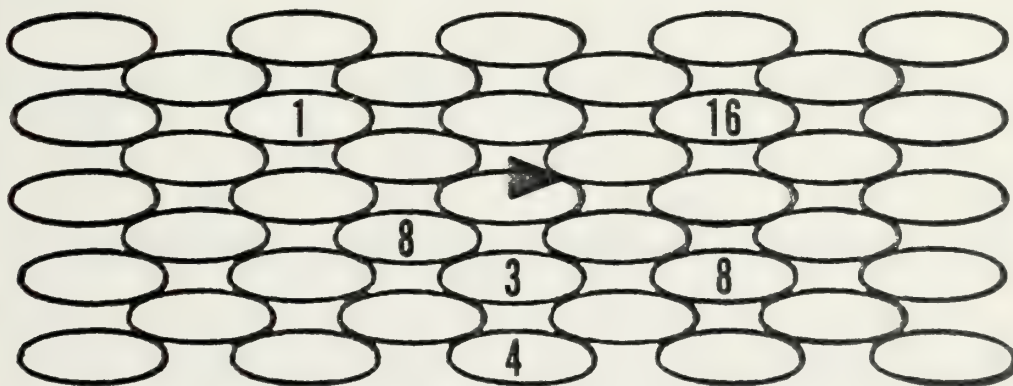
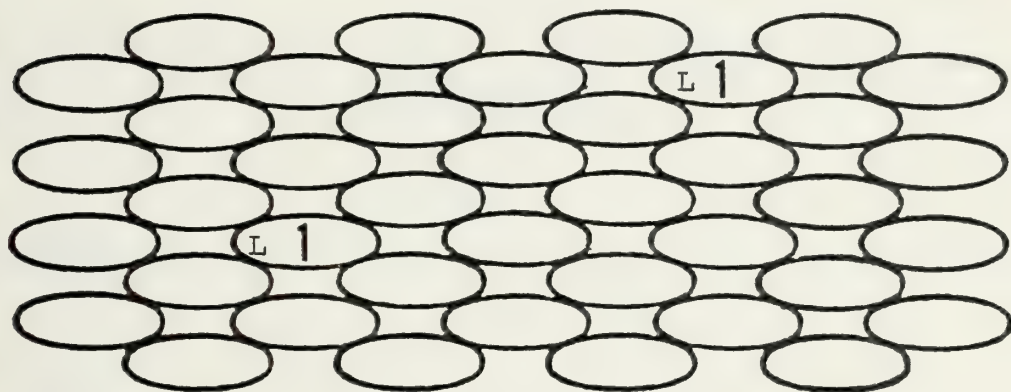


Figure 24 - Angular Dispersion - (100), 100-eV, Cu/Ar⁺
KSE-B



(a) Gibson-II



(b) KSE-B

Figure 26 - Sputtering Summary - (100), 100-eV, Cu/Cu+

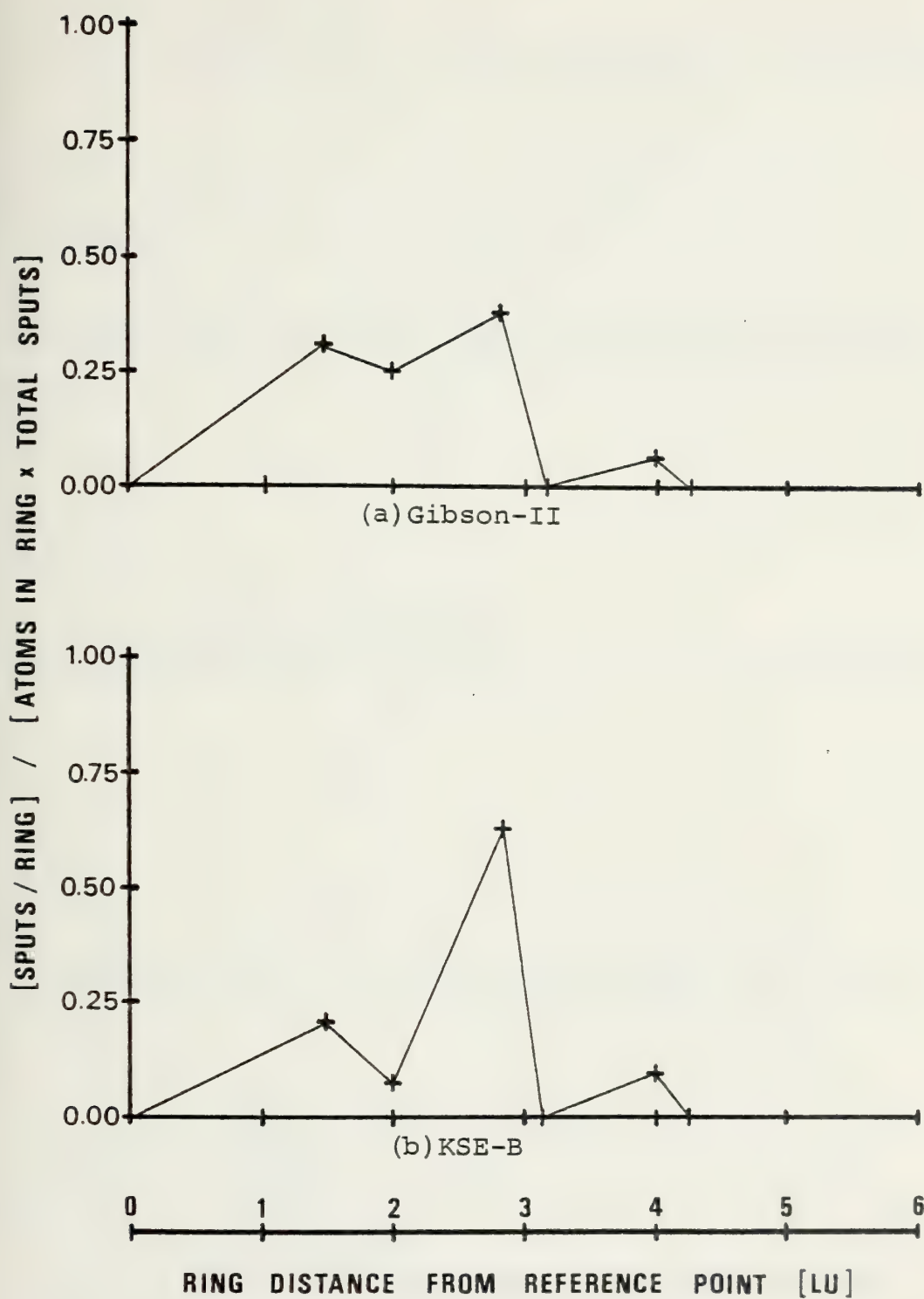
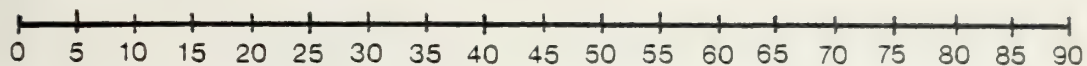


Figure 27 - Ring Probability - (100), 100-eV, Cu/Cu⁺

Ejection Angle (Degrees)



Heavy



Light

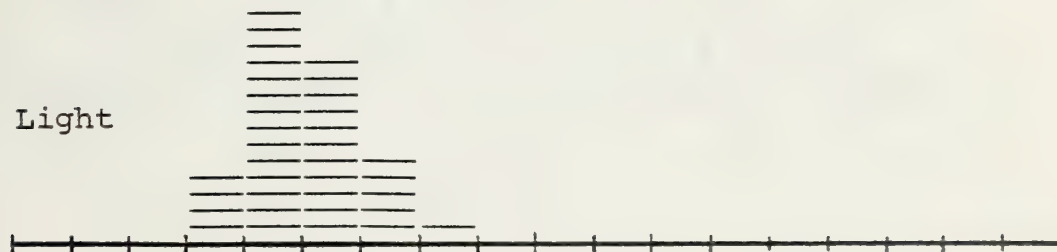


(a) Gibson-II

Heavy

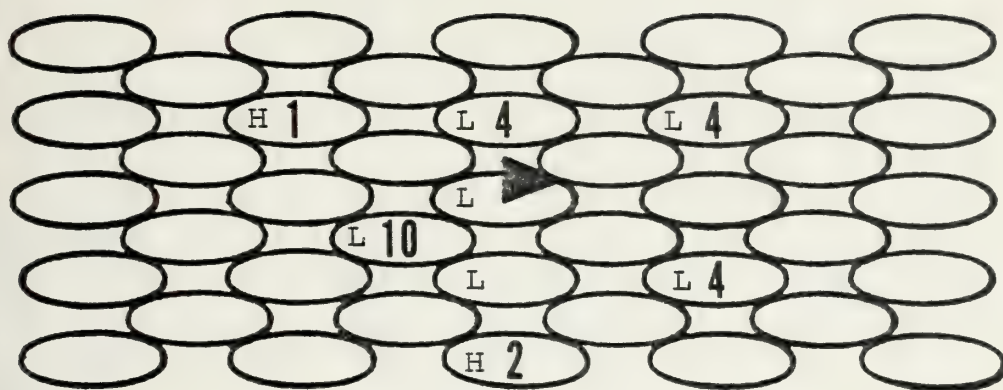


Light

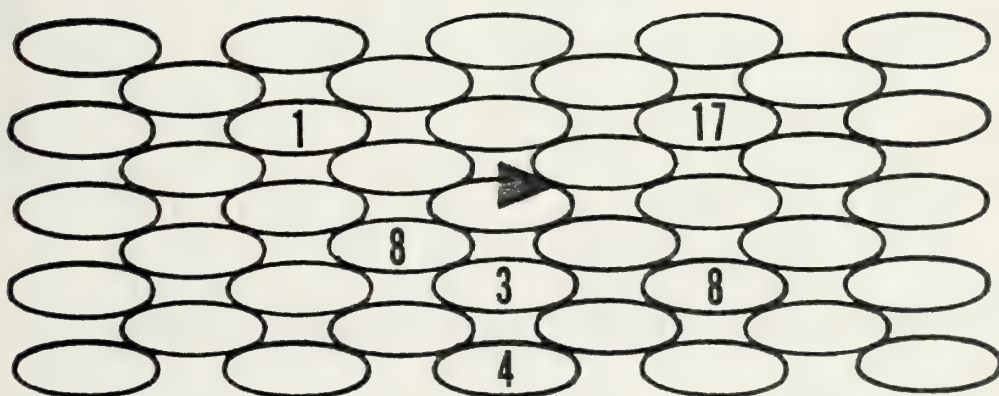


(b) KSE-B

Figure 28 - Angular Dispersion - (100), 100-eV, Cu/Cu⁺



(a) Gibson-II



(b) KSE-B

Figure 29 - Sputtering Summary - (100), 100-eV, Cu/Kr^+

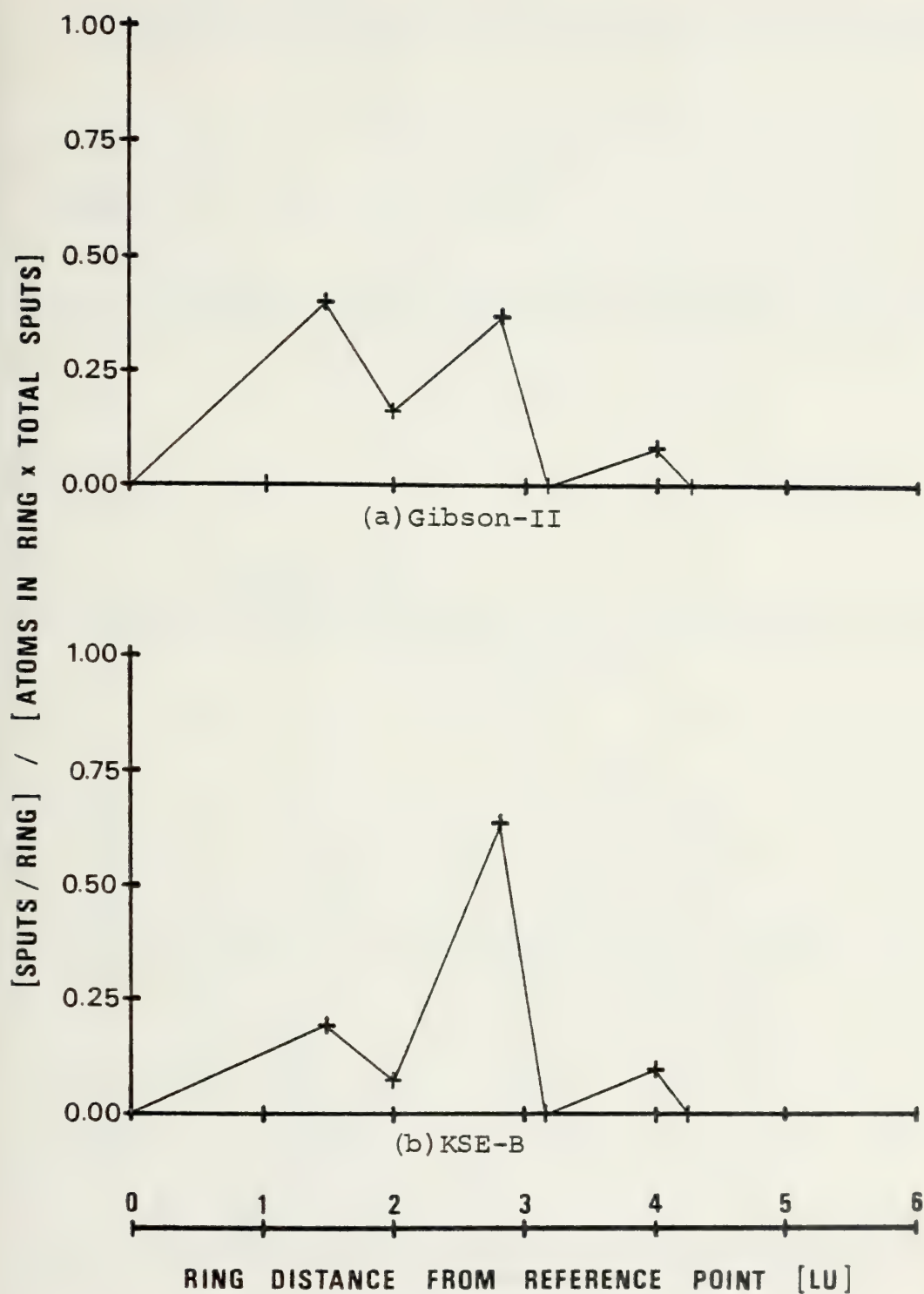
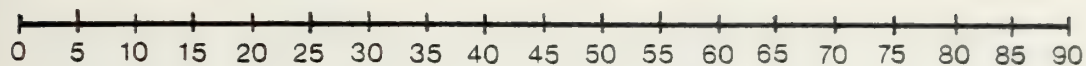


Figure 30 - Ring Probability - (100), 100-eV, Cu/Kr⁺

Ejection Angle (Degrees)



Heavy



Light

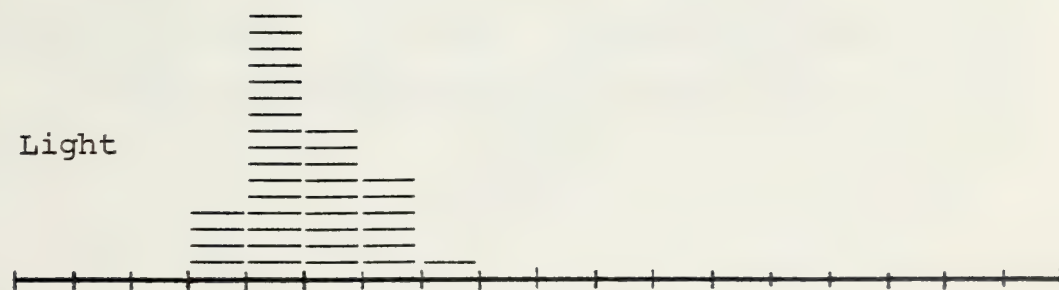


(a) Gibson-II

Heavy

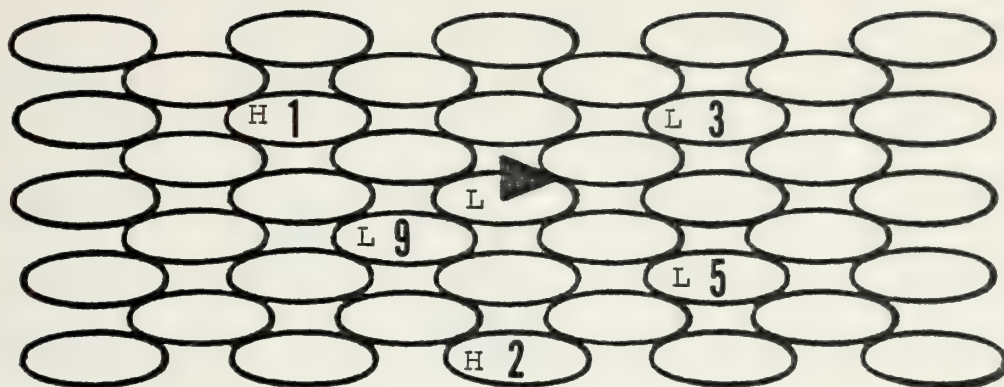


Light

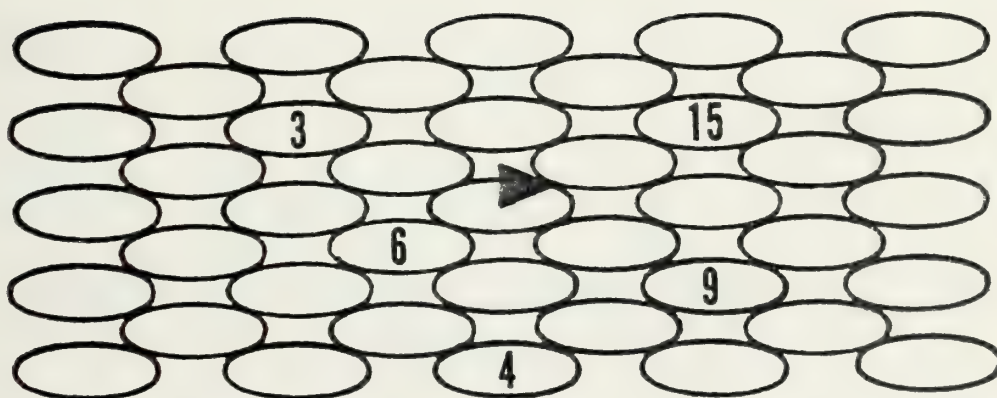


(b) KSE-B

Figure 31 - Angular Dispersion - (100), 100-eV, Cu/Kr⁺



(a) Gibson-II



(b) KSE-B

Figure 32 - Sputtering Summary - (100), 100-eV, Cr/Xe^+

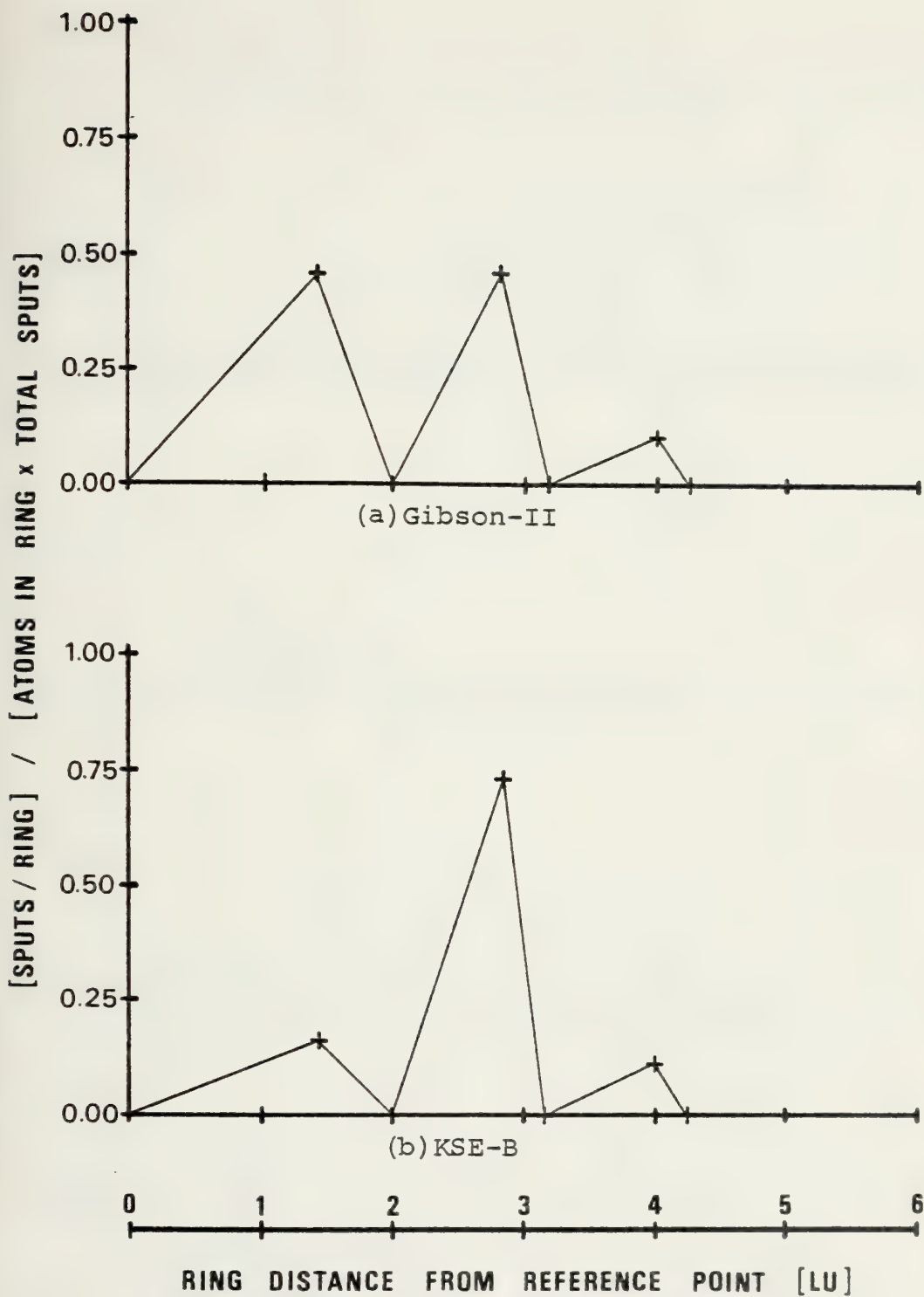
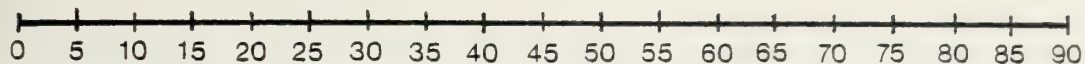


Figure 33 - Ring Probability - (100), 100-eV, Cu/Xe+

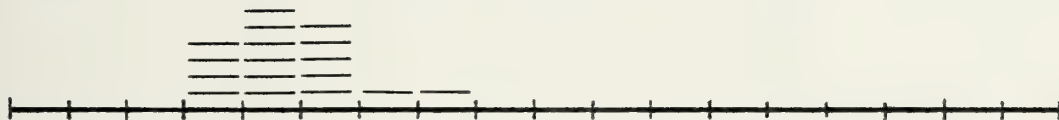
Ejection Angle (Degrees)



Heavy



Light



(a) Gibson-II

Heavy

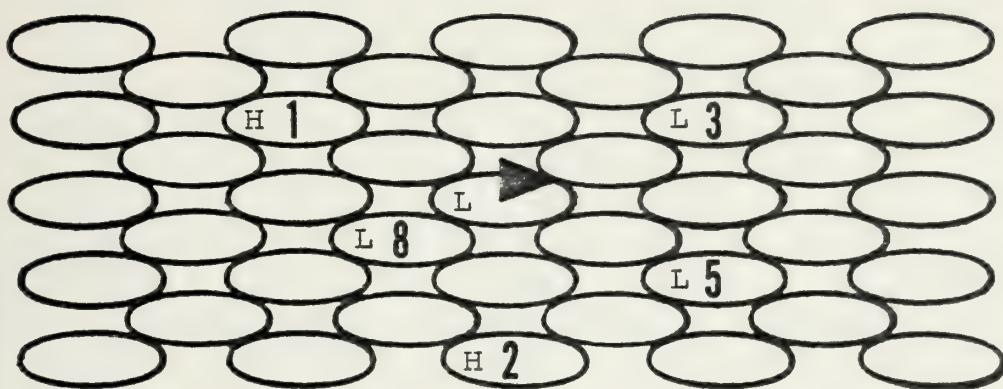


Light

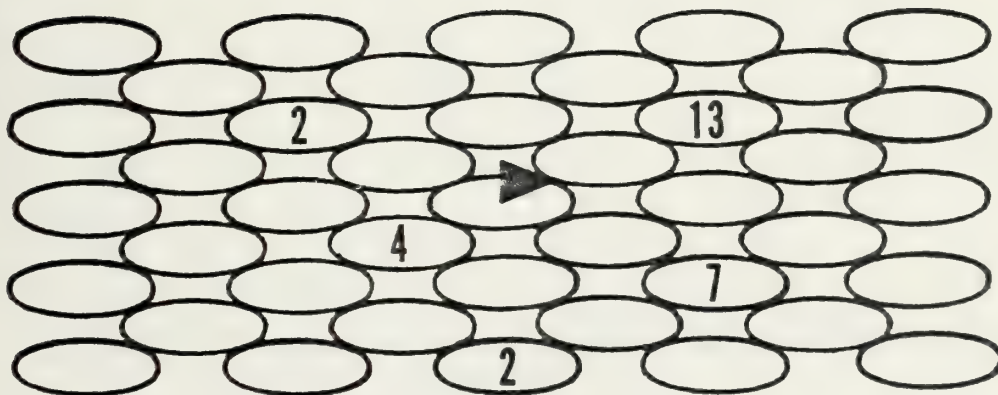


(b) KSE-B

Figure 34 - Angular Dispersion - (100), 100-eV, Cu/K⁺



(a) Gibson-II



(b) KSE-B

Figure 35 - Sputtering Summary - (100), 100-eV, Cu/Au⁺

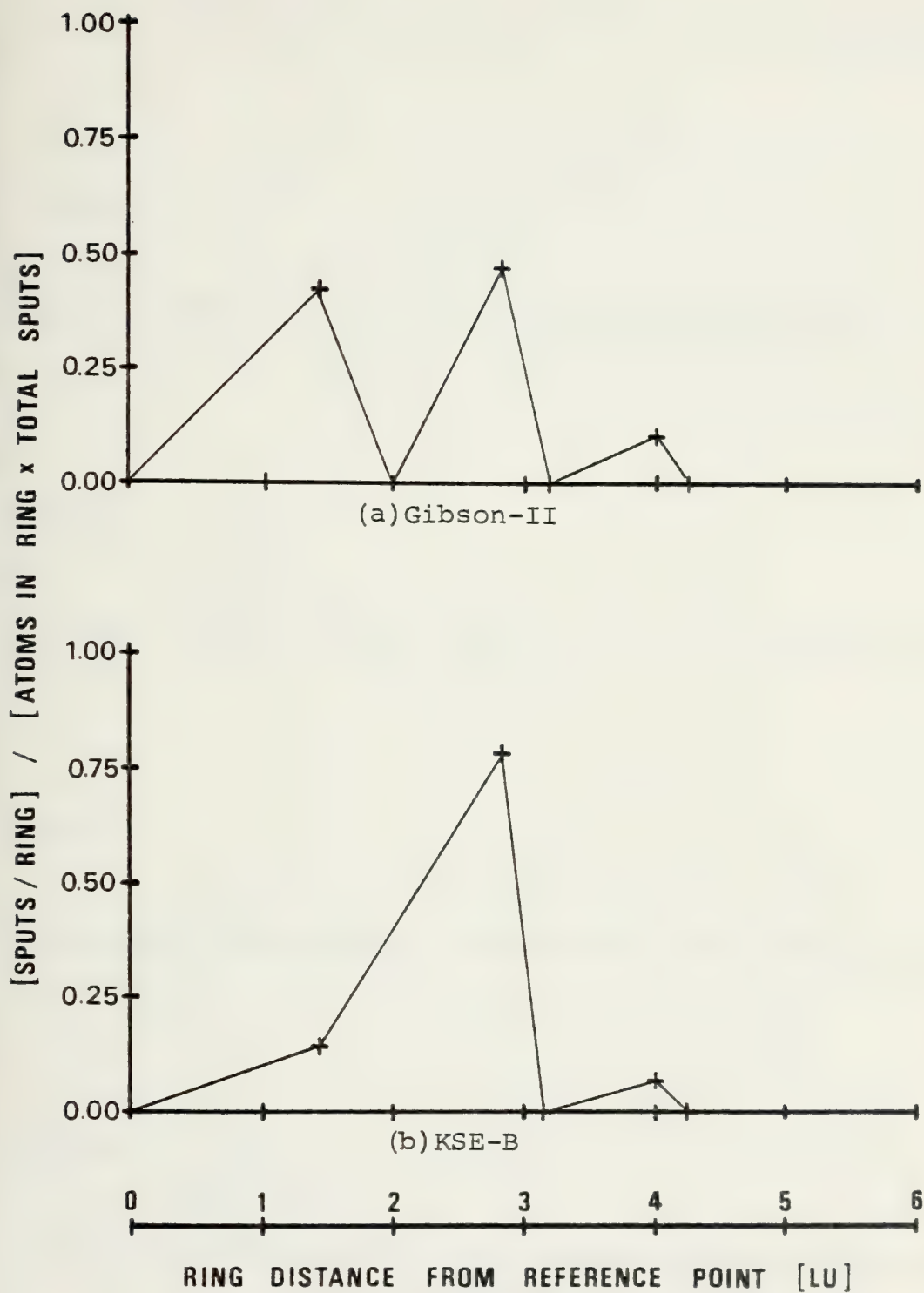


Figure 36 - Ring Probability - (100), 100-eV, Cu/Au+

Ejection Angle (Degrees)



Heavy

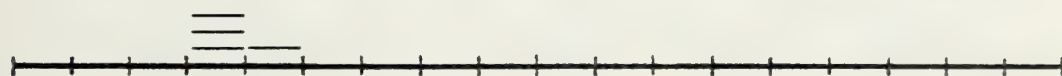


Light



(a) Gibson-II

Heavy

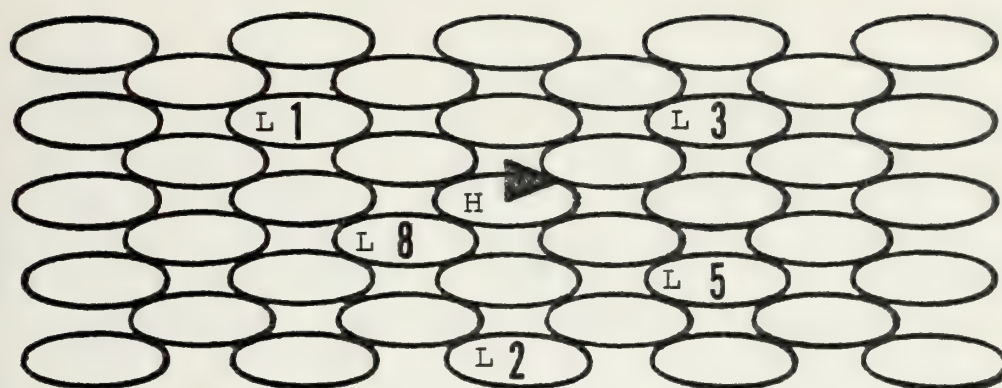


Light

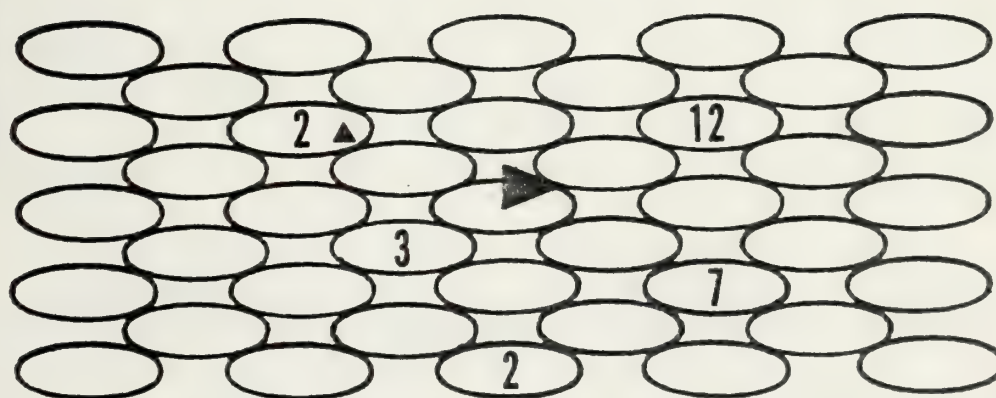


(b) KSE-B

Figure 37 - Angular Dispersion - (100), 100-eV, Cu/Au⁺



(a) Gibson-II



(b) KSE-B

Figure 38 - Sputtering Summary - (100), 100-eV, Cu/Hg⁺

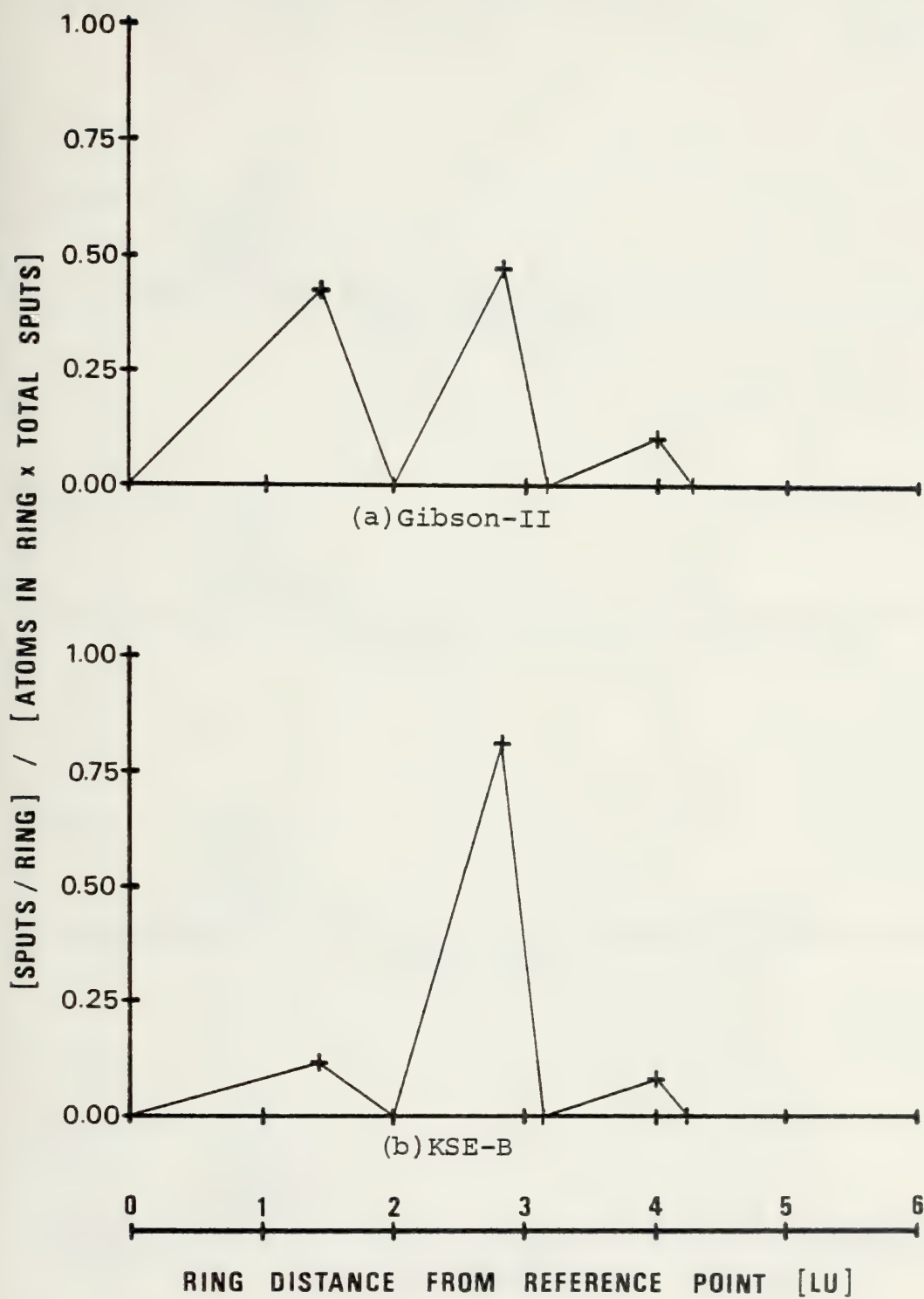
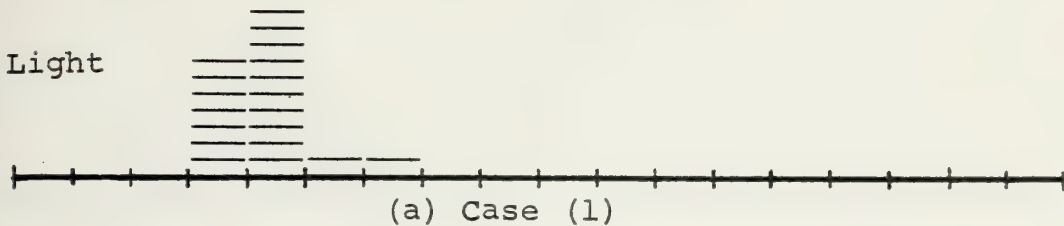


Figure 39 - Ring Probability - (100), 100-eV, Cu/Hg⁺

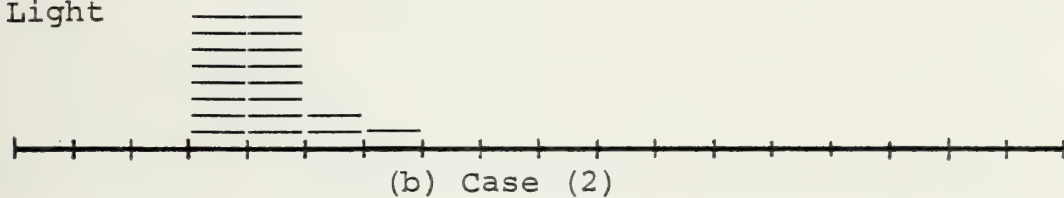
Ejection Angle (Degrees)



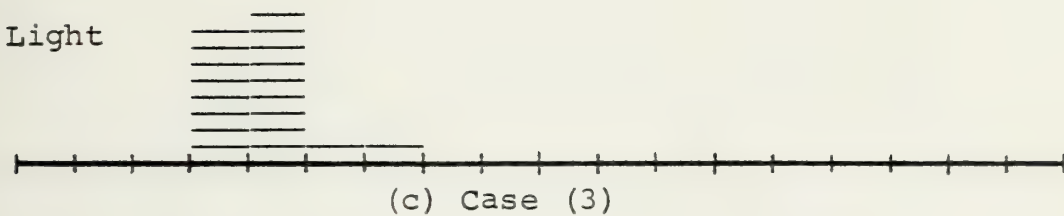
Light



Light



Light



Light

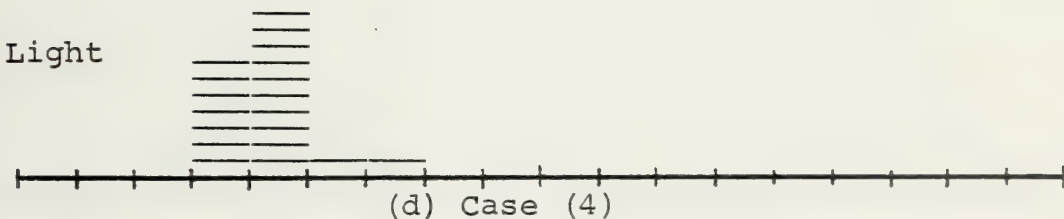
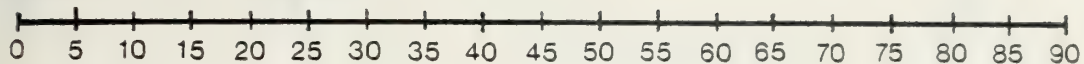
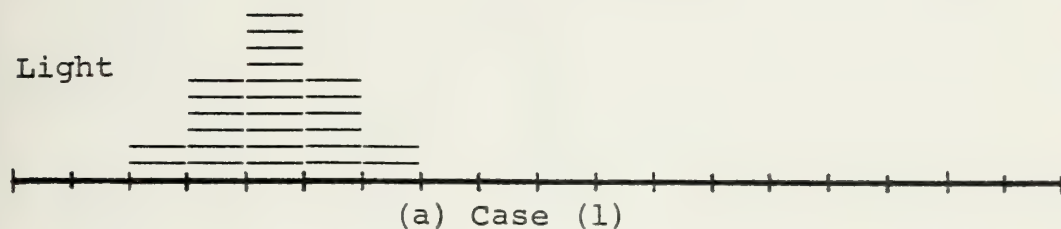


Figure 40 - Angular Dispersion - (100), 100-eV, Cu/Hg+
Gibson-II

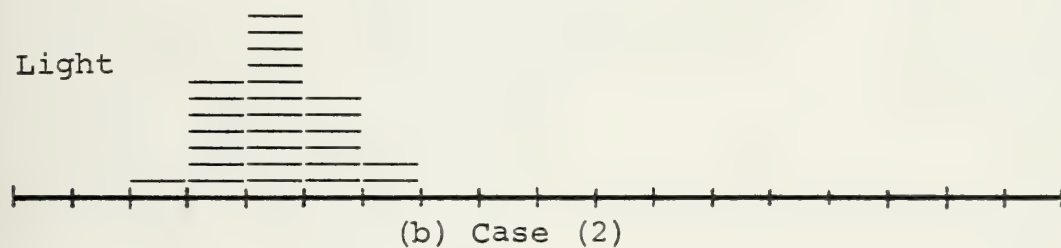
Ejection Angle (Degrees)



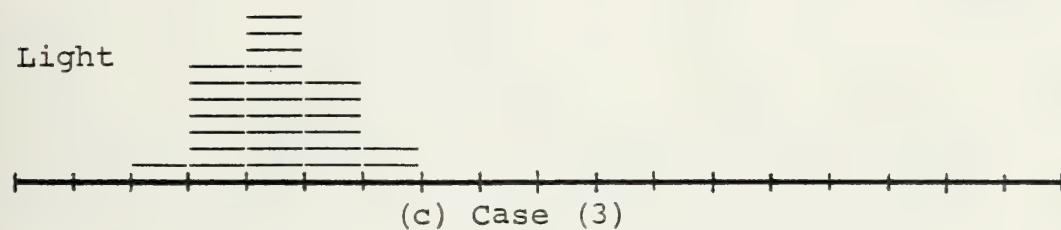
Light



Light



Light



Light

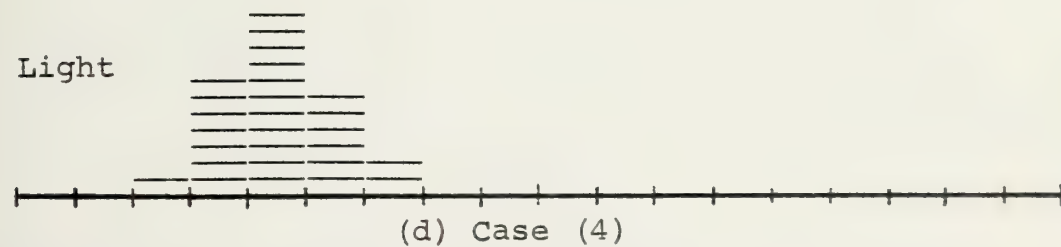


Figure 41 - Angular Dispersion - (100), 100-eV, Cu/Hg⁺
KSE-B

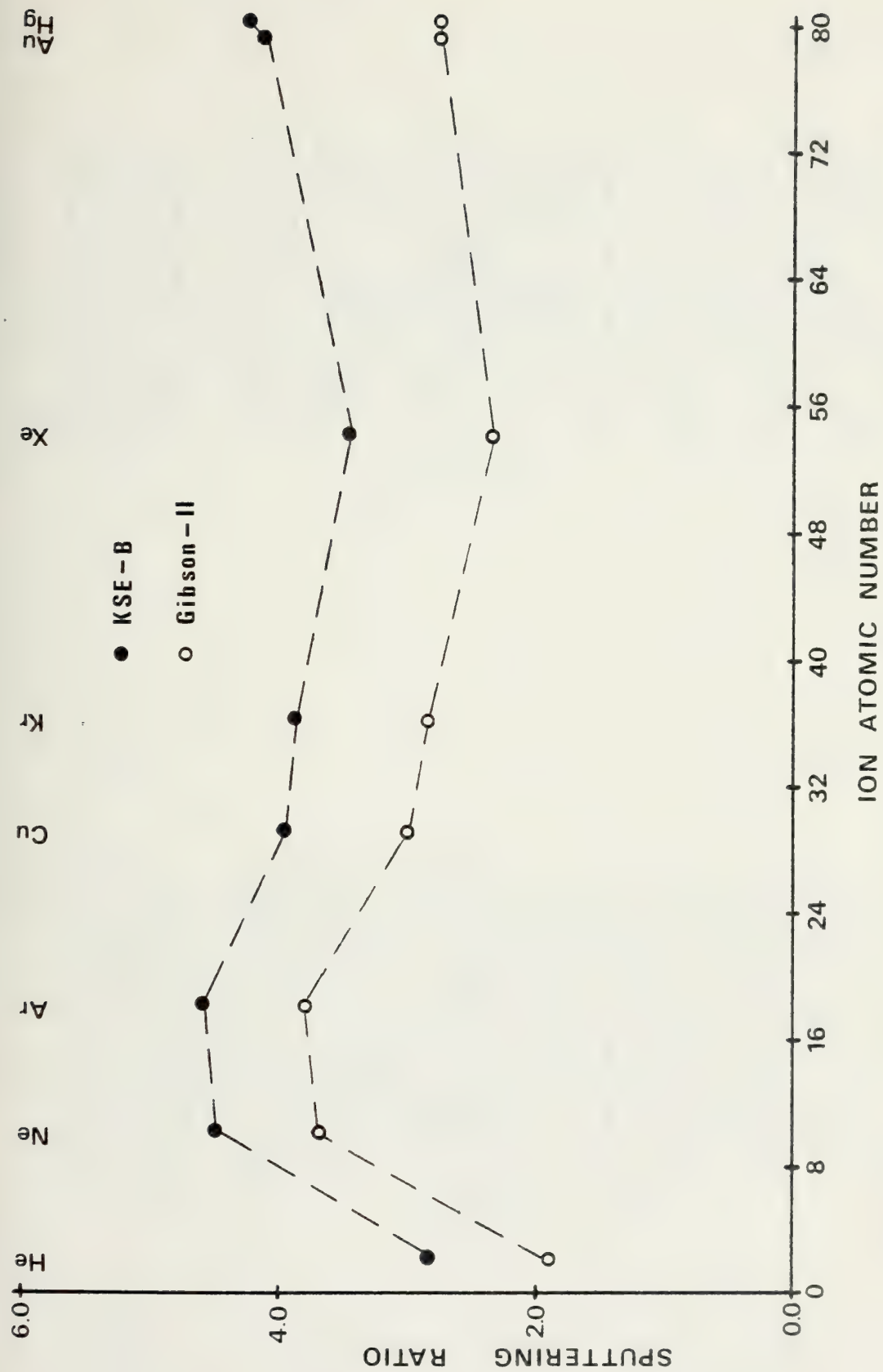
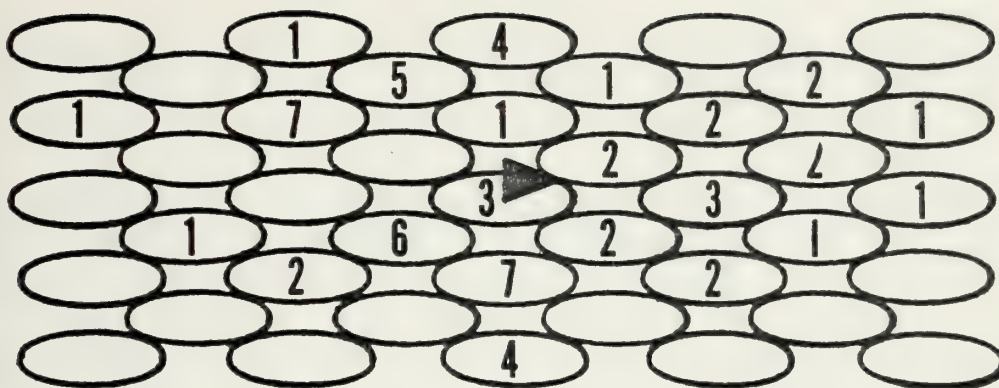


Figure 42 - Sputtering Ratio vs. Ion Atomic Number - (100), 1-keV, 9x4x9



(a) Gibson-II



(b) KSE-B

Figure 43 - Sputtering Summary - (100), 1-keV, Cu/He+

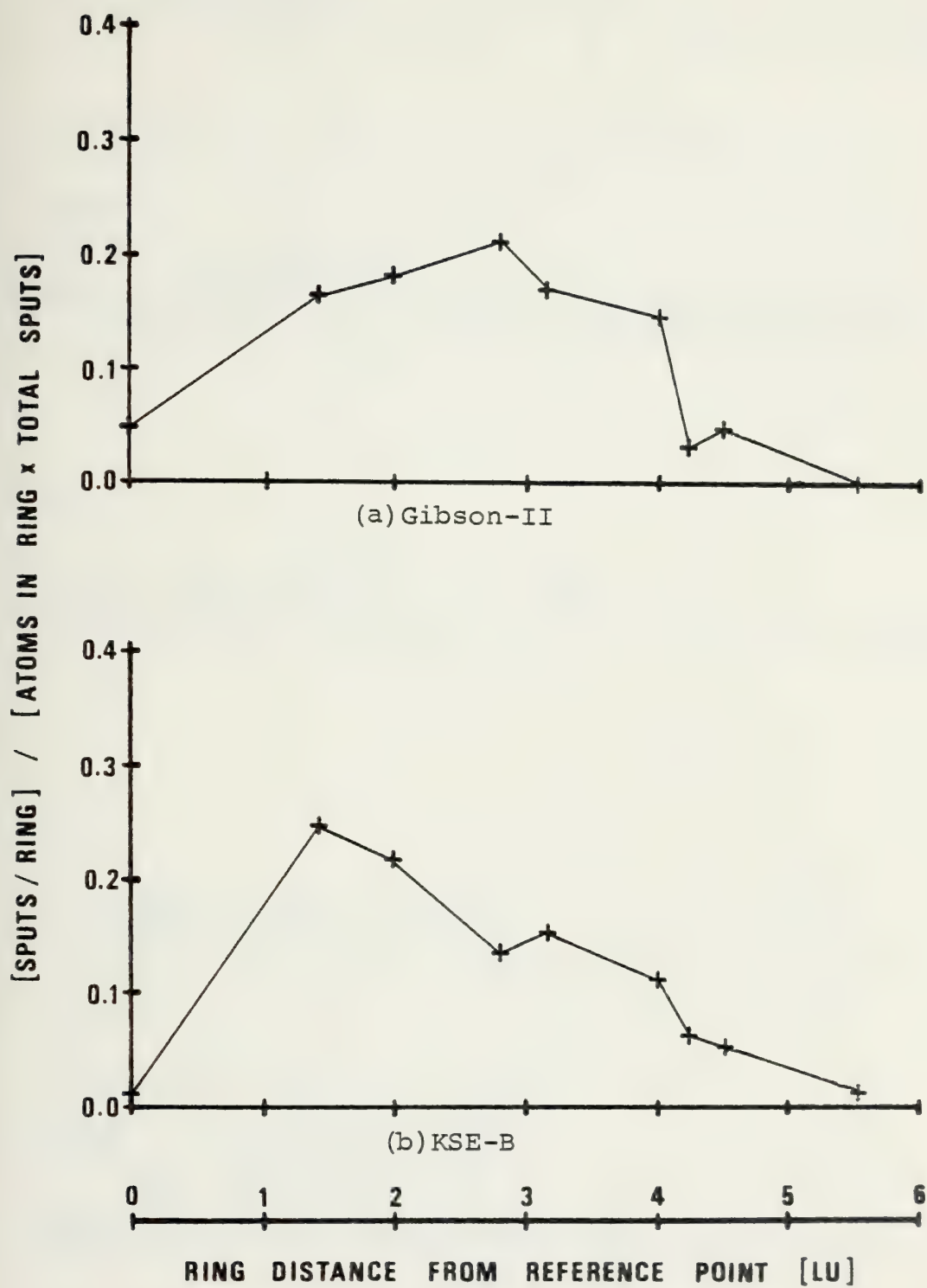
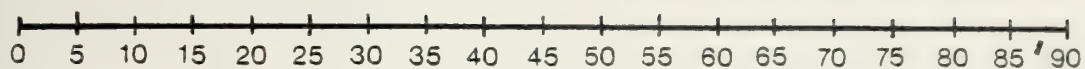


Figure 44 - Ring Probability - (100), 1-keV, Cu/He⁺

Ejection Angle (Degrees)



Heavy



Light



(a) Gibson-II

Heavy

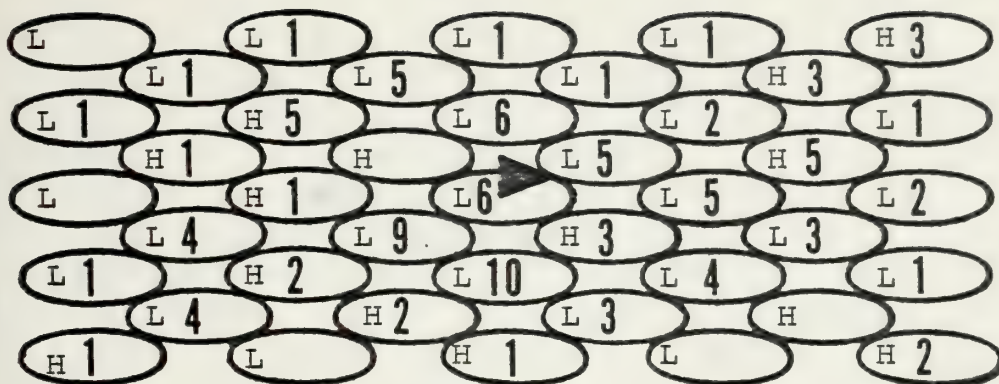


Light

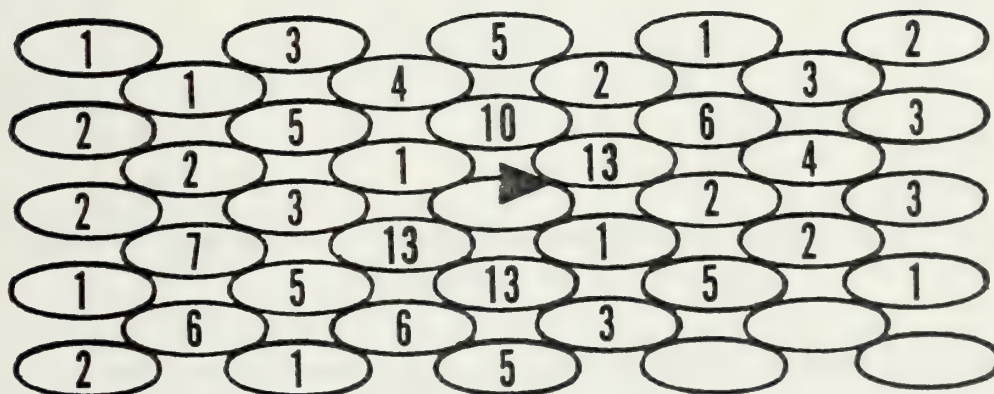


(b) KSE-B

Figure 45 - Angular Dispersion - (100), 1-keV, Cu/He⁺



(a) Gibson-II



(b) KSE-B

Figure 46 - Sputtering Summary - (100), 1-keV, Cu/Ne+

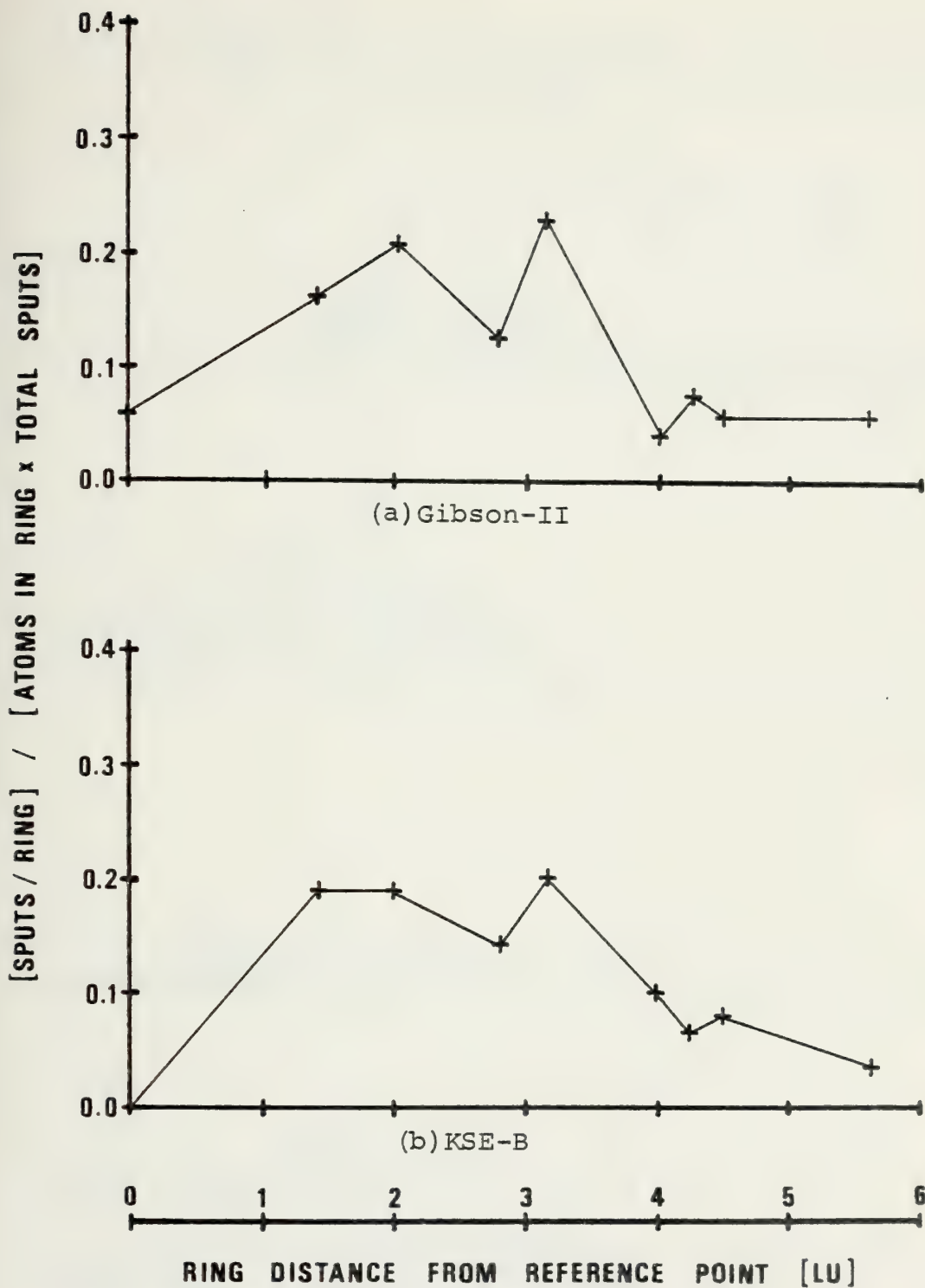
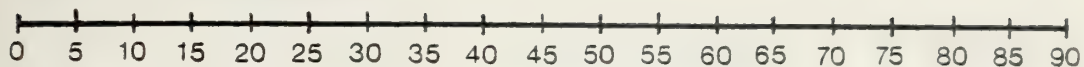
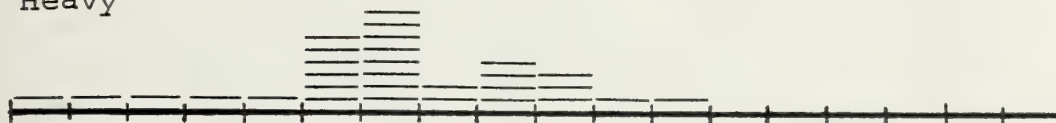


Figure 47 - Ring Probability - (100), 1-keV, Cu/Ne+

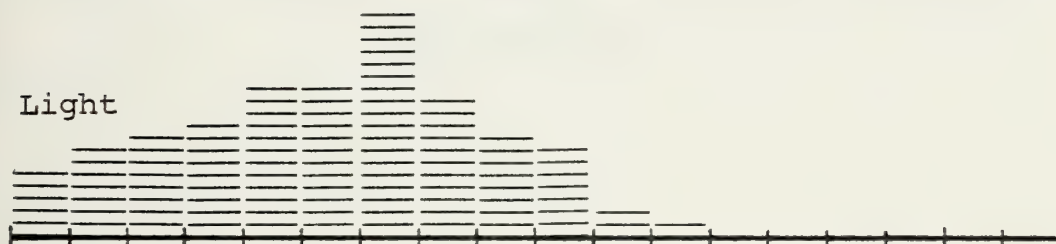
Ejection Angle (Degrees)



Heavy



Light



(a) Gibson-II

Heavy

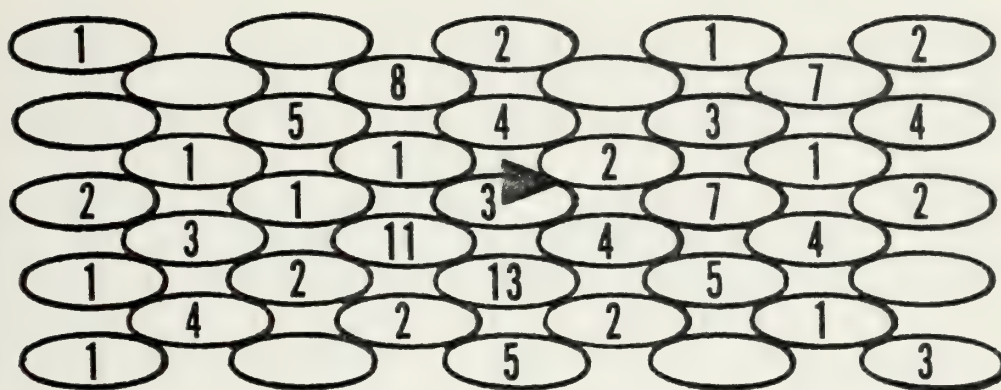


Light

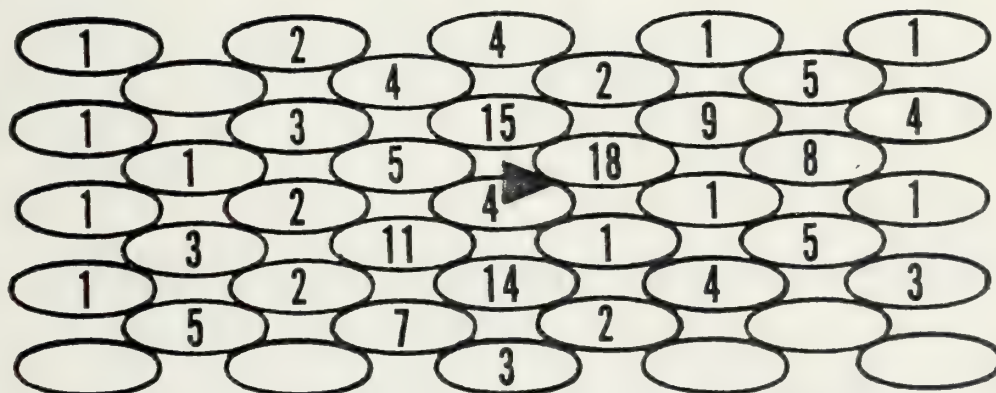


(b) KSE-B

Figure 48 - Angular Dispersion - (100), 1-keV, Cu/Ne⁺



(a) Gibson-II



(b) KSE-B

Figure 49 - Sputtering Summary - (100), 1-keV, Cu/Ar⁺

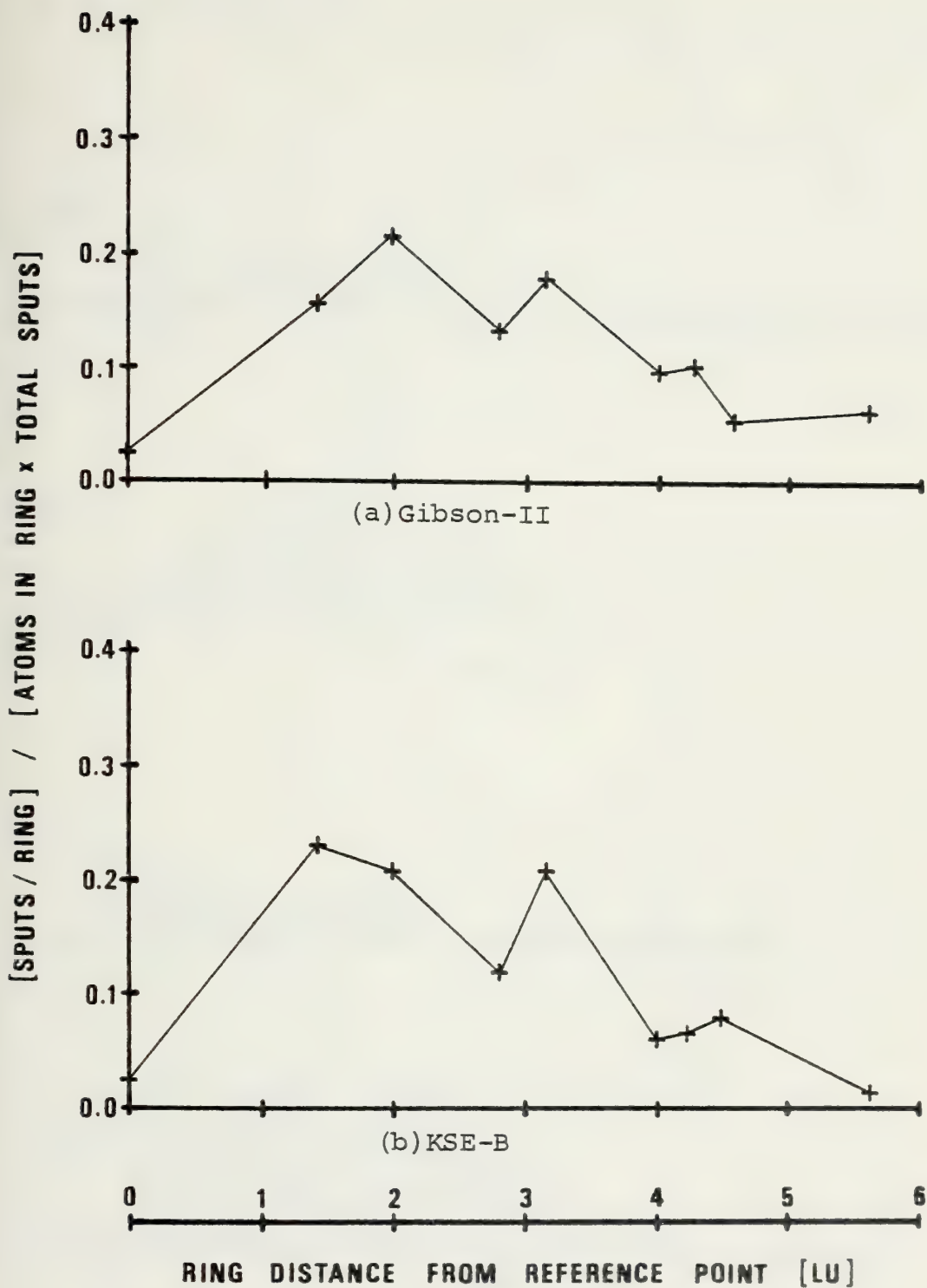
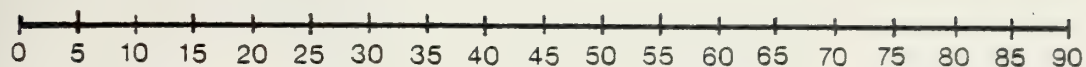
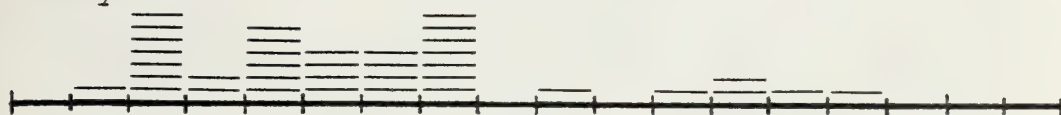


Figure 50 - Ring Probability - (100), 1-keV, Cu/Ar+

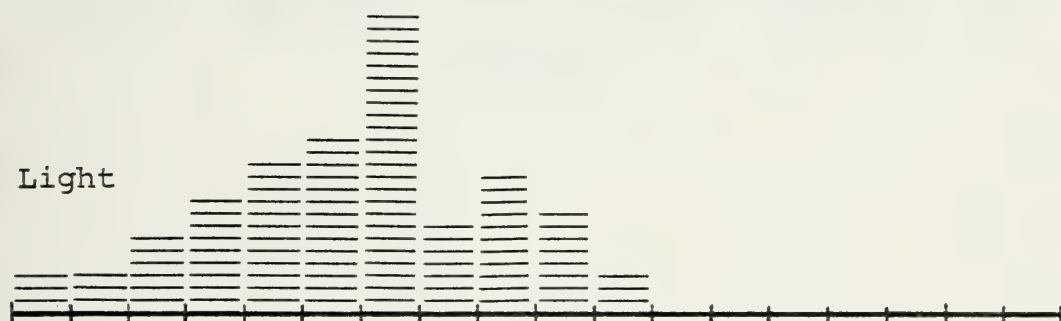
Ejection Angle (Degrees)



Heavy



Light

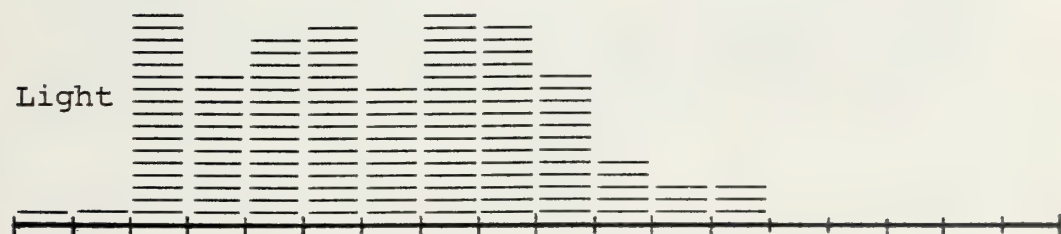


(a) Gibson-II

Heavy

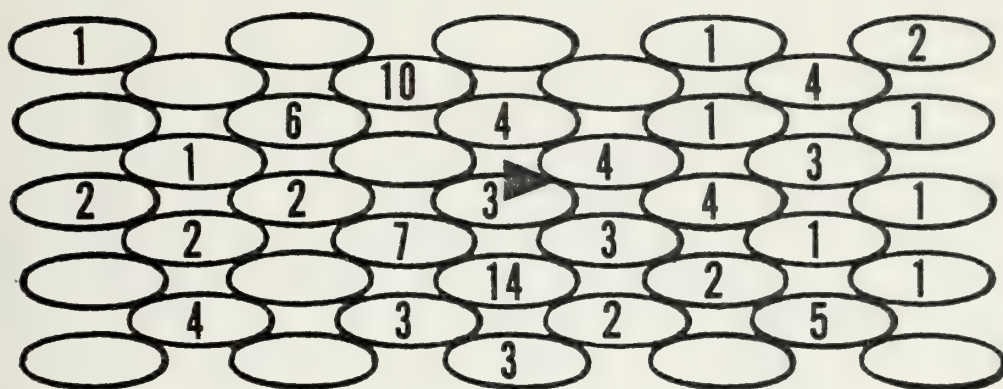


Light

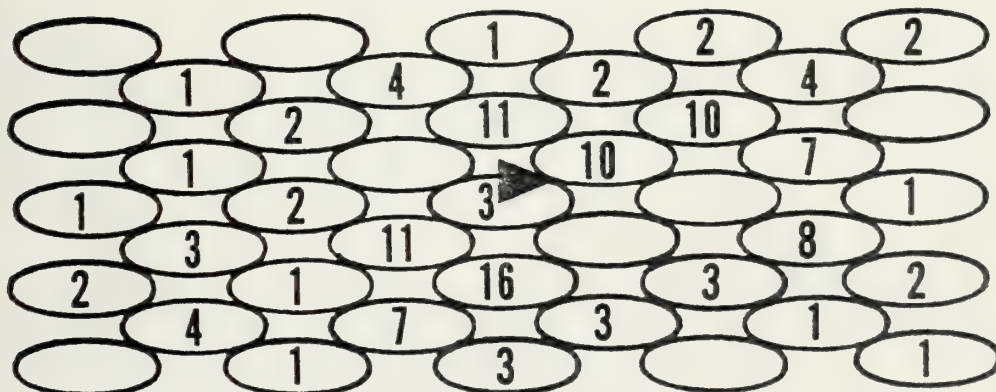


(b) KSE-B

Figure 51 - Angular Dispersion - (100), 1-keV, Cu/Ar⁺



(a) Gibson-II



(b) KSE-B

Figure 52 - Sputtering Summary - (100), 1-keV, Cu/Cu+

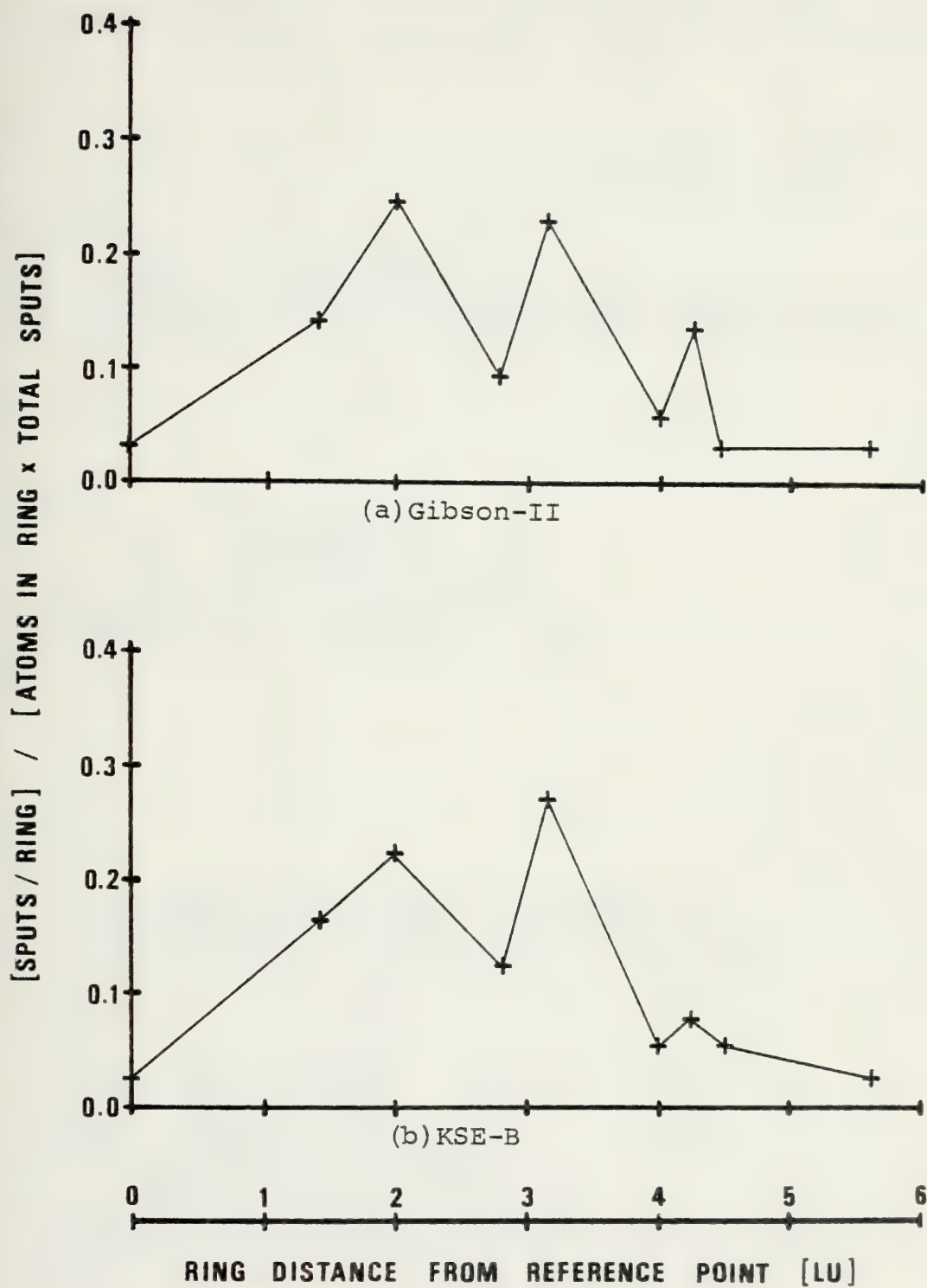
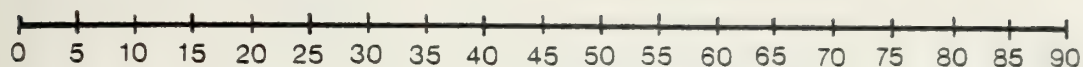


Figure 53 - Ring Probability - (100), 1-keV, Cu/Cu⁺

Ejection Angle (Degrees)



Heavy

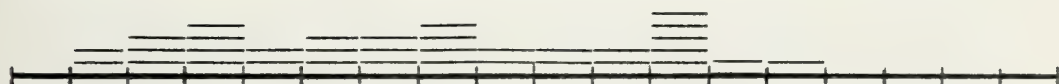


Light



(a) Gibson-II

Heavy

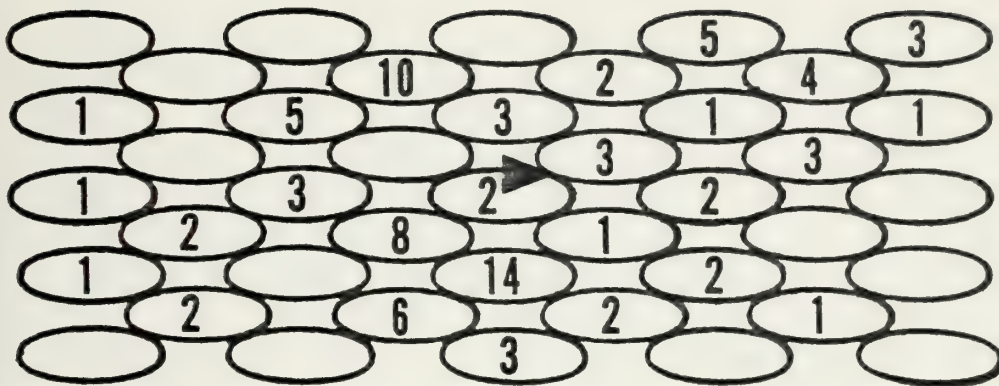


Light

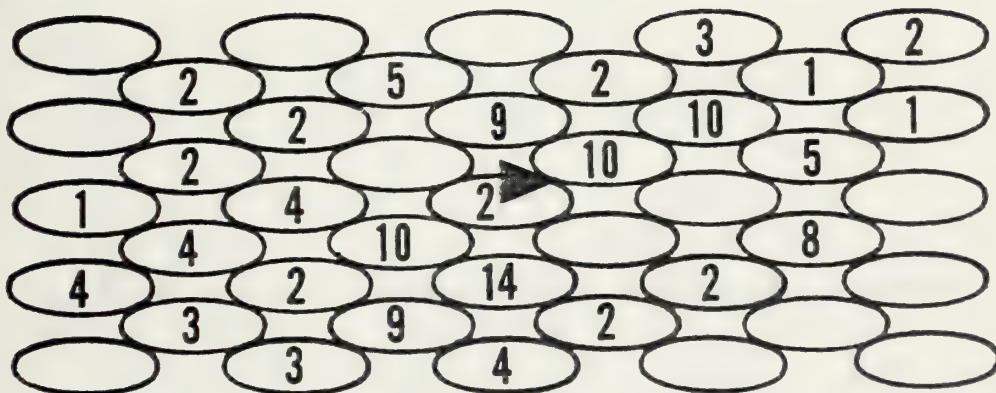


(b) KSE-B

Figure 54 - Angular Dispersion - (100), 1-keV, Cu/Cu⁺



(a) Gibson-II



(b) KSE-B

Figure 55 - Sputtering Summary - (100), 1-keV, Cu/Kr⁺

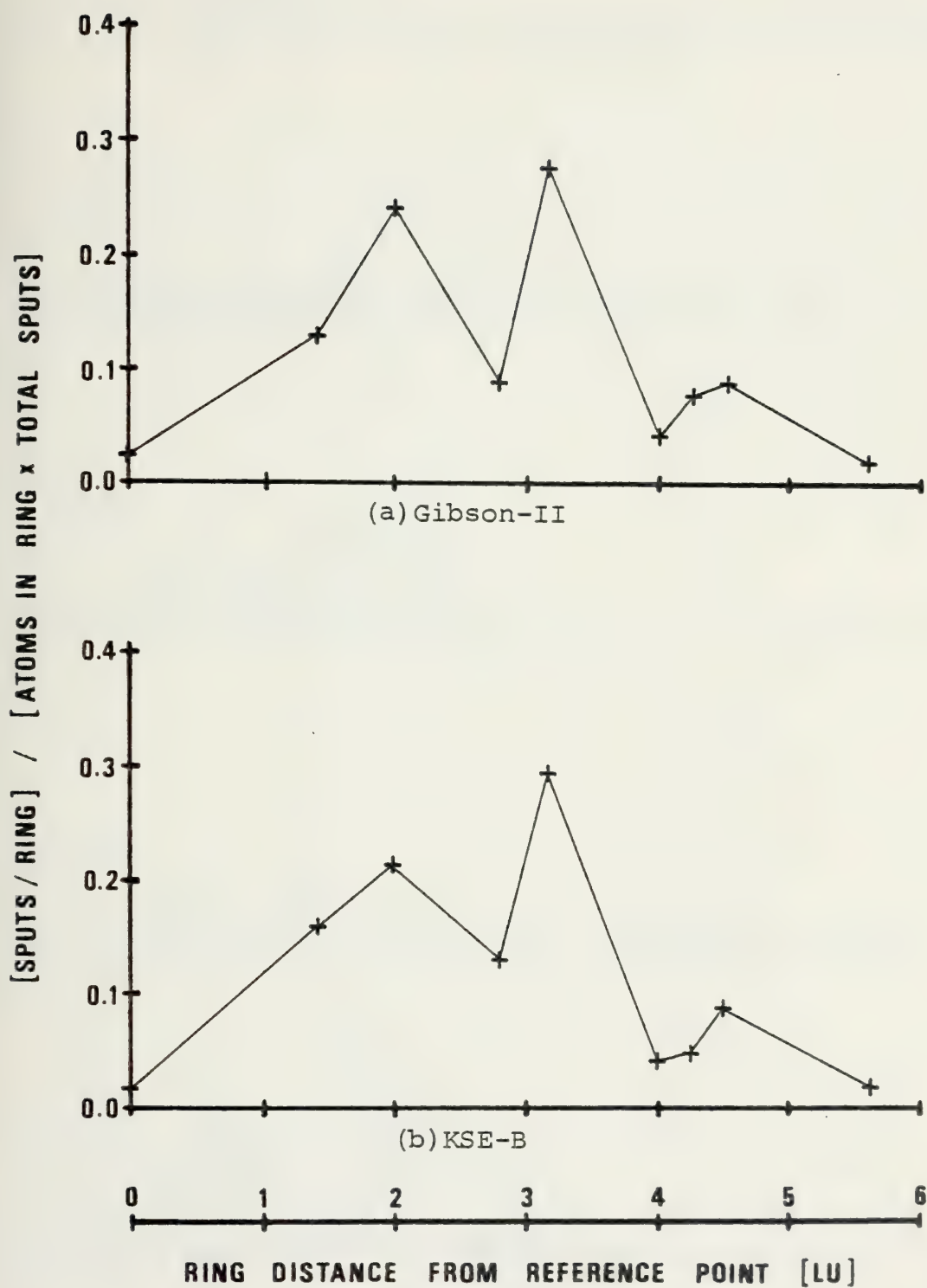
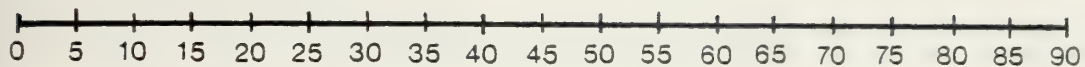


Figure 56 - Ring Probability - (100), 1-keV, Cu/Kr⁺

Ejection Angle (Degrees)



Heavy

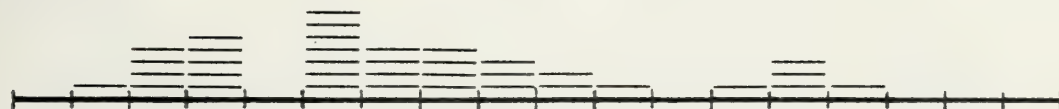


Light

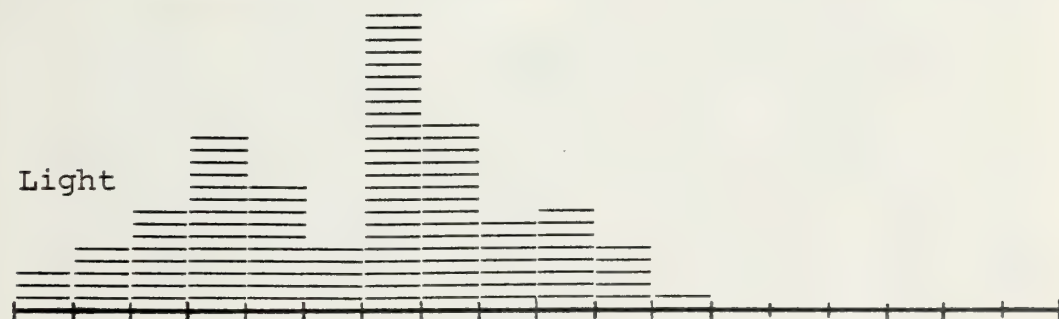


(a) Gibson-II

Heavy

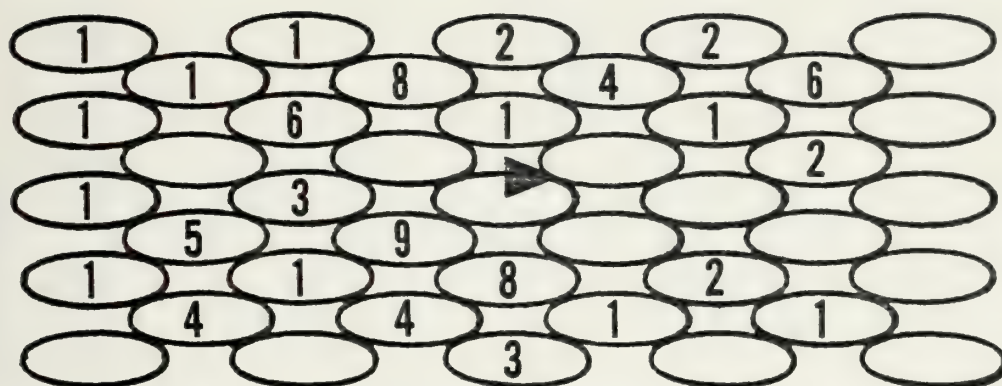


Light

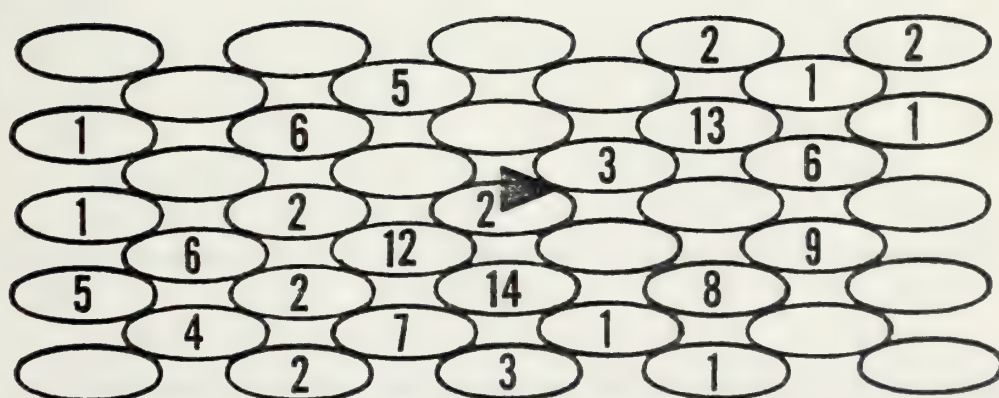


(b) KSE-B

Figure 57 - Angular Dispersion - (100), 1-keV, Cu/Kr⁺



(a) Gibson-II



(b) KSE-B

Figure 58 - Sputtering Summary - (100), 1-keV, Cu/Xe+

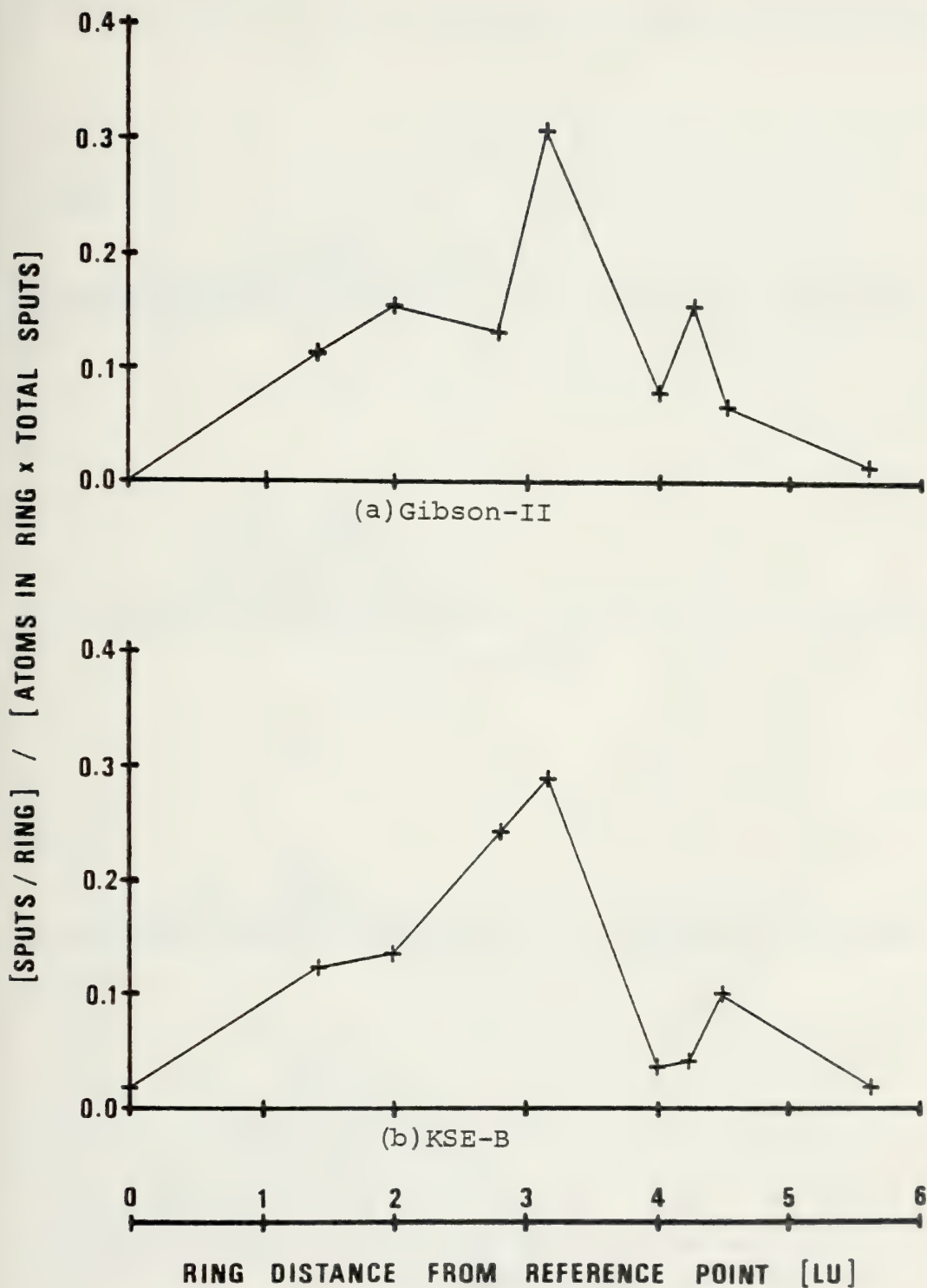
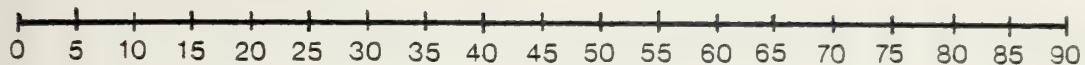
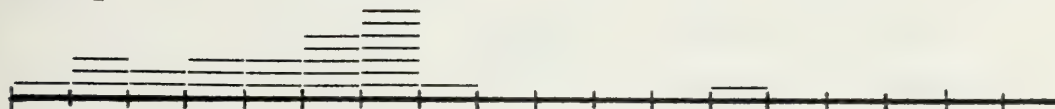


Figure 59 - Ring Probability - (100), 1-keV, Cu/Xe+

Ejection Angle (Degrees)



Heavy



Light



(a) Gibson-II

Heavy

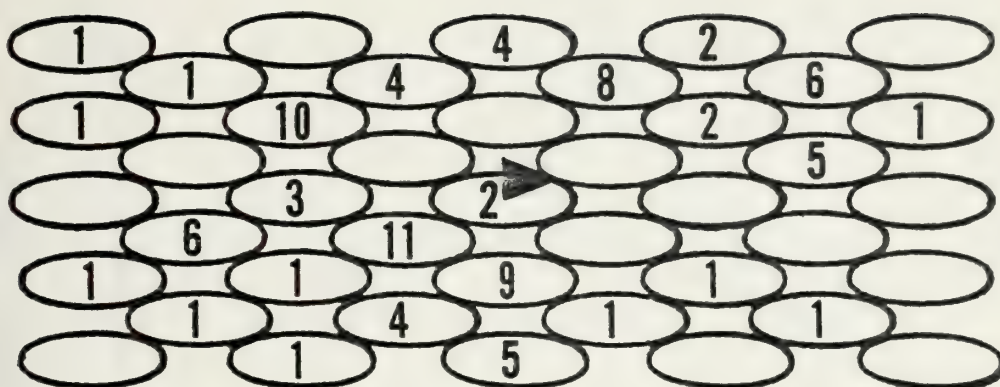


Light

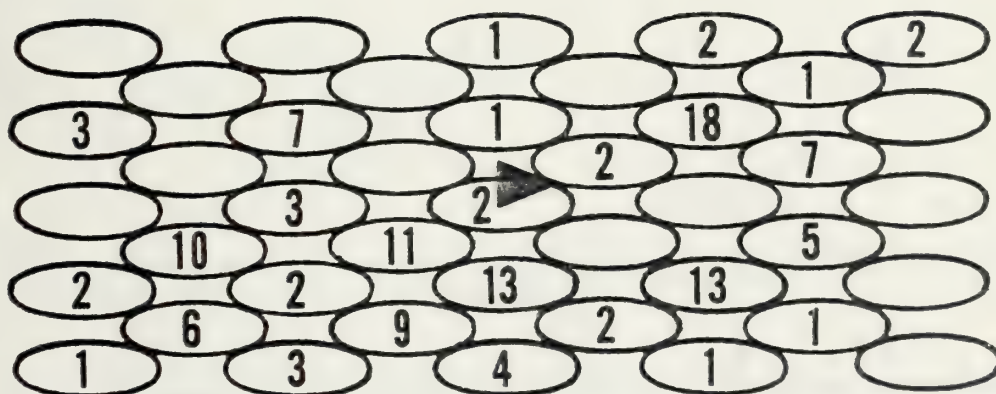


(b) KSE-B

Figure 60 - Angular Dispersion - (100), 1-keV, Cu/Xe+



(a) Gibson-II



(b) KSE-B

Figure 61 - Sputtering Summary - (100), 1-keV, Cu/Au⁺

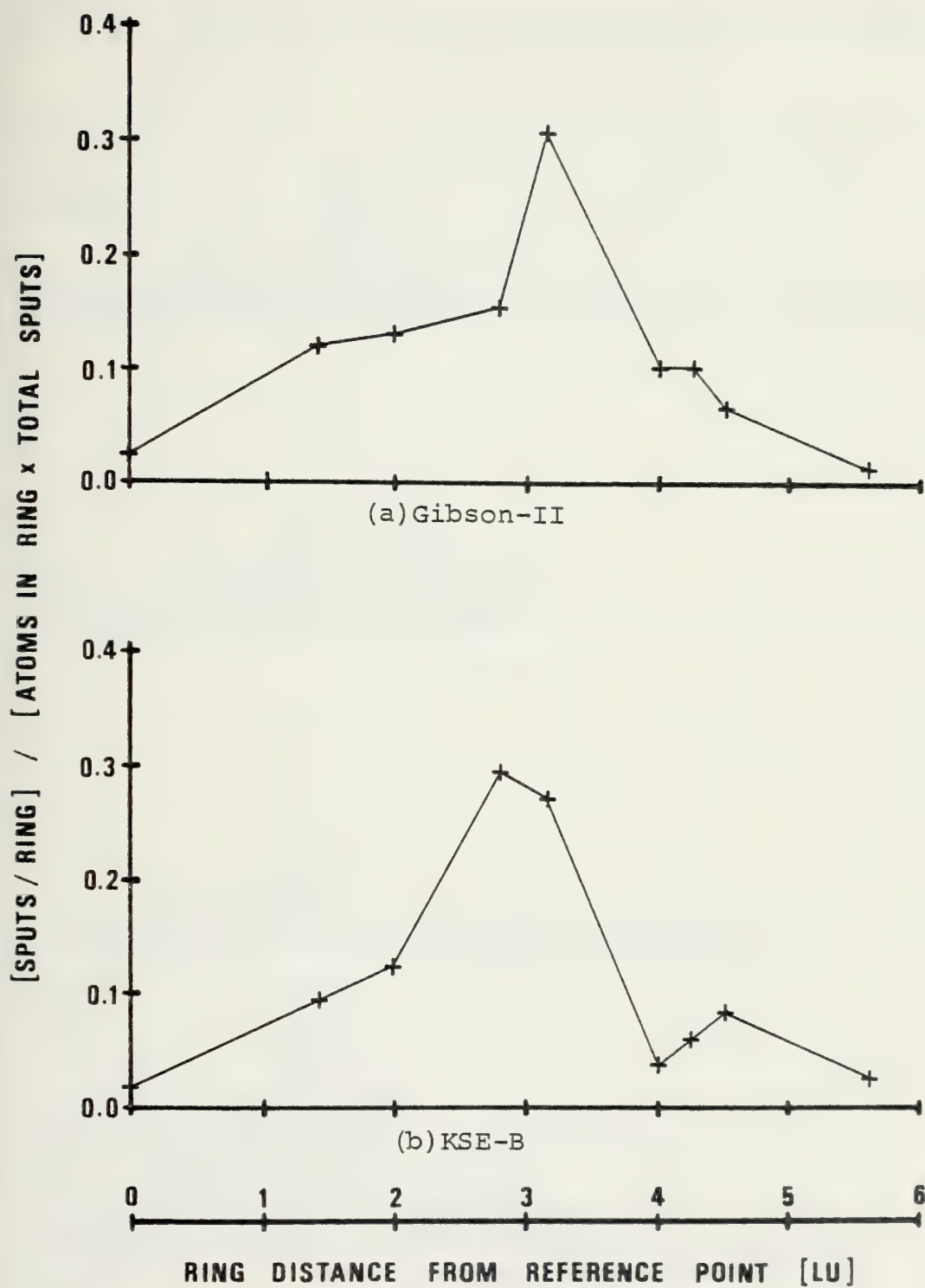


Figure 62 - Ring Probability - (100), 1-keV, Cu/Au⁺

Ejection Angle (Degrees)



Heavy

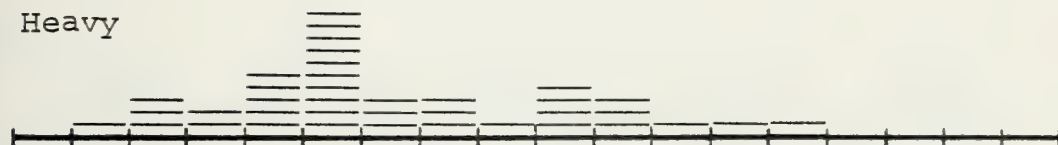


Light



(a) Gibson-II

Heavy

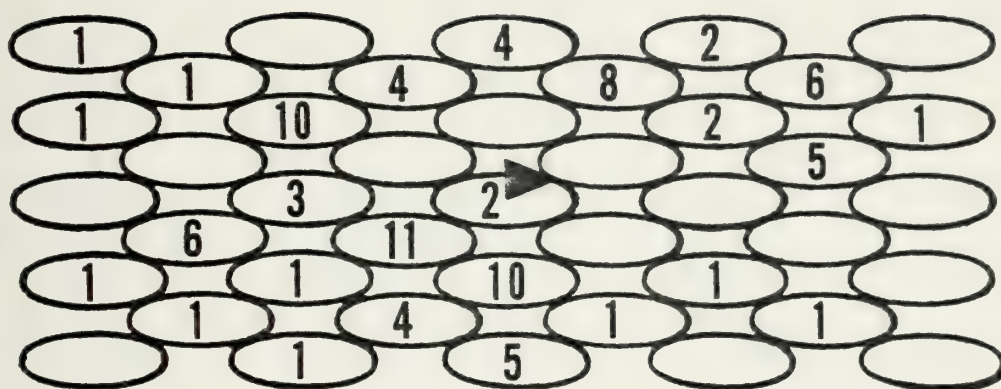


Light

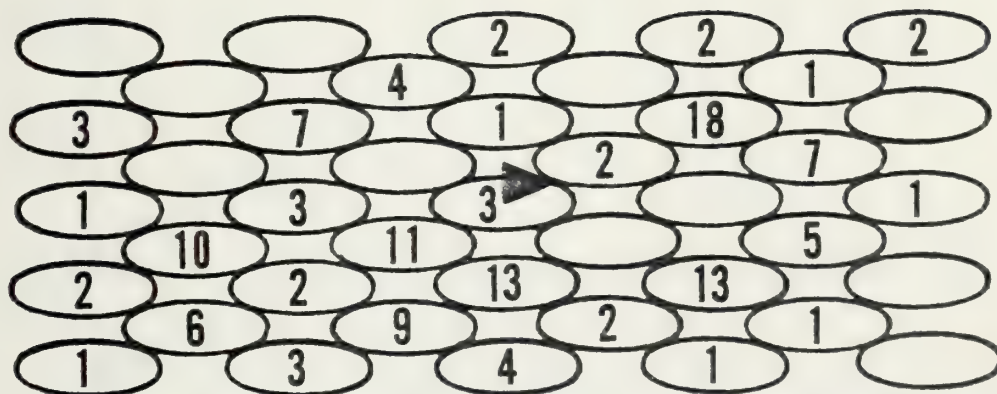


(b) KSE-B

Figure 63 - Angular Dispersion - (100), 1-keV, Cu/Au+



(a) Gibson-II



(b) KSE-B

Figure 64 - Sputtering Summary - (100), 1-keV, Cu/Hr⁺

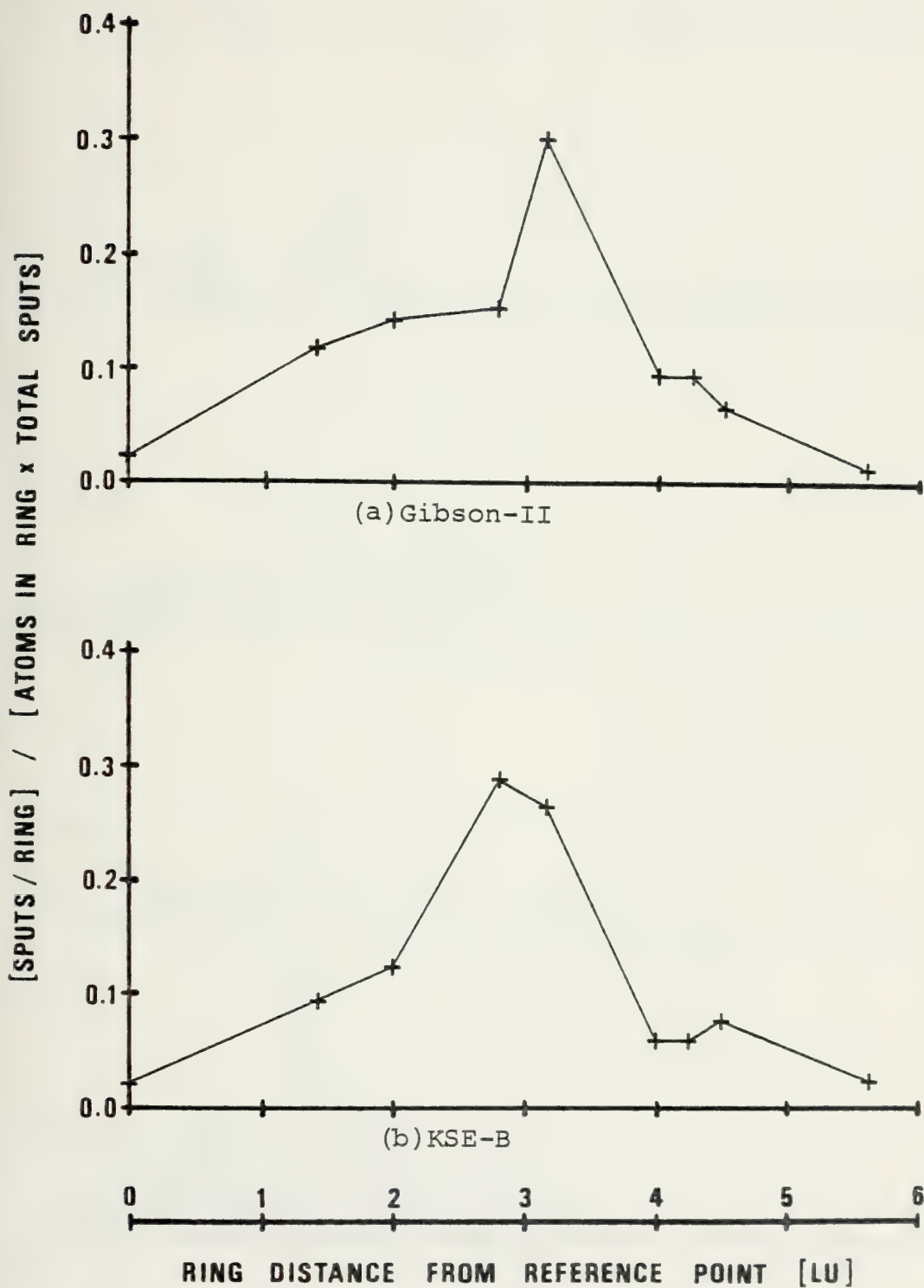
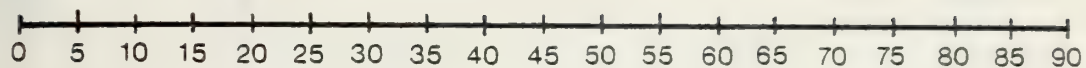
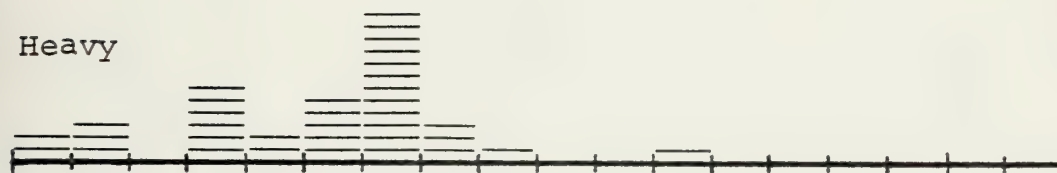


Figure 65 - Ring Probability - (100), 1-keV, Cu/Hg+

Ejection Angle (Degrees)



Heavy



Light

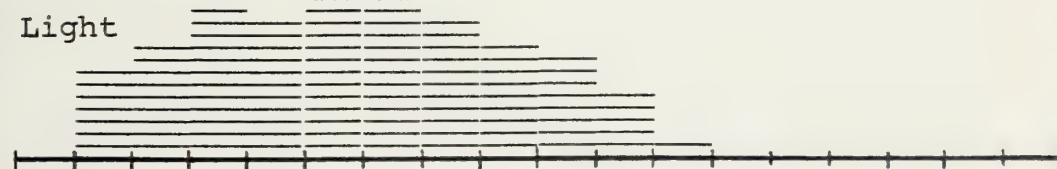


(a) Gibson-II

Heavy



Light



(b) KSE-B

Figure 66 - Angular Dispersion - (100), 1-keV, Cu/H⁺

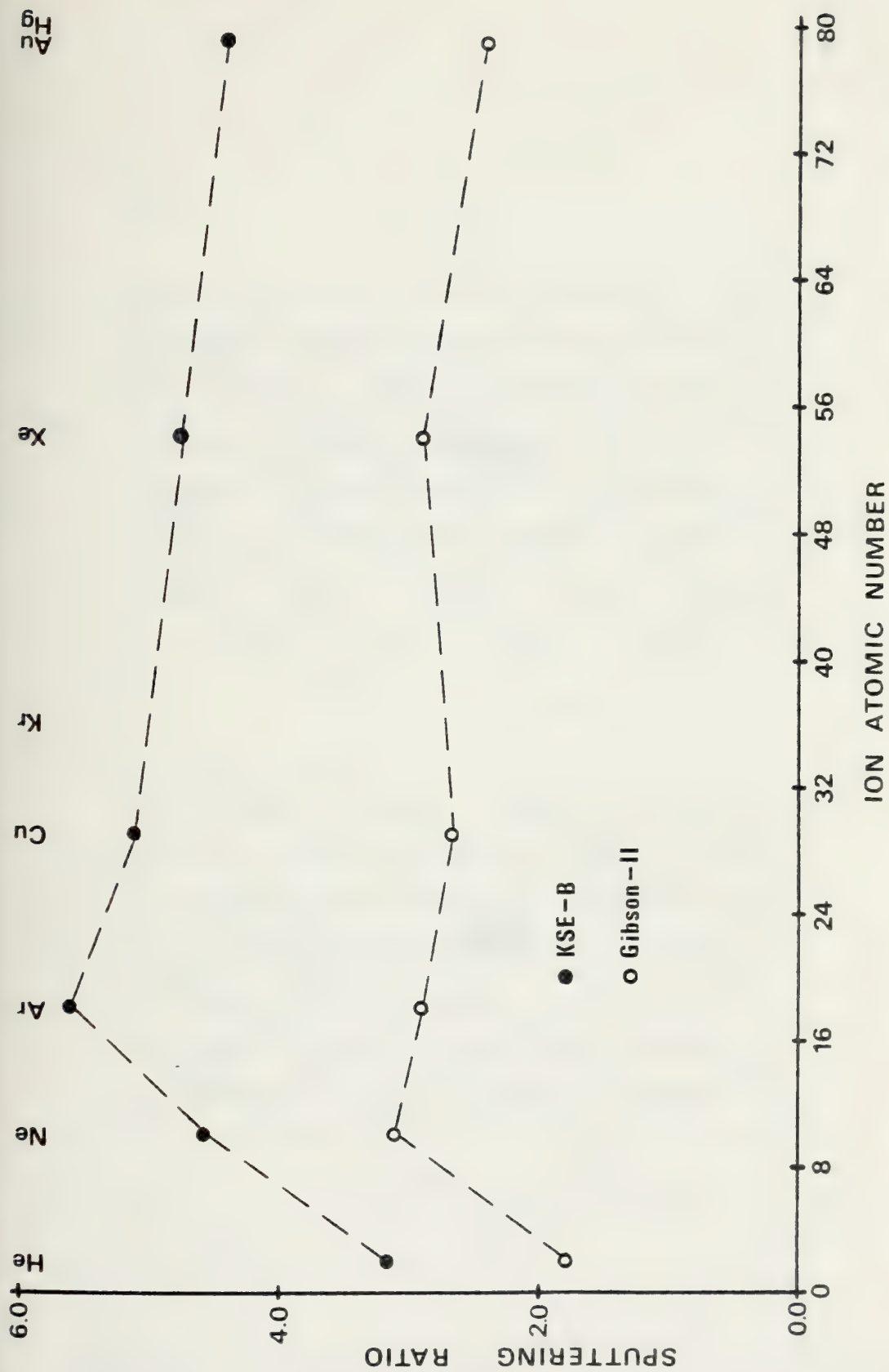
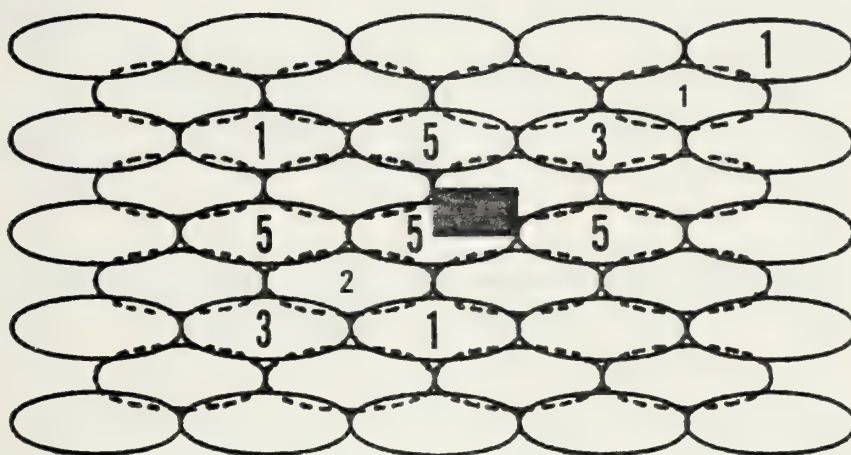
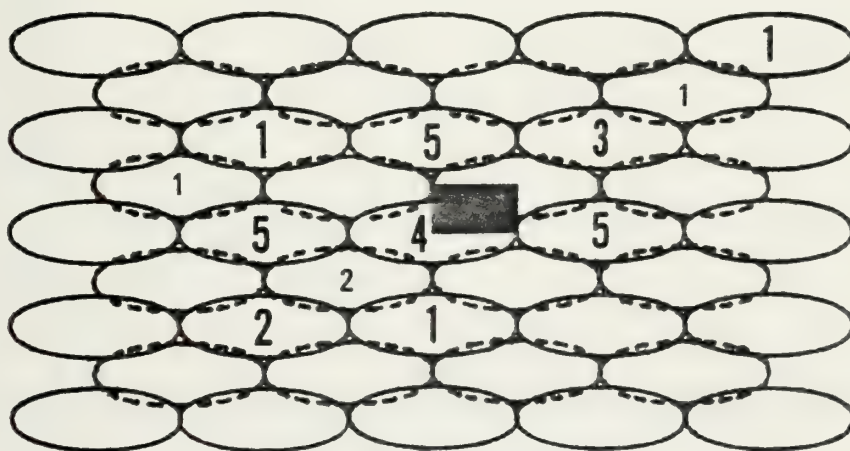


Figure 67 - Sputtering Ratio vs. Ion Atomic Number - (100), 2-keV, 9x4x9



(a) Case (1) and Case (3)



(b) Case (2) and Case (4)

Figure 68 - Sputtering Summary - (110), 100-eV, Cu/Ar⁺
Gibson-II

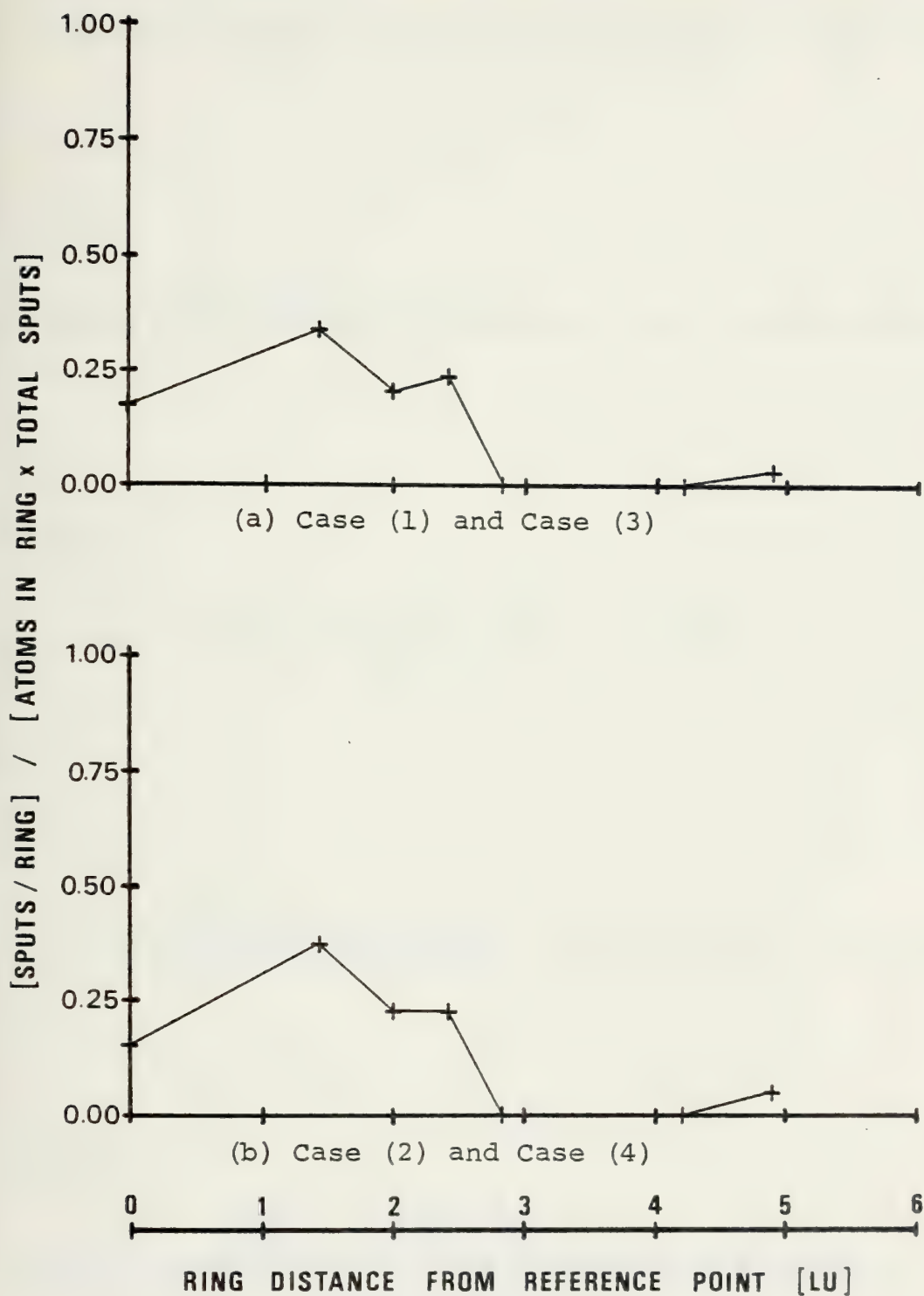
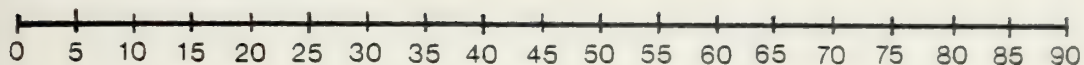


Figure 69 - Ring Probability - (110), 100-eV, Cu/Ar⁺
Gibson-II

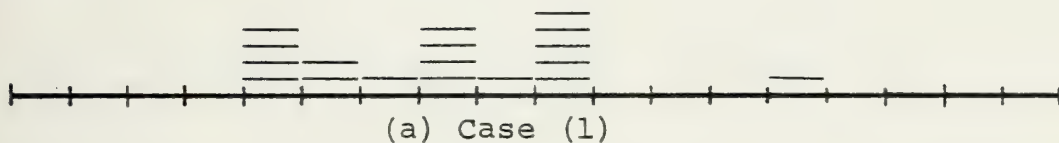
Ejection Angle (Degrees)



Heavy



Light



Heavy



Light

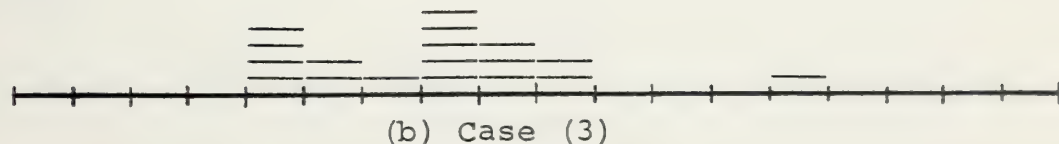
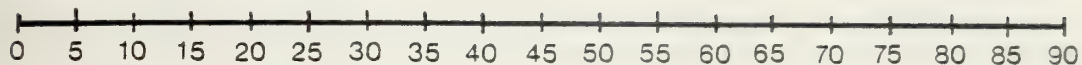
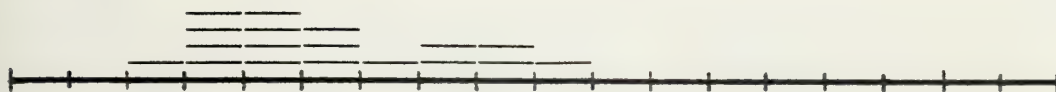


Figure 70 - Angular Dispersion - (110), 100-eV, Cu/Ar⁺
Gibson-II

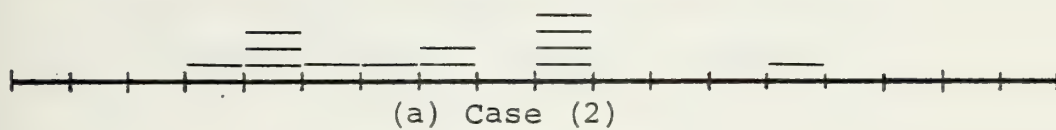
Ejection Angle (Degrees)



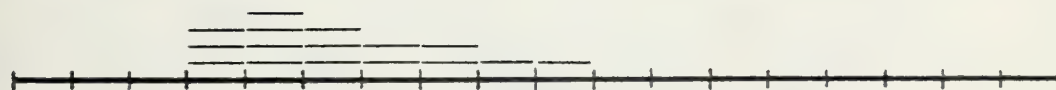
Heavy



Light



Heavy



Light

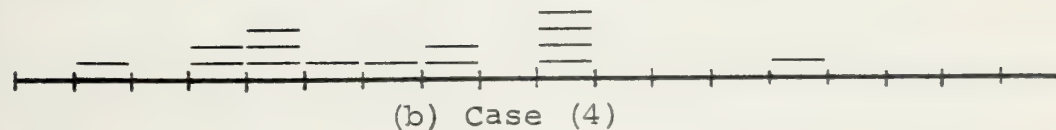
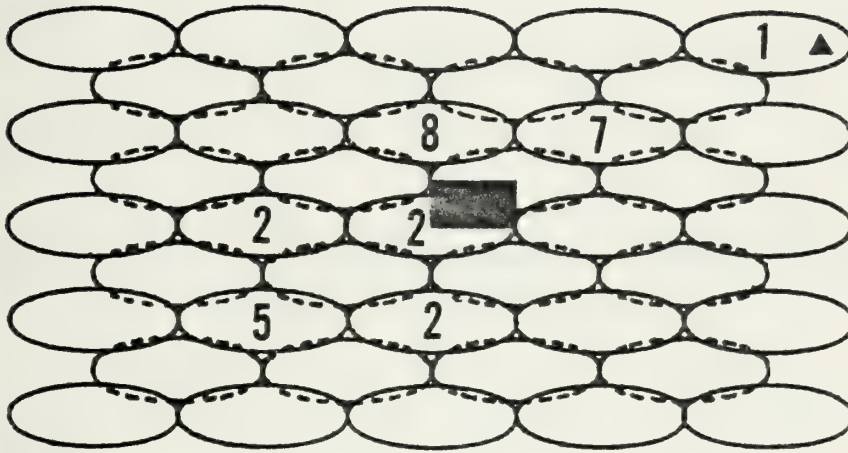
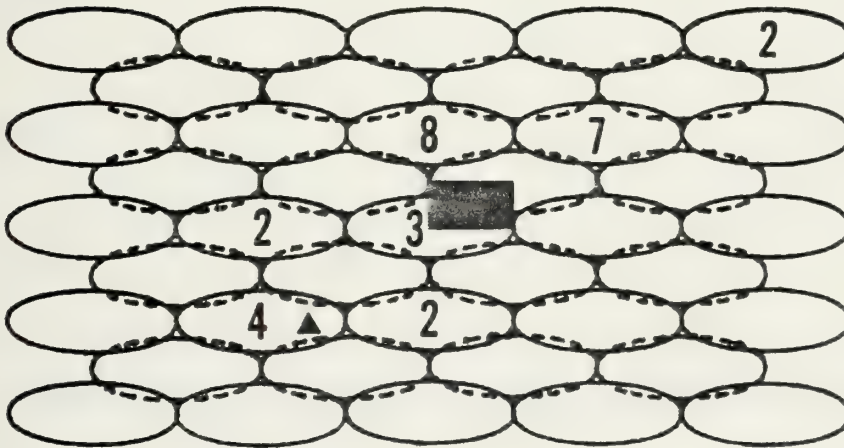


Figure 71 - Angular Dispersion - (110), 100-eV, Cu/Ar⁺
Gibson-II



(a) Case (1) and Case (3)



(b) Case (2) and Case (4)

Figure 72 - Sputtering Summary - (110), 100-eV, Cu/Ar⁺
KSE-B

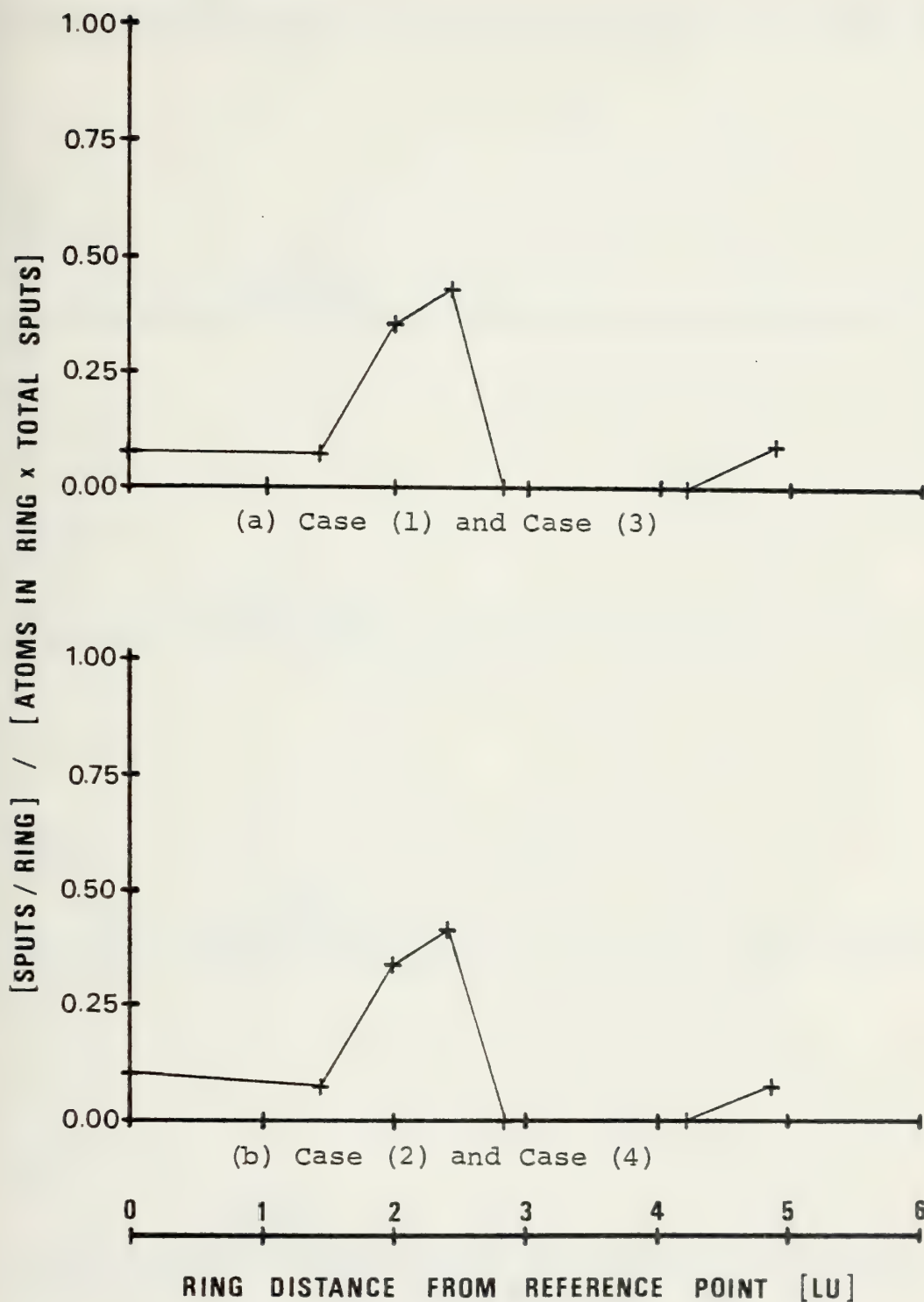
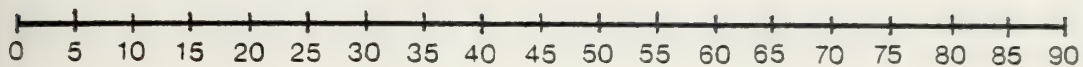
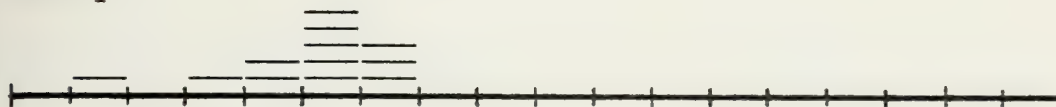


Figure 73 - Ring Probability - (110), 100-eV, Cu/Ar+
KSE-B

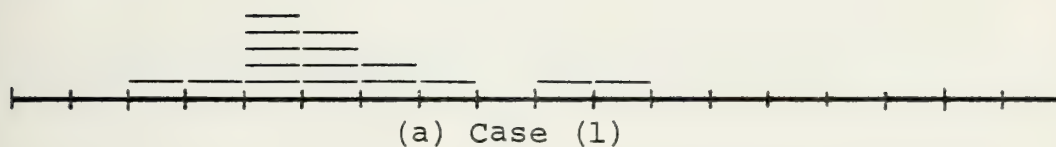
Ejection Angle (Degrees)



Heavy



Light



Heavy



Light

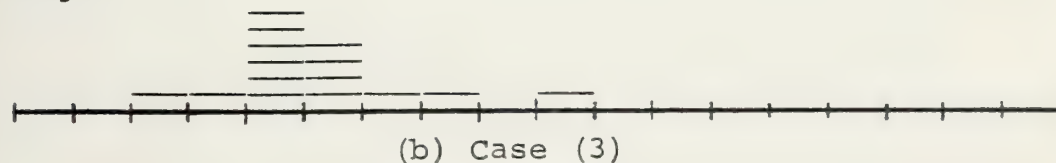
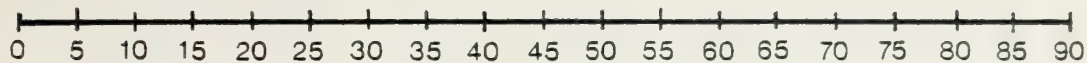
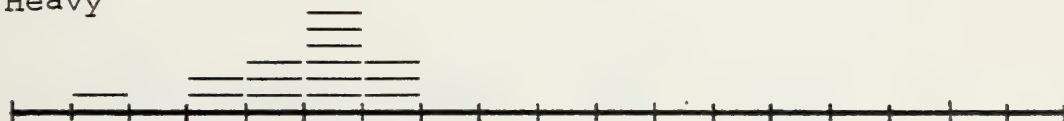


Figure 74 - Angular Dispersion - (110), 100-eV, Cu/Ar⁺
KSE-B

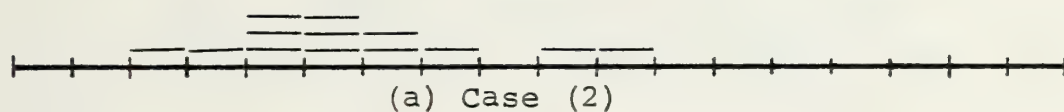
Ejection Angle (Degrees)



Heavy

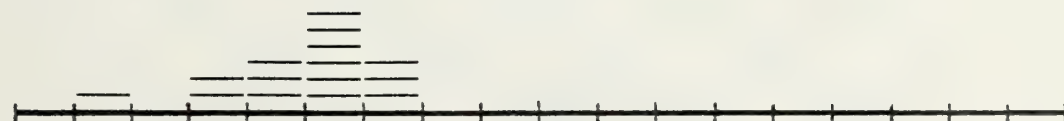


Light

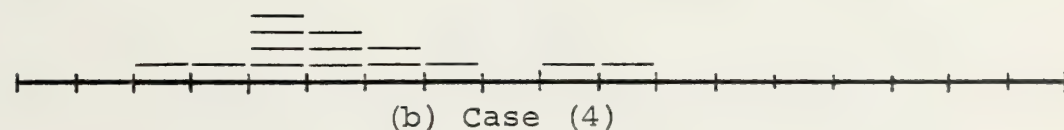


(a) Case (2)

Heavy

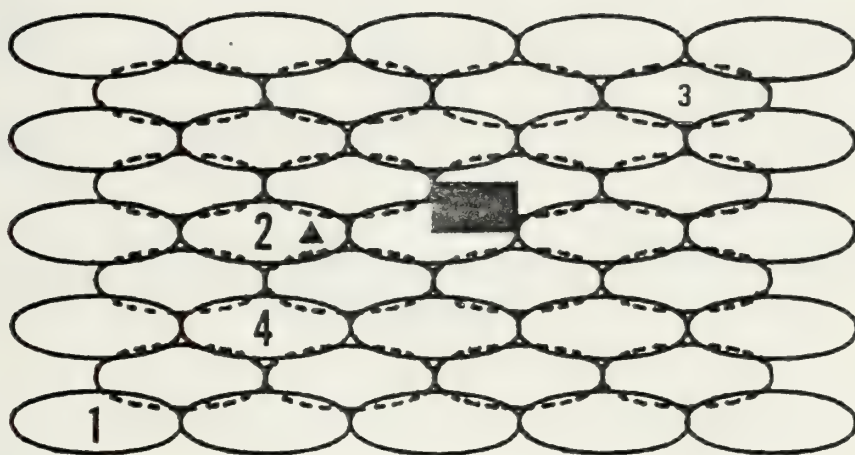


Light

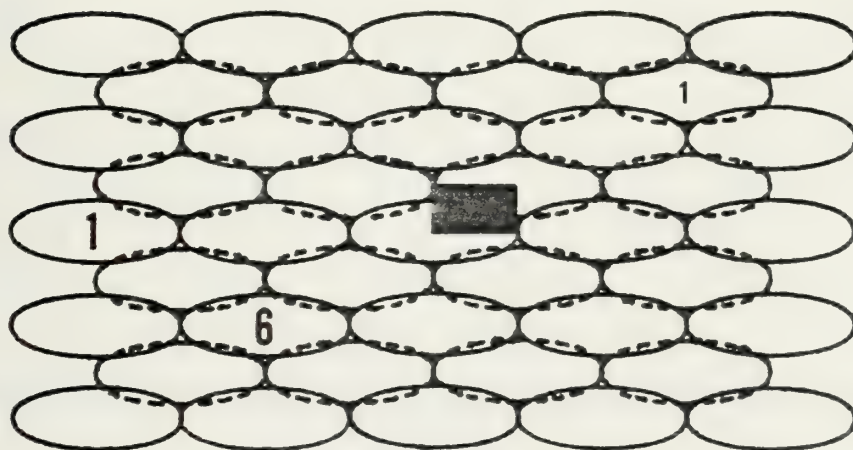


(b) Case (4)

Figure 75 - Angular Dispersion - (110), 100-eV, Cu/Ar⁺
KSE-B



(a) Gibson-II



(b) KSE-B

Figure 76 - Sputtering Summary - (110), 100-eV, Cu/Hg⁺
KSE-B

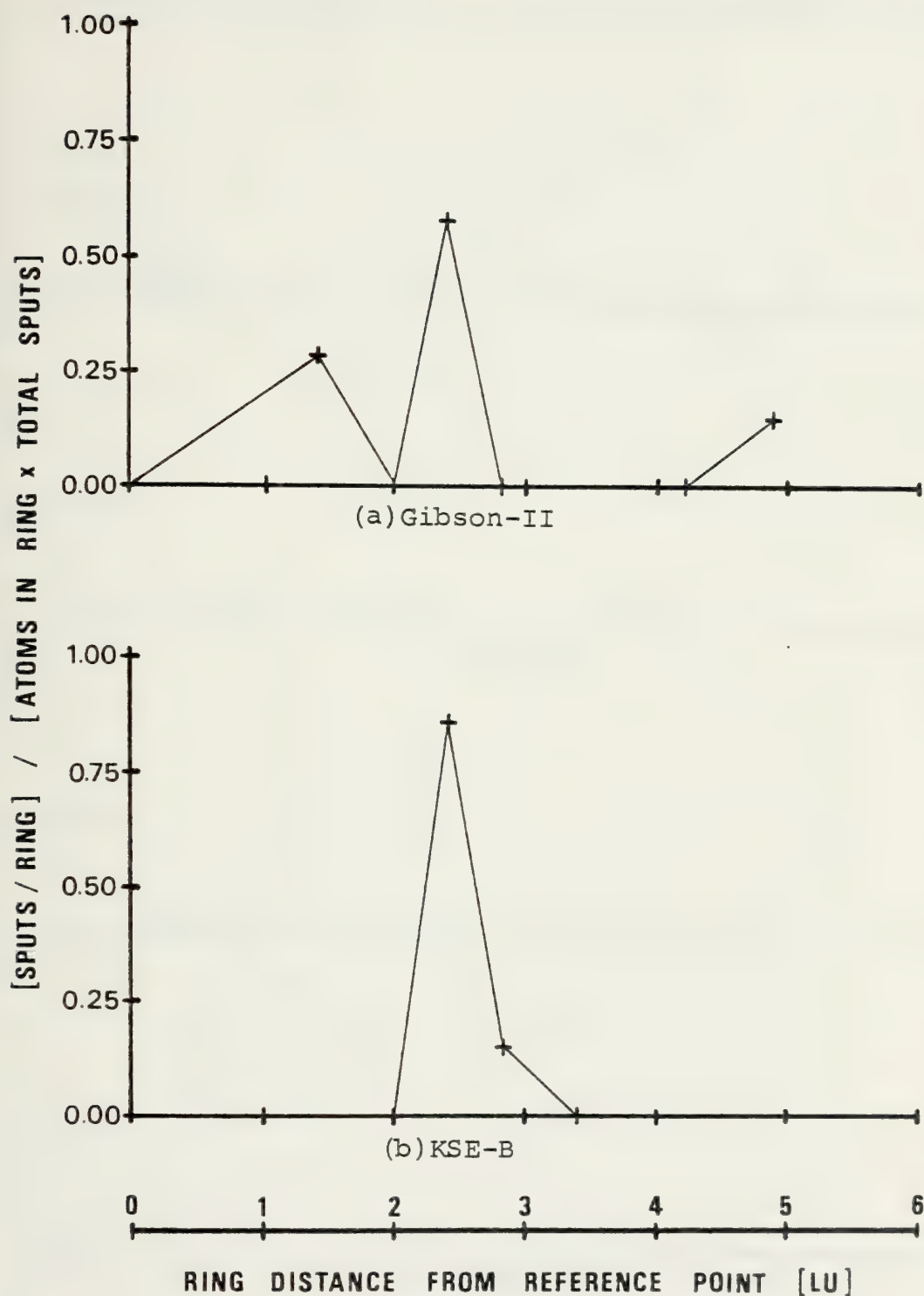
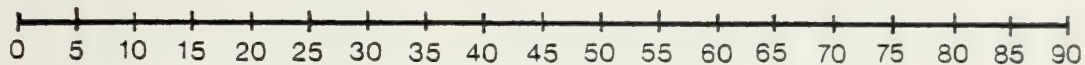


Figure 77 - Ring Probability - (110), 100-eV, Cu/Hg+
KSE-B

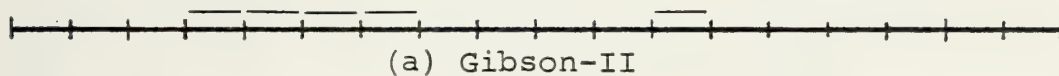
Ejection Angle (Degrees)



Heavy



Light

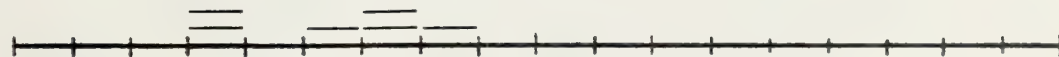


(a) Gibson-II

Heavy

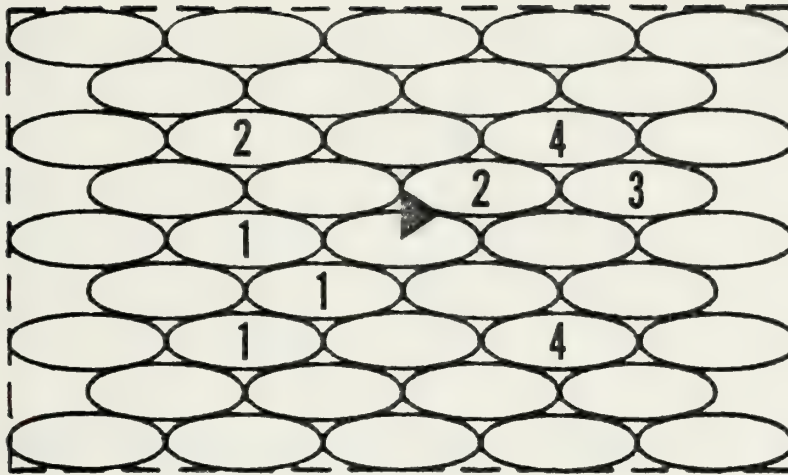


Light

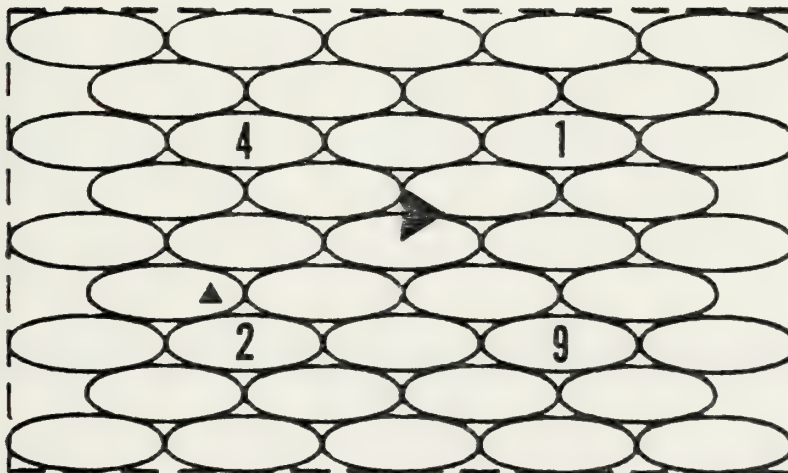


(b) KSE-B

Figure 78 - Angular Dispersion - (110), 100-eV, Cu/H⁺



(a) Gibson-II



(b) KSE-B

Figure 79 - Sputtering Summary - (111), 100-eV, Cu/Ar⁺

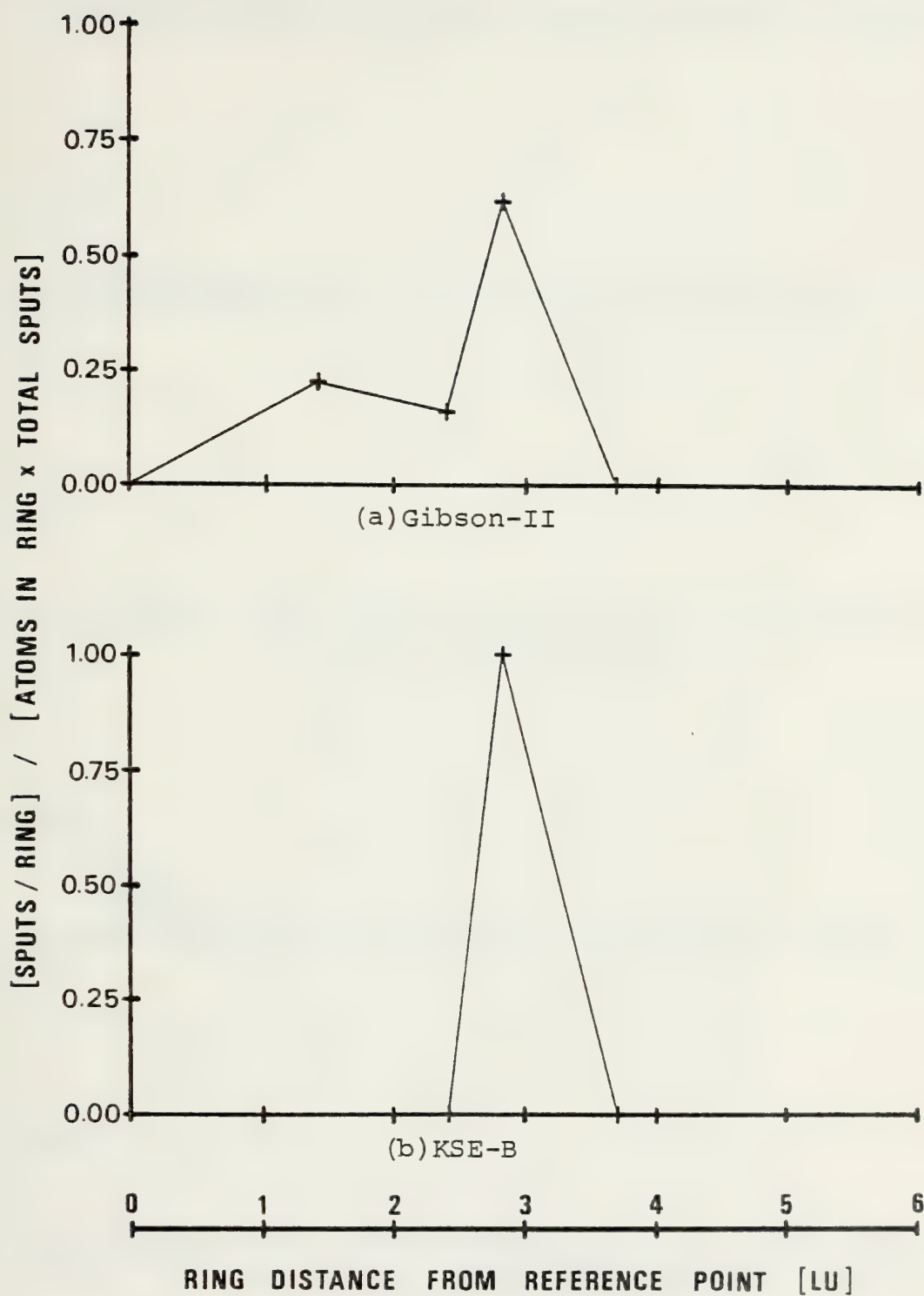
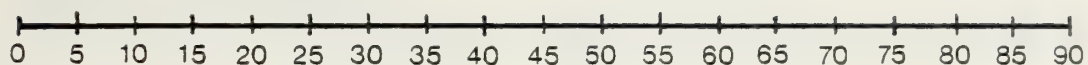
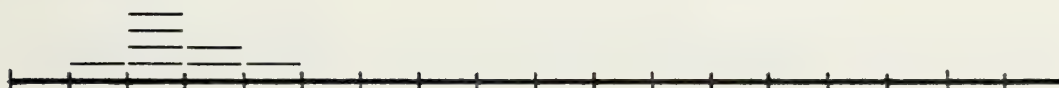


Figure 80 - Atom Probability - (111), 100-eV, Cu/Ar⁺

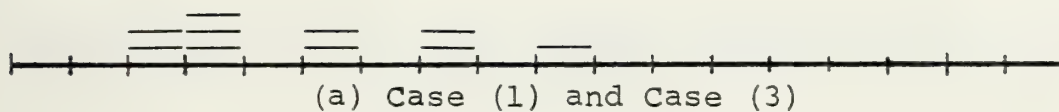
Ejection Angle (Degrees)



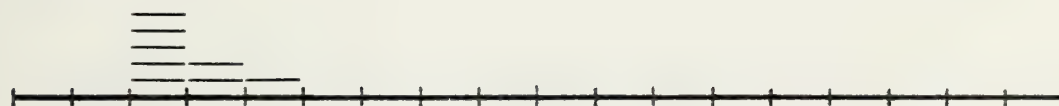
Heavy



Light



Heavy



Light

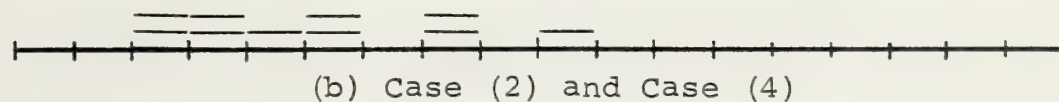
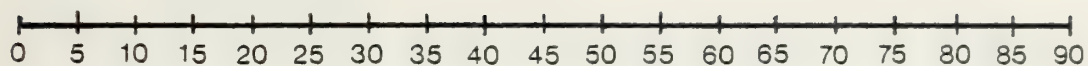


Figure 81 - Angular Dispersion - (111), 100-eV, Cu/Ar⁺
Gibson-II

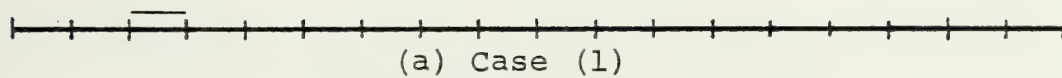
Ejection Angle (Degrees)



Heavy



Light



(a) Case (1)

Heavy



Light



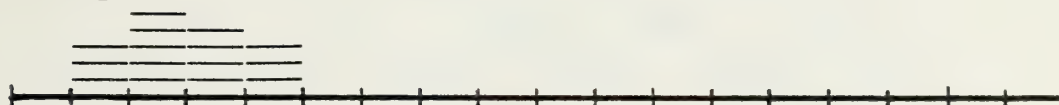
(b) Case (3)

Figure 82 - Angular Dispersion - (111), 100-eV, Cu/Ar⁺
KSE-B

Ejection Angle (Degrees)



Heavy

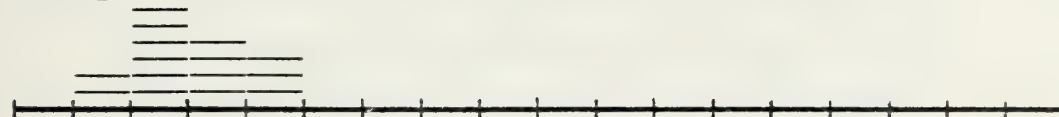


Light

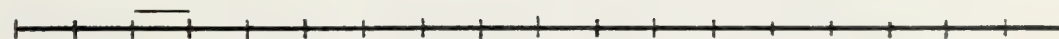


(a) Case (2)

Heavy

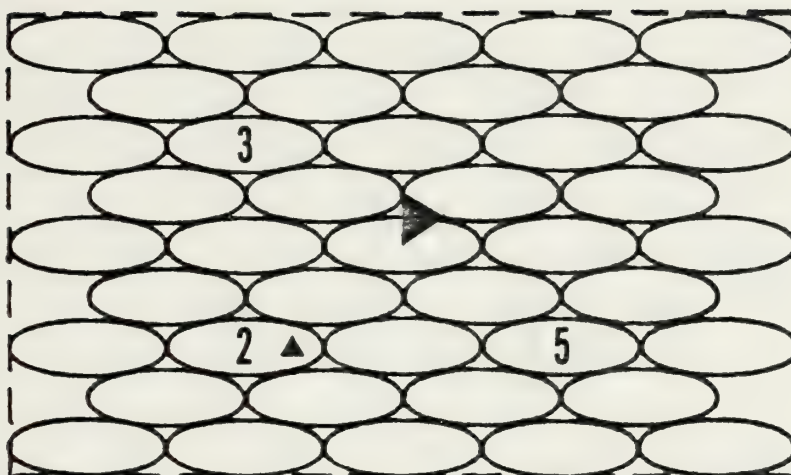


Light



(b) Case (4)

Figure 83 - Angular Dispersion - (111), 100-eV, Cu/Ar⁺
KSE-B



(a) Case (1), Case (2), and Case (4)



(b) Case (3)

Figure 84 - Sputtering Summary - (111), 100-eV, Cu/Hr+
Gibson-II



(a) Case (1) and Case (3)



(b) Case (2) and Case (4)

Figure 85 - Sputtering Summary - (111), 100-eV, Cu/Hg⁺
KSE-B

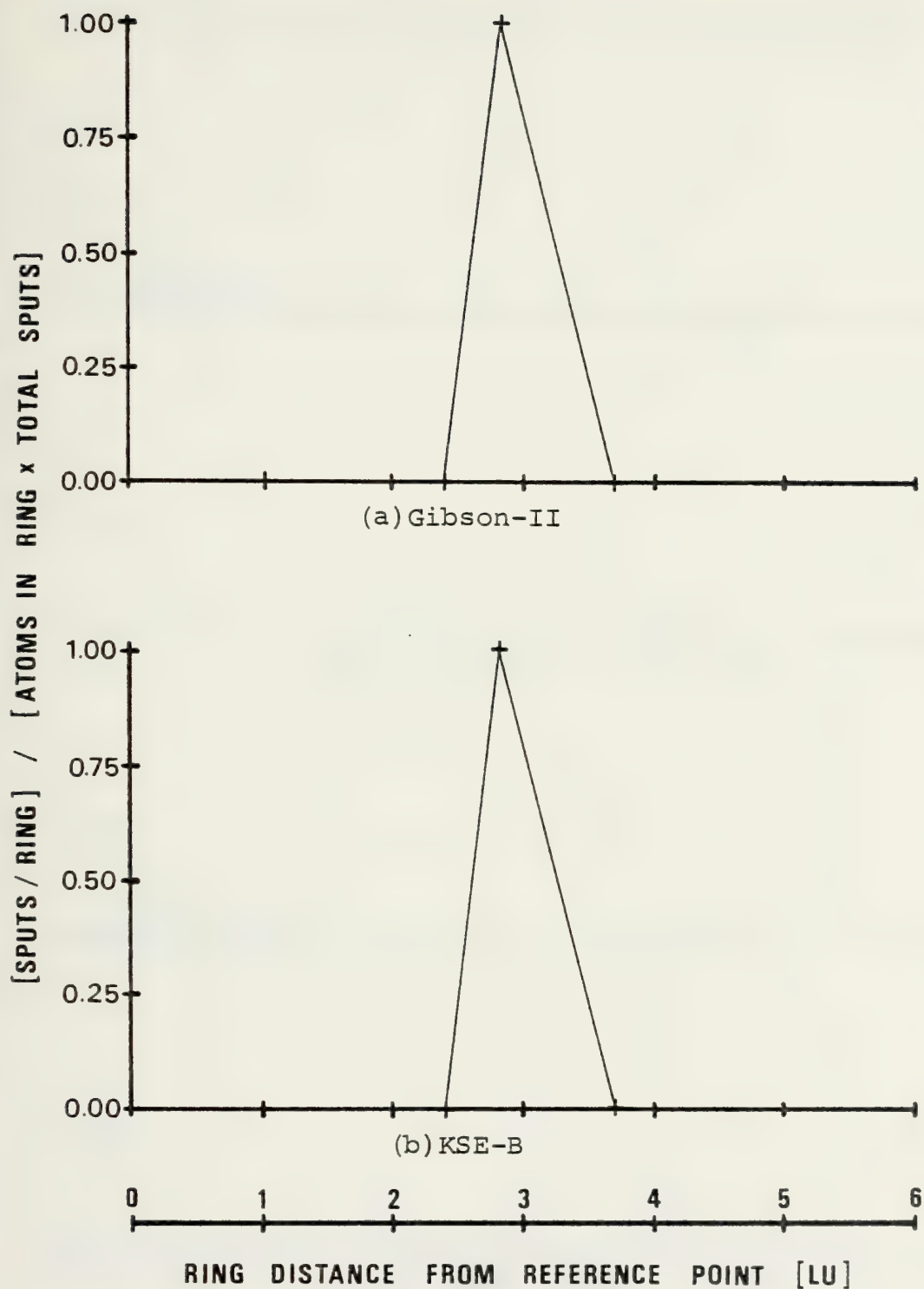
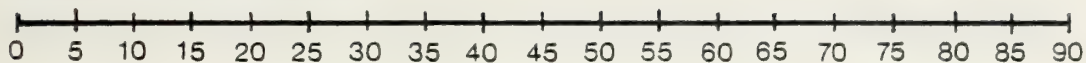
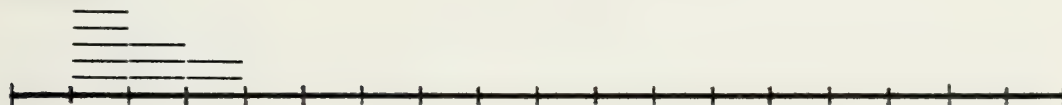


Figure 86 - Atom Probability - (111), 100-eV, Cu/Hg⁺

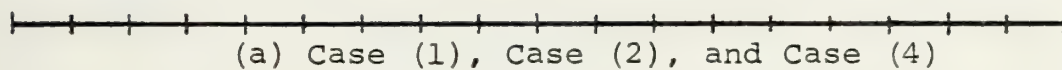
Ejection Angle (Degrees)



Heavy



Light

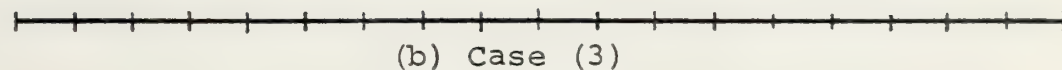


(a) Case (1), Case (2), and Case (4)

Heavy



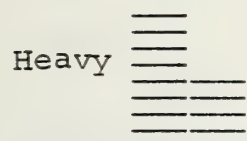
Light



(b) Case (3)

Figure 87 - Angular Dispersion - (111), 100-eV, Cu/Hg⁺
Gibson-II

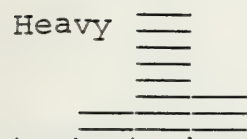
Ejection Angle (Degrees)



Light



(a) Case (1)



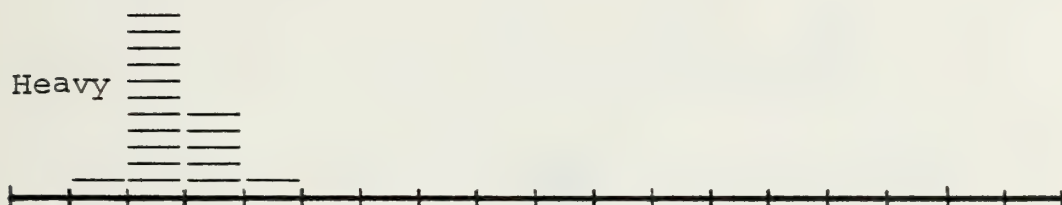
Light



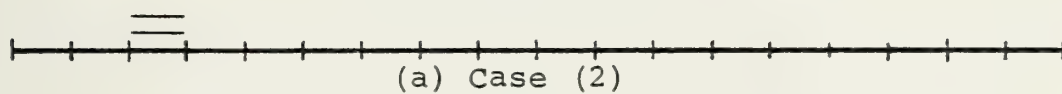
(b) Case (3)

Figure 88 - Angular Dispersion - (111), 100-eV, Cu/Hg^+
KSE-B

Ejection Angle (Degrees)



Light



Light

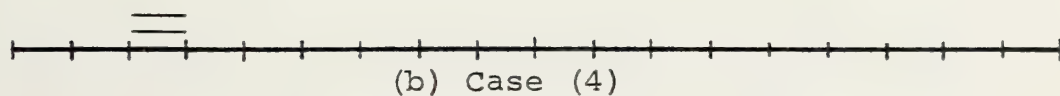
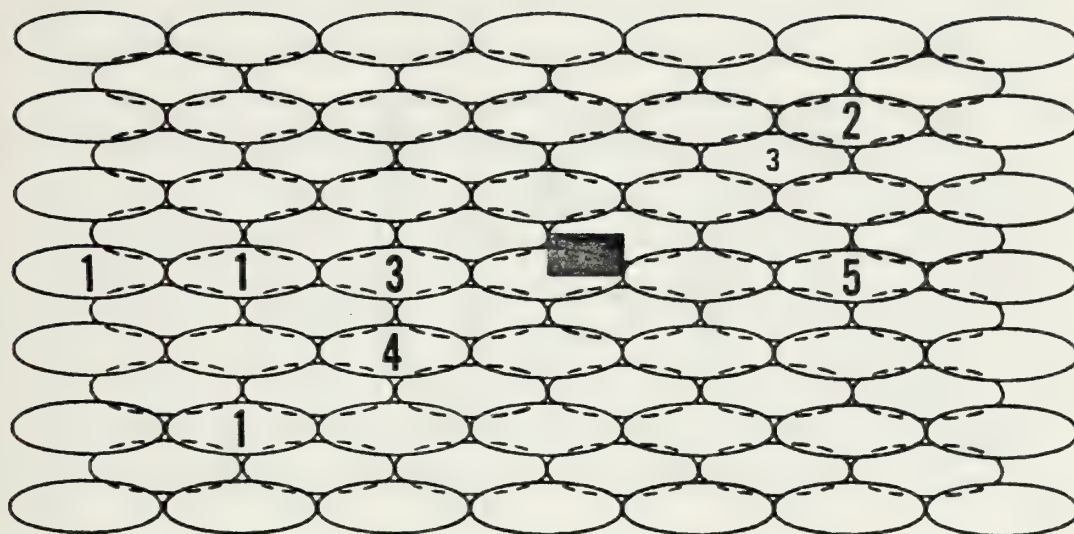
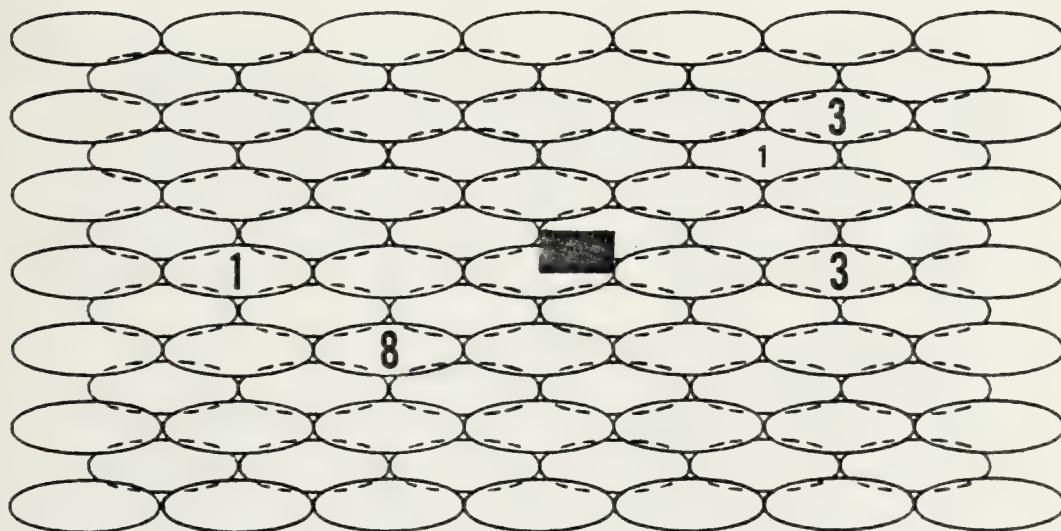


Figure 89 - Angular Dispersion - (111), 100-eV, Cu/Hg⁺
KSE-B

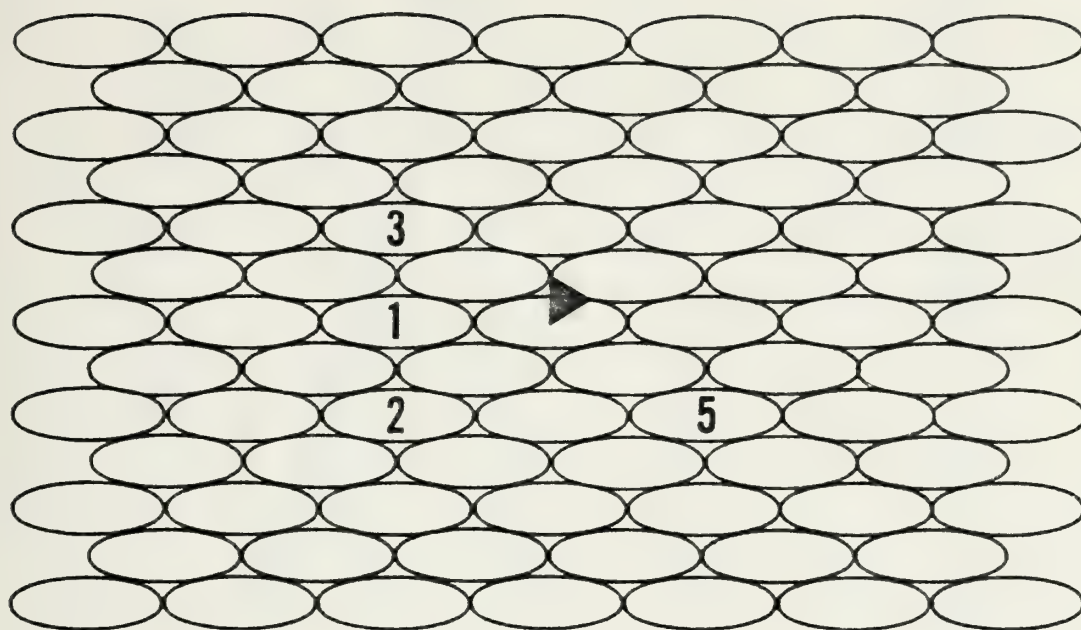


(a) Gibson-II

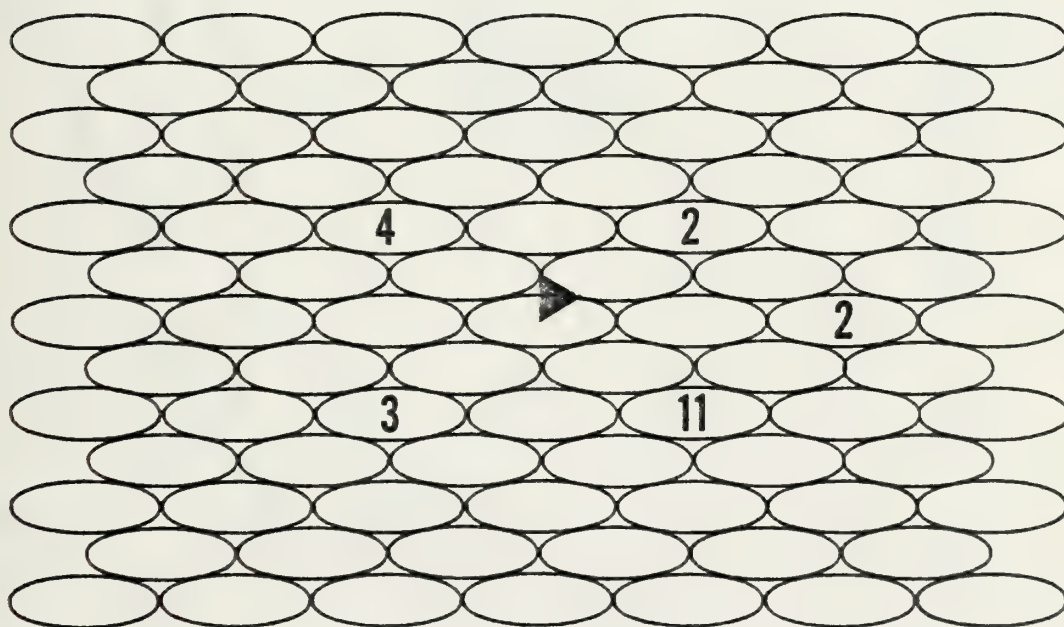


(b) KSE-B

Figure 90 - Sputtering Summary - (110), 100-eV, Cu/Hg+
13x6x13



(a) Gibson-II



(b) KSE-B

Figure 91 - Sputtering Summary - (111), 100-eV, Cu/Hg+
13x4x13

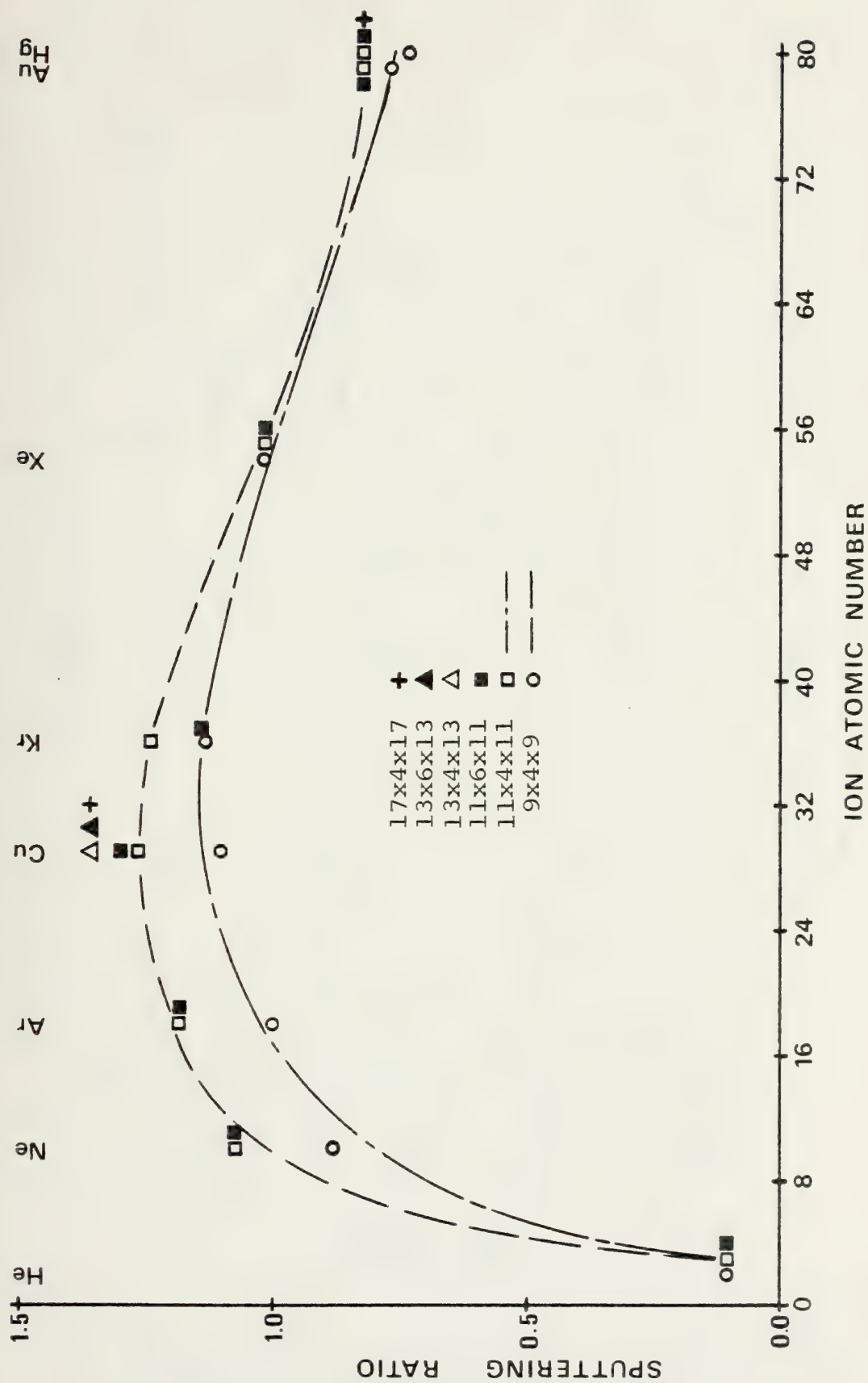


Figure 92 - Sputtering Ratio vs. Ion Atomic Number

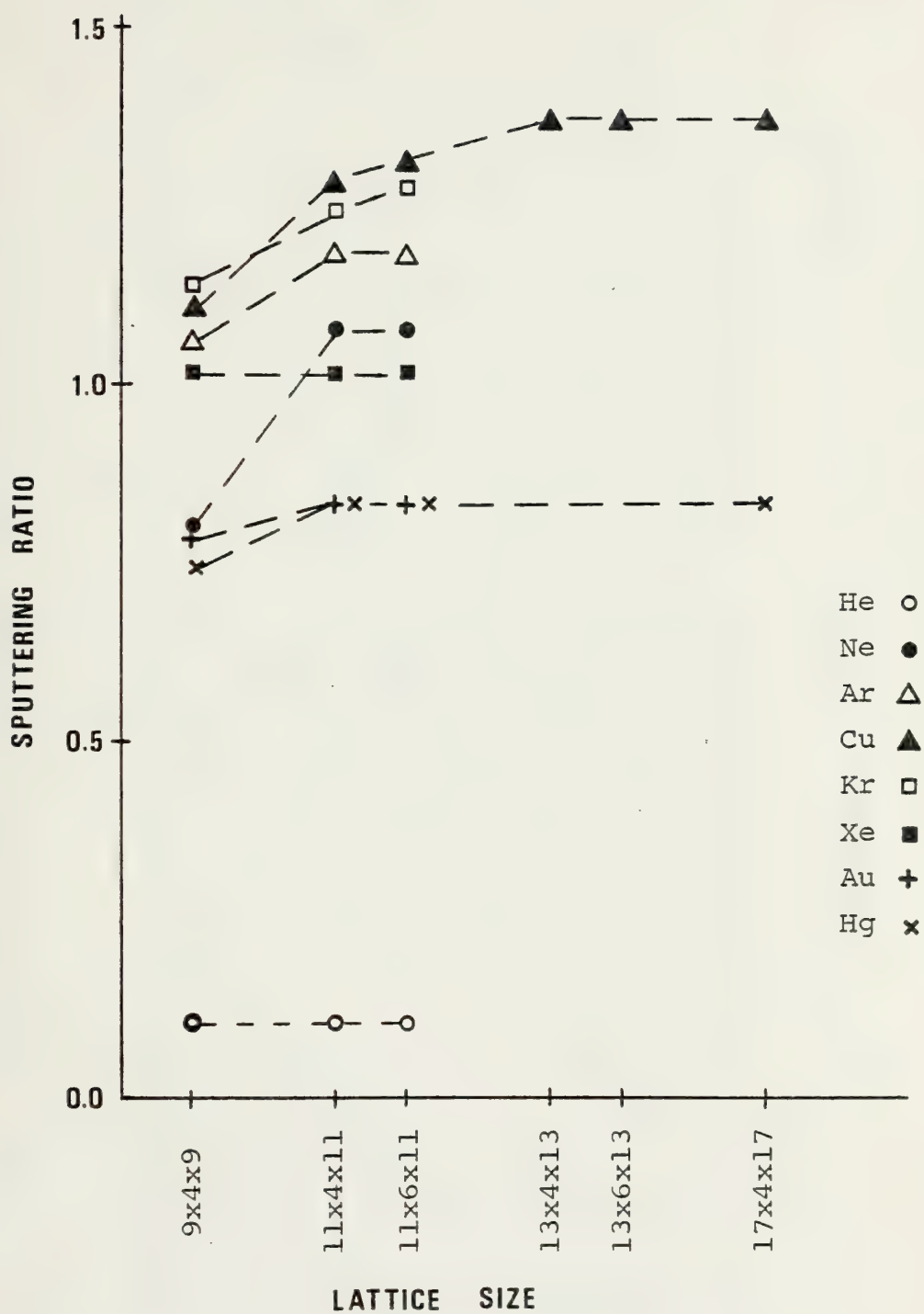


Figure 93 - Sputtering Ratio vs. Lattice Size

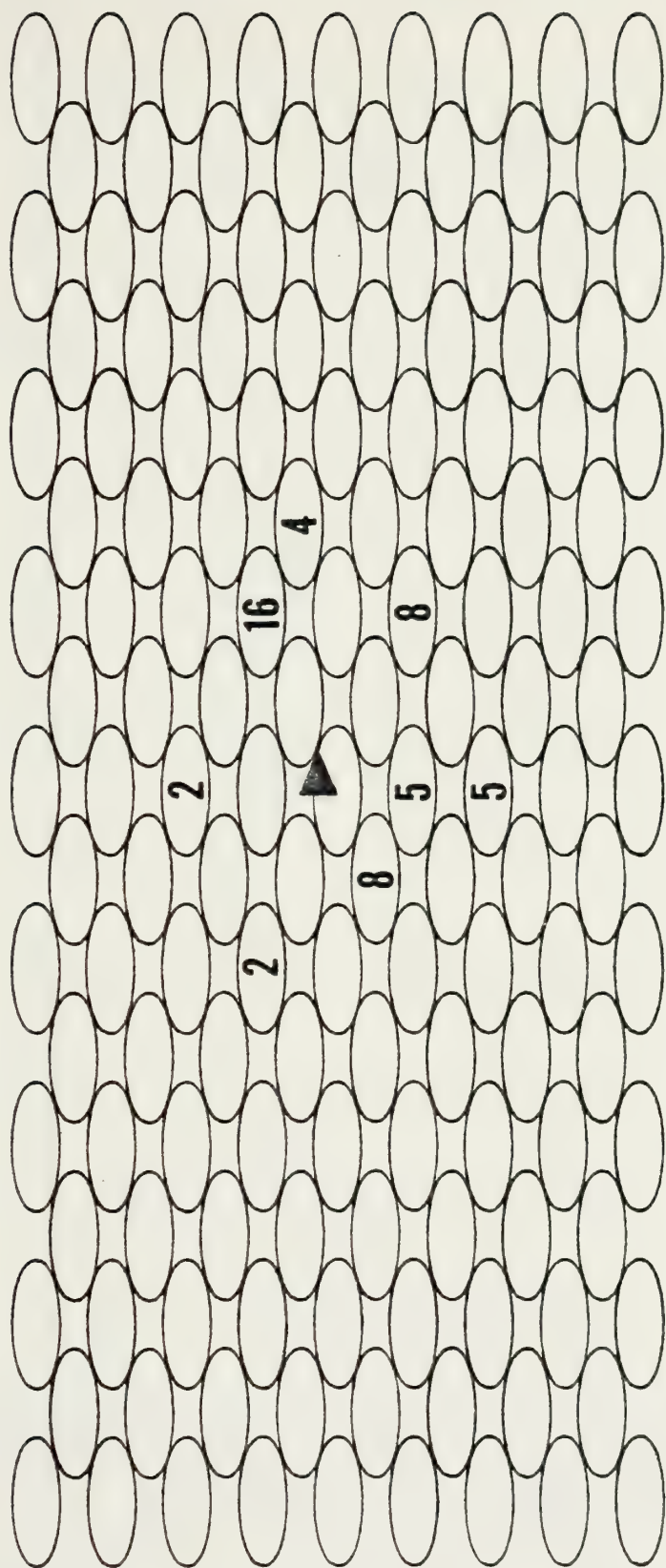


Figure 94 - Sputtering Summary - (100), 100-eV, Cu/Cu^+

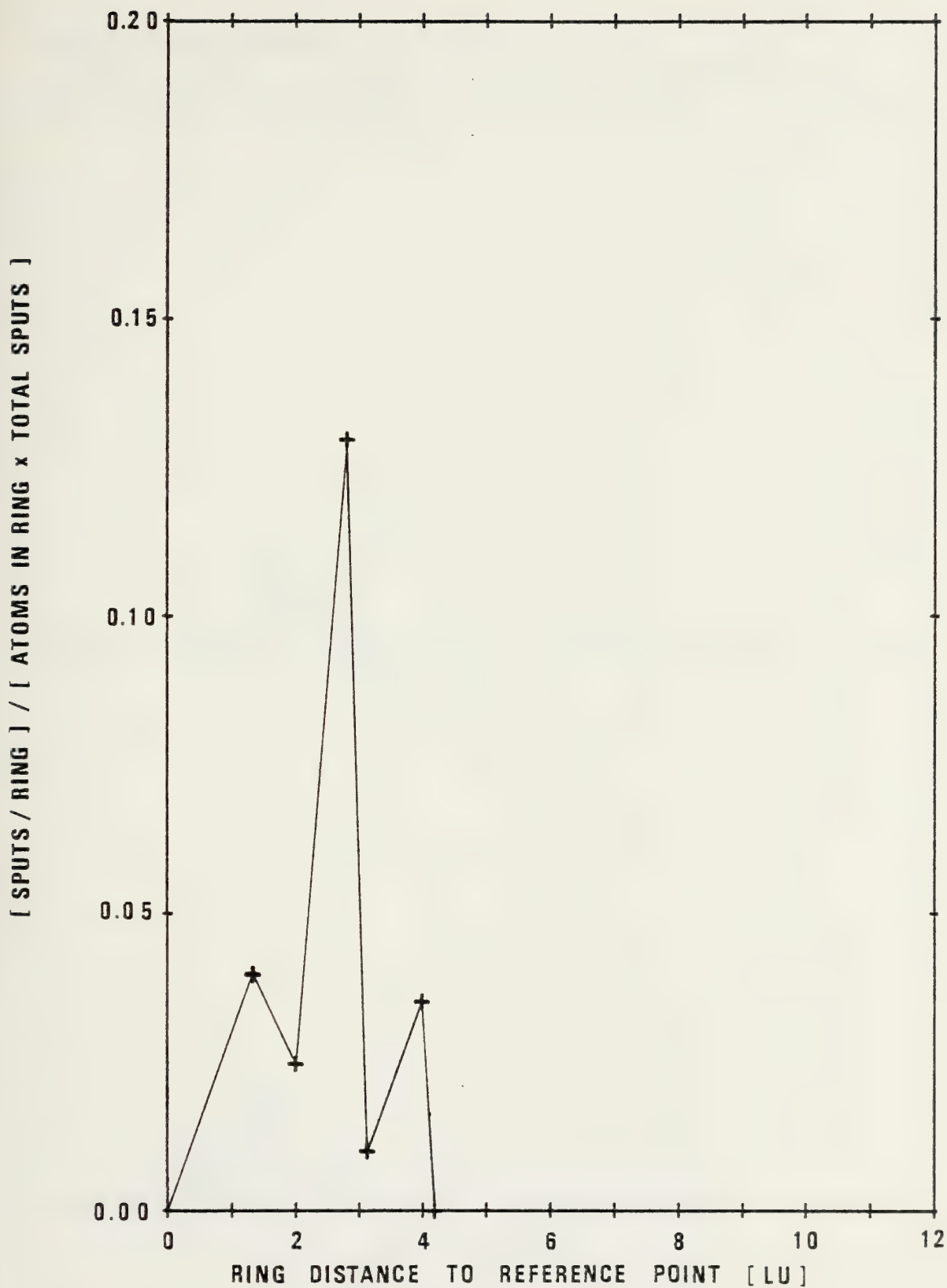


Figure 95 - Atom Probability - (100), 100-eV, Cu/Cu⁺,

Ejection Angle (Degrees)

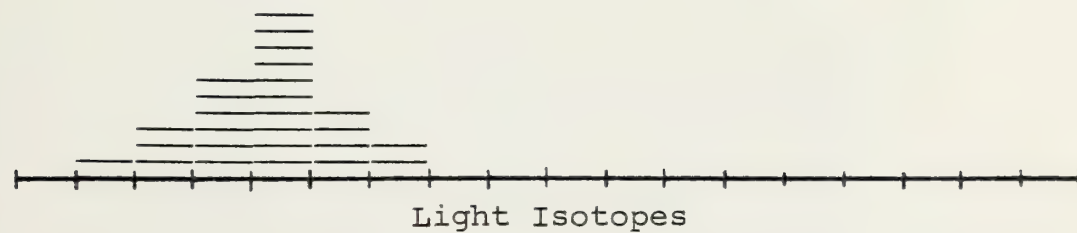
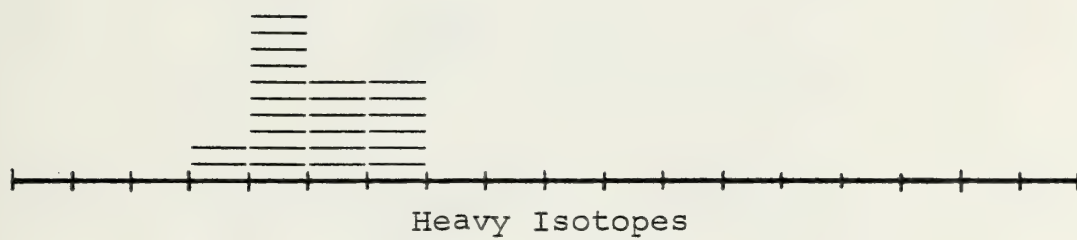
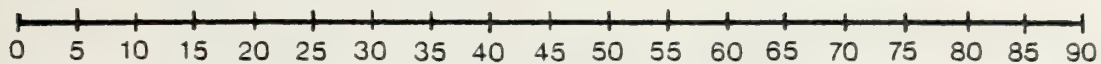


Figure 96 - Angular Dispersion - (100), 100-eV, Cu/Cu⁺

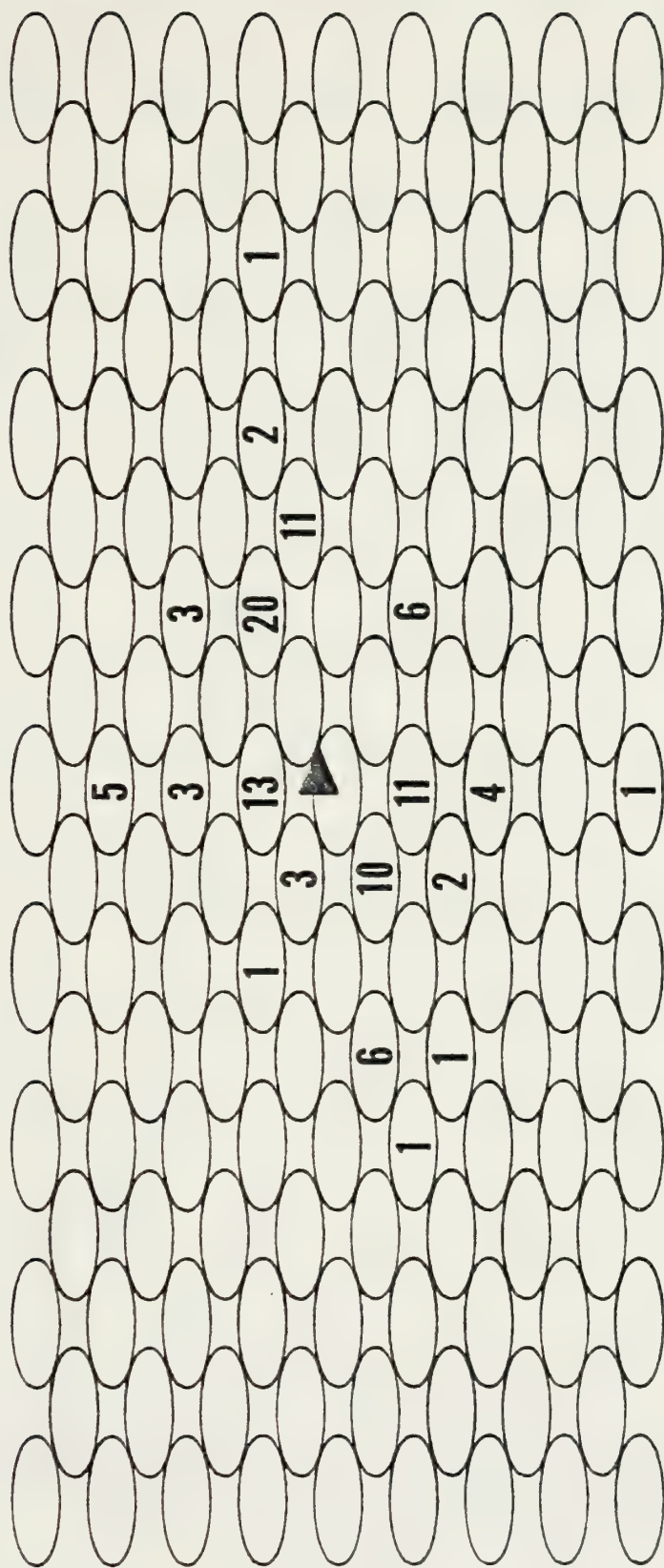


Figure 97 - Sputtering Summary - (100), 200-eV, Cu/Cu⁺

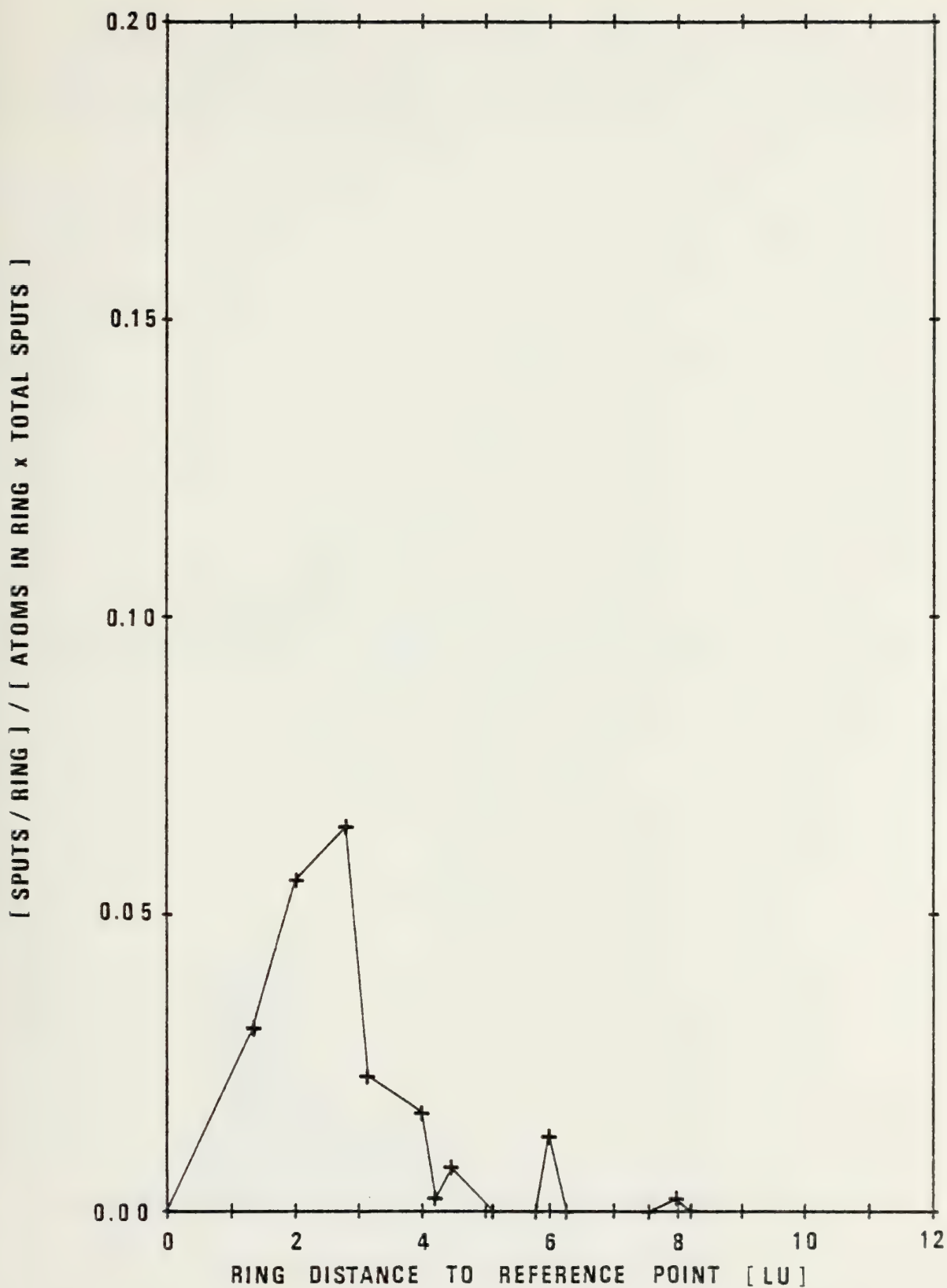


Figure 98 - Atom Probability - (100), 200-eV, Cu/Cu⁺

Ejection Angle (Degrees)

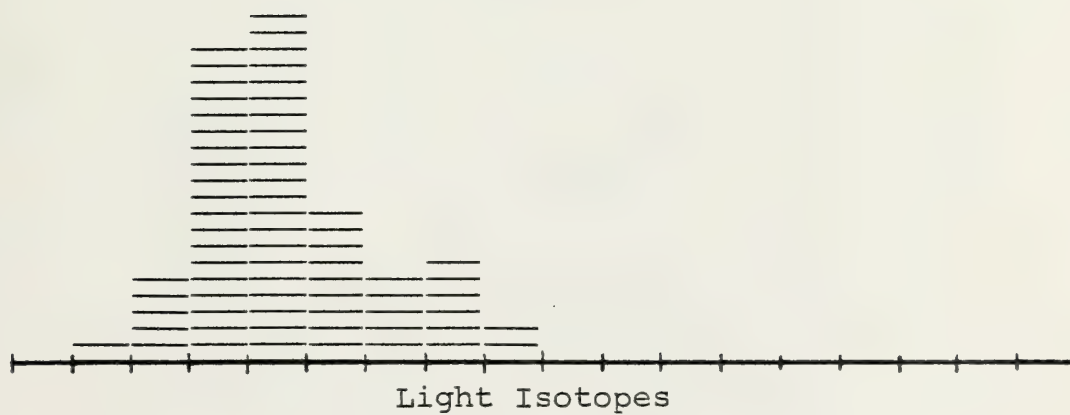
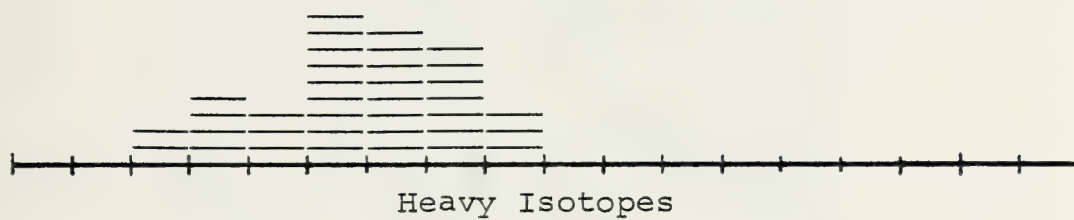
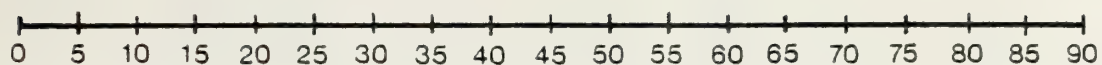


Figure 99 - Angular Dispersion - (100), 200-eV, Cu/Cu⁺

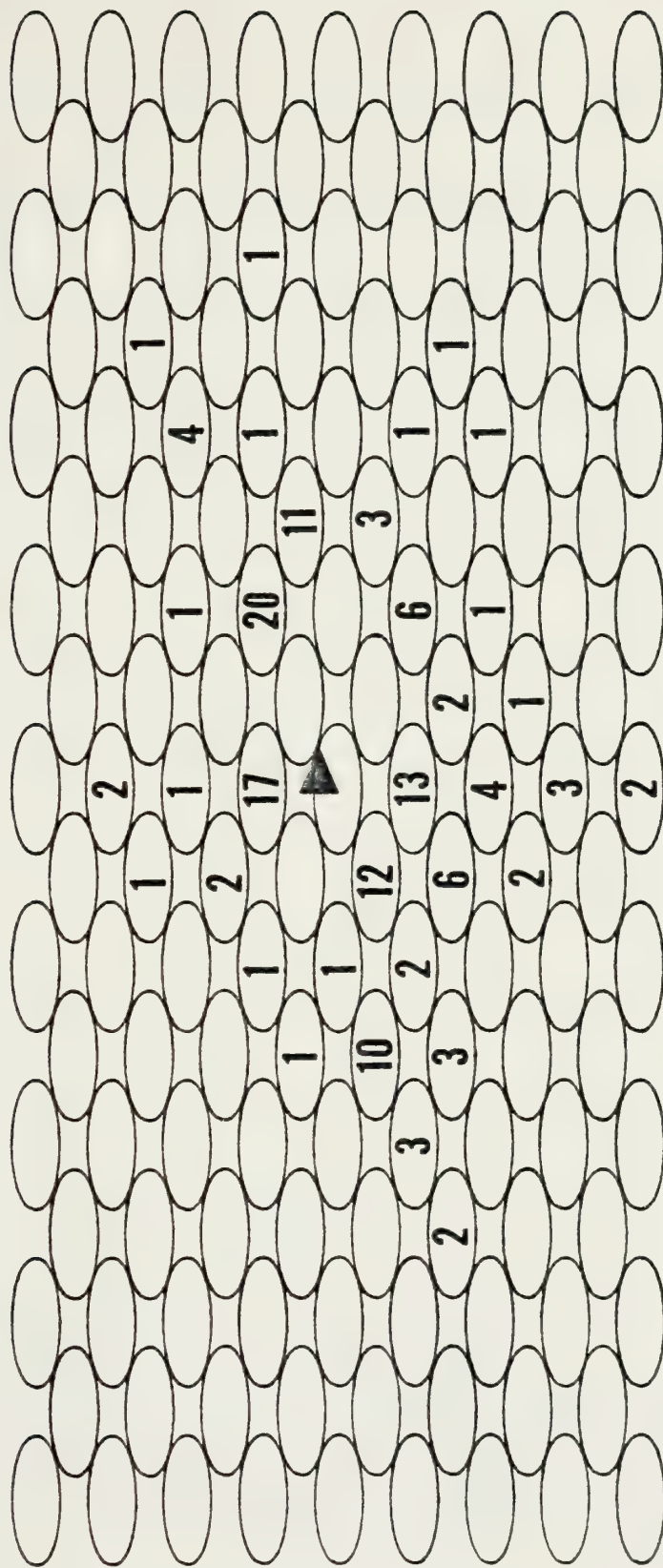


Figure 100 - Sputtering Summary - (100), 500-eV, Cu/Cu^+

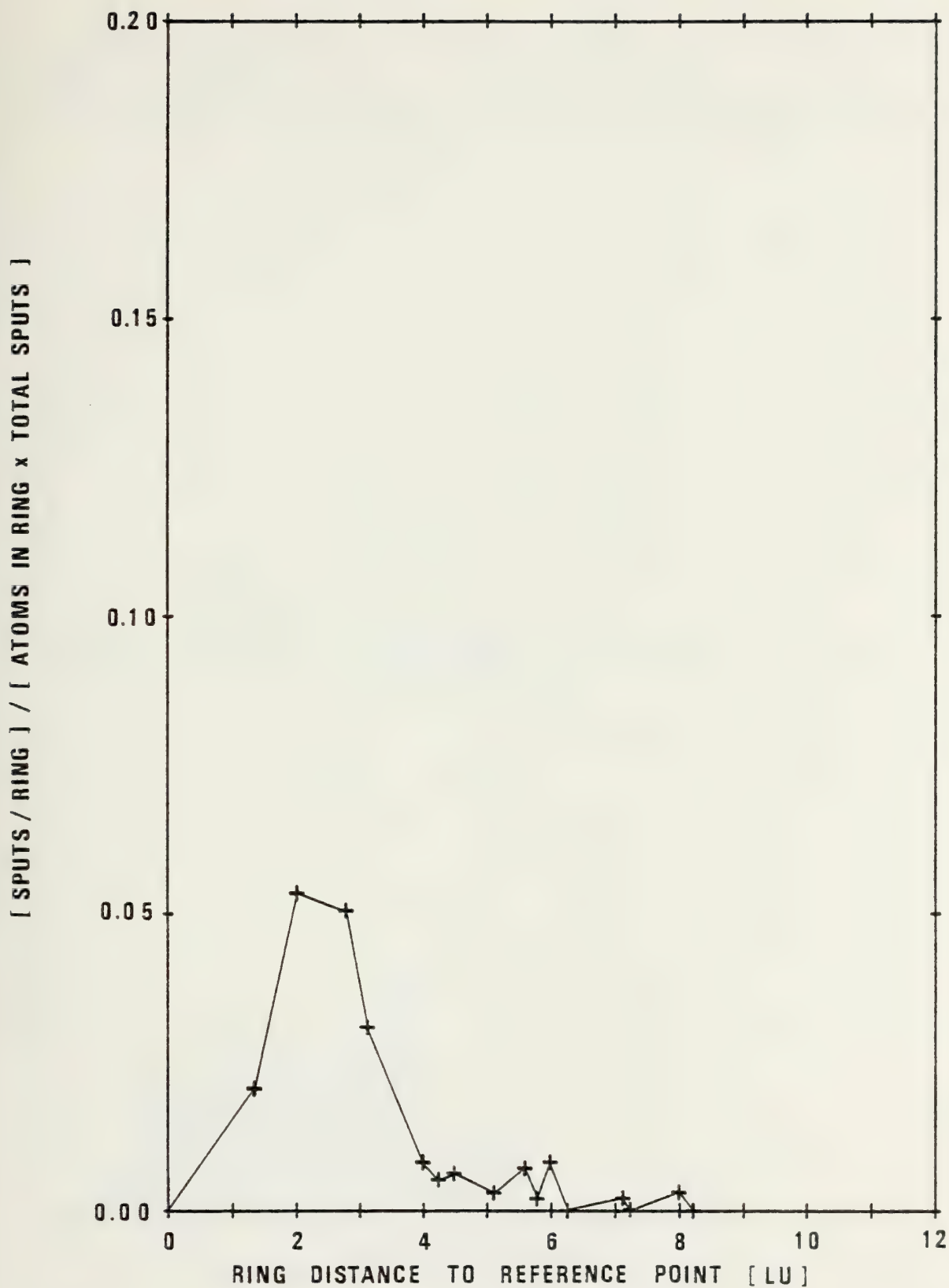


Figure 101 - Atom Probability - (100), 500-eV, Cu/Cu⁺

Ejection Angle (Degrees)

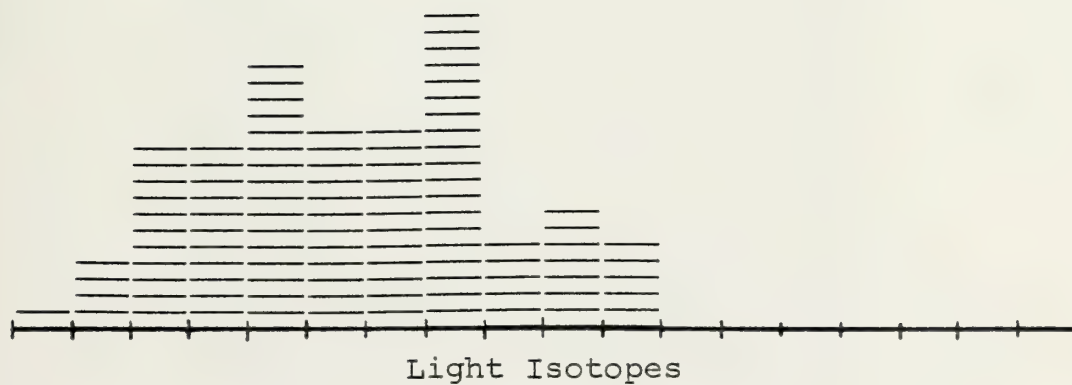
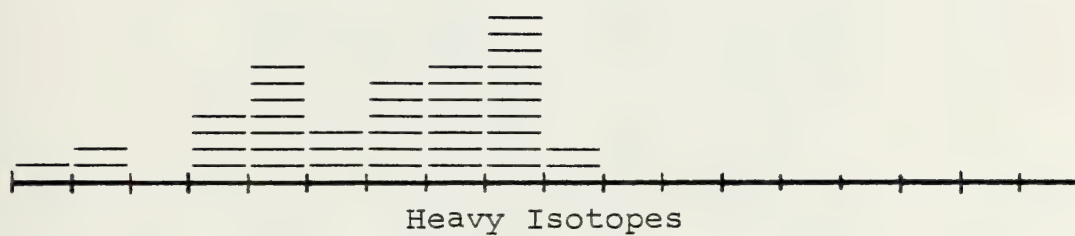
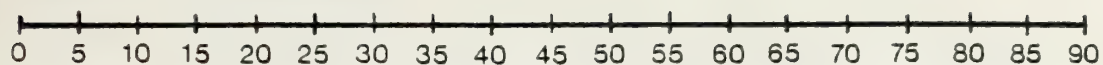


Figure 102 - Angular Dispersion - (100), 500-eV, Cu/Cu+

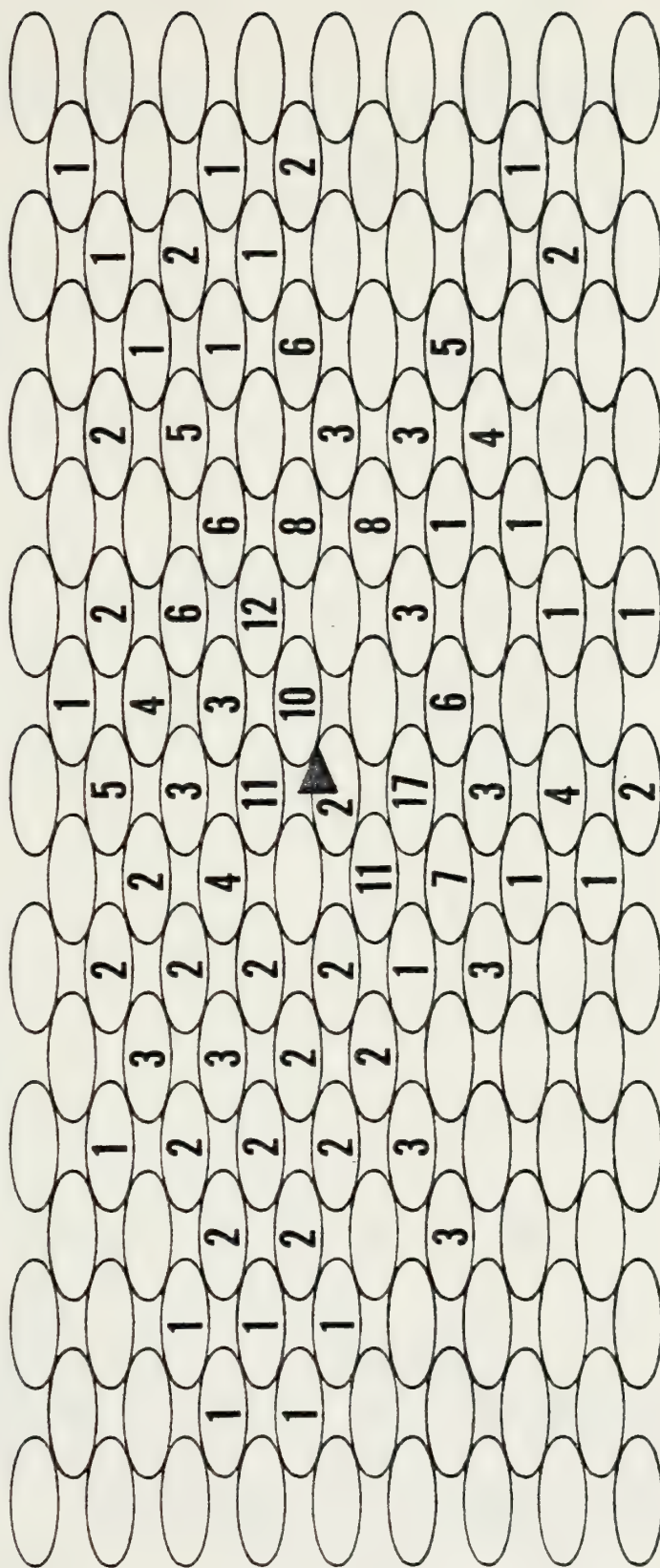


Figure 103 - Sputtering Summary - (100), 1-keV, Cu/Cu⁺

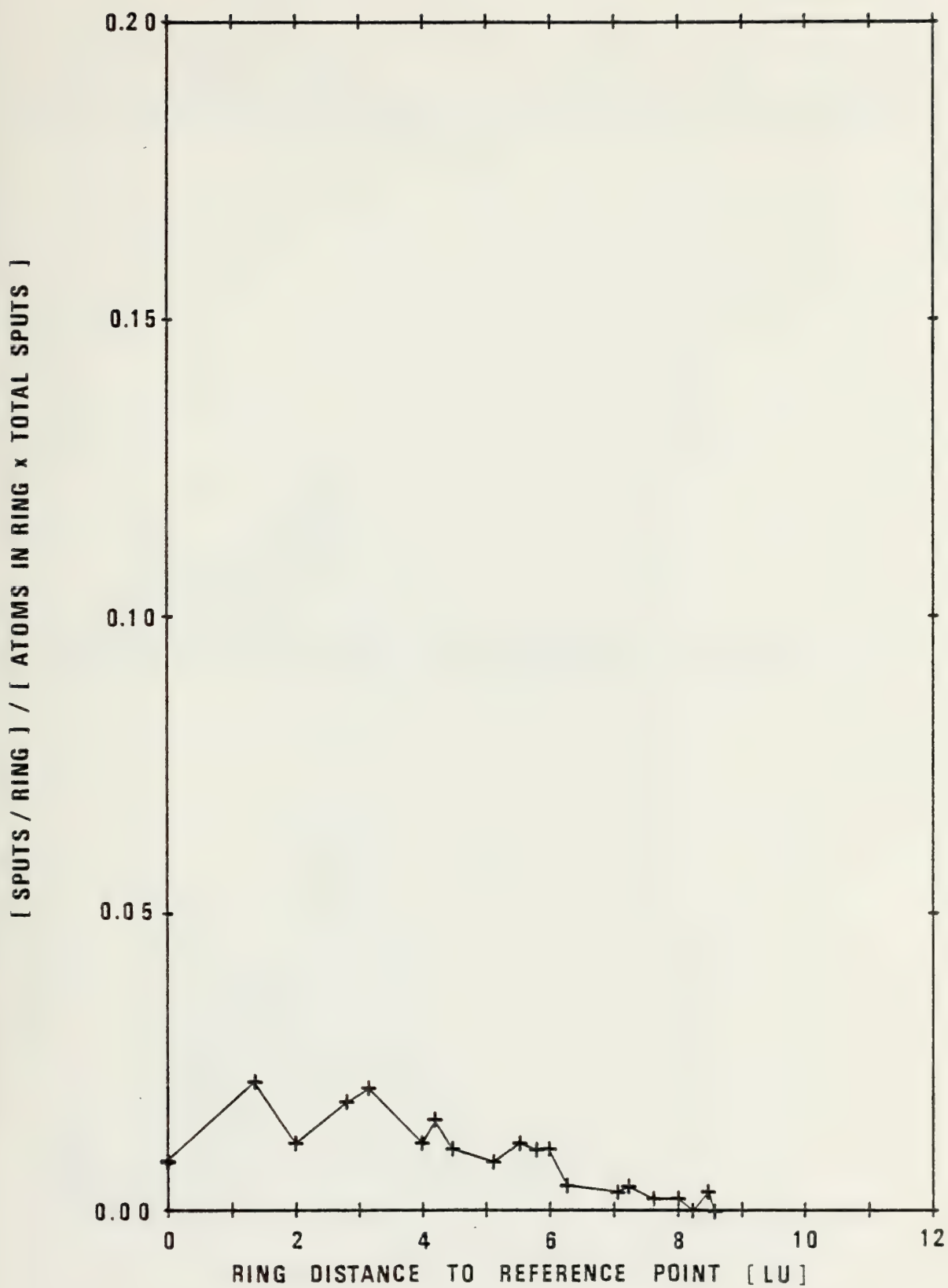


Figure 104 - Atom Probability - (100), 1-keV, Cu/Cu⁺

Ejection Angle (Degrees)

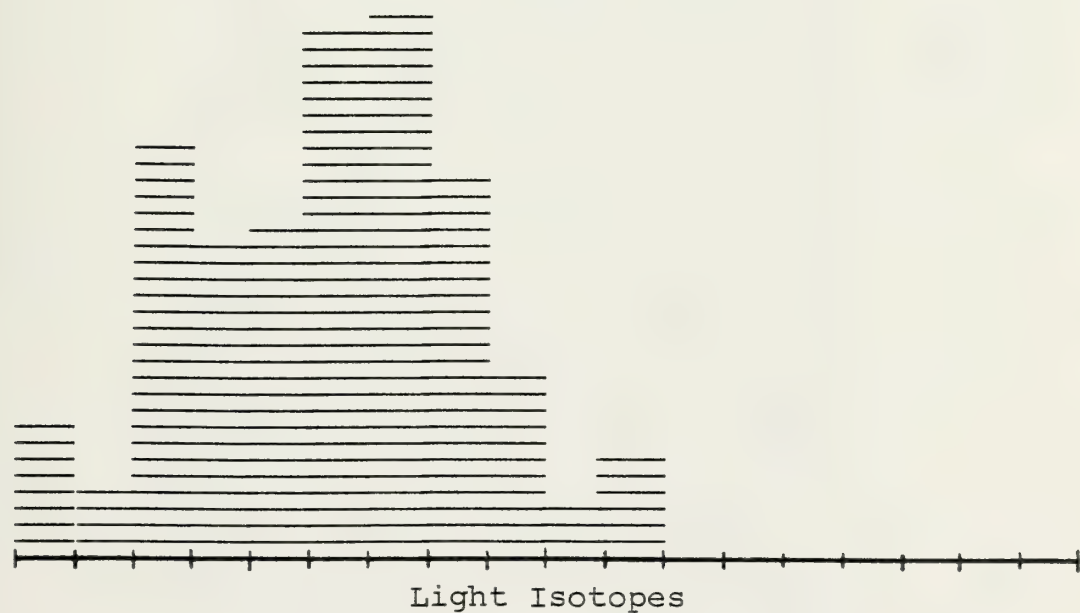
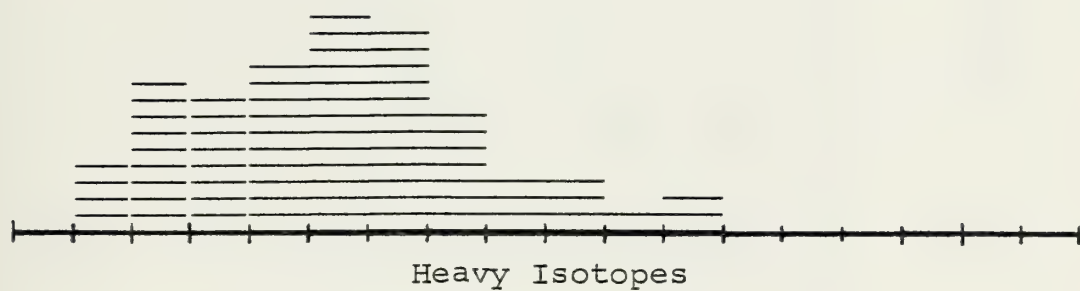
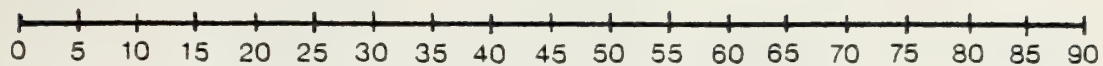


Figure 105 - Angular Dispersion - (100), 1-keV, Cu/Cu+

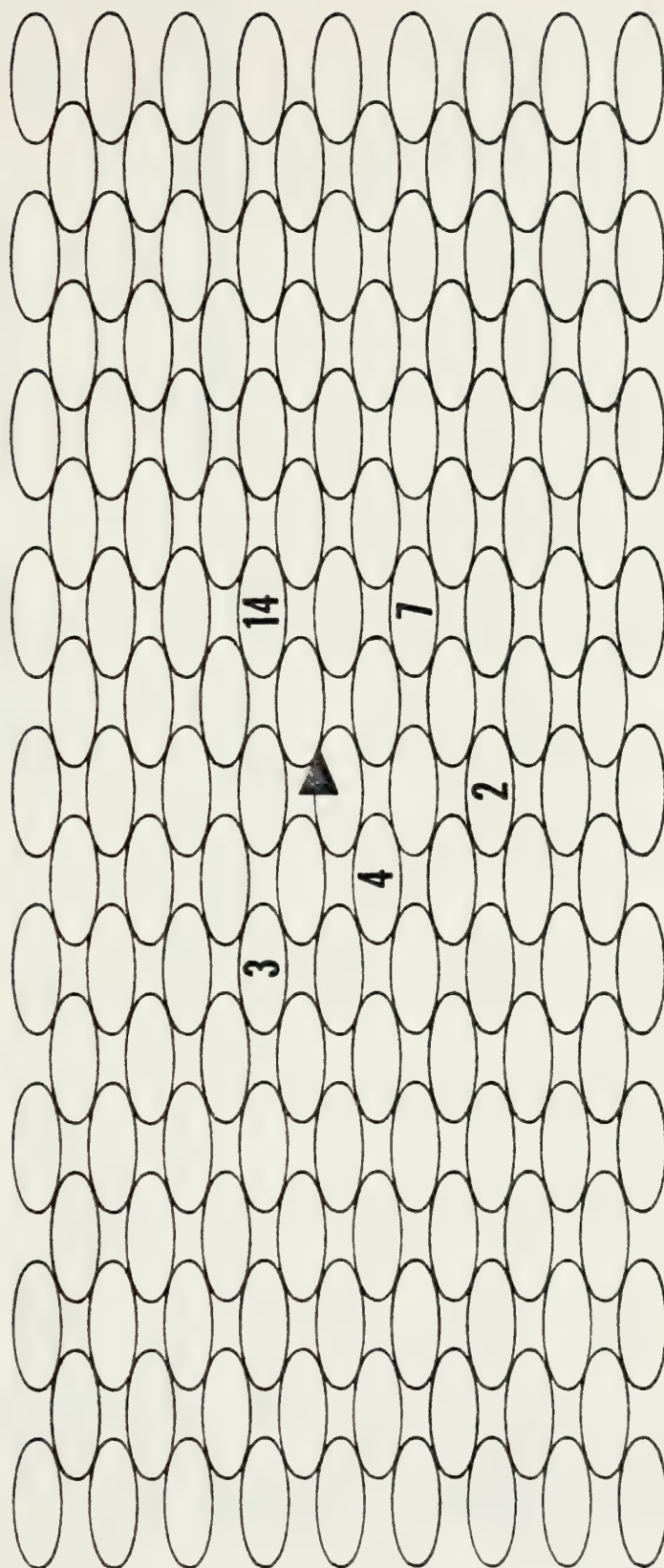


Figure 106 - Sputtering Summary - (100), 100-eV, Cu/Hg⁺

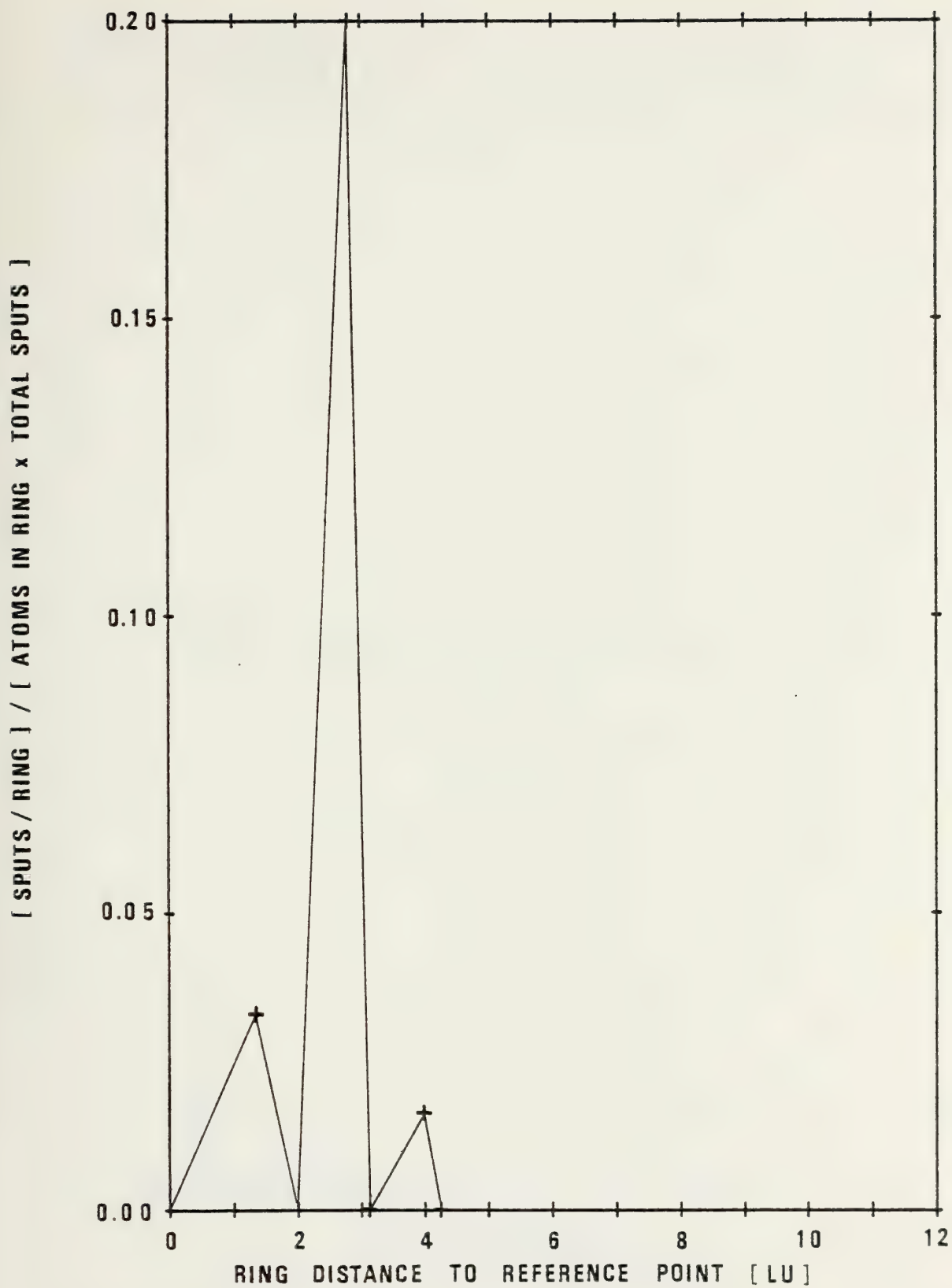


Figure 107 - Atom Probability - (100), 100-eV, Cu/Hg+

Ejection Angle (Degrees)

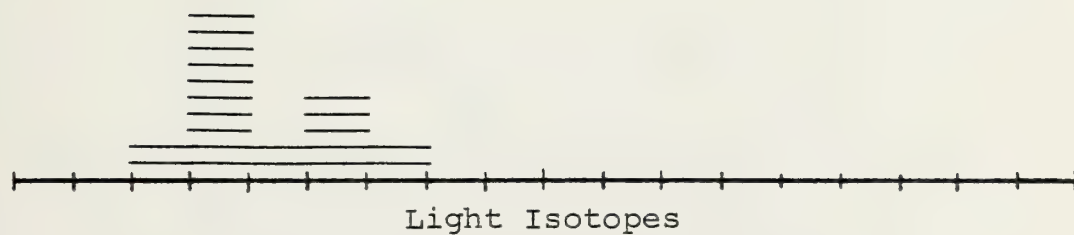
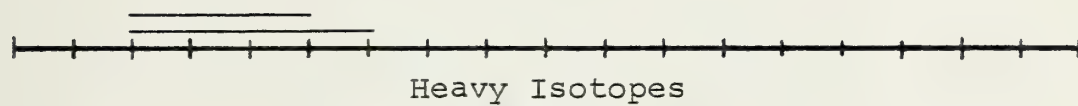
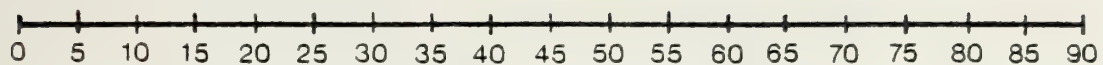


Figure 108 - Angular Dispersion - (100), 100-eV, Cu/ $^{63}\text{J}^+$

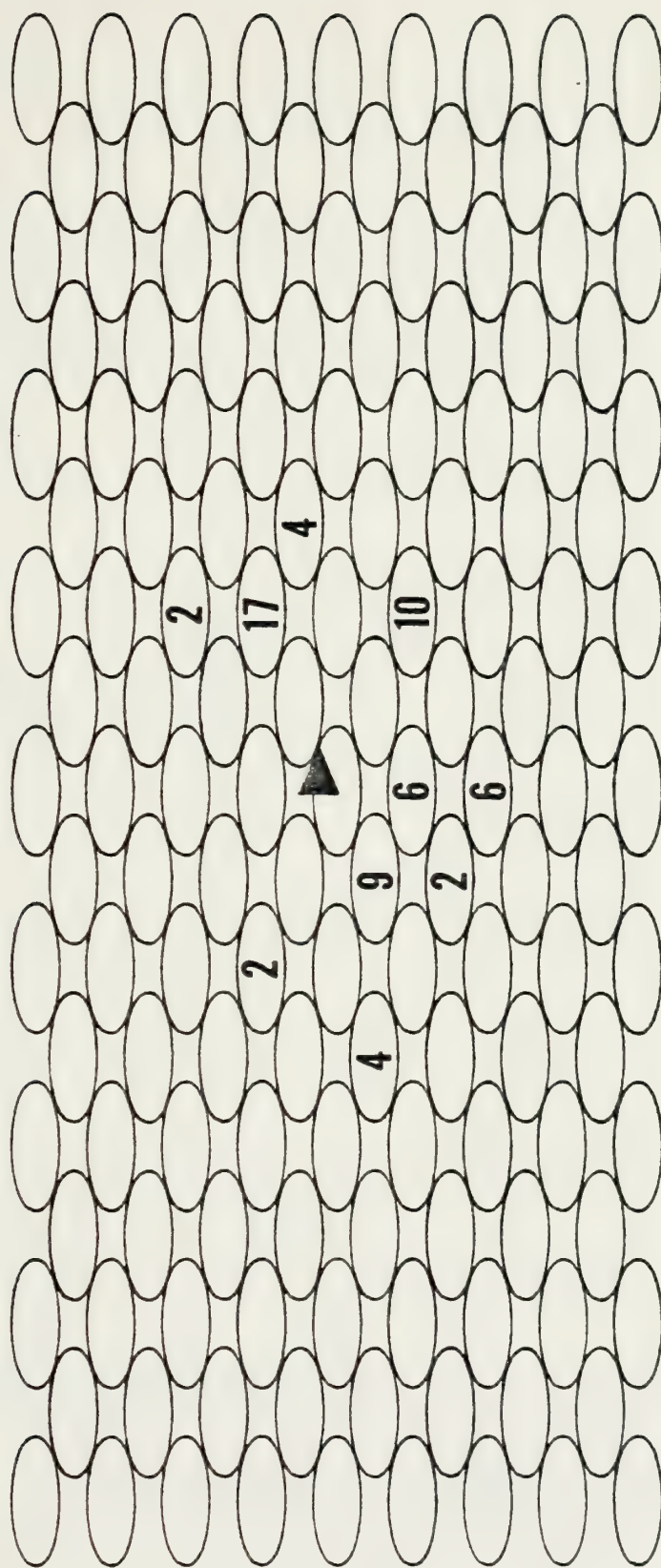


Figure 109 - Sputtering Summary - (100), 200-eV, Cu/Hg⁺

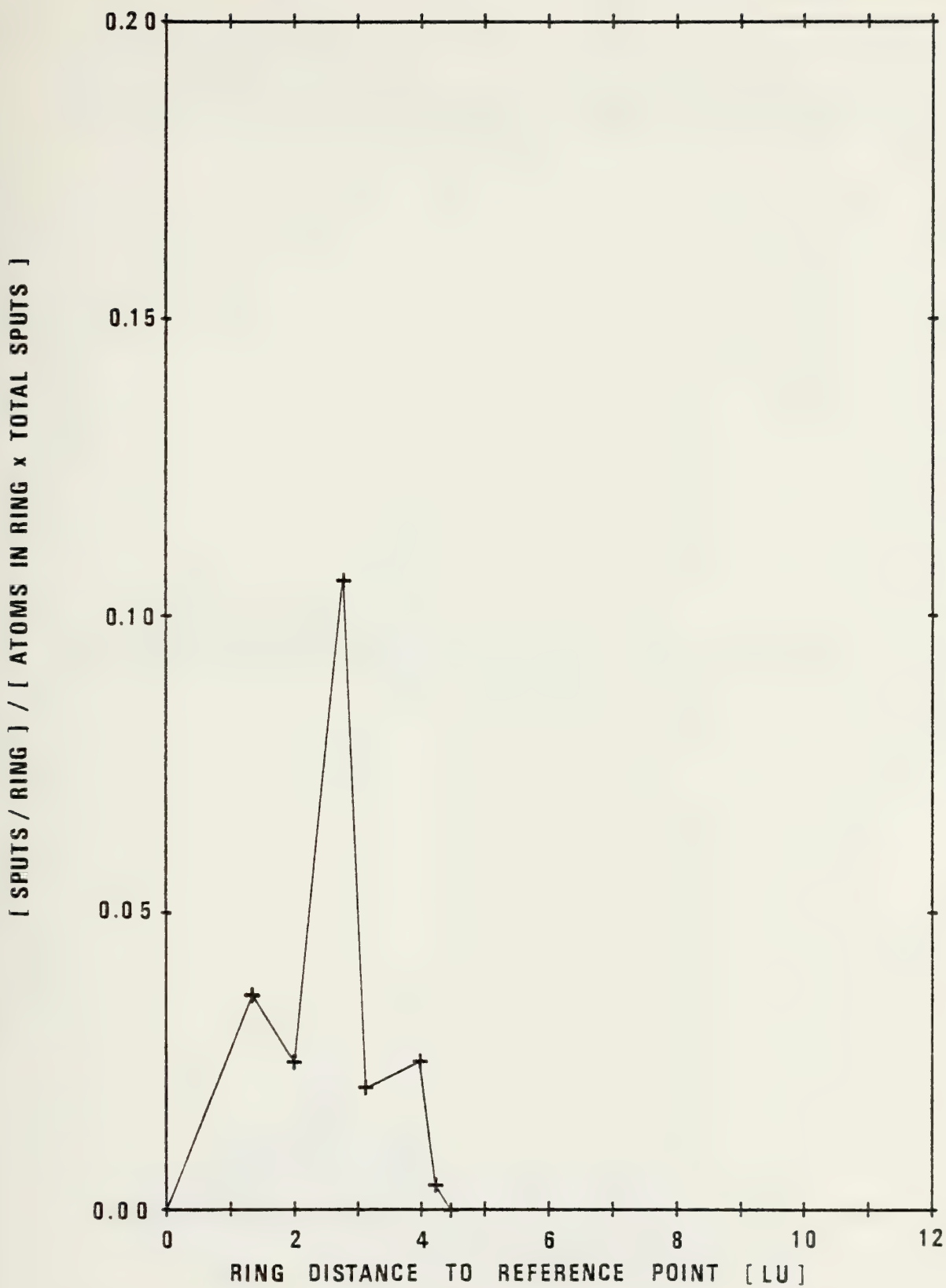


Figure 110 - Atom Probability - (100), 200-eV, Cu/Hg+

Ejection Angle (Degrees)

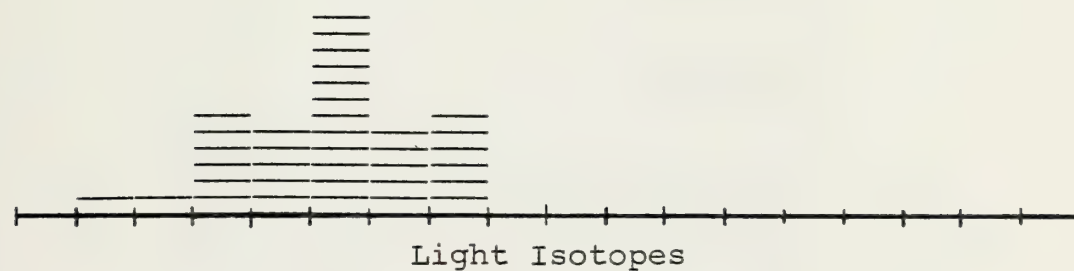
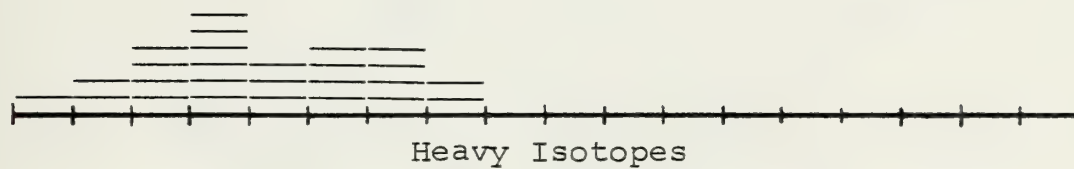
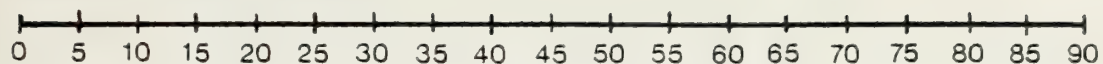


Figure 111 - Angular Dispersion - (100), 200-eV, Cu/Hg⁺

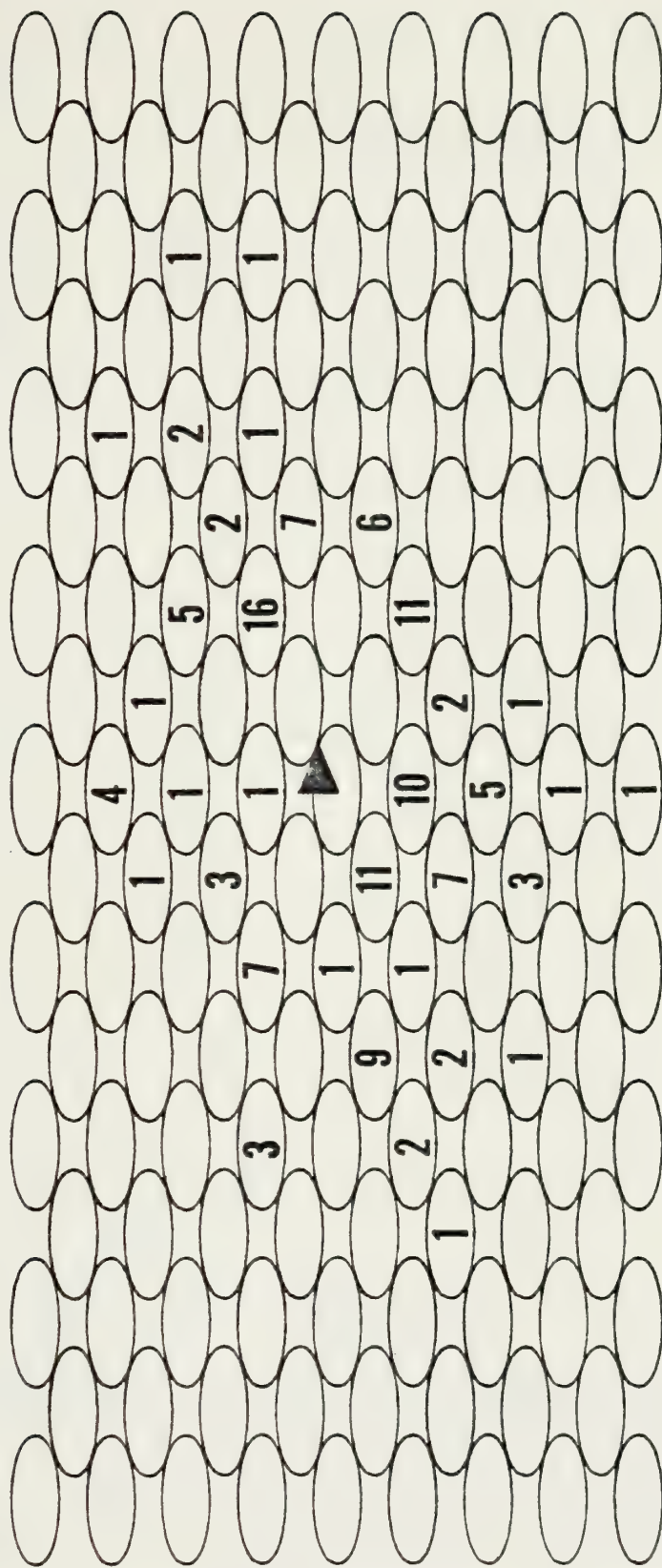


Figure 112 - Sputtering Summary - (100), 500-eV, Cu/Hg^+

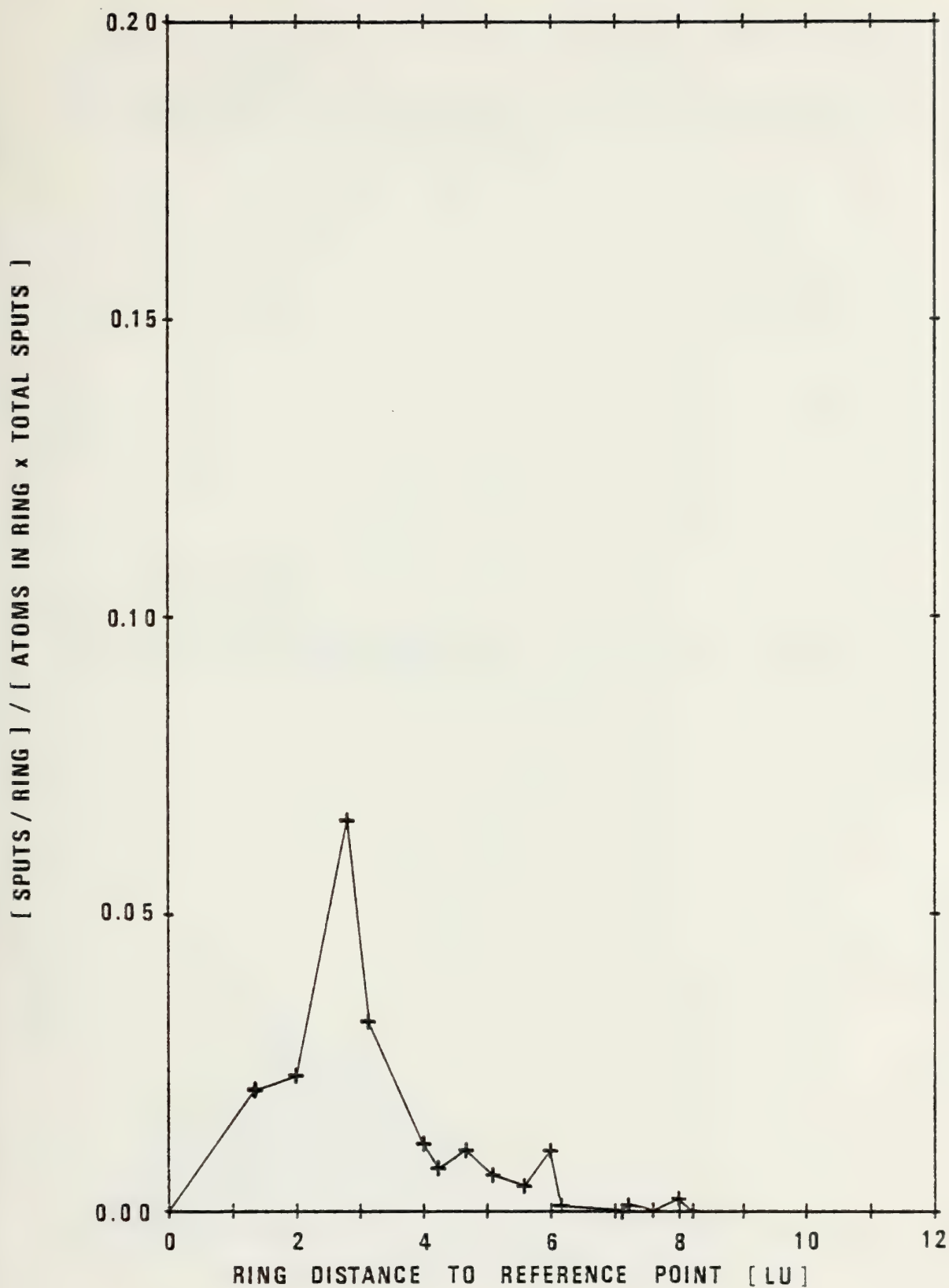


Figure 113 - Atom Probability - (100), 500-eV, Cu/Hg⁺

Ejection Angle (Degrees)

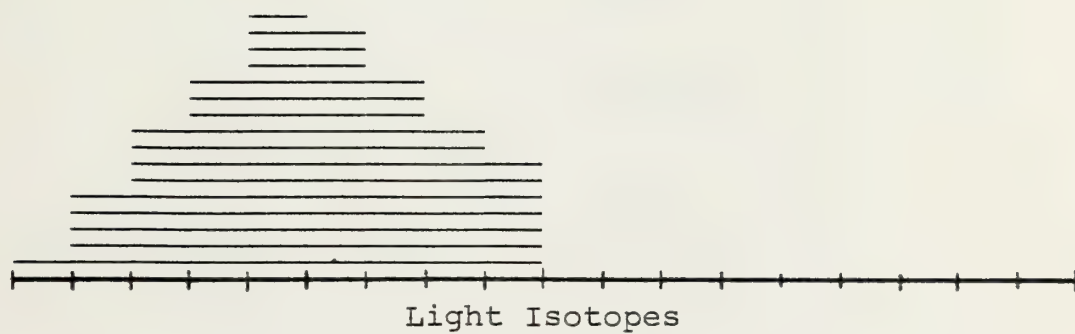
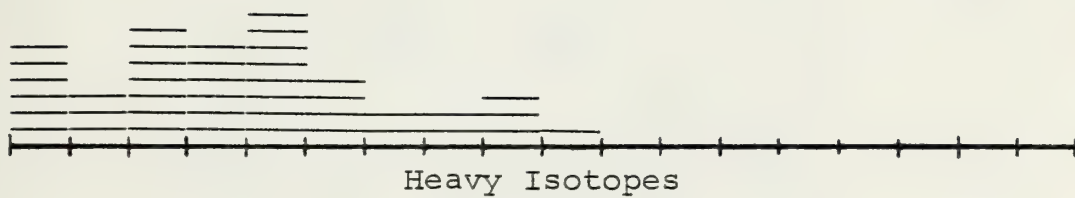
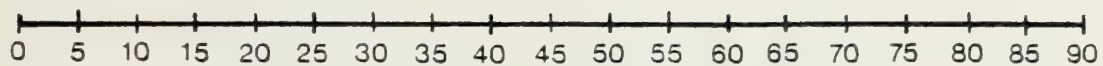


Figure 114 - Angular Dispersion - (100), 500-eV, Cu/Hg+

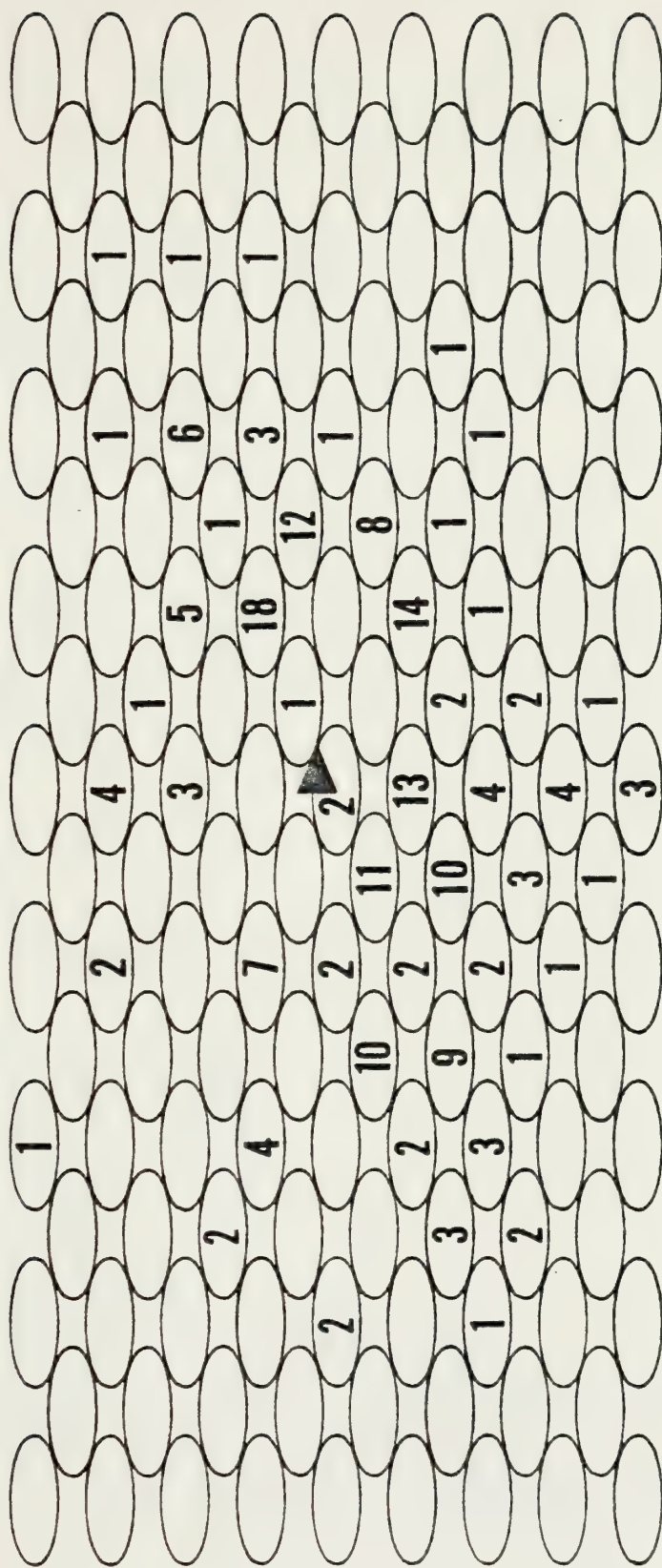


Figure 115 - Sputtering Summary - (100), 1-keV, Cu/Hg⁺

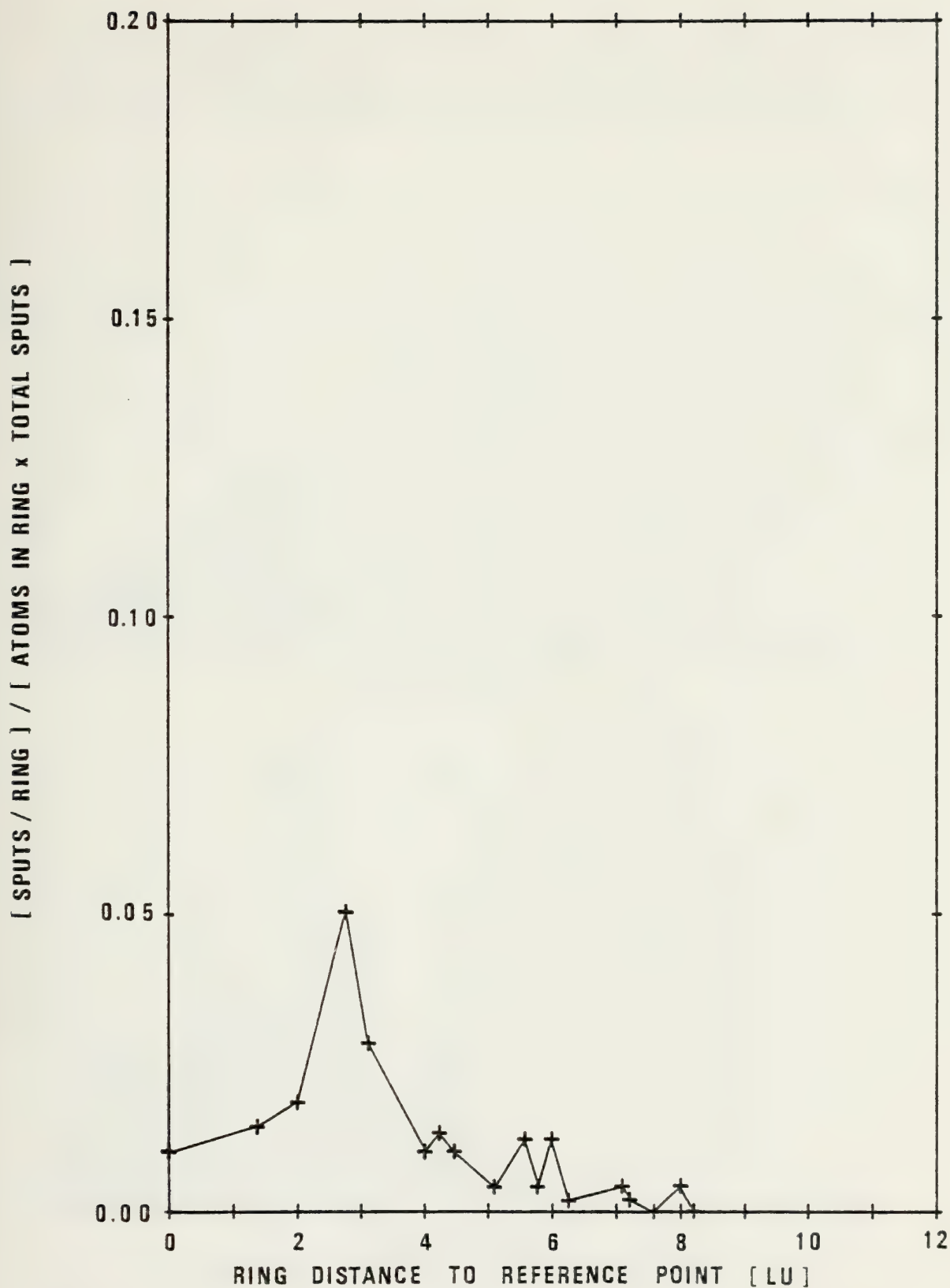


Figure 116 - Atom Probability - (100), 1-keV, Cu/Hg⁺

Ejection Angle (Degrees)

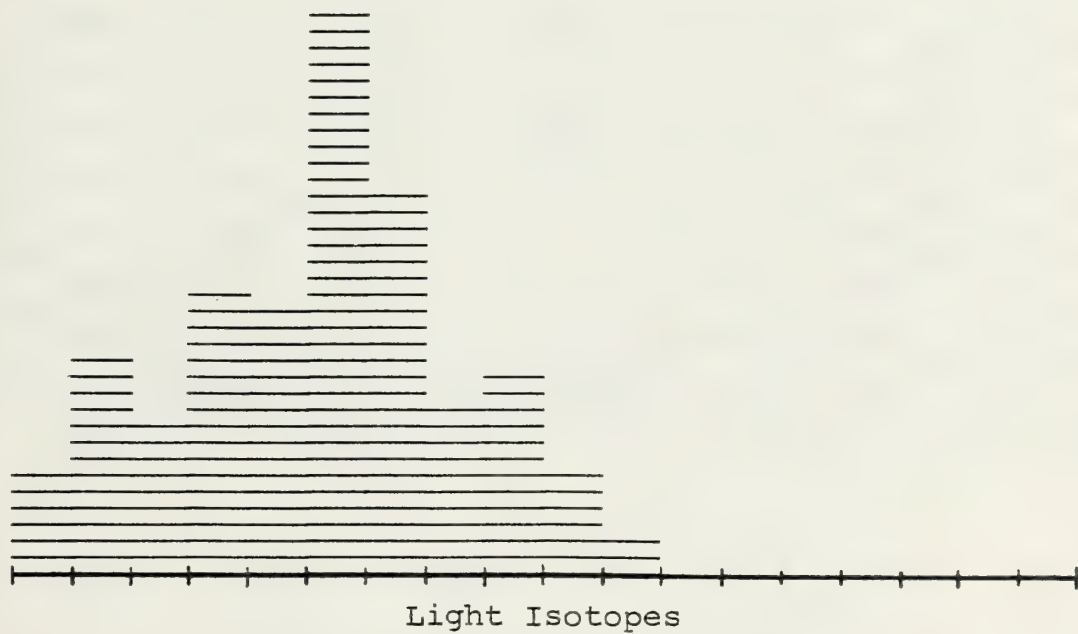
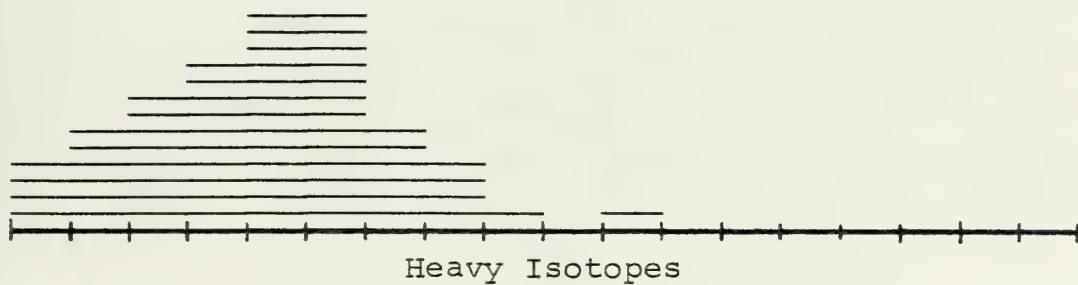
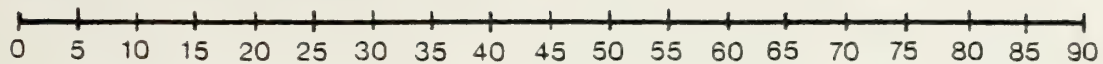


Figure 117 - Angular Dispersion - (100), 1-keV, Cu/Hg+

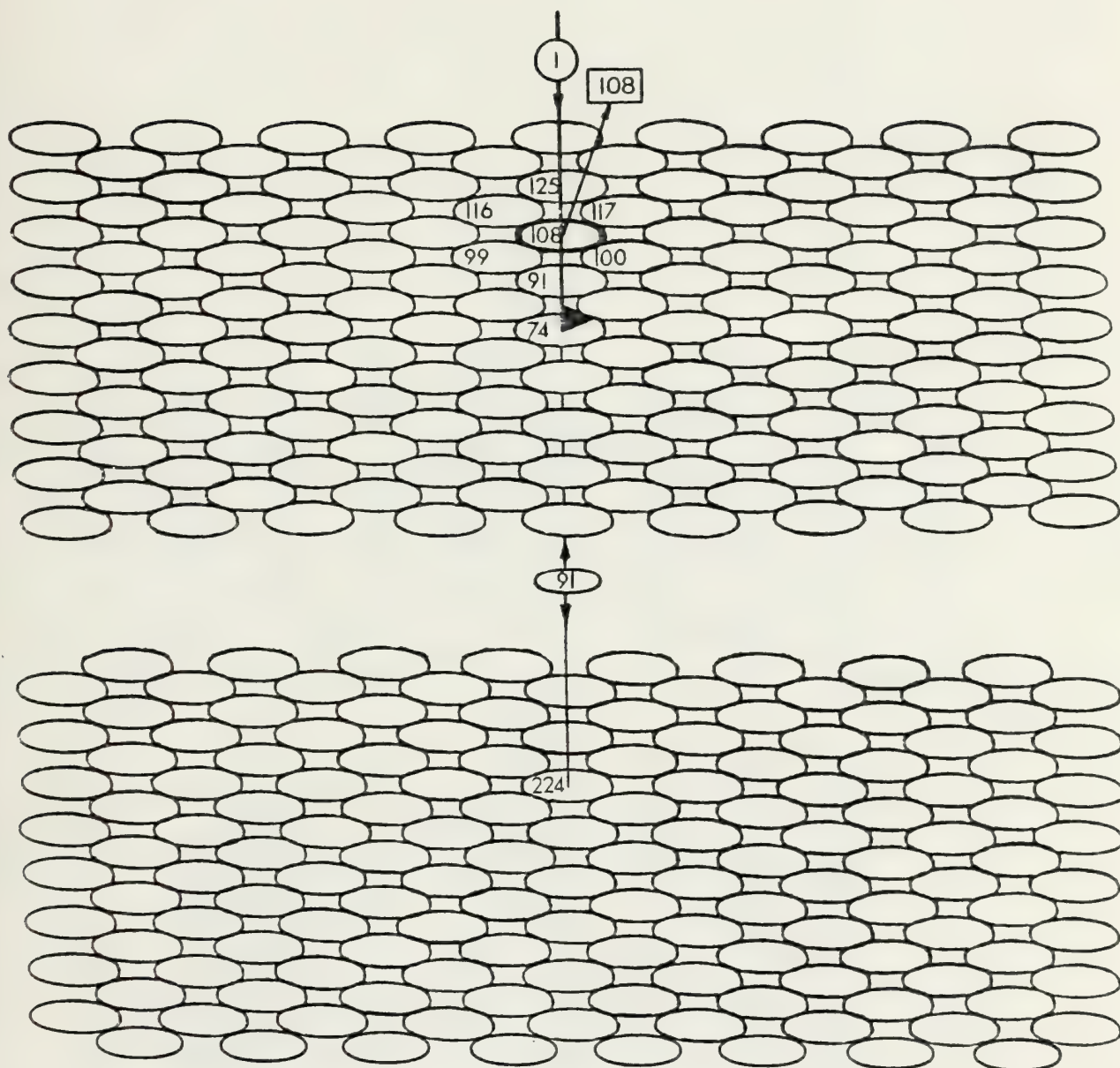


Figure 118 - Sputtering Mechanism Trace
(100), 100-eV, Cu/Cu⁺, KSE-B

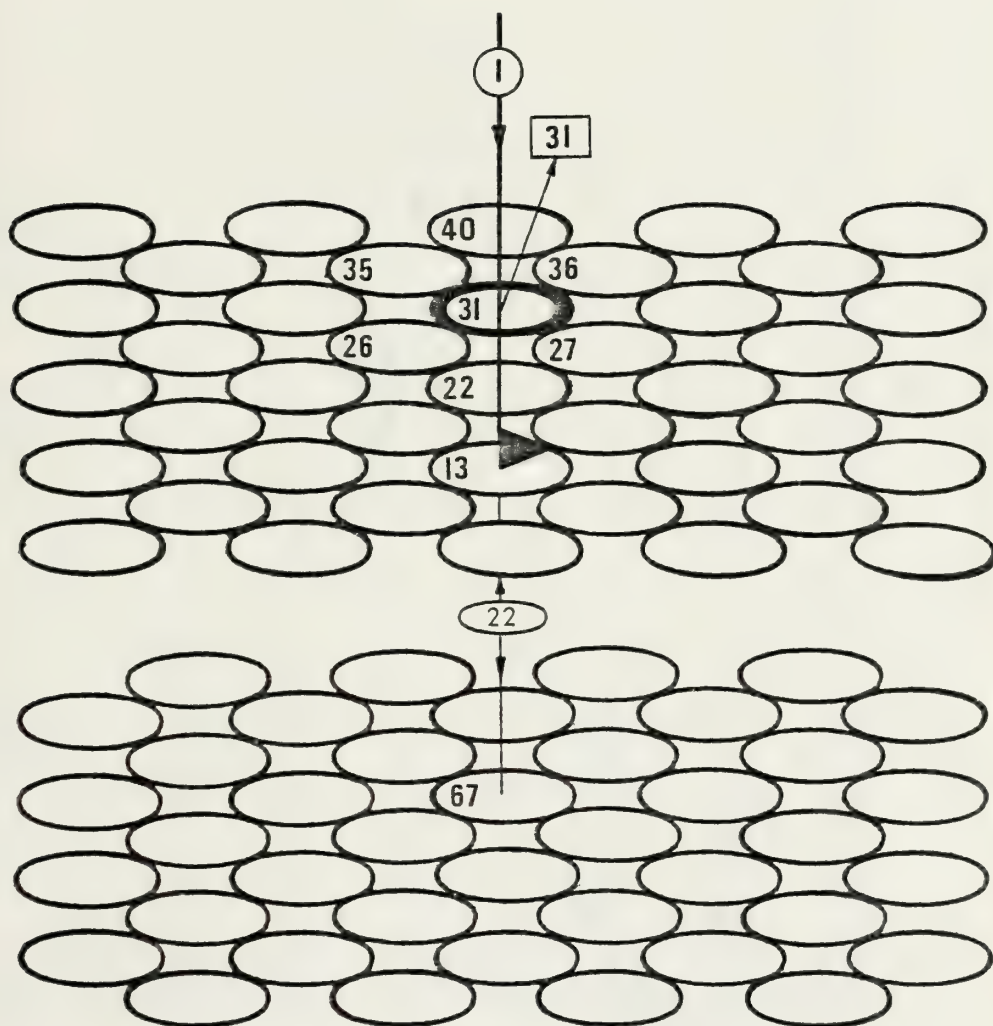


Figure 119 - Sputtering Mechanism Trace
(100), 100-eV, Cu/Cu⁺, KSE-B

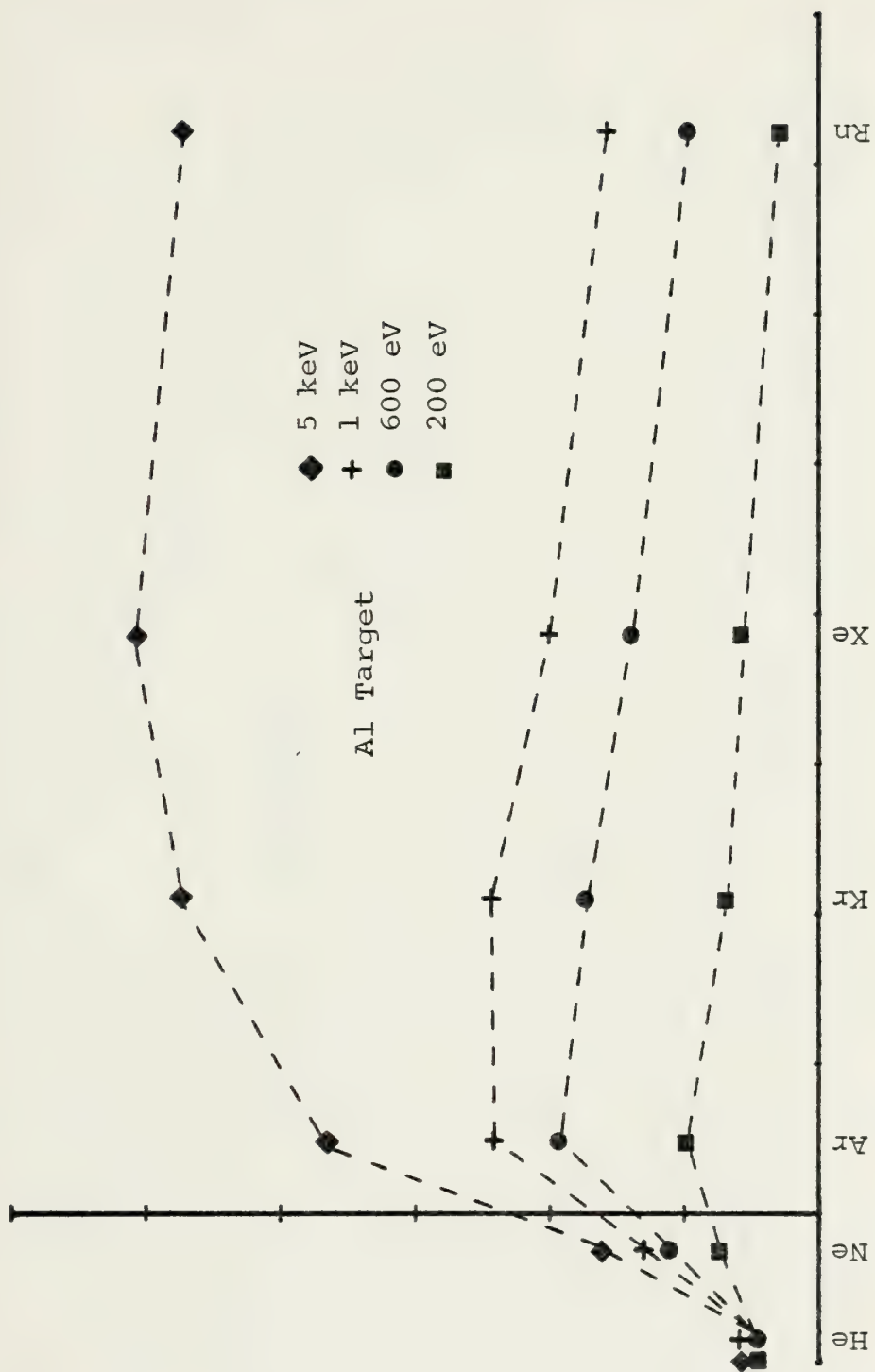


Figure 120 - Sputtering Ratio vs. Ion/Target Atom Atomic Mass Ratio

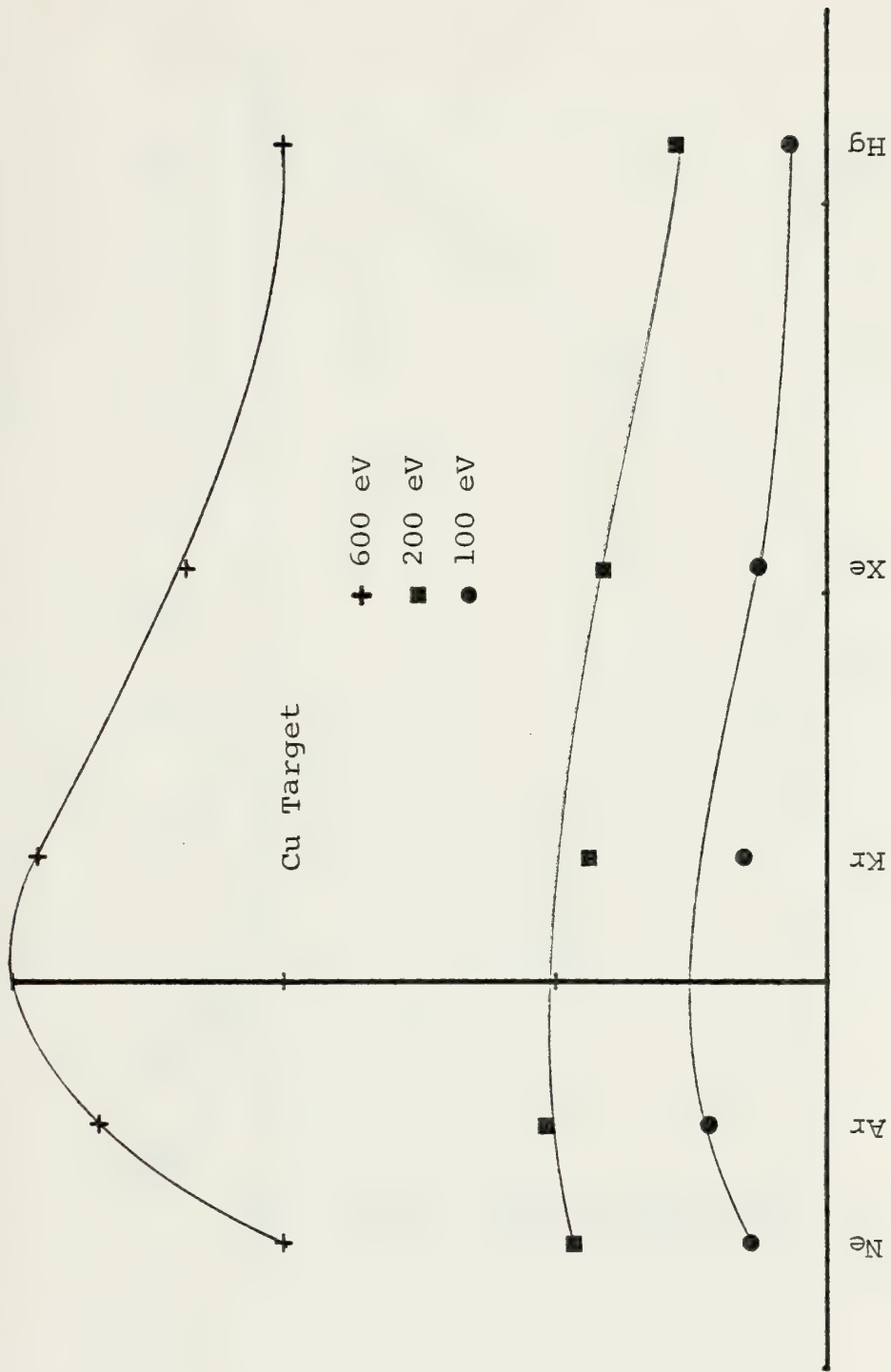


Figure 121 - Sputtering Ratio vs. Ion/Target Atom Atomic Mass Ratio

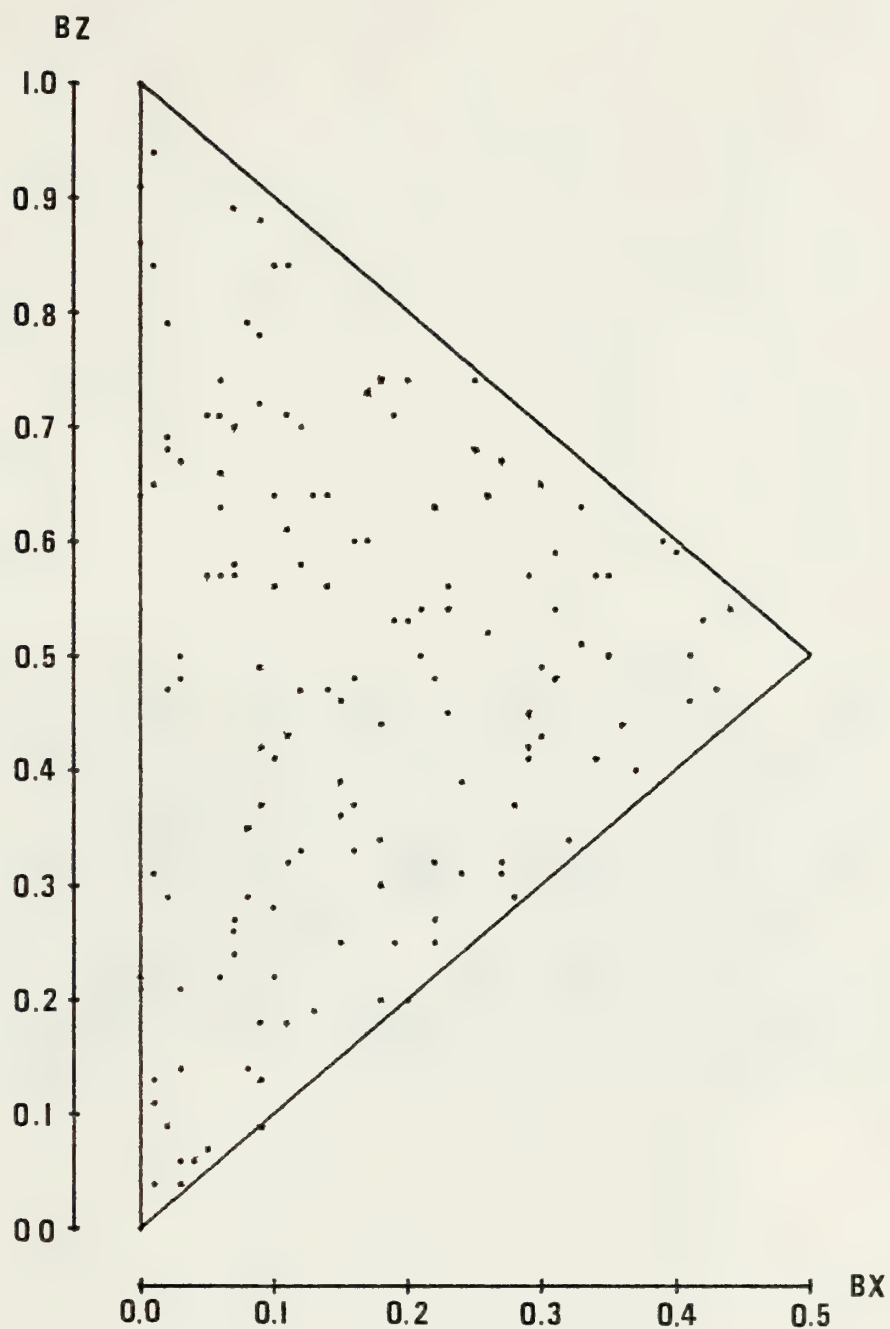


Figure 122 - Placement of 144 Random Shots

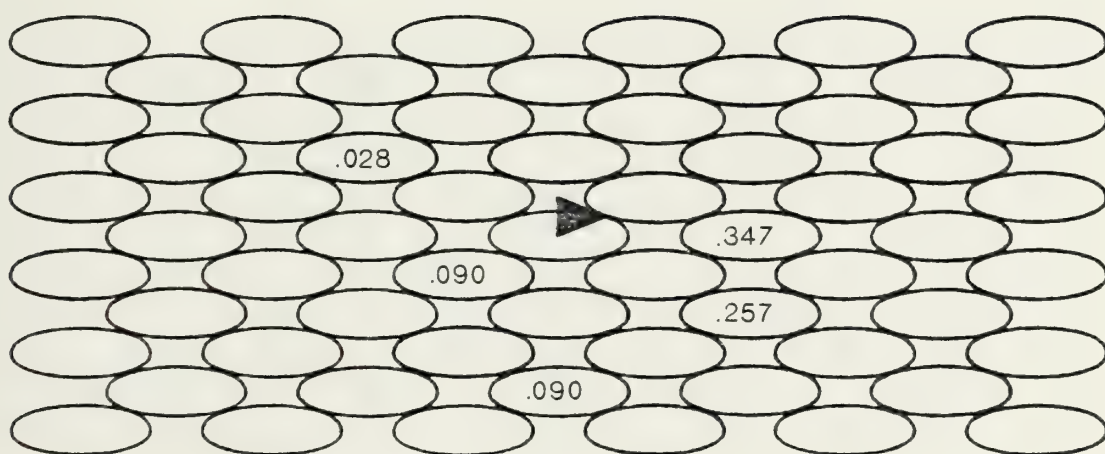


Figure 123 - Sputtering Summary - Random Points
(100) , 100-eV, Cu/Hg⁺, KSE-B, 11x4x11

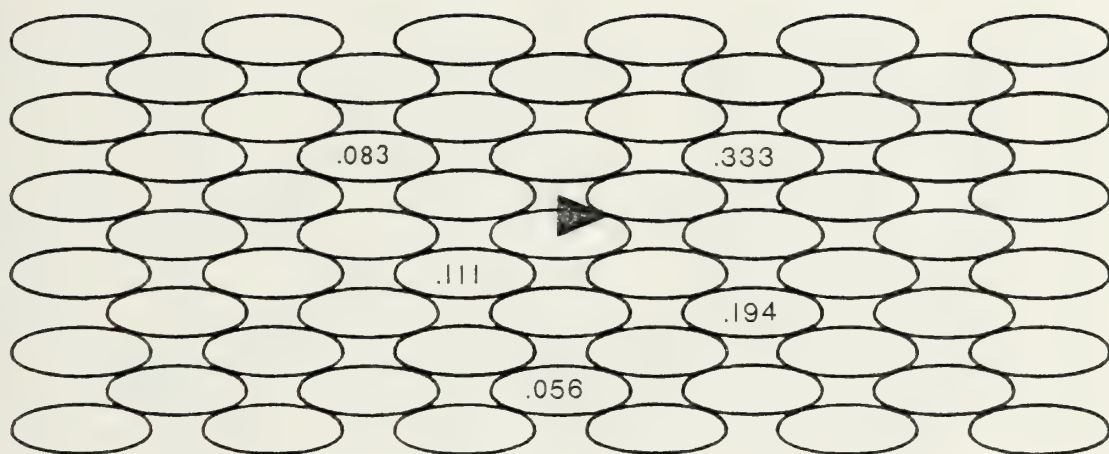


Figure 124 - Sputtering Summary - Grid Points
(100) , 100-eV, Cu/Hg⁺, KSE-3, 11x4x11

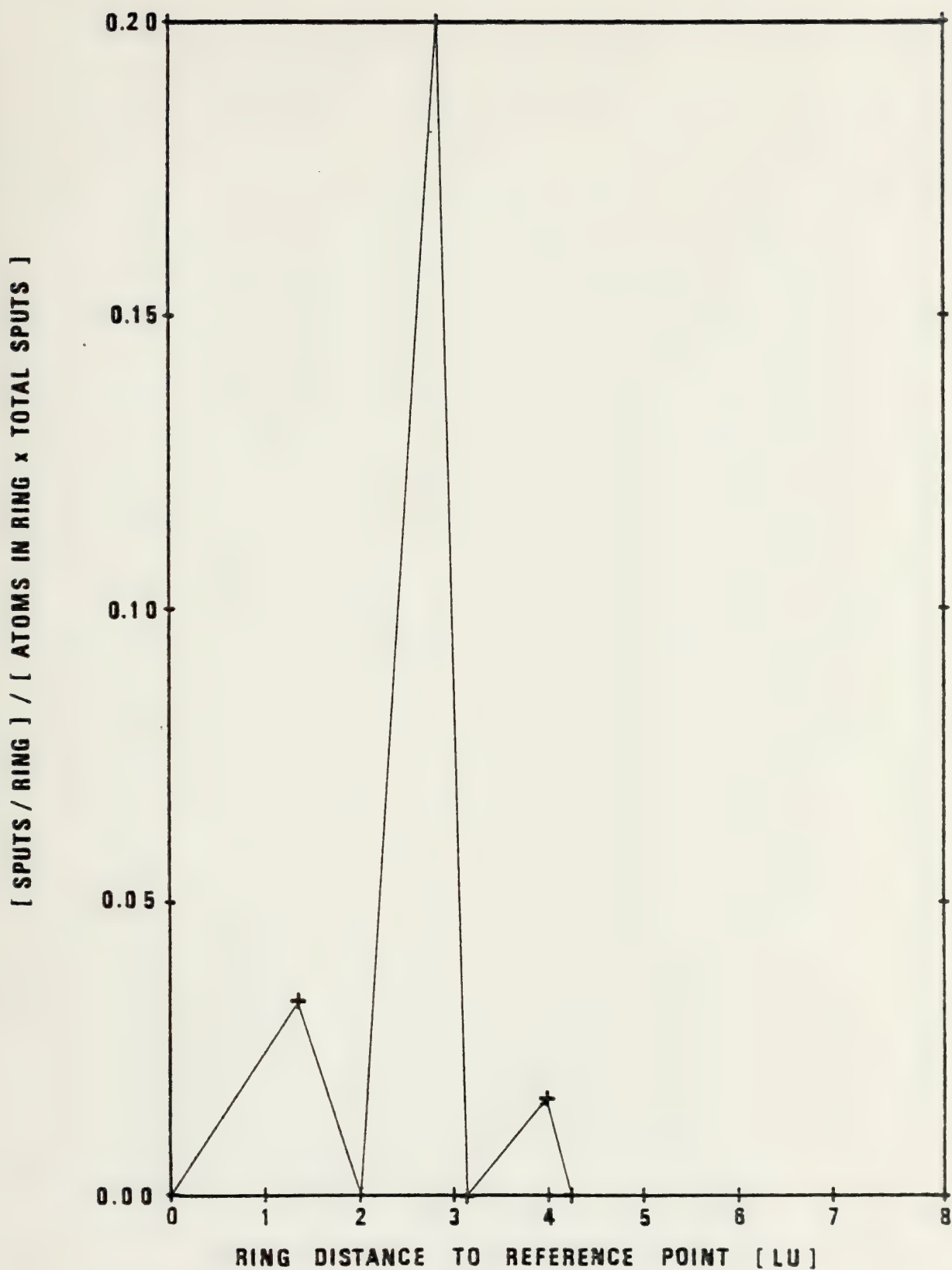


Figure 125 - Atom Sputtering Probability - Random Points

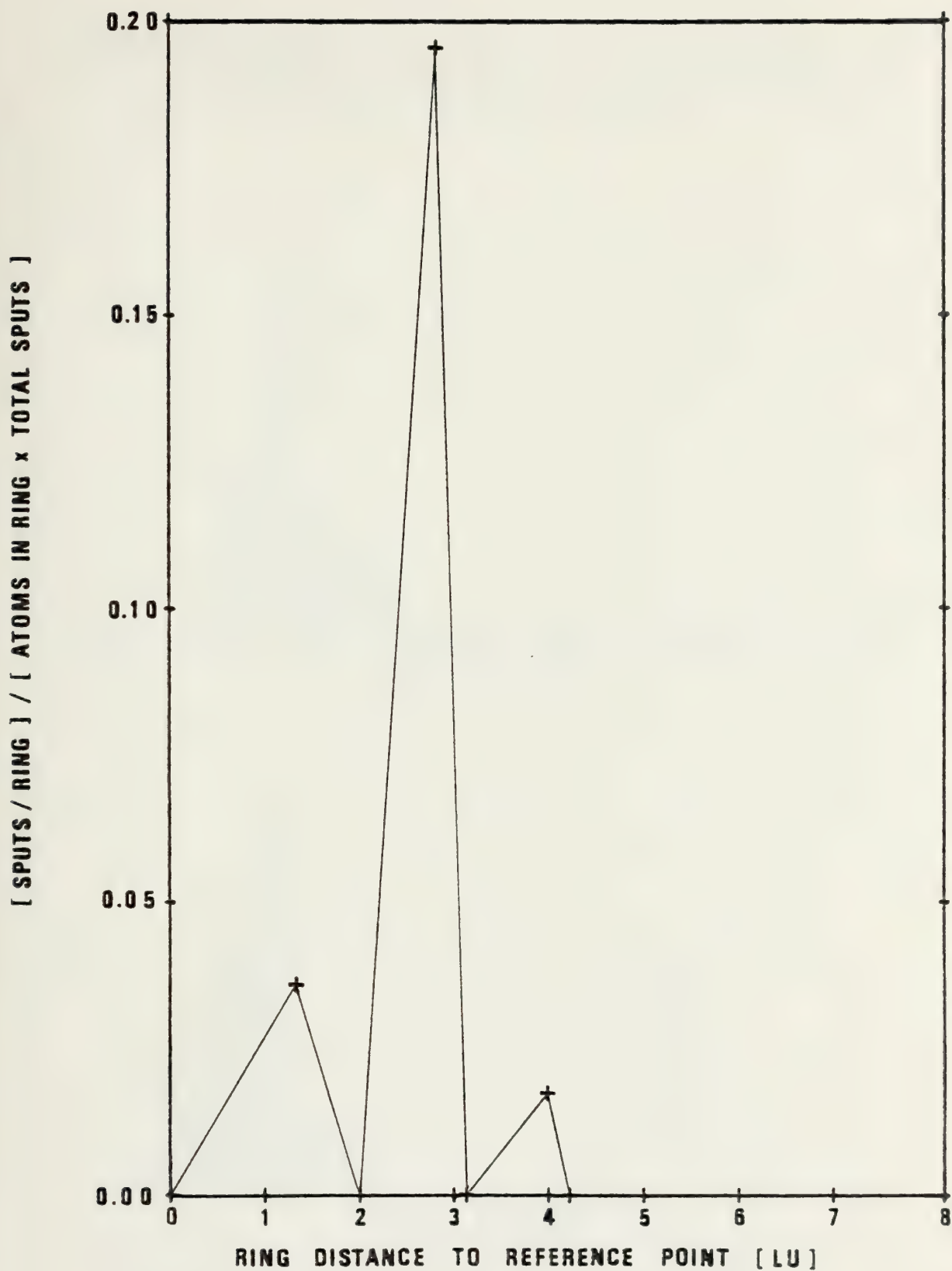


Figure 126 - Atom Sputtering Probability - Grid Points

Ejection Angle (Degrees)

0 5 10 15 20 25 30 35 40 45 50 55 60 65 70 75 80 85 90

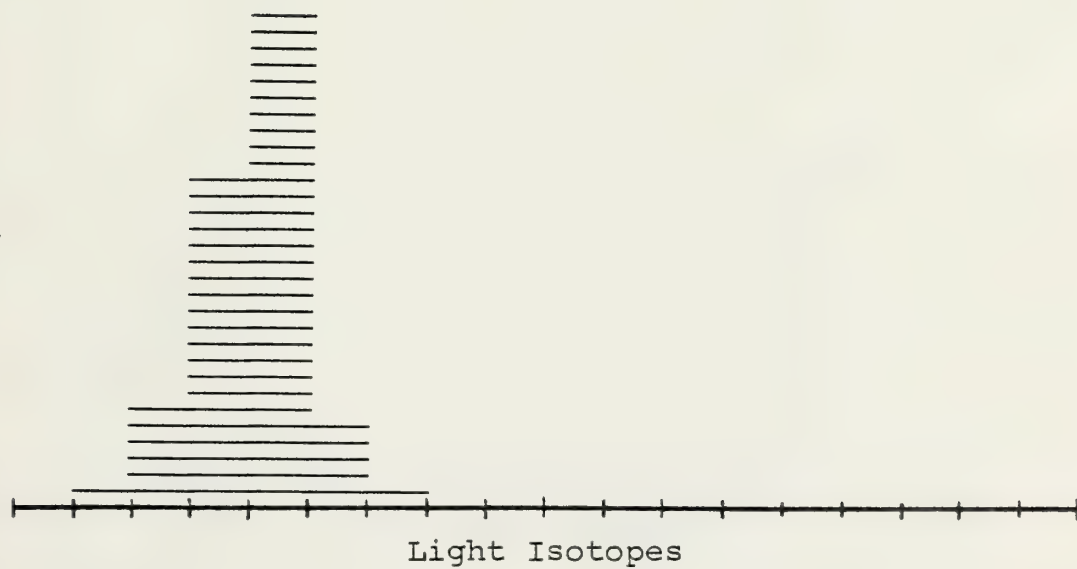
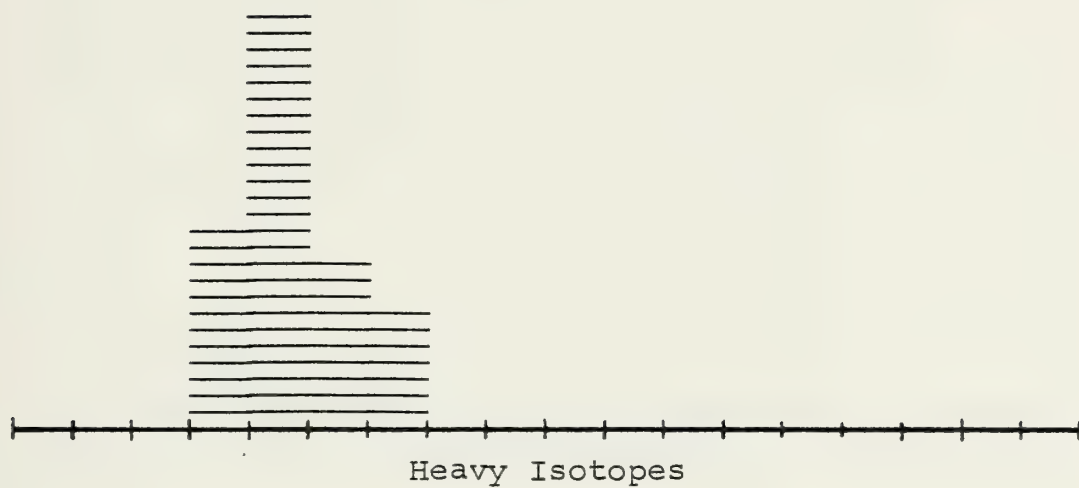


Figure 127 - Angular Dispersion - Random Points

Ejection Angle (Degrees)

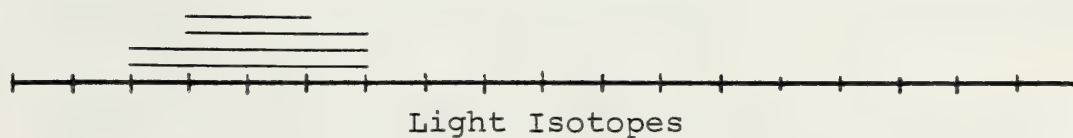
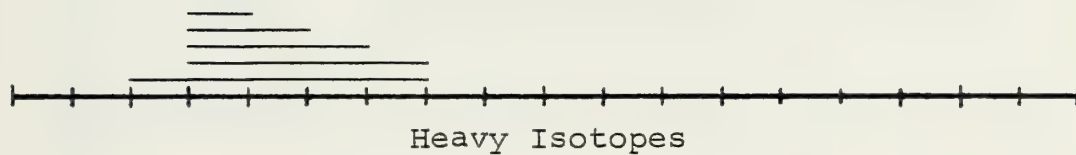
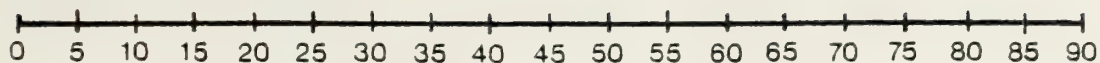


Figure 128 - Angular Dispersion - Grid Points

LIST OF REFERENCES

1. Kingdon, K.H. and Langmuir, I., "The Removal of Thorium From The Surface of a Thoriated Tungsten Filament By Positive Ion Bombardment," Physical Review, v. 22, no. 2, pp. 148-160, August 1923.
2. Blechschmidt, E. and von Hippel, A., "Der Einfluß von Material und Zustand der Kathode auf den Zerstaubungsprozeß," Annalen der Physik, v. 86, no. 15, pp. 1006-1024, 1928.
3. von Hippel, A., "Zur Theorie Der Kathodenzerstaubung," Annalen der Physik, v. 81, pp. 1043-1075, 11 December 1926.
4. von Hippel, A., "Über die Natur und den Ladungszustand der bei Kathodenzerstaubung emittierten Metallteilchen," Annalen der Physik, v. 80, no. 15, pp. 672-706, 1926.
5. Harrison, D.E. Jr., "Theory of Sputtering Process," Physical Review, v. 102, no. 6, pp. 1473-1480, 15 June 1956.
6. Wehner, G.K., "Momentum Transfer in Sputtering by Ion Bombardment," Journal of Applied Physics, v. 25, no. 1, pp. 270-271, January 1954.
7. Henschke, E.B., "New Collision Theory of Cathode Sputtering of Metals at Low Ion Energies," Physical Review, v. 106, no. 4, pp. 737-753, 15 May 1957.
8. Wehner, G.K. and Rosenberg, D., "Angular Distribution of Sputtered Material," Journal of Applied Physics, v. 31, no. 1, pp. 177-179, January 1960.
9. Anderson, G.S. and Wehner, G.K., "Atom Ejection Patterns in Single-Crystal Sputtering," Journal of Applied Physics, v. 31, no. 12, pp. 2305-2313, December 1960.
10. Winters, H.F. and Sigmund, P., "Sputtering of Chemisorbed Gas (Nitrogen on Tungsten) by Low-Energy Ions," Journal of Applied Physics, v. 45, no. 11, pp. 4763-4765, November 1974.
11. Harrison, D.E. Jr. and Magnuson, G.D., "Sputtering Thresholds," Physical Review, v. 122, no. 5, pp. 1421-1430, June 1961.
12. General Mills Report 2309, Sputtering Yield Data in the 100-600 ev Energy Range, 15 July 1962.
13. Applied Science Division, Litton Systems, Inc., Litton Industries Report 3031, Surface Bombardment Studies, by G.K. Wehner, G.S. Anderson, and C.E. KenKnight, 27 September 1966.
14. Almen, O. and Bruce, G., "Collection and Sputtering Experiments With Noble Gas Ions," Nuclear Instruments and Methods, v. 11, pp. 257-278, January 1961.

15. Southern, A.L., Willis, William R., and Robinson, Mark T., "Sputtering Experiments with 1- to 5- keV Ar⁺ Ions," Journal of Applied Physics, v. 34, no. 1, pp. 153-163, January 1963.
16. Zanuk, E.J. and Wolsky, S.P., "Sputtering of Single-Crystal Copper and Aluminum with 20-600 eV Argon Ions," Journal of Applied Physics, v. 36, no. 5, pp. 1683-1687, May 1965.
17. Snouse, T.W. and Haughney, Louis C., "Sputtering of Single-Crystal Copper," Journal of Applied Physics, v. 37, no. 2, pp. 700-704, February 1966.
18. Tishchenko, V.D., "Cathode Sputtering of Copper, Silver and Tungsten Single Crystals in the Near-Threshold Region of Ion Energies," Radio Engineering and Electronic Physics, v. 13, no. 9, pp. 1431-1434, 1968.
19. Gibson, J.B., Goland, A.N., Milgram, M., and Vineyard, G.H., "Dynamics of Radiation Damage," Physical Review, v. 120, no. 4, pp. 1229-1253, 15 November 1960.
20. Heiland, W. and Taglauer, E., "Low Energy Ion Scattering: Elastic and Inelastic Effects," Nuclear Instruments and Methods, v. 132, pp. 535-545, January 1976.
21. Harrison, D.E. Jr., Levy, N.S., Johnson, J.P. III, and Effron, H.M., "Computer Simulation of Sputtering," Journal of Applied Physics, v. 39, no. 8, pp. 3742-3761, July 1968.
22. Harrison, D.E. Jr., Gay, W.L. and Effron, H.M., "Algorithm for the Calculation of the Classical Equations of Motion of an N-Body System," Journal of Applied Physics, v. 10, no. 7, pp. 1179-1184, July 1969.
23. Harrison, D.E. Jr., Moore, W.L. Jr., and Holcombe, H.T., "Computer Simulation of Sputtering II," Radiation Effects, v. 17, pp. 167-183, 1973.
24. Wehner, G.K., "Isotope Enrichment in Sputter Deposits," Applied Physics Letters, v. 30, no. 4, pp. 185-187, 15 February 1977.
25. Harrison, D.E. Jr. Private communication.
26. Macklin, W.C. and Metaxas, J., "Splashing of Drops on Liquid Layers," Journal of Applied Physics, v. 47, no. 9, pp. 3963-3970, September 1976.
27. Eer Nisse, E.P., "Sputtering of Au by 45-keV Ions For Different Fluences," Applied Physics Letters, v. 29, no. 1, pp. 14-17, 1 July 1976.
28. Sigmund, P., "Theory of Sputtering. I. Sputtering Yield of Amorphous and Polycrystalline Targets," Physical Review, v. 184, no. 2, pp. 383-416, 10 August 1969.
29. Harrison, D.E. Jr. Private communication.
30. Harrison, D.E. Jr., Carlston, C.E. and Magnuson, G.D., "Kinetic Emission of Electrons From Monocrystalline Targets," Physical Review, v. 139, no. 3A, pp. 737-745, 2 August 1965.
31. Harrison, D. E. Jr., "Additional Information of Computer Simulation of Sputtering," Journal of Applied Physics, v. 40, no. 9, pp. 3870-3872, August 1969.

32. Harrison, Don E. Jr. and Delaplain, C. B., "Computer Simulation of the Sputtering of Clusters," Journal of Applied Physics, v. 47, no. 6, pp. 2252-2259, June 1976.

INITIAL DISTRIBUTION LIST

	No. Copies
1. Defense Documentation Center Cameron Station Alexandria, Virginia 22314	2
2. Library, Code 0212 Naval Postgraduate School Monterey, California 93940	2
3. Department Chairman, Code 61 Department of Physics and Chemistry Naval Postgraduate School Monterey, California 93940	2
4. Dr. Don E. Harrison, Jr., Code 61HX Department of Physics and Chemistry Naval Postgraduate School Monterey, California 93940	5
5. Dr. G.K. Wehner Department of Electrical Engineering University of Minnesota Minneapolis, Minnesota 55455	1
6. LT. Patrick W. Kelly, USN USS THOMAS EDISON (SSBN 610) (GOLD) FPO San Francisco, California 96601	1

Thesis

K2864 Kelly

c.1

Computer simulation
of the angular disper-
sion of sputtered cop-
per isotopes and a pos-
sible "liquid splash"
effect.

170400

thesK2864

Computer simulation of the angular dispe



3 2768 002 12078 4

DUDLEY KNOX LIBRARY